AN EXPERIMENTAL AND THEORETICAL INVESTIGATION OF SHOT CLOUD BALLISTICS

by

David John Compton

November 1996

A thesis submitted for the Degree of Doctor of Philosophy in the University of London

University College London
(University of London)
Department of Electronic and Electrical Engineering
Torrington Place
London

ABSTRACT

This thesis is concerned with an investigation of the evolution in time and space of shot clouds. The shot cloud is produced by launching a number of spherical projectiles from a shotgun barrel. With limited detailed information on the distribution of pellets within a shot cloud generated from previous studies, a considerable part of the investigation is dedicated to the design and implementation of a measurement facility to acquire accurate experimental data. Opto- and acousto-electronics were employed to meet contractual and research requirements in generating timing and positional information on the distribution of pellets in a shot cloud travelling, typically, at transonic velocities. The nature of the measurement facility also allows three-dimensional graphical reconstruction of shot cloud outlines. From the experimental data statistical analysis on the distribution of pellets within shot cloud was performed.

Theoretical models are introduced which describe the dispersion of pellets within a shot cloud as it develops in flight. The preliminary work involved the motion of a single sphere in free flight and with the experimental data the deceleration characteristics of pellets were determined. Using this information a model was developed which predicted the development of the shot clouds from the point where the pellets become independent of one another. Finally, a stochastic model was developed to describe the behaviour of a shot cloud. The equation of motion of a single sphere was perturbed by the addition of a random force term, and the width and length of the cloud were determined by performing ensemble averages. The prediction of these theoretical models were then compared to the experimental data to assess their validity.

ACKNOWLEDGEMENTS

"What goes up must come down" - an appropriate phrase for the emotions endured whilst striving to complete a PhD. In the process of trying to keep my feet firmly on the ground or giving me a helping hand up during this PhD, I acknowledge my gratitude to the following people and organizations.

I would like to start by thanking Roger Giblin for his supervision, as he was a constant source of encouragement and inspiration, especially when I was staring down the barrel of the proof gun. He also had the amazing ability, along with the spell chequer!, to sort out my remarkable use of the English language. My special gratitude is also due to Paul Radmore for his advice and guidance throughout the mathematical stages of this investigation, without his help the solution of some of my double integrals would have turn into *monogrels*. I would like to like to thank the Department of the Environment for making this work possible by funding the project over the past three years, for which I am very grateful.

To the many people that provided valuable help, and advice in the assembling of the measurement facility, I am particularly grateful to Alan Gorrod and Trevor Hamer in manufacturing the ballistics target; Ian Porter for installing the electrics in the measurement hut; the continued help and support of Holland and Holland's staff during field trials; Martin Eccles (Sabre Computers) in his involvement with the data acquisition equipment and John Bebb for manufacturing the 32 channel interface and summing units. In order to complete this investigation several items of equipment have been kindly lent or donated to the project, so I am also grateful to Bob Pitcher (London Proof House) for the use of the proof barrel; Nigel Teague and Russell Wilkin (Holland and Holland) for modifying the barrel's chokes and chambers, respectively; Ian Charlton and Arthur Phillips for the special loads of cartridges supplied for research purposes; Colonel L. McNaught (Ordnance Board, Ministry of Defence) for the use of the skyscreens; Derek Allsop (Royal Military College of Science) for the use of the high speed photographic equipment; Ed Lowry for his permission to include his spark

shadowgraphs in this thesis; Peter Fuller for the ionization probe idea; John Brindle for the translation of large sections of Journée's book and Margitte Giblin who kindly prepared food for every field trial. Special thanks must go to all my many friends in and out of college for their unwitting support and help. Finally may I thank my family for the encouragement and support given in everthing I do.

Pull!

TABLE OF CONTENTS

SYMBOLS AND ACRONYMS

#	Nominal shot size
(?.?)	Reference to an equation
BRL	Ballistics Research Laboratory
χ^2	Chi-squared, represents the goodness of fit
C_D	Drag coefficient
C_p	Pattern coefficient
d	Diameter
d_n	Normalized deviation, (4.13), mainly used to determine the most appropriate fit to experimental data from a section of models or functions
EOTS	Electro-Optical Target System
F_D	Drag force
ICAO	International Civil Aviation Organization
k_2	Deceleration constant associated with the square law
k_3	Deceleration constant associated with the cube law
M	Mach Number
pv	Percentage variation
r	Distance from the pattern centre, or radius of a circle
Re	Reynolds Number
RMCS	Royal Military College of Science
SCP	Shot cloud profile
SE	Standard Error
t_0	Time the shot column exits the muzzle
t_1	Flight time from muzzle to target for first pellet in the shot cloud
t_2	Flight time from muzzle to target for first pellet in the main section of the shot cloud
t_3	Flight time from muzzle to target for last pellet in the main section of the shot cloud
t_4	Flight time from muzzle to target for the last pellet in the shot cloud

v	Velocity
v_0	Initial velocity
v_c	Speed of sound
x-axis	Represents the horizontal
y-axis	Represent the vertical
z-axis	Represent the axis of the barrel

LIST OF FIGURES

LIST OF TABLES

Chapter 1

Introduction

1.1 BACKGROUND

A shot cloud, most commonly associated with shotguns, is produced by launching a number of spherical projectiles. There are many opinions as to how the pellets from a shotgun cartridge behave after firing, and the majority of these have no scientific evidence to support them. Over the last century, notable work on shotgun ballistics has been carried out by Journée [1] and Lowry [2], and some of Journée's work is reported in detail by Burrard [3]. It has emerged clearly from their work, and from ours, that no satisfactory theory existing can predict the downrange behaviour of shot clouds in sufficient details to render practical measurements superfluous. Ballistics therefore remains very much an experimental science. In this thesis it is shown how modern day technology has been employed to answer some of these questions. It also attempts to develop the limited work on an ensemble of spheres travelling in the vicinity of Mach 1.

The aerodynamic performance of single spheres in the transonic velocity regime (Mach number 0.5-1.4) has been the subject of several studies [4-9], but there is however a scarcity of comprehensive work on clusters of multiple spheres [1,2,10,11]. It is believed that this scarcity is due to the lack of military interest in this class of projectile, and in part to the special problems associated with this type of measurement.

In 1992 the UK Department of the Environment announced a policy decision to encourage the phasing out of lead in shotgun ammunition used over wetlands. This decision arose because of the growing concern of the increasing incidences of waterfowl poisoning in the UK and other parts of Europe [12]. The proposed time scale included a requirement that by September 1995 a range of "non-toxic shot" ammunition should be available to shooters which met four principal criteria: the alternative shot materials should be non toxic, safe to use, affordable, and effective.

In 1993 a three year contract was awarded to the Department of Electronic and Electrical Engineering at University College London to establish a shotgun external ballistics testing facility. The facility was to make measurements of kinetic energy and hit probability distribution of pellets in a shot cloud but not to address the issue of

effectiveness. The project was approximately 90% funded by the Department of the Environment, with the remaining contributions coming from Holland and Holland Ltd., the British Association for Shooting and Conservation, ammunition manufacturers and other interested organizations.

Ammunition manufacturers have sent lead reference loads as well as non-lead loads to be tested at the Ballistics Research Laboratory (BRL) in the UK. The results were fed back to provide advice and guidance for manufacturers and the shooting community [13]. This unique experimental facility has also provided the foundation for research into the dynamics of shot clouds as they evolve in space and time.

1.2 ORGANIZATION OF THESIS

The introductory chapter presents the background to the project and explains how the modern shotgun is used to research into the dynamics of multiple spheres. It reviews relevant past work that has been carried out on shotgun ballistics, as well as experimental and theoretical work on the behaviour of spheres in free flight.

Chapter 2 describes the measurements facility which has been designed to address the issue of effectiveness for cartridge loads. It will explain the different requirements and experiments that where needed to meet the contract and research work plan. The contract required routine measurements on the cartridges which had been sent for testing, and the research developed the equipment to obtain measurements on the behaviour of a shot cloud as it travels downrange.

Chapter 3 discusses the shot cloud phenomenon through experiments which address the effects of altering the internal ballistics of a shotgun, via choke and chamber length, on the ballistics and patterns. With the basic test facility designed to meet the contract requirements, the introduction of multiple recording channels is used to produce three-dimensional outlines of the shot cloud downrange. Using the pattern, ballistics and three-dimensional data the pellet density distribution in the shot cloud can be obtained and the hit probability on standard areas is examined.

Chapters 4 and 5 are concerned with the dynamics of a shot cloud as it develops in time and space. They use different approaches in modelling the behaviour of the spheres (pellets) as they evolve.

Chapter 4 uses two expressions derived from the equation of motion for a single sphere to condense the experimental data, and summarize the ballistic characteristics of shot clouds. A general relationship is obtained between the leading and trailing edge pellets and their deceleration constants. Using this information and assuming the pellets in a shot cloud are in free flight, a model is developed from the equation of motion for a single sphere to predict the ballistic characteristics of a shot cloud over the measurement range.

A random force approach to the theory of shot cloud dispersion is used in Chapter 5, which develops a stochastic model to describe the behaviour of a cloud of spherical projectiles travelling around Mach 1. The equation of motion of a sphere is perturbed by the addition of a random force term, and the width and length of the cloud are determined by performing ensemble averages, and analytical expressions containing two parameters are derived.

The models in Chapter 4 and 5 are then compared with experimental data on the pellet distribution in a shot cloud from a variety of different cartridge loads. To conclude, Chapter 6 summarizes the main achievements and identifies possible areas for further research.

1.3 THE SHOTGUN AND CARTRIDGE

1.3.1 Use of shotgun and cartridge in this investigation

Single-projectile ballistics have been studied for hundreds of years and it was the work of Leonardo da Vinci (1452-1519) which lead to the early development of modern ordnance engineering. Over the centuries many sophisticated methods of measurement on single projectiles have evolved, yet by comparison, multiple spheres and especially

shotgun ballistics have been largely neglected in terms of systematic and scientific study. This may be in part due to the lack of military interest in shotguns, and in part to the special problems of measurement in this topic of research.

The main interest in this thesis is to determine the downrange ballistic characteristics of pellets in shot clouds. To launch the pellets into the format of a shot cloud the shotgun and cartridge are used. The measurements and experiments described in this thesis involve the use of shooting terms, so for completeness the basic elements of a shotgun and cartridge are described. For further information on the construction and manufacture of shotguns and cartridges refer to books such as 'Shotgun shooting techniques and technology' [1,3,14].

1.3.2 Basic principles of the shotgun cartridge

The projectile used in a shotgun consists of a large number of small pellets. The pellet count in a cartridge can be as few as 100, each 4mm in diameter, or as many as 800, 2mm in diameter. In the shooting community the pellet diameters are stated as a nominal shot size, indicated by #, table A.1 shows the equivalent metric units. The combined mass of the shot (pellets) load is generally in the range of 25-50g. Fewer larger pellets or even single projectiles can also be used in shotguns but do not form part of this study. The pellets are only one of the components which make up the shotgun cartridge.

The principle behind the cartridge has not changed over the last century. It is designed to keep the shot load complete until it is are propelled from the muzzle of the gun. The cartridge case forms a container for the components, as shown in Figure 1.1, into which the pellets are placed, wadding and propellant are packed behind, and a small explosive cap (percussion cap) is in the base. The fibre wad cartridge (ii) uses biodegradable components, where the casing is made of paper and the wad is fibre (traditionally felt). In the more modern cartridge a plastic shot cup (i) replaces the wad and holds the pellets.

Firing the gun ignites the propellant charge, via a flame from the percussion cap, and a build up of pressure is produced from the expanding gasses. The wad, which acts like a

piston, seals the bore of the gun between the expanding propellant gases and the shot load as they are driven out of the barrel at high velocities (typically 400m/s or Mach number 1.2). For cartridges with plastic shot cups the pellets are held and buffered from the bore of the gun. After leaving the muzzle the shot cup separates away from the shot and falls to the ground, due to its relatively inferior aerodynamic performance caused by the petals of the shot cup opening.

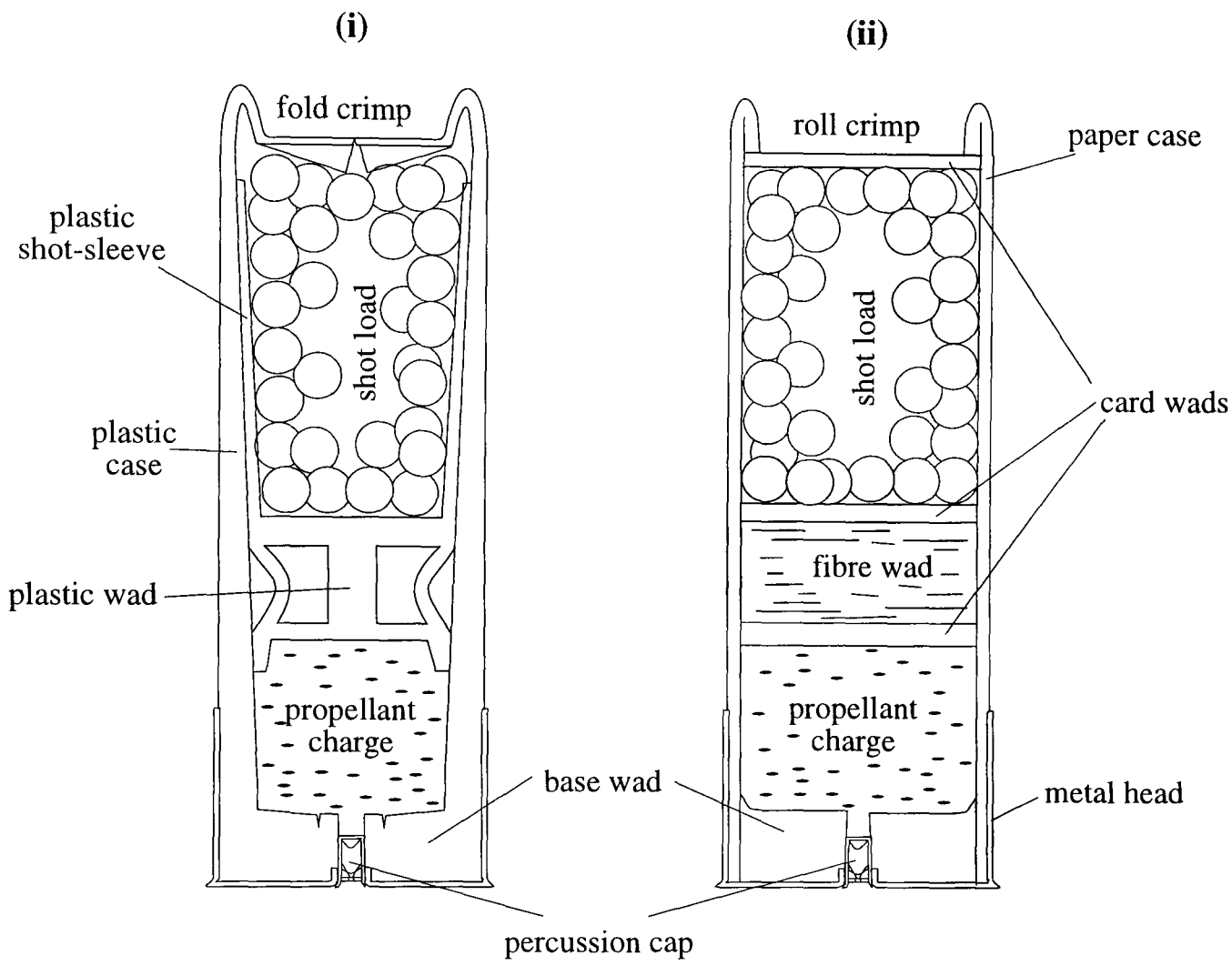

Figure 1.1 *Cross section of a shotgun cartridge with a plastic shot cup and a fibre wad.*

For mass production it is very difficult to control the loading of the cartridges by weights. The manufacturers load by volume, and it has been noticed and discussed further in section 3.2 that the number of pellets in a mass produced cartridge has a typical standard deviation, as a percentage of the mean, of 2%. For some experiments it has been necessary to have loads specially hand loaded by weight to limit the possible variation and also to achieve velocities which would not be commercially safe when used through standard guns.

1.3.3 Brief description of the modern shotgun

The main purpose of a shotgun is to fire 'small shot'. The shotgun is defined as *"Shot-gun, shotgun, org. US 1828 A smooth-bore gun used for firing small-shot, as dist. from a rifle for firing a bullet"* [15].

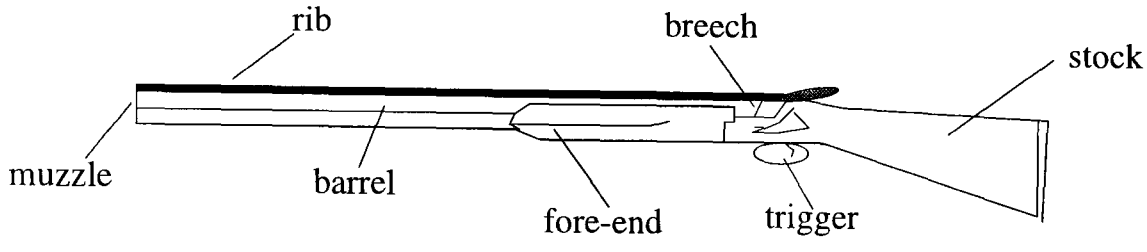

Figure 1.2 *Basic elements of a over and under shotgun.*

The principles behind the modern shotgun have been used for the last hundred years and it is made of three main sections, as shown in Figure 1.2 . The stock fits the shotgun into the shoulder of the shooter and gives it its stability. The trigger action creates pressure on the percussion cap which ignites the cartridges, and the barrel helps the propulsion of the shot (pellets). In shotguns there can be one or two barrels which are configured side by side or over and under. There are many other configurations, but the principles are mainly all the same.

One factor that can alter the performance of the shot cloud after firing is the choke of the gun. The choke is an internal constriction at the muzzle to some degree of the barrels bore. An analogy of the effect of choke is the squeezing of a hose pipe at the end to spray the water further. Within limits, decreasing the diameter of the choke constriction (Figure 1.3) increases the shot column length and tightens its width as it emerges from the muzzle, this is discussed in greater depth in the next section.

Figure 1.3 *Cylinder choke and a choke with a linear tapered constriction.*

The choke of a shotgun has relatively more effect on the width of the shot cloud compared to the length. Depending on the shooting discipline, it is desired to obtain certain pellet densities in the shot cloud pattern. This has meant the development of a variety of chokes, a selection are shown in Figure 1.4, where the angle of constriction and profile are experimented with to achieve the optimum pattern for a gun-cartridge combination.

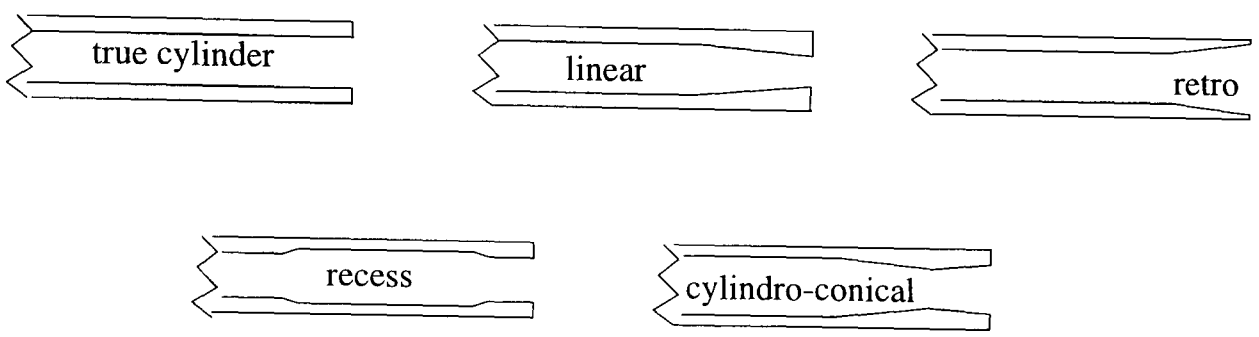

Figure 1.4 *A selection of different types of muzzle profiles.*

The breech end of the shotgun barrel is internally enlarged to take the cartridge. This enlargement is called the "chamber" of the barrel and is usually long enough to hold the full length of the cartridge after it has been fired. Due to different loads used in shooting the cartridge case length varies with component volumes (mainly the pellets). This means that there are different chambered guns to take the different length cartridge cases.

1.3.4 Shot cloud development

The resemblance between a shotgun projectile and a bullet ends even before the charge leaves the gun muzzle. In the shotgun the pellets accelerate up the barrel as a compact mass which to some extent is compressed as it passes through the "choke". As soon as this mass exits the muzzle it starts to disperse. The development of the pellets after leaving the muzzle is made up of several complex stages. Experiments by Lowry [16] have shown (Figure 1.5) that for the first metre of flight the shot column of pellets behaves like a single semi-fluid object. The drag force of air resistance and interaction between pellets causes a gradual separation of pellets after the shot cup has fallen away

from the load. At some point the pellets have separated sufficiently apart that they are travelling in free air and their only interaction is with air resistance.

Image removed due to third party copyright

Figure 1.5 *Spark shadowgraph produced by Lowry [16] showing the dispersion of pellets from a felt wad #7.5 lead cartridge at 4 feet from the muzzle when passed through a cylinder chokes (top) and a full choke barrel (bottom).*

The shot cloud length is defined as the distance between the first and last pellets in flight and the pattern gives an overview of the pellet distribution across the width of the shot cloud. Generally, at ranges close to the muzzle a more constricted choke will produce a longer shot cloud which patterns tighter. Shadowgraphs produced (Figure 1.6) by Lowry [16] show the effects of a full choke, where the front pellets in a shot cloud separate away leaving turbulent wakes. He explained that the pellet behind in the wake experience less resistance, due to slip stream effects of the leading pellets, and disperse less rapidly compared to a cylinder choked shot cloud. With the greater dispersion from a cylinder choke the pellets spend a shorter period in a protected atmosphere. Therefore they achieve free flight quicker and become subjected to the full force of air resistance.

In the cartridge a vital component is the wad or plastic shot cup (described in section 1.3.2), it controls the performance of the cartridge after exiting the muzzle. The shot cup holds the pellets, in theory, until a short period after exiting the muzzle, after

which it falls away from the load. If it does not release the pellets consistently then it will alter the initial spread of the pellets, creating a great variation in the ballistics, especially patterns.

Image removed due to third party copyright

Figure 1.6(a) *Spark shadowgraph produced by Lowry [16] showing the dispersion effects on a shot cloud from a cylinder choke (right) and a full choke (left) at 6 and 10 feet for a #7.5 lead load.*

Image removed due to third party copyright

Figure 1.6(b) *Spark shadowgraph produced by Lowry [16] showing the dispersion effects on a shot cloud from a cylinder choke (right) and a full choke (left) at 14 and 18 feet for a #7.5 lead load.*

1.3.5 Traditional measurement techniques

Lead has been extensively used for the manufacture of the small spherical projectiles in shotgun cartridges. It has been shown to have excellent ballistic characteristics for this purpose because it is dense and malleable. The development of these traditional loads has been by trial and error over the last three centuries and experiments were designed to give comparative results. Testing the penetration of the shot charge on special card pads, tin sheets or telephone directories was one of the earliest methods employed for measuring comparative velocities, where the velocity of the pellets were assessed as a function of the depth of penetration.

Later experiments on velocity were based on the "observed velocity" of the cartridge. This was measured by firing at a metal sheet 20 yards from the gun muzzle and timing the flight time of the leading edge pellets over this fixed range. The flight time was used to estimate a velocity at 10 yards and assumed that the deceleration of the projectiles were constant.

The process of timing between two ranges and giving the mid point velocity was extended with the use of an array of wire meshes spread downrange. When the shot cloud broke the wires the timing information would be recorded for that particular range. From the different array positions downrange it was then possible to calculate the mid-point velocities for a number of ranges. This method relied on a pellet breaking part of the wire mesh to give the flight time at that particular range. Unfortunately it was not possible to know the position of the pellet in relation to the leading edge of the shot cloud.

The experimental procedures described in this section and also the majority of data available in the shooting community [3,17] only state single ballistic figures. These figures generally refer to the leading edge data, as it is the easiest to measure and shows the highest velocity and energy values. It cannot, however, be assumed that every pellet in the shot cloud has the same value as there is a lateral and longitudinal distribution.

It has been easier to measure the lateral spread than the longitudinal spread of the shot cloud. This has been traditionally done by firing the cartridge at a steel plate (normally whitewashed) or sheet of paper, where the area of interception must be large enough to collect the majority of the pellets from the cartridge. To analyse the pattern, the centre would be judged by the eye and from this a pellet count in a 30" diameter circle would be made. The result is the "pattern", and the process itself is termed "patterning".

The lateral spread or pattern would represent the pellet distribution seen by a going away or driven target to the shooter. Experiments by Burrard [3], and reassessed by Lowry [18], showed the lateral pattern seen by a crossing target. Metal pattern sheets were attached to the side of a car and driven at constant speeds, distances and angles away from the shooter. They both concluded from these patterning tests that the pattern seen by a crossing target were measurably different but not of practical significance from that obtained on a stationary plate. It must be noted that they both judged patterns by eye and did not use any statistical analysis.

There have been several comprehensive projects undertaken to assess the performance of shotgun cartridges. These methods are more experimental and not traditional; they are reviewed later in this chapter.

1.4 MOTION OF A SINGLE SPHERE IN FREE FLIGHT

1.4.1 Theory of the motion of a sphere in free flight

Shot clouds have been shown in section 1.3.4 to be complex structures which contain many pellets. Near the muzzle the pellets travel in close proximity to one another and at a range >20m they have probably (see section 4.5.4) separated sufficiently to be regarded as being in free flight. Due to the complexity of the interaction between an ensemble of pellets, most of the preliminary work involves the principles of a single sphere in free flight. The methods for treating the problem of an ensemble of spheres (or pellets) can be built upon an understanding of this motion. There are many references [19-23] which deal in-depth with the forces on a single sphere in a steady flow.

A sphere experiences a number of forces when in free flight. The main component of force is in the direction of the undisturbed air stream and termed the drag force. The drag force (F_D), described by (1.1), acts in the negative direction to the spheres flight and is dependent on four parameters: the cross sectional area of the sphere (A), the atmospheric density (ρ_a), the instantaneous velocity of the sphere (v) and the drag coefficient (C_D).

$$F_D = -\frac{1}{2}\rho_a A v^2 C_D \qquad (1.1)$$

There has been limited work carried out on single sphere drag coefficients [4-10,24-26]. It is a non-dimensional coefficient dependent on velocity (strictly, the Mach number), shape, and Reynolds number.

The Reynolds number given by (1.2) describes the type of flow around a sphere and is seen as the ratio between inertia and viscous forces, where velocity (v), diameter (d) of the sphere and viscosity(U) are its components. This makes it non-dimensional. For low values of Reynolds number the viscous forces are predominant and a laminar flow is produced which slides smoothly over the sphere, whereas for large values of Reynolds number the inertia forces are of much greater importance and a turbulent flow is created. To summarize, the degree of turbulence or the relative importance of inertia to viscous forces in a given flow is uniquely defined by the Reynolds number for that flow.

$$\mathrm{Re} = \frac{inertia\ force}{viscous\ force} = \frac{vd}{U} \qquad (1.2)$$

The Reynolds number for a 3mm diameter sphere, or pellets in a shot cloud, which has a velocity distribution from 400m/s (Re=8x10^4) to 100m/s (Re=2x10^4) over the measurement ranges (20-50m) is approximately 5x10^4. The value for viscosity can be found in Goldstein [19] as 1.5x10^{-5} m^2/s at 20°C.

The major parameter of the drag coefficient is the Mach number, which is the ratio of the speed of the sphere to the velocity of sound in the surrounding medium. From previous experiments [4-6,24] it has been shown that a sphere's drag coefficient (C_D) obeys different force laws depending on its velocity for a Reynolds number of 5×10^4. In Figure 1.7 the drag coefficient is reproduced using data from Braun's [24] experimental data. It can be seen that at subsonic velocities below Mach 0.5, the drag coefficient is constant and a square law of air resistance is obtained from (1.1), with the force of air resistance proportional to the square of the magnitude of the velocity. At transonic velocities between Mach 0.5 and Mach 1.4 the drag coefficient is approximately proportional to the velocity (illustrated in Figure 1.7 as the extrapolated dotted line). At higher supersonic velocities (greater than Mach 1.4) the drag coefficient becomes approximately constant again.

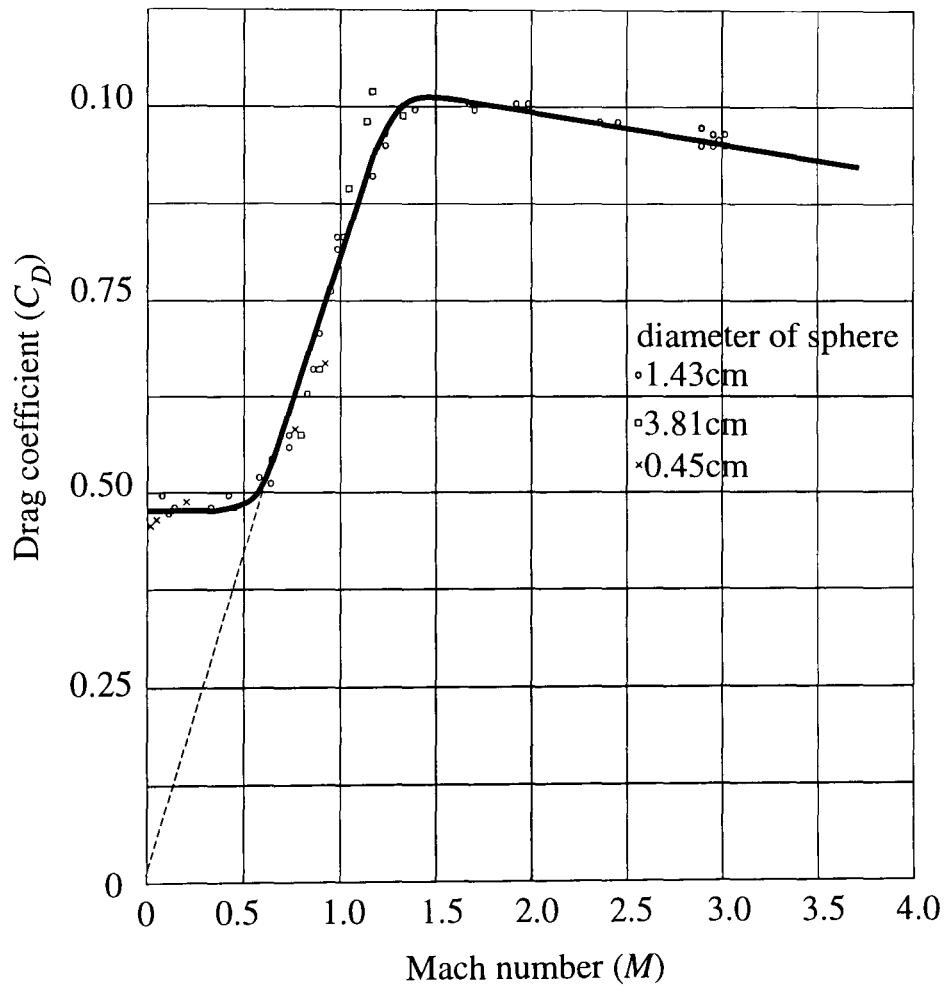

Figure 1.7 *Drag coefficient curve of a sphere around the transonic regime using Braun's experimental data [24]. The extrapolated dotted line illustrate the approximation that the drag coefficient is proportional to Mach number between 0.5 and 1.4.*

A sphere is described as a "bluff body", meaning that it is not streamline. From experiments summarized in several books [20,22,23], the drag on a sphere is shown to be influenced by the cross-sectional area of the wake. A broad wake is accompanied by a relatively high drag coefficient and vice versa. The flow past a sphere and the wake produced, is changed dramatically as the Reynolds number is varied. For the pellets in a shot cloud with Reynolds number of $5x10^4$, it can be seen in Figure 1.8 that the laminar boundary layer (boundaries between different pressure flows) separate at points, S, on the front half of the sphere. This forms a large wake which produces a relatively high drag coefficient (C_D).

Figure 1.8 *Flow past a sphere for different Reynolds numbers as illustrated by Houghton and Carpenter [20].*

A smooth sphere has a critical Reynolds number at approximately $3x10^5$ (log Re=5.48) where the drag is dramatically reduced (Figure 1.9). When the Reynolds number reaches this critical value a turbulent boundary layer around the sphere is produced. In Figure 1.8 it is shown that the laminar boundary layer transforms into a turbulent flow

after the separation points and reattaches as a turbulent boundary layer, creating a separation bubble. Due to the better sticking properties of turbulent boundary layers the wake is decreased and reduces the drag. Spheres have been used to ascertain the turbulence levels in the air steam of wind tunnels working section. With regular calibration of wind tunnels, the onset of turbulence (critical Reynolds number) has been found to depend on the roughness of the sphere's surface, such as on its precise shape. With a small increase in the surface roughness the critical Reynolds number can be reduced for the same velocity. This method is used in sports to helps golf balls go further in flight from their driving velocity. Unfortunately this idea cannot be used in the shot cloud context as the associated Reynolds numbers are below this critical point and there is also a great variation in the pellet shapes after firing, shown in section 3.2.1.

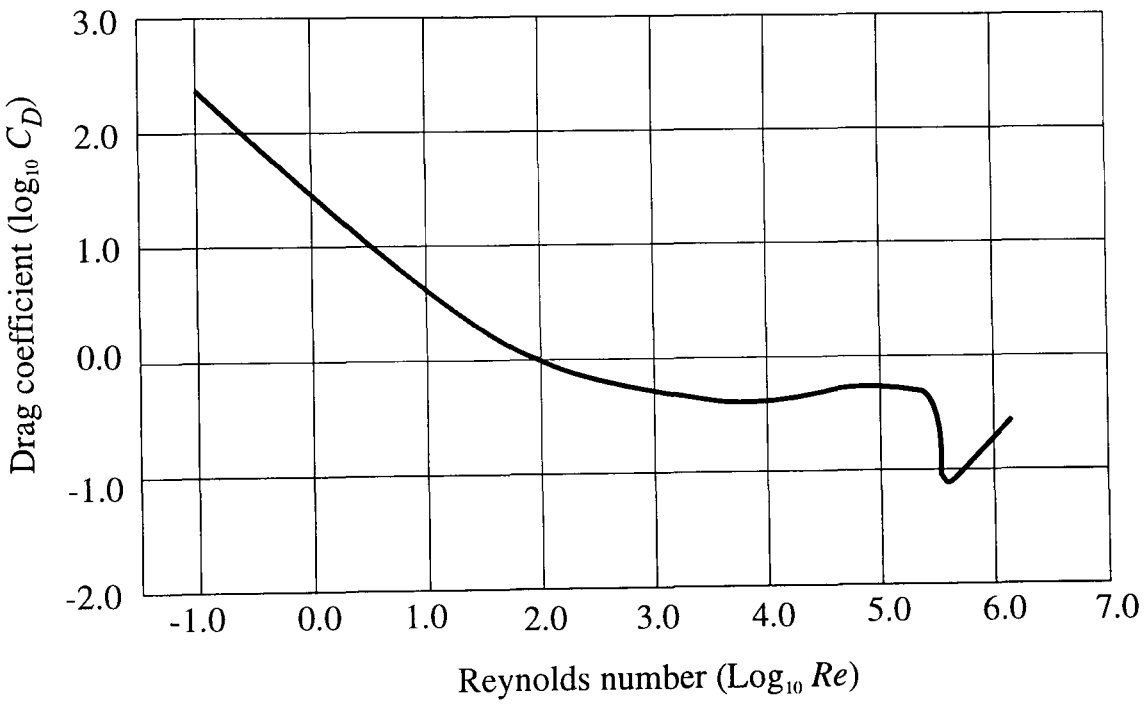

Figure 1.9 *The standard drag curve taken from Golstein's data [19]. The logorithms of both axis are taken here to emphasize the critical Reynolds number.*

When a fluid is incompressible the standard drag curve (Figure 1.9) is applicable for the relationship between Reynolds number and Drag coefficient. However, when compressibility plays an essential part, such as at Mach number >0.5, the dimensionless drag coefficients depend on both the Mach and Reynolds number parameters (Figure 1.10). For low Mach number it can be seen that the curve for M=0.3 is practically coincident with that in Figure 1.9 for incompressible flows and it suggests that

Mach number has negligible effect. However, with greater Mach numbers its influence increases and there is less of a critical Reynolds number present.

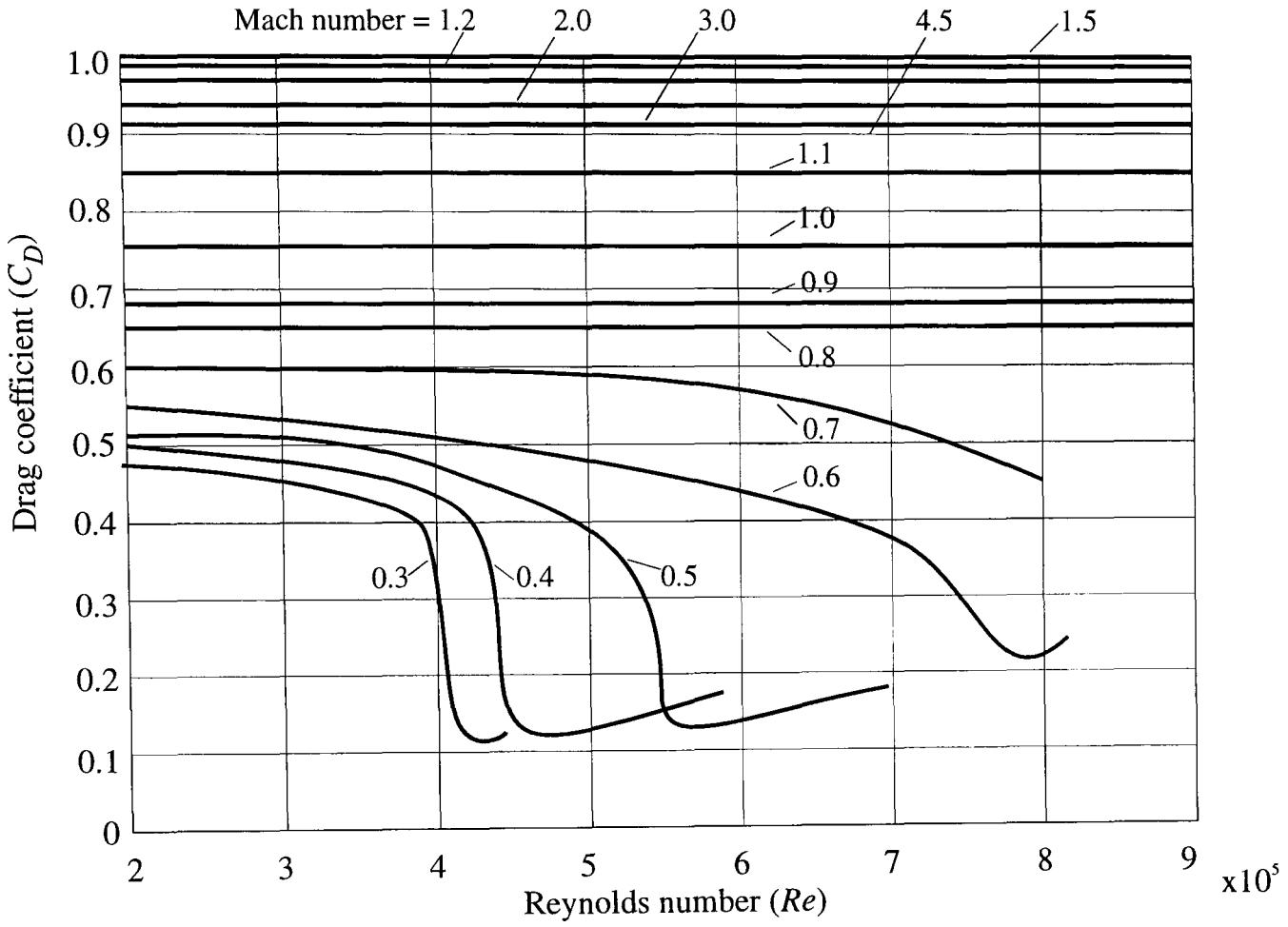

Figure 1.10 *Drag coefficient of spheres in terms of Reynolds and Mach numbers as reported by Schlichting [21].*

1.4.2 Past work

The behaviour of a sphere moving through a fluid has generated interest ever since the first recorded measurements relating to sphere drag made by Newton. More recently the sphere has been extensively used for the calibration of turbulence in wind tunnels, producing a multitude of studies on sphere aerodynamics. There are and have been experimental programmes [2,13,16] (including this work) which require an accurate knowledge of a sphere's aerodynamics over a particular range of Reynolds number and Mach number. In addition to such programs the study of flow round a sphere is of continued interest [9] due to the lack of understanding of bluff-body flows.

In many textbooks [19,20,22,23] since 1938 graphs have been produced, which are called the "standard" drag curve (Figure 1.9), summarizing the relationship between drag coefficient and Reynolds number by a straight line. Figure 1.9 shows the effect of Reynolds number on the drag coefficient and it can be seen that there is a critical number where the drag is dramatically reduced, as described in section 1.4.1. Even though there have been many investigations into the aerodynamic performances of spheres, the basic relationship between drag coefficient and Reynolds number (C_D and Re respectively) are somewhat indefinite for a steady-flow. Roos and Willmarth [25] reported that the scatter in existing data amounts to at least 10% over much of the Re range. The "standard" drag curves had a common shape but the critical Reynolds number and drag coefficient differed.

The majority of wind tunnel experiments on a sphere used strain gauges inside hollow spheres which are then supported on a thin wire mount. This structure is placed in a wind tunnel where a steady flow of air passed over the sphere. It has been recognized [8,26,27] that the available data differs from one another because of the many parameters which influence the flow. These parameters are the turbulence level of the flow, the effect of the supports, surface roughness, tunnel blockage and Mach number. The method of supporting the sphere is very important to obtain reliable data. The support cannot interfere with the formation or natural movement of the boundary of discontinuous flow or it will prevent the sphere from free flight. As there was no consistency between the early experimental configurations it is reasonable to expect differences in the results.

The importance of turbulence in the wind-tunnel was first acknowledged after discrepancies were found on similar bodies at the same Reynolds number between tests made in different low-speed wind tunnels, particularly over certain ranges of Reynolds number. The critical Reynolds number was observed to vary from tunnel to tunnel due largely to the variation of stream turbulence and this is now used to specify the turbulence of a wind tunnel. It was also indicated by Sherman [29] that the a single wind

tunnel does not have sufficient operational flexibility to cover the entire flight regime for a broad range of Mach ($0.05<M<20.0$) and Reynolds numbers ($2x10^{-1}<Re<10^{6}$).

The scatter of existing data points is more uncertain in the case of accelerated motion. Experiments by Lunnon [7] and Bacon [8] dropped spheres through fluids and air. These methods do not represent a free moving sphere as they are affected by the additional force of gravity which causes the sphere to accelerate. The effect of gravity were apparently ignored and resulted in the scatter of drag curves. Ross [25] concludes that the result of free-fall tests affects the coupling of the spheres dynamics with the unsteady wake processes.

More recently, detailed experiments [9,30] have made measurements on the pressure distribution around a sphere in a transonic flow. With the advances in Computational Fluid Dynamics, there is an increasing demand for experimental data in all ranges of flow conditions, for the verification of numerical techniques. There is a great interest in this area of study, especially in missile and aircraft aerodynamics, and also as velocity probes in subsonic and supersonic flow fields.

The main interest for this work is on a spheres ballistics at velocities in the vicinity of Mach 1 and Reynolds numbers of $5x10^{4}$, this corresponds to the shotgun projectiles as they pass through, depending on initial velocity, the three regions of supersonic, transonic and subsonic before terminating. The main requirement is to have accurate data on the drag coefficient of a sphere around the speed of sound (Mach 1) and especially the transonic regime (approximately $0.5<M<1.4$).

There are very few experimental measurements on sphere drag in the transonic regime. To determine the aerodynamic characteristics (drag coefficient) of a sphere around the transonic regime, Bailey [5] experimented with the effect of Reynolds and Mach numbers. The experiments used fixed intervals of Mach number and plotted the drag coefficients for a derived Reynolds number, using the spheres diameter. It can be seen in Figure 1.11 that the drag coefficient versus Mach number variation at $0.9<M<1.1$ is a function of free stream Reynolds number and the curves have different trends. It is

apparent that for small values of Reynolds number ($Re<2x10^2$) a relatively large change in drag coefficient is observed for a small change in Mach number when changing from subsonic to supersonic. For high Reynolds number ($Re>10^4$) there appears to be a smooth transition from subsonic to supersonic drag values. The drag coefficient curve for a Reynolds numbers of 10^5 seem to show good agreement with Braun [24] data (Figure 1.7). All of Bailey's experiments were carried out in the same wind tunnel, reducing the variation in flow condition, which shows the relative effects of changing the Reynolds number around the transonic regime.

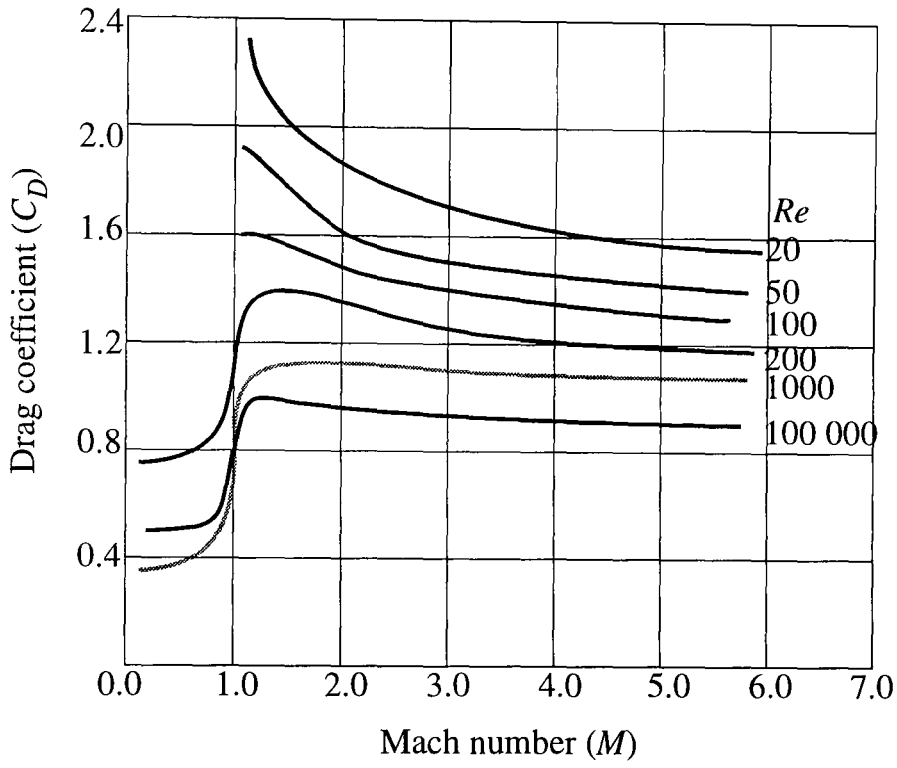

Figure 1.11 *A sketch of the variation of drag coefficient on a sphere for different Mach numbers [5].*

The most accurate known deceleration measurements relevant to this work ($Re=5x10^4$) are those obtained by the Ballistics Research Laboratory at the Aberdeen Proving Ground, USA. Measurements on drag coefficient as a function of Mach number where carried out by Charters and Thomas [4] and Braun [24] on several diameters of steel spheres. The two separate experiments involved firing single spheres down a range and recording the flight times.

The timing measurements were obtained by spark photography which captures the image of the sphere travel downrange by six separate cameras set at defined distances. From

these measurements the velocity of the sphere was found by a least square fit. Using the velocity and manipulating the drag force equation on a sphere in free flight, described by (1.1), the drag coefficient was obtained. Braun used C_D (Figure 1.7) and Charter and Thomas (Figure 1.12) used K_D, which is $^{\pi}/_{8}C_D$. Comparing the two sets of experimental data it can be seen that they show good agreement even though the experiments were carried out 30 years apart.

From the experimental data which gives drag coefficient as a function of Mach number, it is thought that the data contained in Figures 1.7, 1.11 and 1.12 represent the most comprehensive set of results in the transonic velocity regime. They show that there is a smooth transition from the two different drag coefficient constants representing subsonic (M<0.5) and supersonic (M>1.4) velocity. The change from subsonic to supersonic drag values is accompanied by a relatively large change in drag coefficient for a small change in Mach number. This experimental data has been the basis of the limited work and calculation of shotgun ballistics by Lowry [2,16].

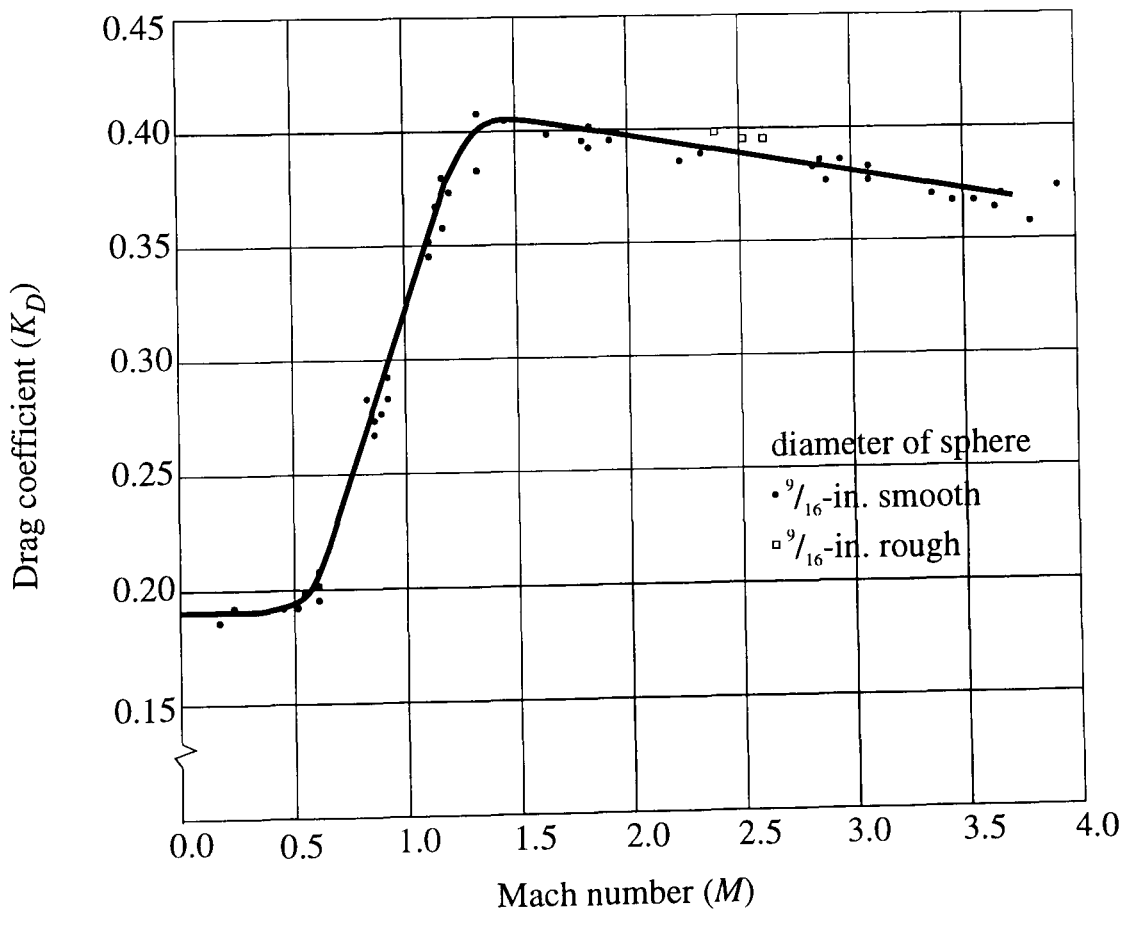

Figure 1.12 *Charters and Thomas [4] data showing the drag coefficient of a sphere around the transonic regime.*

Another important experiment that Charters and Thomas tried was to see the effect of surface roughness on the drag coefficient. Their results showed that the drag coefficient increases with surface roughness (e.g. poor shape) as a function of Mach number, but the shape of the curves stays the same but were offset. Achenbach's [27] experiments showed that an increase in surface roughness decreased the critical Reynolds number, but at the same time the transcritical drag coefficient became greater. This result agrees with Goldstein's [19] and other experimentalists opinion, that under certain circumstances surface roughness can greatly change the drag on a sphere.

Suryanarayana [31] showed that it was possible to reduce the drag by ventilation. This concept of reducing drag may be of benefit as it allows a sphere to travel further from the same initial velocity. The principle was that the drag of a sphere at high Reynolds number can be reduced to less than half its value by means of passive ventilation, such as the sphere would have a combination of holes through it. This was effective for a stable sphere in motion. The drag reduction by ventilation is very sensitive to the quality of the external surface and this sensitivity to surface roughness can completely offset the benefit obtained.

1.5 MULTIPLE SPHERES

1.5.1 Past work on multiple spheres

The aerodynamic performance of single spheres and their flow have been studied extensively, but the behaviour of clusters or multiple spheres has received little attention. There have been experiments on the behaviour of clusters of spheres falling in a viscous fluid [32-34], but due to the low velocities associated with this type of work the Reynolds numbers are small (Re<100). The majority of this data was used to verify the Navier-Stokes equation (using Stokes or Oseen approximations) where this is only applicable for very small Reynolds numbers. Hamielec [35] concluded that an analytical solution of the complete Navier-Stokes equations is difficult due to its non-linearity. Although numerous approximate solutions [22] have been obtained, virtually the only exact solution available are those of Stokes, for Reynolds number is less than 1.

The work on clusters of spheres falling through a viscous fluid and the Navier-Stokes equations are of little relevance to this work due to the very low Reynolds numbers compared to the work (Re=5x10^4), which consequently produces a stable laminar boundary layers. Although this data is not appropriate for this work, Jayaweera's [32] observations are of interest. The experiments on clusters of 6 equal spheres for Reynolds number between 0.06 and 7 showed that their speed of fall is greater than that of a single sphere. This enhancement of rate of fall was greater the more compact the cluster. This suggests that the cluster is more aerodynamic the tighter the spheres are together. Jayaweera also observed that even if the spheres are separated by a few diameters they can arrange themselves back into a compact cluster. This effect stopped when the separation of the sphere exceeded a certain value (about 6 diameters).

Lee [11] carried out the simplest form of multiple sphere interaction on two spheres. The experiments showed that there are considerable forces, which are caused by aerodynamic interaction, between closely spaced spheres. The experiments were designed to measure the aerodynamic forces in magnitude and direction on spheres with Reynolds numbers approximately 10^4. Two hollow spheres of the same diameter with strain gauges inside of them were rotated around one another at different separation and angles in a wind tunnel. The forces acting upon a sphere were found to be dependent on the position of the other sphere. Lee expressed the forces in terms of the ratio of drag coefficients, re-arrange (1.1), between the free stream drag (C_D) of a single isolated sphere and the actual force (C_F), calculated from the net resultant of the two measured components (parallel and normal to the main air flow), for the same flow. Figure 1.13 shows that there are considerable forces on the spheres when they are close abreast (90° to flow) of one another. These forces at close separation are shown to increase the drag by 50% at the minimum separation. When the sphere separation is increased the drag force rapidly diminishes in some exponential form until at separation of greater than 3.5 diameters the effects are negligible.

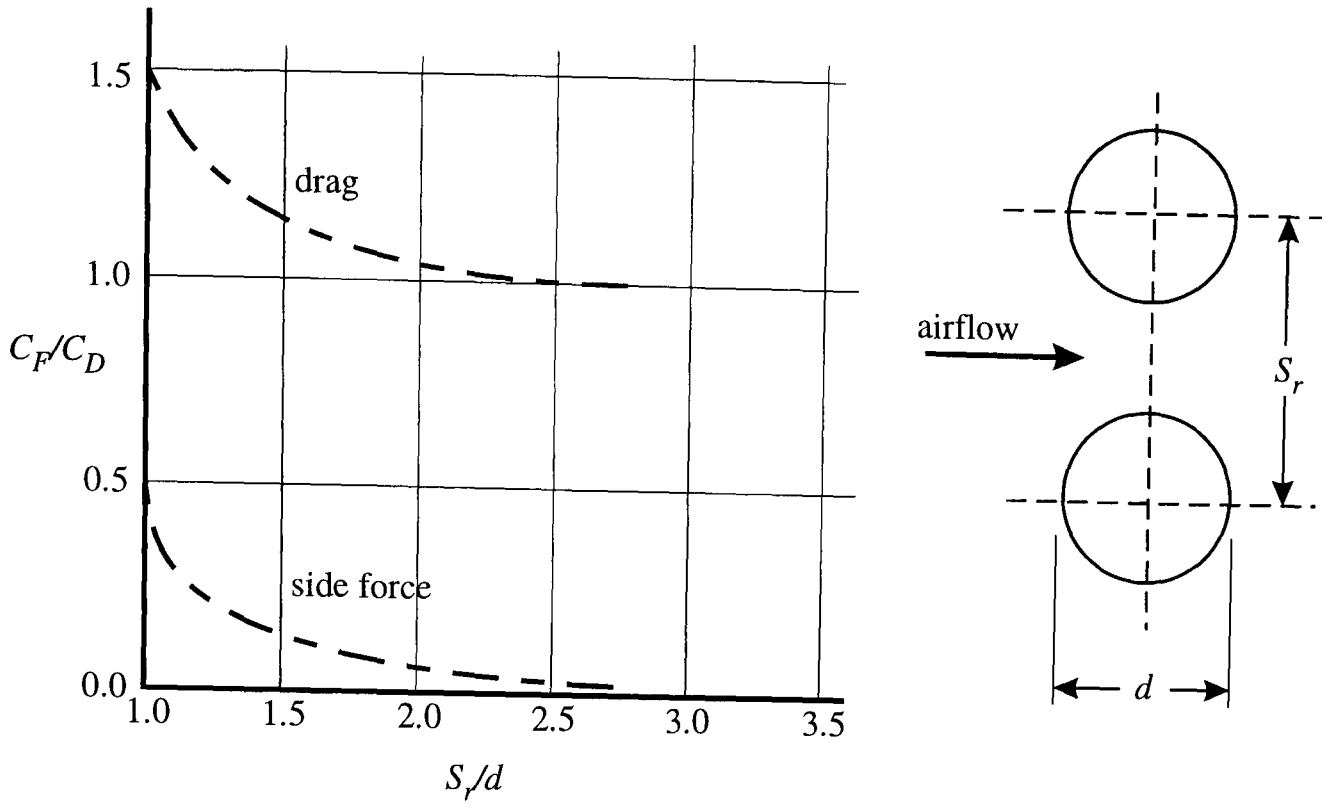

Figure 1.13 *The drag force on two spheres abreast of one another using Lee [11] experimental data.*

For spheres in line (180° to flow) with one another the trailing edge sphere can be seen in Figure 1.14 to experiences a very marked decrease in drag until a separation of 3.5 diameters. Unlike the abreast case, the in-line trailing edge sphere will be affected more by the leading edge wake downstream. The leading edge sphere does not seem to be affected too much by the presence of a trailing edge sphere. The only limitation to Lee's work was that the spheres were mounted and fixed in position, therefore the effect of repulsion, attraction and rotation could not be seen. For instance, at close separation the abreast forces are large which could separate the spheres, and when the spheres are in-line of one another the reduction in drag means that the trailing edge sphere would catch the leading edge sphere up and affect its performance.

For spheres positioned in other orientations, Lee concluded that the behaviour is more complex and a formal manner of description is difficult. The general conclusion made was that the spheres at the leading edge of the stream will experience greater drag than those to the rear and causing a bunching up of the cluster of spheres in the direction of relative airflow. This was also found by Jayaweera for clusters of spheres falling in a viscous fluid. Lee's results also suggested that when two spheres are greater than 3.5

diameters apart the influences of interaction are dramatically reduced. These results are considered to be sufficiently accurate and comprehensive to give some basic understanding of the phenomena occurring within a shot cloud. Although, they are of slightly low Reynolds number and that the airflow is of a constant velocity, producing a constant drag coefficient, unlike the transonic regime associated with this work.

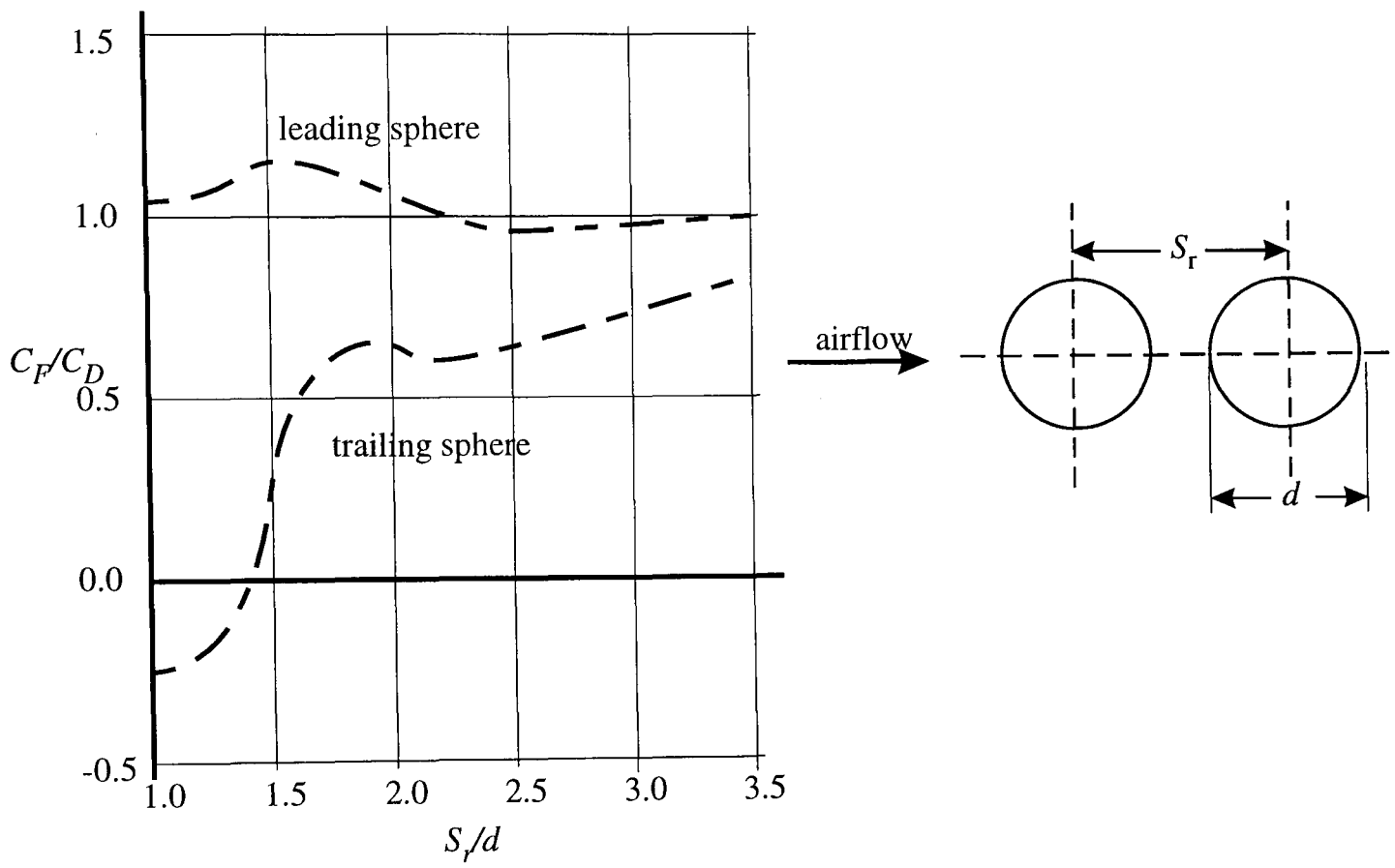

Figure 1.14 *The drag force on two spheres in-line with one another using Lee [11] experimental data.*

1.5.2 The aerodynamic performance of shot clouds

The main interest in this work is to explain how shot clouds develop over time and space by studying the external ballistics of shotguns which use spherical pellets. If the pellets emerged from the muzzle of the gun in a constant order and shape, the interactive forces and downrange performance of the shot cloud could perhaps be modelled by theory. Unfortunately in shotguns there are many variations, for instance the diameter, shape, and surface roughness of the pellets, which alter the drag coefficient of a sphere. Another major influence on the spread of the pellets in a shot cloud is the choke and shot cup behaviour. As no satisfactory theory yet exists to predict the downrange behaviour of shot clouds, practical measurements are not rendered superfluous.

At the beginning of the century more extensive experiments were carried out in France by Journée on the exterior ballistics of shotguns. During this period of time the cartridges were manufactured slightly different and resembled the wadded cartridge shown in Figure 1.1. The introduction of the modern designed cartridges with plastic shot cup produces a high pellet density (first report by Journée [36]) in the patterns compared to that of fibre wads.

Experiments by Journée to measure the velocity of the shot cloud were made up of flight time as a function of range calculations. He measured the flight time over a limited range of distances by several different experimental techniques and obtained an instantaneous velocity for the mid-point. In France at the turn of the century the flight time measurements of shot pellets were at 30m, measured from the muzzle of the barrel, used to obtain a velocity at 15m. These early measurements of shot cloud velocities were only able to produce timing information on the first pellet to trigger the system. This was the cause of strange results, as stray pellets that fly off at the front of the shot cloud give an illusion of a higher velocity. There was also an error incurred by using timing information which had been influenced by the complex behaviour of all of the pellets travelling together after leaving the muzzle. A better measurement by Journée was the velocity at 50m where he measured the flight time between 40 and 60m, at these ranges the pellets have separated sufficiently to behave like single spheres in free flight. It is easy to be critical of the accuracy of the measurements and results produced by Journée, but he had limited technology compared with what is available now.

Although Journée's results may not have the greatest accuracy, the interesting point about his work was he tried simple but effective experiments to show relative effects. The main conclusion was that the pellets in a shot cloud have various trajectories and are subject to random paths. Journée [1] confirmed this by shooting at the edge mn of target A which partially covered another target B further away from the gun. A line was drawn on target B which projected the edge mn of target A from the line of sight (Figure 1.15). The trajectories of the pellets were shown to be fairly sinuous because some struck target B in the area shaded by target A. With the pellet striking an unseen area from the firing

point it shows that they do not travel in a constant and straight trajectory for their whole flight period. Another experiment carried out by Journée showed the effect of random trajectories of pellets by colour coding different layers of the pellets in the cartridge and using high speed photography and pattern plates. From this it could be seen that the different coloured pellets moved around in the shot cloud with no constant order. Journée did show that in the final pattern the pellets which were at the rear of the cartridge seemed on average more dispersed than those from the middle and front. He also did an early study on drag function and work on hit probabilities, where he observed that the pellet density of patterns were increased when hard shot or large pellet diameters were used.

Figure 1.15 *Journée's experimental set up to investigate the randomness of the trajectories of pellets.*

In Journée's book statements were made but no theory or measurements where shown to back them up. For instance he stated that the pellets required to be 150 diameters apart so that there is no interactive effects between one another. These points are of interest but without justification the accuracy is uncertain. In conclusion Journée showed great imagination and innovation to complete the largest single study of shotgun ballistics.

The most recent work on the aerodynamics of shot clouds was carried out in the 1970's by Lowry [2]. The specific objectives of these experiments were to measure the deceleration characteristic of pellets travelling in a shot cloud fired from a shotgun. These deceleration constants were better than measurement data from the flight of single

pellets, as they included the interactive effects of the shot cloud. The deceleration characteristics of the shot cloud were then based on assumptions obtained from previous work on single spheres [4], where the drag coefficient (Figure 1.12) is proportional to velocity ($0.5<M<1.4$) or constant ($M<0.5$). Using the assumption of a single sphere travelling at velocity between 0.5 and 1.4 Mach, a cube law of air resistance, given by

$$\frac{dv}{dt} = -k_3 v^3 \quad , \tag{1.3}$$

is obtained. The deceleration constant (k_3) was given as

$$k_3 = \frac{2t}{R^2} - \frac{2}{Rv_0} \quad , \tag{1.4}$$

and then calculated by means of time (t), range (R), and the effective initial velocity (v_0), such as a constant to fit the data, for different parts of the shot cloud.

Lowry's measurement system, high speed photography, used 100ft of 16mm film for each round fired to obtain the initial velocity and flight times of every pellet. The camera was set up to capture the image of the pellets penetrating a 30" diameter circular aperture at various range between 20 and 50 yards. The flight times where measured by searching for the frames (6500 frames per second) which first showed the pellets arriving. This method gave accurate timing data for all the pellets in the shot cloud, but was very time consuming. The nature of the ballistic performance of shotgun cartridges is variable and to obtain a reliable result an average is required, this leads to greater time analysing data and high costs in film. For these reasons Lowry only performed very limited test at various ranges for each batch of cartridges using extreme chokes, such as cylinder and full.

From the timing information Lowry calculated the deceleration constants (k_3) for the leading and trailing edge pellets. Lowry defined the leading edge of the shot cloud as the point where 10% of the pellets had arrived and the trailing edge as 90%. When using an

aperture of only 30" stray pellets must of missed the aperture at long range (>30yds) with the full choke and even at 30yds with the cylinder choke. Therefore the actual percentage measured will differ and a error will occur in the timing data.

On the basis of these measurements, Lowry calculated the deceleration constants for a limited range of pellet diameters which in turn he used to predict the external ballistic performance for any diameter pellet. He used a novel approach in combining the cube and square laws of air resistance, explained in section 4.2.3 with a transitional stage. This allowed the drag coefficient to change as the pellets velocity fell below 0.5 Mach upon which it became constant (Figure 1.12).

Lowry used measurements on the initial velocity and flight time data for different distances to calculate, from (1.4), the deceleration constants on different parts of the shot cloud. It has already been shown by Lowry that there is interaction between the pellets at the near muzzle distance (Figure 1.5). With the shot cloud having different deceleration characteristics at the muzzle and flight time ranges interpolation of this data has produced an uncertainty in the accuracy of Lowry's downrange performance calculations. Lowry also only took timing information at two ranges for one pellet diameter. This data covers only a small proportion of the total history and different types of shot cloud. Lowry tried to cover a large unknown subject with relatively little raw data. However, his work was a good start to an area that had not been reported on for a long time, with a limited budget.

High speed photographic techniques were also used by Donovan [10], to show the influences of damaged or deformed pellets in a shot cloud. The drag coefficients were obtained for individual pellets, as they were marked for recognition, from time-range data. The results showed that for slightly damaged pellets there was a small increase in C_D and for major deformation the drags were 20 to 30 percent higher than a well formed pellet. The classification of deformation from the film was subjective but the result coincided with the factors which influence the drag coefficient on a sphere (section 1.4.1). Some pellets in the shot cloud were observed to have a lower drag than

the undamaged leading edge pellets, this is thought to be caused by slip stream (Lee [11] showed that pellets behind one another experience a reduction in drag) where the leading edge pellets are subject to a greater deceleration than the pellets in the centre of the cloud. As a result the pellets in the middle of the shot cloud caught up with the front pellet, since they experience less air resistance. The work also showed that with an increase in pellet deformation in the shot cloud there was a greater initial spread.

An important issue which Donovan recognized was that when using near muzzle measurements, particularly when presented as a function of velocity or Mach number, there are conditions where both damage levels and the degree of interaction between pellets occurs. The damage is a function of the acceleration forces experienced by the pellets, and the region of interaction is influenced by the distance from the gun and the muzzle velocity. He therefore did not recommend direct extrapolation of these types of results to other conditions. This was a sensible limitation to his work. He also could not recommend the use of high speed photography for routine data acquisition unless the probable importance of the results was high. This was because the processing of a single round required a large amount of human effect which did not lend itself to mechanization. This was the problem that Lowry [2] found in obtaining his limited data.

There have been many books written about shotguns [3,14,37,38], most of these have reviewed the work of Lowry and Journée in some detail. These authors designed their own experiments to try and explain certain shot cloud behaviour, but never attempted any theory. The majority of this type of work had no substantial funding, therefore the exterior ballistics testing of the shotgun loads are usually restricted to pattern tests and muzzle velocity determination. Burrard [3] wrote a set of books on the "Modern Shotgun" but there are many doubts about the method and accuracy of his velocity results. He measured the flight time for the first pellet to arrive at 20 yards and then obtained the velocity at 10yds in the same way as Journée. This gives only one point and does not allow for the velocity distribution and the non-uniform deceleration in the shot cloud. Burrard also ignores the complex area close to the muzzle and uses a single sphere theory which does not represent the true aerodynamics for a pellet in a shot cloud

from the muzzle to 10m. He then says that "this velocity provides excellent data from which the velocities for all other sporting ranges may be calculated and tabulated ..." [3]. From this one reading a lot of assumptions are used to predict the downrange performance of cartridges making his results unreliable.

Oberfell and Thompson [38], like the other experimentalists mentioned in this section, recognized that the patterns seem to follow a Gaussian distribution. They tried to assess patterns for areas where there were no pellets, or patches, and came up with some interesting methods. The problems in the theory of the random clumping of particles, or patches, in two dimensional and even three dimensional models simulating such phenomena seem tantalizingly simple, but in fact few solutions have yet been discovered. Roach [39] stated that even today an approximate solution to an over-simplified model is the best that mathematics can provide the technologists in this area.

The experiments and research discussed in this section have produced the majority of the work on shot cloud aerodynamics. It can be seen that there is a large area of new and more accurate research requiring development.

1.6 RESEARCH OBJECTIVES AND MOTIVATION

The author developed an interest in the behaviour of pellets in shot cloud from a background in clay pigeon shooting. It has been shown in this chapter that the amount of work carried out on multiple spheres is very limited. As far as the author is aware there was no theory until this research was carried out which could model a shot cloud as it evolves in time and space.

The first objective of this research was to design and implement a measurement facility which could assess the external ballistics of shotgun cartridges. From the measurements information was passed to the cartridge manufacturers to help develop non-lead loads and to educate the shooting community [13]. This fulfilled the contractual requirements set by the Department of Environment and laid the foundation for the research into shot clouds, which was carried out in parallel.

Secondly, with actual external ballistic measurements an understanding of the complexities involved with the flight of multiple spheres has been developed. Models have been produced to predict the spread of the shot cloud in length and width terms, and have been assessed for accuracy by comparison from experimental measurements. The final requirement was to fill part of the large gap in modern shotgun ballistics which has been left empty due to a lack of interest from the military.

1.7 ORIGINAL CONTRIBUTIONS

In the process of completing this investigation the following results are the most significant of the research and are, to the best of my knowledge, original work. During the research, results have been published and a list of the publications is given.

In Chapter 2 a measurement facility is described which was designed and implemented to measure the external ballistics of shotguns. It consisted of two parts: firstly, the ballistics target produced timing information on different parts of the shot cloud to determining its ballistic performance. The target also produced limited positional information which allowed 3-dimensional reconstruction of the shot clouds outline to be performed. Secondly the traditional method of obtaining the lateral distribution of pellets, from patterns, was refined and automated using image processing techniques to generate the pellet co-ordinates in the x- and y-axis. A paper containing a description of this measurement system has been submitted for publication [3].

In Chapter 3, detailed analysis of the experimental data gathered from the measurement facility is used to establish, statistically, the nature of the pellet distribution within a shot cloud. An attempt was also made to examine the effects of choke on the pellet distribution.

In Chapter 4, the experimental data is condensed to summarize the deceleration characteristics of pellets in a shot cloud. This work was initially introduced at the first conference on Non-Toxic Shot[2] and the results used to present comparative ballistics to the Department of the Environment (the sponsor) and the shooting community[1].

Continuation of the work led to a simplified model of the drag coefficient (C_D) characteristics of pellets in a shot cloud. This information has been used to develop a synthesis model, based on the equation of motion for a single sphere, which predicts the shot cloud ballistics over the measurement range.

In Chapter 5, a novel random force approach to the theory of shot cloud dispersion is presented[4] in the form of a stochastic model. The equation of motion of a single sphere is perturbed by the addition of a random force term and by performing ensemble averages the shot clouds width and length were determined. This is the first theory, to the author's knowledge, which can model a shot cloud as it evolves in time and space.

1.7.1 Publication list

1. Giblin R. A. and Compton D. J., "A ballistics measurement system to assist the development and evaluation of non-toxic shot", Report for the UK Department of the Environment, March 1996.

2. Compton D. J. and Giblin R. A., "A measurement system for the external ballistics and pattern analysis of shot clouds", *Proceedings of the 1st Conference on non-toxic shot*, Royal Military College of Science (Cranfield University), ISBM 0 86038 022 X, pp 33-55, July 1996.

3. Compton D. J., Giblin R. A. and Radmore P. M., "Measurements on an ensemble of spheres in the transonic velocity regime", Submitted to the *IEE Proceedings of Science, Measurement and Technology*, October 1996.

4. Compton D. J., Radmore P. M. and Giblin R. A., "A stochastic model of the dynamics of an ensemble of spheres", Accepted for publication in the *Royal Society Proceedings A*, November 1996.

Chapter 2

Implementation of the measurement facility

2.1 INTRODUCTION

2.1.1 Required measurements

The measurement facility was required to produce timing and positional information on the distribution of pellets in a shot cloud at various ranges. From the ballistic and pattern measurements the velocity and energy distributions and pellet density within the shot cloud, respectively, could be calculated. An additional requirement imposed by the contract was that the facility must be capable of testing ammunition at a sufficient rate that statistically significant results could be reported to the suppliers within a reasonable period of time (within a few days of the tests being carried out).

Using the timing and positional information obtained, comparative ballistics (comprising of over 150 ballistics reports) were presented to the Department of the Environment [13] and the shooting community [40] on the alternatives to lead shot. More importantly this unique measurement system has laid the foundation for this research into the dynamics of shot clouds as they evolve in time and space. With the experimental results, theoretical models can be evaluated for their accuracy.

The following part of this section describes existing methods of measuring the ballistic properties of projectiles and comments are made on their applicability to shot clouds. The proposed measurement systems will be discussed at the end of this section and explained in greater depth later in the chapter.

2.1.2 Acousto-electronics : Impact detectors

The use of piezo-electric transducers are used to detect impacts in industry, e.g. sports gear, crash dummies, shock wave sensor and impact printer diagnostics, and due to their versatility they have been used to develop a method of registering the impact of projectiles. The transducers produce an electrical pulse when struck and are attached to the back surface of a protective plastic sheet to prevent being damaged and to increase their area of sensitivity. In Figure 2.1 the data acquisition system records the output response of the transducer after being triggered by the shot exiting the muzzle. This

enables timing information to be obtained for every projectile intercepted by the plastic sheets. An analogy of this system is standing behind a metal door when a hand full of stones are thrown at it. If time was slowed down each stone would be heard hitting the metal door and a timing measurement could be made.

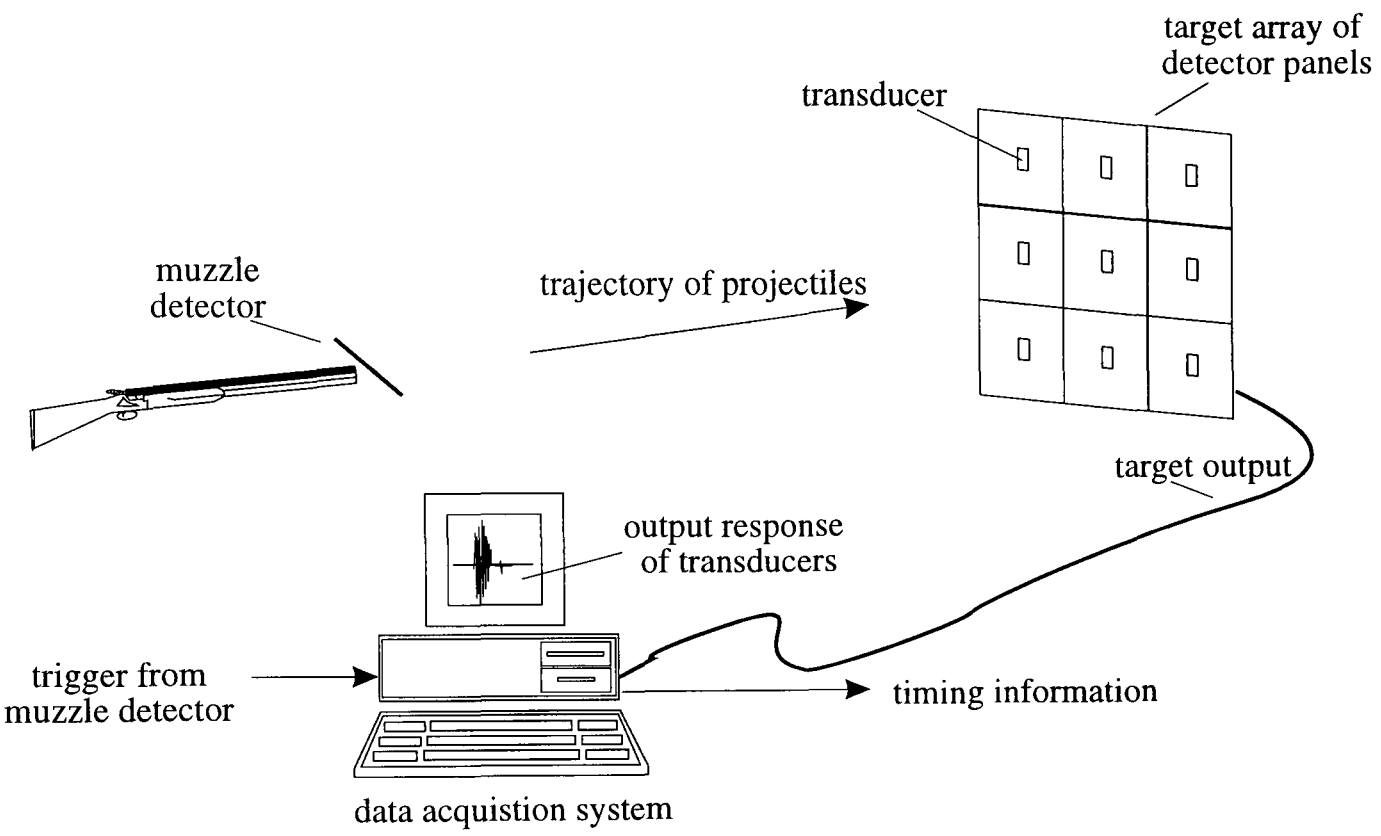

Figure 2.1 *A target array of impact detector units with data acquisition system.*

A target array of impact detector units can then be built to encompass the whole spread of the projectiles. By moving the target array to set distances from the muzzle, the flight time, velocity and energy distribution in a shot cloud can be obtained as well as the shot cloud length.

There are many other impact oriented measurement systems and the majority are based on Journée's [1] experimental procedures. The pellet flight times are measured by the use of wire grid targets, or metal plates, which when struck closed an electrical circuit and stopped a timer. The problems with these methods are that the wire grid may not intercept all the projectiles and the metal plate requires a hard enough impact to make the switch close. Therefore they only produce data on the leading edge of the shot cloud (t_1) or the first object to strike them.

2.1.3 Opto-electronics

The work of Lowry [2,16] in the 1960's and early 1970's laid the foundations of modern shotgun ballistics measurements using high-speed photographic techniques. This photographic technique was also used by Journée [1] and Quayle [41] in the early part of this century. Lowry's work has been discussed in section 1.5 and Figure 2.2 illustrates the equipment he used to record the flight time of the shot cloud from the instant it left the muzzle until the final pellet penetrated the downrange target.

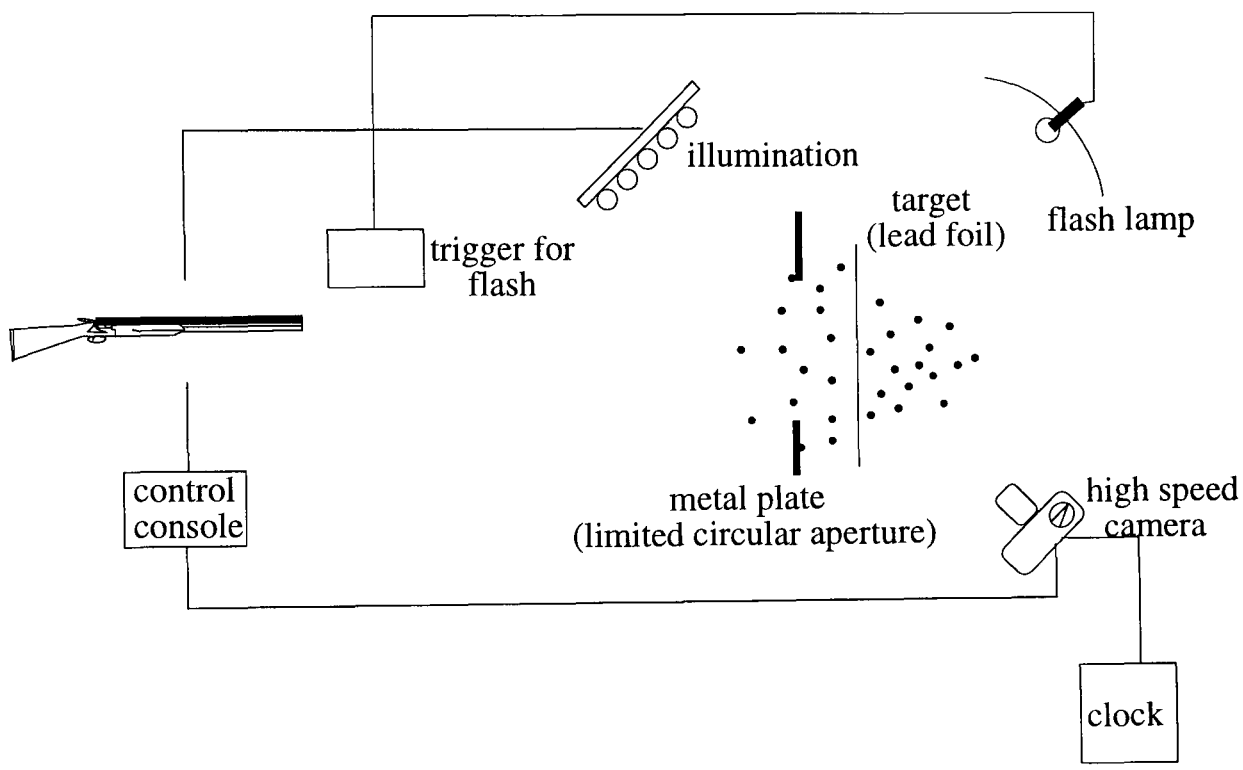

Figure 2.2 *Schematic diagram of Lowry's [2] photographic set up.*

The control console is used to synchronize events leading to the firing of the test shot, including the target illumination. A muzzle detector triggers the flash lamp at a set period after the shot leaves the muzzle and it gives the high-speed photographic camera its initial reference point. The camera records the illuminated holes after the pellets have penetrated the target. The target is a sheet of lead foil placed behind a metal plate which had a 30" diameter circular aperture. The flight times for each pellet can then be obtained by extracting the data from the frame when the illuminated pellet holes first appear. Combining this data with the "pattern" on the target, the relative position of every pellet in three dimensions is made possible.

Chronographs are widely used in rifle and pistol ballistics and consist of two optical detectors (Figure 2.3). The detectors are frequently referred to as skyscreens, because they are often used to detect the silhouette of an object such as a bullet passing immediately above them. They use light sensitive detectors and a cylindrical lens to create a detection zone above the units which looks V-shape from the firing point, the angle of the "V" being typically 30° either side of the vertical. A projectile passing within this sector will generate a pulse which triggers a timer, when the projectile passes over the second screen another pulse stops the timer and the average velocity over the distance is calculated and assumed to equal the instantaneous velocity at the mid-point.

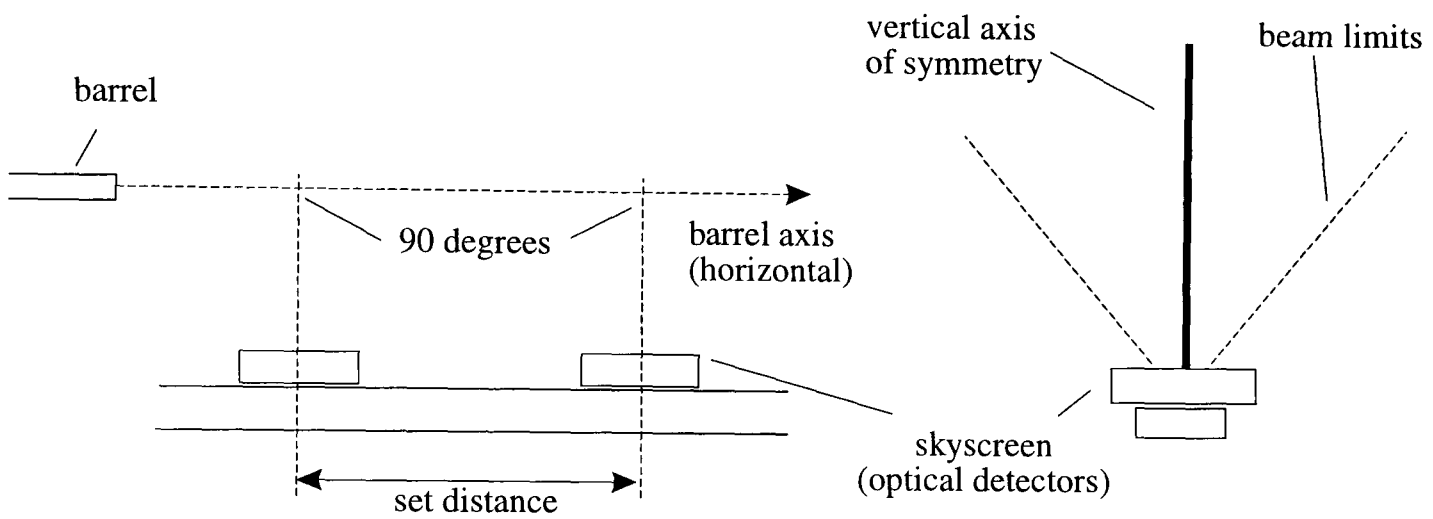

Figure 2.3 *Two optical detectors set at a known distance apart to measure the velocity at the mid-point.*

A recent paper [42] introduced an electro-optical target system (EOTS) that could measure velocity and positional information for projectiles. It was based on a microcomputer system with a novel structure which showed its capability of precisely detecting the position as well as the velocity of small calibre projectiles in real time. Laser beams were directed onto a cylindrical mirror which reflected the beams in a fan-shaped light sheet onto two banks of photodiode arrays (Figure 2.4). Each light sheet was combined with its own signal processing unit to construct an optical gate. With two sets of parallel arrays at a fixed distance apart, a projectile can be measured for its position and velocity when it passes through the optical gates.

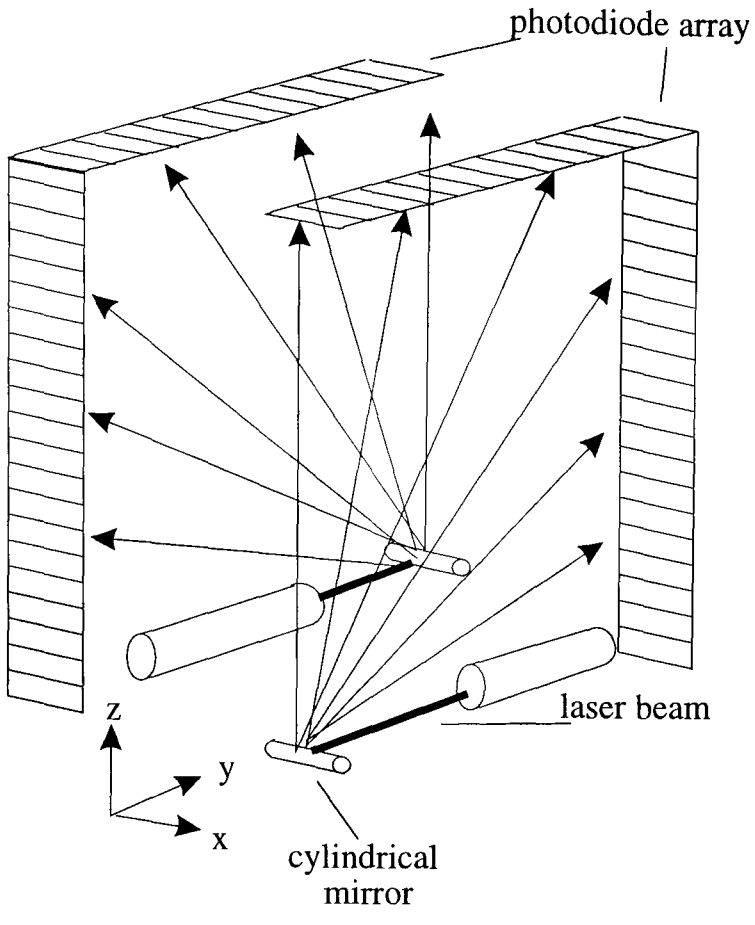

Figure 2.4 *Optical configuration of EOTS [42].*

2.1.4 Electromagnetics

Radar is an electronic device used for the detection and location of targets by radiating electromagnetic energy and examining the reflected energy. It operates by transmitting a particular types of waveforms, a pulse modulated sine wave for example, and detects the nature of the echo signal. The term "target" is applied to any reflecting object which interferes with the transmitted wave and reflects part of its energy. Figure 2.5 shows a simplified diagram of a radar set consisting of separate transmitting and receiving antennas.

A portion of the transmitted signal is intercepted by the reflecting object (target) and radiated in all directions. It is the energy radiated back towards the radar that is the prime interest. The receiver antenna collects the returned energy and delivers it to a receiver, where it is processed to detect the presence of the target. From timing measurements and the known velocity of the transmitted waveform, which is constant, the location and velocity of target are calculated.

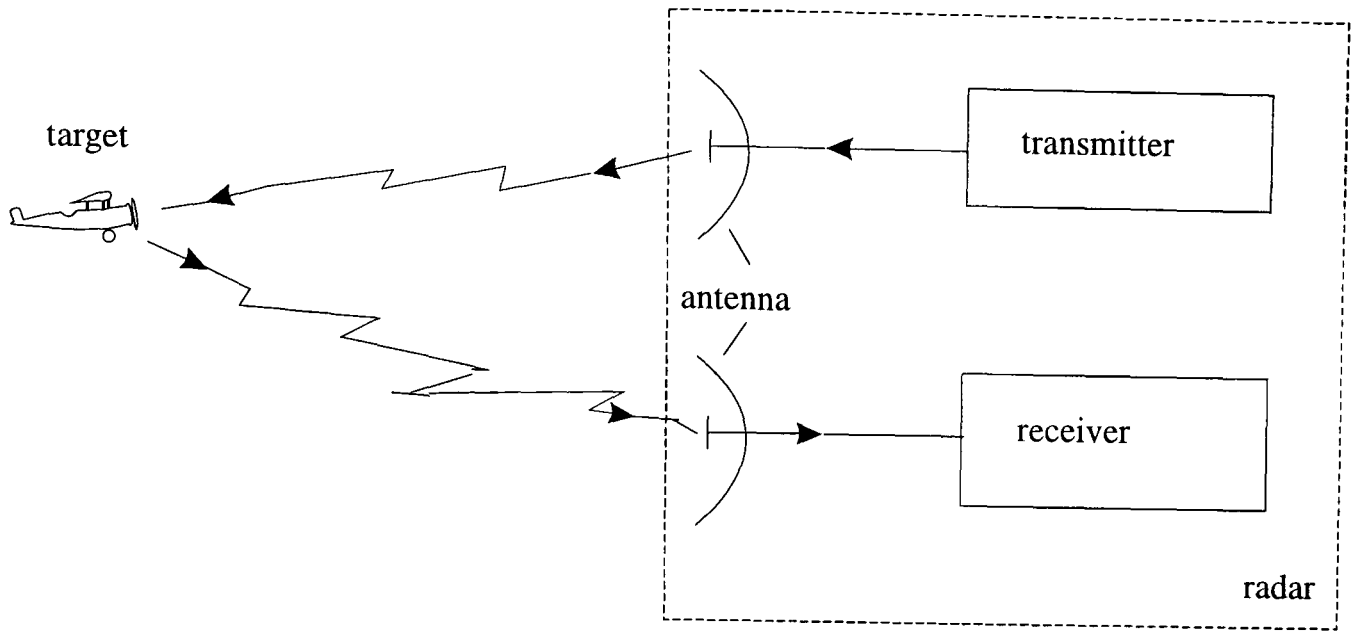

Figure 2.5 *Block diagram of an elementary form of radar.*

2.1.5 Proposed measurement system

It is not possible to obtain accurate timing information on the distribution of pellets in a shot cloud by the use of traditional wire grids and metal plates, due to their inadequacy in detecting all the pellets. Another method described in the previous section which is unable to gather sufficient detail on the shot cloud is the conventionally radar. During feasibility studies, radar was investigated for its possible application to shotgun ballistics [43], but when directed along the line of fire the radar beam detected the shot cloud as an "object" and could not resolve individual pellets. Nevertheless, the radar gave an average (weighted) velocity for the cloud and as such was the only check on the proposed system [43].

The introduction of EOTS by Lu [42], described a system primarily designed to register single projectiles. The expanse of the shot cloud creates a mechanical problem where a larger aperture would be required. This places the laser and photodiode detectors further apart, decreasing the signal to noise ratio and reducing individual pellet resolution. At the time of writing the EOTS would not of been able to register the high frequencies of projectile arrival associated with shot cloud because of the response time of the electronic components. There would also be a problem with multiple reflections and scattering generated from the pellets fouling the detectors.

High-speed photographic techniques [2,10,16] are able to obtain both timing and positional distribution of every pellet that passes through a given aperture at a given range. This approach was not adopted for the present investigation, primarily because the size of target aperture needed to intercept the whole shot cloud (measured on pattern plates to be up to 3m in diameter at 50m) would make an enclosed range and the associated high-speed photographic equipment prohibitively expensive. Another reason is that the variation associated with shotgun ammunition requires a large enough sample of firings obtained statistically accurate data. The processing of a single round requires a large amount of human effort to acquire timing and positional information. It also does not seem to lend itself to automation processes. Hence Donovan [10] recommended that photography is not used for routine data acquisition unless the probable importance of the results are high.

Conventional chronographs, or skyscreens, have a limited operation range which is dependent on the dispersive nature of the shot cloud. This is because the resolution of the skyscreens do not allow reliable detection of individual pellets, less than 5mm and at the velocities associated with this research, once the shot cloud has reached a certain dispersion. It is shown in section 2.4.3 that the operational use of the skyscreen stops typically at 10m, but is dependent on the shot size and choke. Therefore this instrument is proposed to be used at near-muzzle ranges to track an individual shot cloud downrange to 10m.

An array of electronic impact detectors (described in section 2.5) has been adopted for this investigation as they are cheap, robust, easy to use and are particularly well suited to direct computer links for digital data storage and processing. The array of impact detector units can be built to any size which intercepts the whole shot cloud. It has been established that this type of acousto-electronic ballistic target is sufficiently sensitive to record impacts from all shot sizes greater than 2mm at ranges between 20 and 60m. By recording the output signals from the impact detectors, the flight times of the pellets from the gun muzzle to the target can be measured. This can be repeated for as many cartridges, chokes, and ranges as required for a given batch of ammunition. The combined data can then be used to calculate averaged velocities and pellet energy

distributions together with the shot cloud length. It is also possible to obtain limited positional information, as the detectors cover individual areas of the total array, producing three-dimensional outlines. The limitation of the impact detectors is a safety factor and data cannot be obtained for distances closer than 20m from the gun muzzle as the ricochets from the target are dangerous and its rapid destruction becomes too costly.

In principle, a matrix of impact detectors with recording channels could provide the lateral shot distribution information on the pellet positions. In practice, the positional accuracy requirement for each impact (within a few mm) means that thousands of such detectors and recording channels would be needed, making the cost prohibitive. Instead the shot patterns are recorded on a sheet of paper and anlaysed by a CCD camera which is interfaced directly to a computer. From the pattern image from the camera, the co-ordinates of all the pellet hole centres are obtained and stored on disk for analysis.

In combination, these novel approaches have allowed the required information to be obtained for an investigation into shot cloud ballistics. The remainder of this chapter is devoted to detailing information of the experimental procedures and set-up.

2.2 LAUNCH CONDITION

2.2.1 Proof barrel

A test barrel was used to launch spheres, or pellets, into the format known as a "shot cloud". It was a proof barrel of 29" in length which is conventionally used to measure the pressures created by cartridges. Using this type of barrel throughout the research allowed confidence in safety with experimental loads and also reduced the possible variables in the experiments. Figure 2.6 shows the test barrel in position during field trails projecting slightly from the firing window, which was made from 10mm thick polycarbonate to protect against dangerous ricochets. The barrel could be adjusted for azimuth and elevation and was locked in position after being aligned, by bore-sighting the barrel on the target centre. By checking the patterning of the shot cloud at each range the barrel could be adjusted, if necessary, to centre the pattern on the target and

therefore allow for the effects of gravity. The gun was then fired by allowing a pendulum hammer to swing 90°, under its own weight, before striking the firing pin. This ensured that the same force was applied to each primer cap.

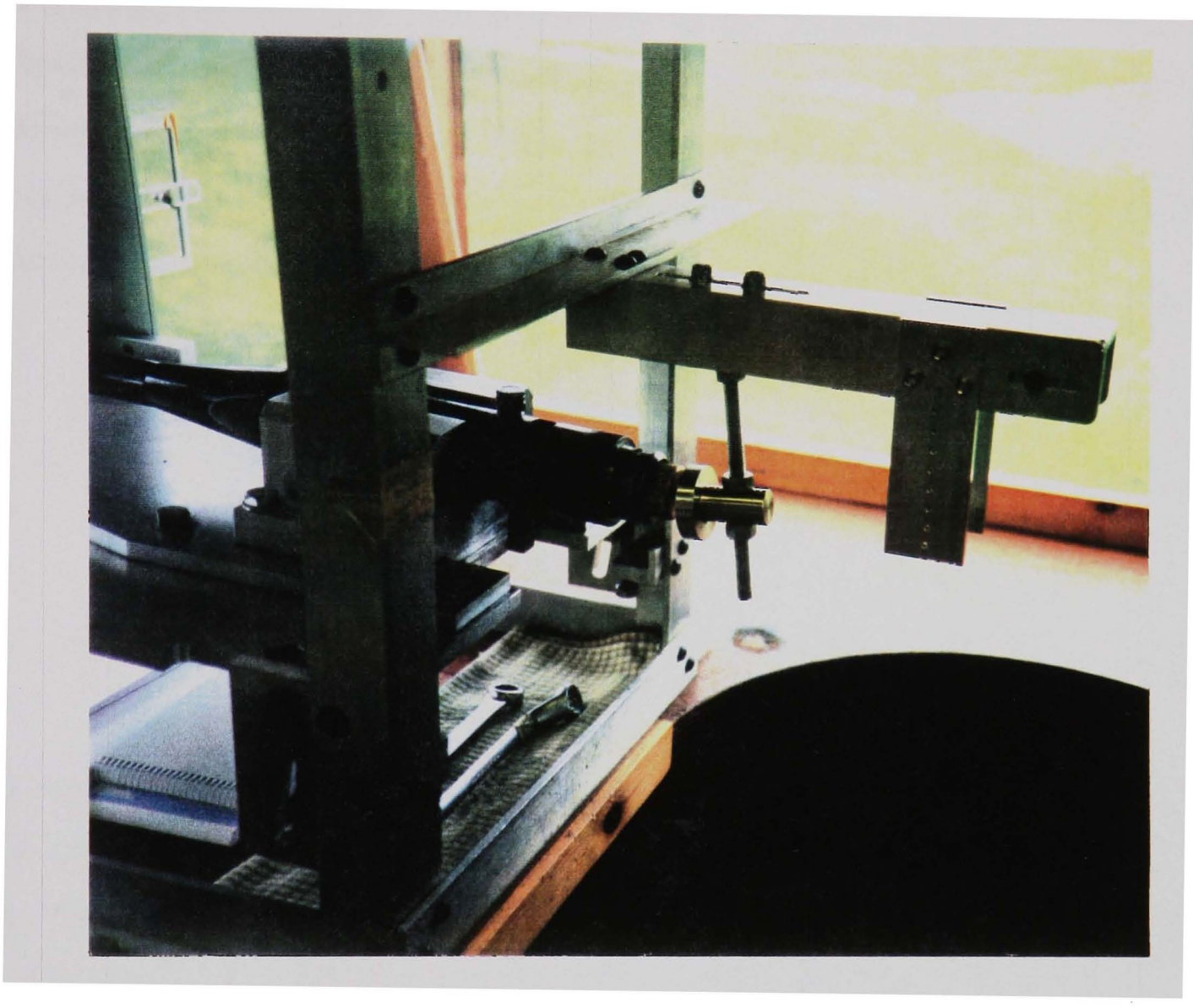

Figure 2.6 *The proof barrel in position during field trials.*

The proof barrel was modified to allow interchangeable choke tubes and chamber sleeves, so that different cartridges lengths could be used. The choke tubes were $2^{3}/_{4}$" long (70mm) and had linear tapers which varied from cylinder (0.000" constriction) to 0.050" (1.3mm constriction) in steps of 0.005" (0.13mm). There was also a limited selection of different choke profiles which were used to investigate their effects on the shot cloud ballistics. The chamber sleeves had chamber lengths of $2^{1}/_{2}$" (63.5mm but conventionally referred to as 65mm), $2^{3}/_{4}$" (70mm) and 3" (76mm).

2.2.2 Atmospheric conditions

A variation in the ballistic performance of cartridges from the same batch when tested on different days was found. This was due to the variability in the cartridges and the change in atmospheric condition. It was preferable to obtain comparative ballistics with experiments carried out on the same day and under identical conditions, but this was not always possible. Therefore to make comparative results, correction had to be made (section 4.3) to a standardized set of weather conditions. It was thus convenient to use the existing standard atmospheres (ICAO), shown below, for this purpose.

Air temperature :	288 K
Air pressure :	1.01 kPa
Air density :	1.225 kg/m^3
Relative humidity :	0%
Gravity (g) :	9.80665 m/s^2
Speed of sound (v_c) :	340.5 m/s

A weather station was built into the hut permitting recordings of wind direction and velocity, air temperature, atmospheric pressure and relative humidity to be made during the course of the field trials. From these measurements the air density could be calculated and its effects on the ballistic properties of shot clouds analysed.

The effects of gravity have been ignored in this research because bore-sighting and checking the pattern centre automatically allowed for gravity. In the case of the ballistics, gravity would cause a drop of 30cm at 50m, using

$$s = ut + \frac{1}{2} g^2 t \qquad (2.1)$$

where s is the distance, g the gravitation acceleration, u the initial velocity in the vertical direction and t the flight time, for a shot cloud that took 300ms. Using Pythagoras' theorem the shot cloud will have travelled an extra 0.9mm than expected, thus producing a negligible timing error.

2.3 DETECTION OF SHOT EXITING THE MUZZLE

2.3.1 Ballistics measurement system

The proposed measurement facility acquires timing information from several sources. A data acquisition process was necessary to store the output signals from the measurement systems so that the timing information can be extracted. The signals from the skyscreens (section 2.4) and the ballistics targets impact detectors (section 2.5) were fed into high-speed data acquisition boards. The boards sampled the analogue input signals and converted them into a digital output. The data acquisition system had 32 separate input channels, made up from four ADC cards with onboard memory of 1 megasample per board with 12 bit resolution. The maximum acquisition rate of each board was 1 megasample/sec (1MHz), allowing a sample rate in excess of 100kHz per channel on all 32 channels simultaneously and a total acquisition time of 1 second. Once the digital presentation of the shot cloud had been acquired, various information could be determined. For example, the leading and trailing pellets flight times.

All the timing information had to have a reference point relative to the shot exiting the muzzle (t_0=0). This meant that there was a requirement for a reliable detection unit which registered the shot leaving the muzzle and produced a TTL output to trigger the data acquisition process. It was important to minimize the uncertainty in the detection of t_0 as it effects the reliability of the other timing measurements. It was therefore required that the errors in t_0 were small compared to the uncertainty in the other measurements. It then could be assumed to be of negligible influence on the overall error of the system.

2.3.2 Alternative methods of muzzle detection

In the early development stages of this system an "ionization probe" was used to detect the shot exiting the muzzle. It consisted of a conductor placed in front of the muzzle, as shown in Figure 2.7. When the shot and wad exited the muzzle the ionized gases, which forced the wad up the barrel, escape inducing a voltage on the conductor. The coaxial cable is connected to a high-impedance detector to register the very small charge which leaks away (seen in Figure 2.8 and 2.9 as the exponential decay). Interpretation [44] of

the voltage waveform in Figure 2.8 shows a voltage drop produced by the blast wave, or precursor pulse (a), from the air being forced out the barrel ahead of the shot at high velocity. The reference for t_0, as the shot exits the muzzle, is shown as the maximum positive voltage peak followed by a sharp reduction in voltage when the ionized gases (b) made contact with the conductor.

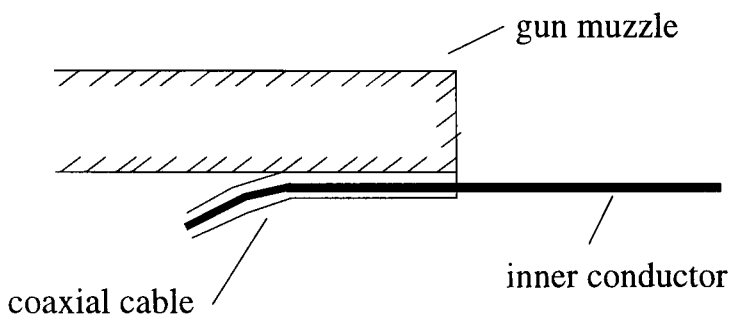

Figure 2.7 *Ionization probe attached to the muzzle.*

From the classical waveform (Figure 2.8) for the ionization probe it was clear when the trailing edge of the shot column exited the muzzle. It was found that the waveforms varied between cartridges, especially different wads and shot types, producing great uncertainties, typically 1ms, in their interpretation. An example of an ambiguous waveform is shown in Figure 2.9 where the location of t_0 is difficult and increased the chance of error. These uncertainties are significant on the remaining timing information as they are of the same order as the variation in flight times at 20m seen between cartridge from the same batch. It is desired for the uncertainties in t_0 to have negligible (such as <50μs, discussed in section 2.8.1) influence on the remaining measurement, therefore an alternative method was adopted.

The problem of detecting the shot exiting the muzzle seemed a simple task, but there were several difficulties brought on by the nature of shotguns. The air in the barrel is forced out at high velocity causing a 'precursor' pulse (see Figure 2.8) before the shot exits. Depending on the gas seal of the plastic, or felt wads, gases can escape past the load and exit before the shot load. This blast wave caused false triggering for some detectors and generates an incorrect value of t_0.

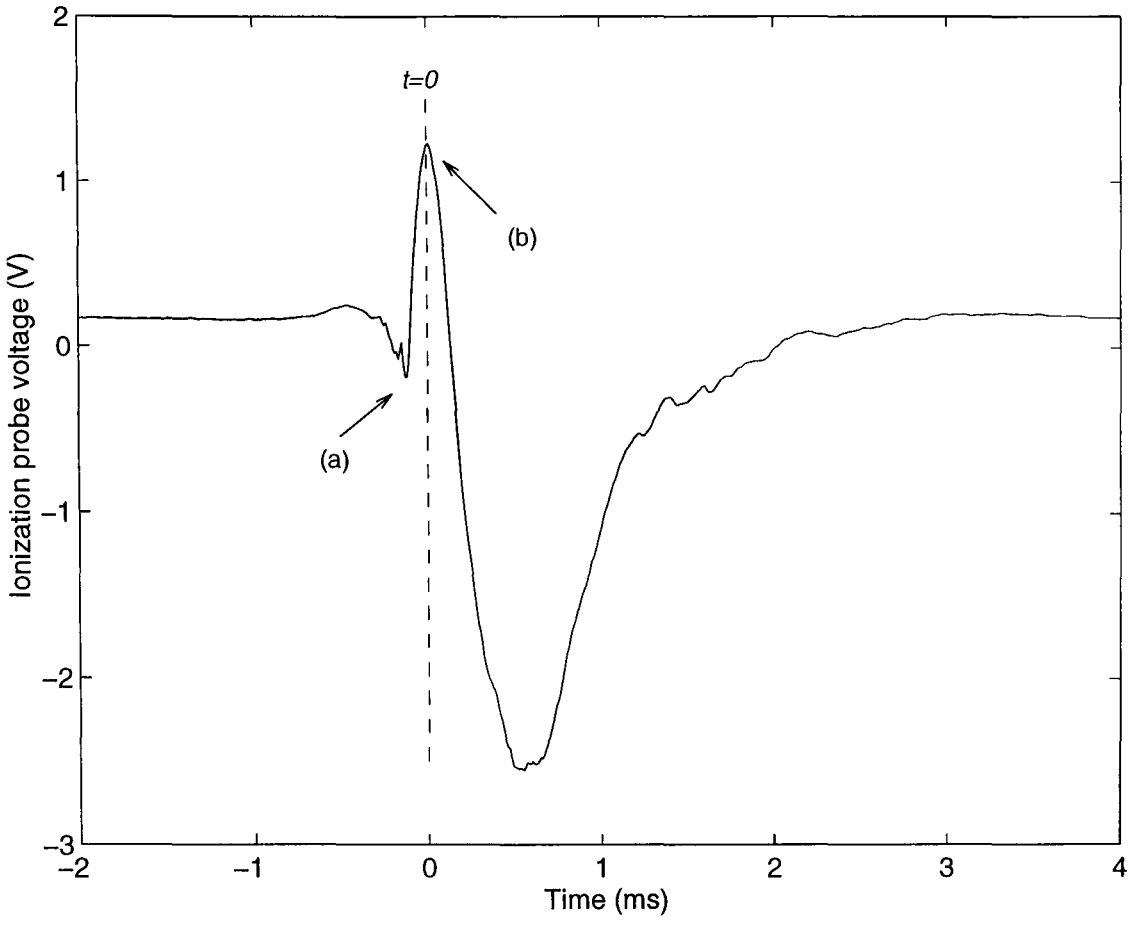

Figure 2.8 *A classical ionization probe waveform where (a) represents the Precursor pulse and (b) the base of the shot cup.*

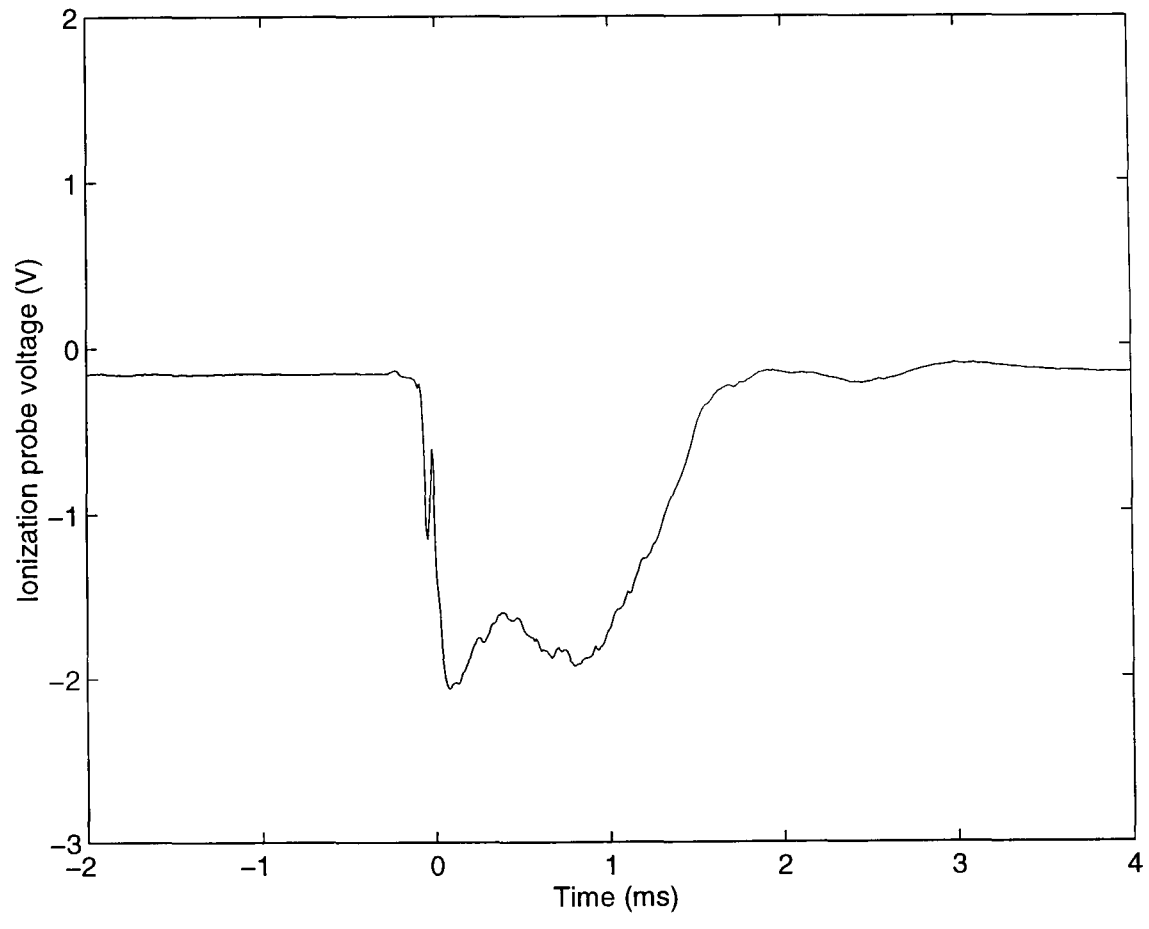

Figure 2.9 *An ambiguous ionization probe waveform.*

The use of an optical detector required a beam of light to be broken and was susceptible to false triggering. This was because the "precursor" pulse refracts the optical beam away from the photodetectors and the beam was assumed to be broken. The optical devices were also sensitive to the muzzle flame, which is produced as the shot exits the muzzle, causing confusion in the shot columns detection and possible damage to the photodetectors.

Magnetic fields have been used extensively in the USA to detect the shot at near muzzle distances. A copper wire coil is placed in front of the shot clouds path and AC current passed through it, creating a magnetic field in the space inside the coil which forms part of a resonant circuit. If a metallic object passes through the magnetic field some of the energy is absorbed by the object, thus lowering the Q-factor. The coils cannot be placed close to the shotgun, typically set up 0.5m from the muzzle, because the recoil effects of the barrel (its movement) also produce a voltage drop. The maximum reduction in voltage corresponds to the centre of mass, such as the densest part of the shot cloud. The relative position in the shot cloud to the maximum voltage drop is unknown due to the inconsistency in shot cloud shape.

2.3.3 Implementation of broken wire probe

The requirement of the muzzle probe was to detector the shot exiting the barrel and ideally locate the leading edge of the shot column. For the majority of detectors the actual triggering point in relation to the shot column is unknown, introducing an uncertainty imposed by their reaction times and threshold settings. The most reliable method of detecting the shot exiting the barrel found during this investigation was by means of breaking a wire. This method kept the detection process simple and minimized the problems associated with shotguns, as mentioned earlier. A piece of wire (15A fuse wire) was placed across and 1-2mm in-front of the muzzle and connected to the circuit shown in Figure 2.10. When the wire broke the circuit created the 5V TTL output trigger required by the data acquisition system. This corresponds to the leading edge of the shot cloud assuming the wire did not stretch.

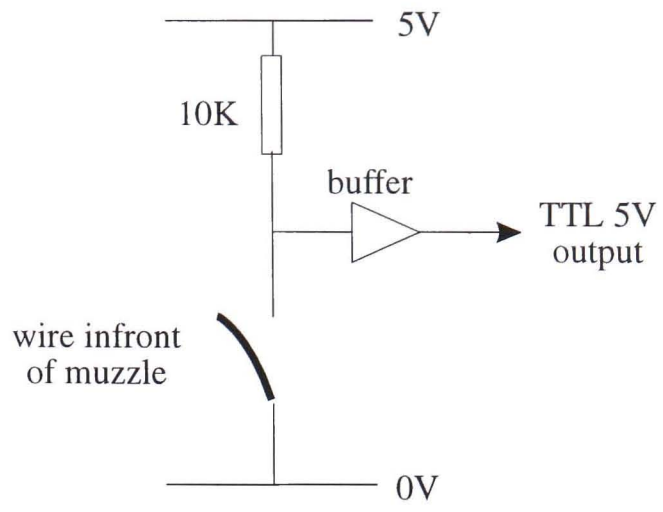

Figure 2.10 *Circuit diagram of broken muzzle wire probe.*

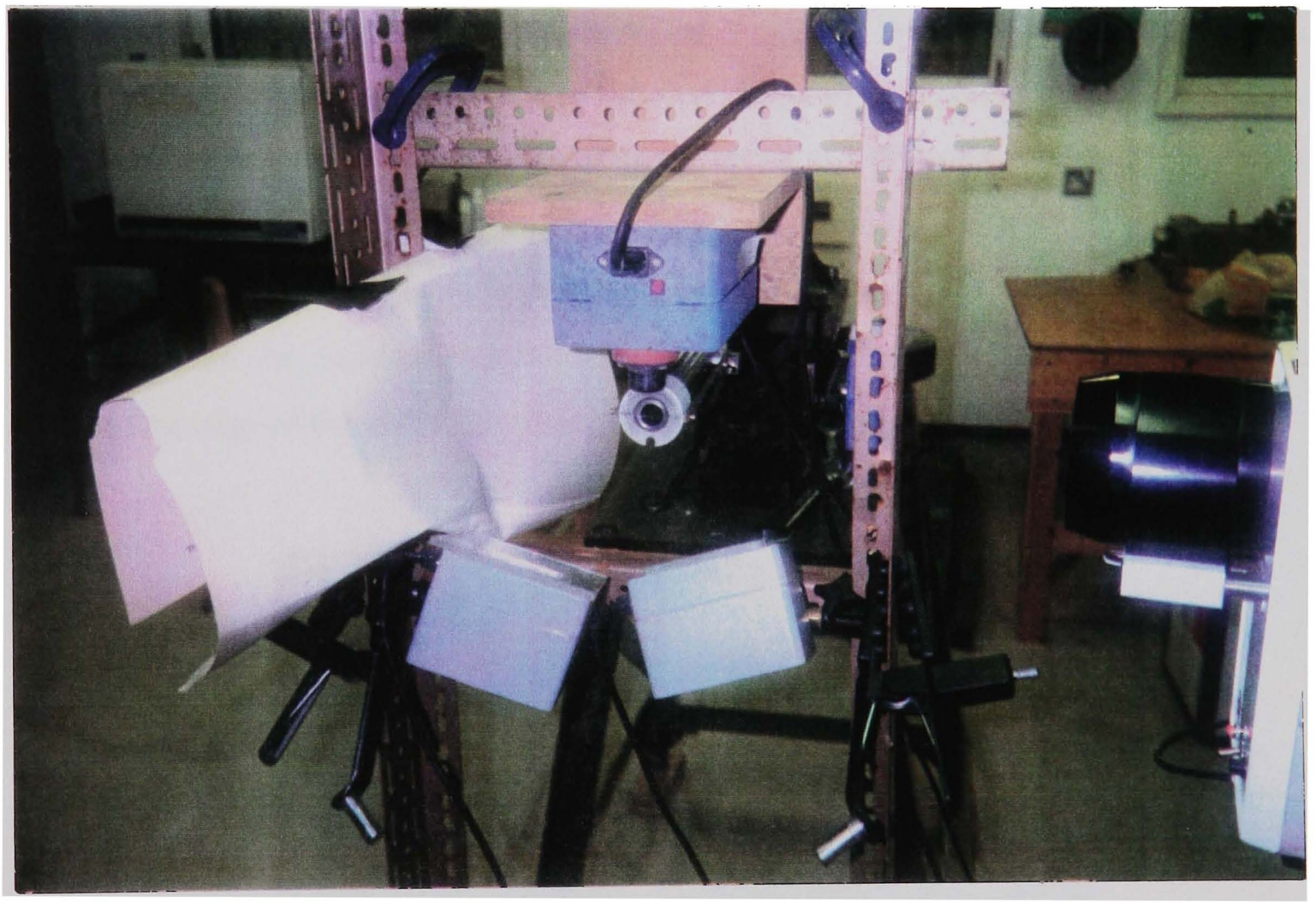

Figure 2.11 *Experimental set up used to capture the image of the shot exiting the muzzle by high speed photography.*

2.3.4 Verification of broken wire probe

High-speed photographic techniques were used to determine if the wire broke before the shot column exited the muzzle and if the wire stretched before breaking. A time window of 200μs allowed the IMACON camera to capture the shot column, via 10 exposures,

exiting the muzzle. Figure 2.11 shows the experimental set up used with the camera positioned on the right pointing at the muzzle. A strain gauge registered the vibration through the barrel after the gun was fired was used to trigger the system. At defined periods in time, a bank of flash lights, set up around the muzzle, were triggered followed by the cameras exposure.

The shot column can been seen exiting the muzzle in Figure 2.12, which reads from bottom to top then left to right, as time develops. A reflection is produced from the flash lamps on the tin fuse wire and can be seen clearly in the first four frames where the shot column is not visible. The wire is present in frame 5 and 6 when the shot column starts to appear, proving the wire is not broken on the 'precursor' pulse or blast wave. In frame 7 the wire has slipped down the side of the shot cup petals but is still not broken. At the bottom of frame 8 there is a slight reflection pointing in a different direction to the early frames suggesting that the wire was broken between frame 7 and 8 (20μs uncertainty). This is backed up as there is no sign of the wire reflection in any of the following frames. It can therefore be assumed that the wire was broken somewhere between the leading and trailing edge of the shot column and the effects of the wire stretching are negligible.

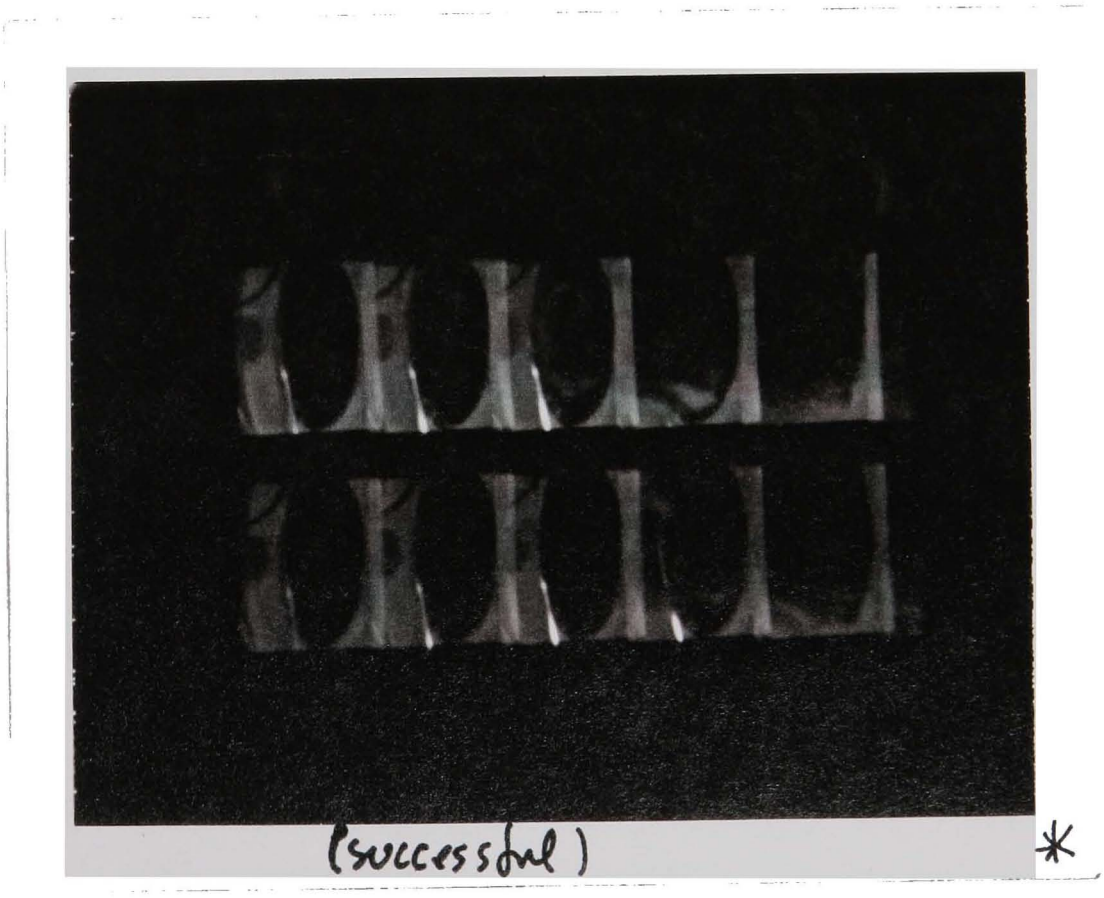

Figure 2.12 *High speed photographs of the shot breaking the wire probe on exiting the barrel. The frames read from bottom to top then left to right as time develops in 20μs time intervals.*

2.4 NEAR-MUZZLE SHOT CLOUD DETECTION

2.4.1 Implementation of skyscreens

During the investigation a growing interest was developed in the near-muzzle characteristics of shot clouds. It has already been discussed in section 2.1.3 that it is not cost effective and time efficient to use photographic techniques for ranges 20-50m, although it would give a greater insight into the interactive effects and other irregularities between the motion of pellets in a shot cloud. The introduction of skyscreens enabled limited data to be obtained at the initial stages of a shot cloud development by tracking them individually downrange without interruption. The principle of how the skyscreens work has already been described in section 2.1.3.

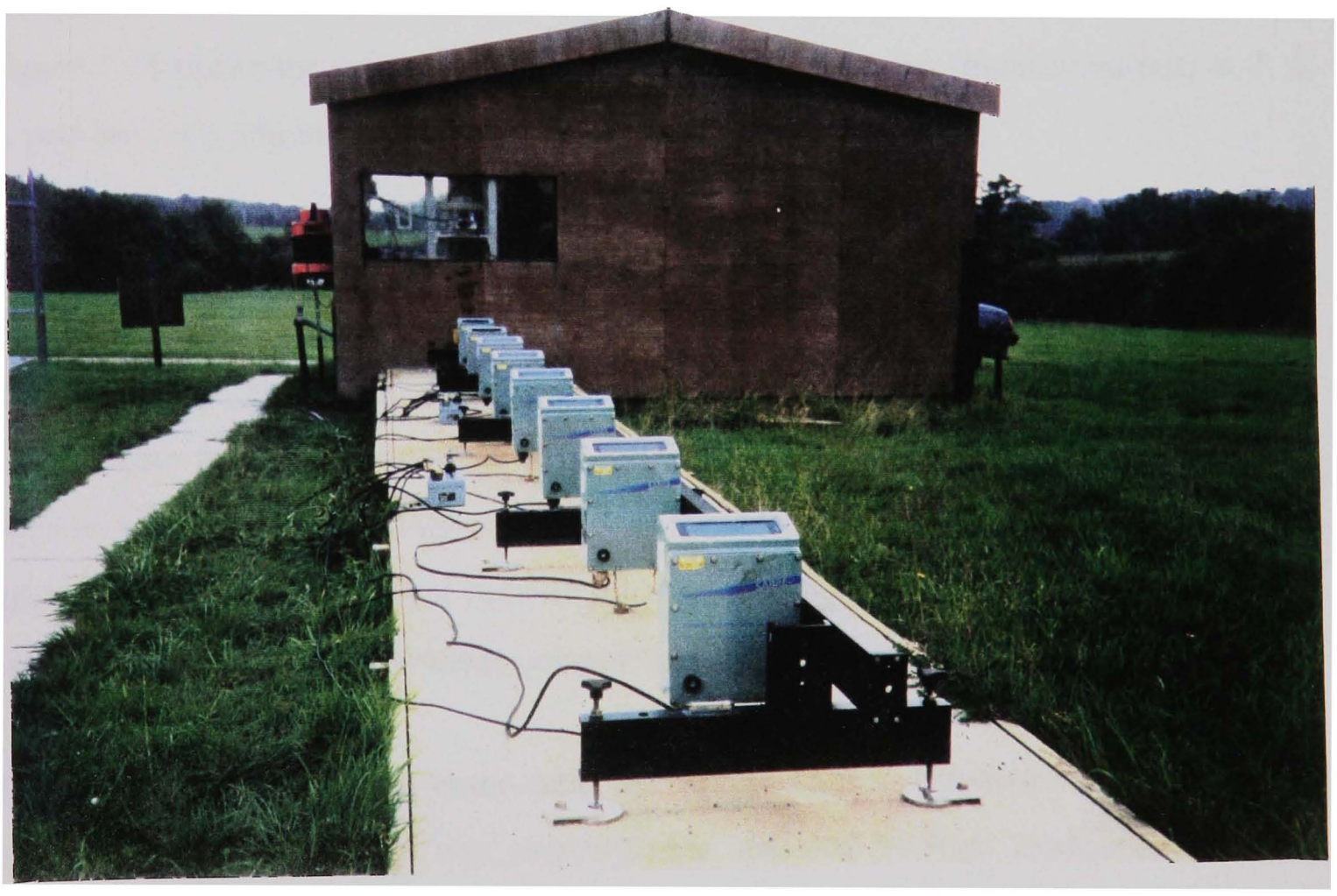

Figure 2.13 *The set of 8 skyscreens at 1m intervals from the gun muzzle.*

The eight skyscreens (with monitor and chronograph outputs) shown in Figure 2.13 were set up accurately at 1m intervals from the muzzle to obtain time-range data. To minimize the range errors, the acceptance beam of the skyscreens had to be set parallel and perpendicular to the axis of the barrel, as shown in Figure 2.3, by using the

adjustments on the support bars. The barrel was aligned horizontally and 1m above the skyscreens to obtain maximum resolution. The beam limits of the skyscreens were then set symmetrically about the barrel axis by bore-sighting on a pole held vertically in the centre of the fan beam. They were also adjusted vertically by the use of a plumb line and the alignment spots on the skyscreens. If the optical axes of the beams were not set parallel and vertical to the line of fire an error would occur in the time range measurements, as the beams would be at different distances apart 1m above ground level.

2.4.2 Interpretation of skyscreen output

When the shot column broke the wire at the muzzle the data acquisition system was triggered. The data acquisition system then continuously sampled the analogue output voltages simultaneously for each skyscreen at 100kHz on 8 separate channels. Figure 2.14 shows the recorded waveforms from the skyscreens (monitor output) at 2, 4, 6, and 8m for a 36g load of #3 lead shot using 0.030" choke.

The gradual separation of the plastic shot cup from the main shot charge is clearly seen in Figure 2.14(a) where the first downward spike from the origin represents the edge of the shot charge passing through the detection plane at the 2m skyscreen. The double spike shows that the shot charge was still in close proximity to the plastic shot cup. Figures 2.14(b), (c) and (d) show the second spike (shot cup) gradually falling behind the main charge. This is expected because the shot cup encounters a greater drag due to its inferior aerodynamic performance compared to the shot cloud.

The skyscreens have given extra detail on the interaction between the shot cup and pellets near the muzzle. It was observed that some of the early designed steel loads occasionally had pellets embedded in their plastic shot cups, giving them a greater momentum and a different ballistic behaviour. These shot cup would stay in close proximity to the shot cloud (seen in Figure 2.15 by the second spike) for a greater distance. With the shot cup separation occurring later, the corresponding ballistic characteristics, especially patterns, for an early 32g load of #3 steel shot using a 0.020" choke produced a greater variation.

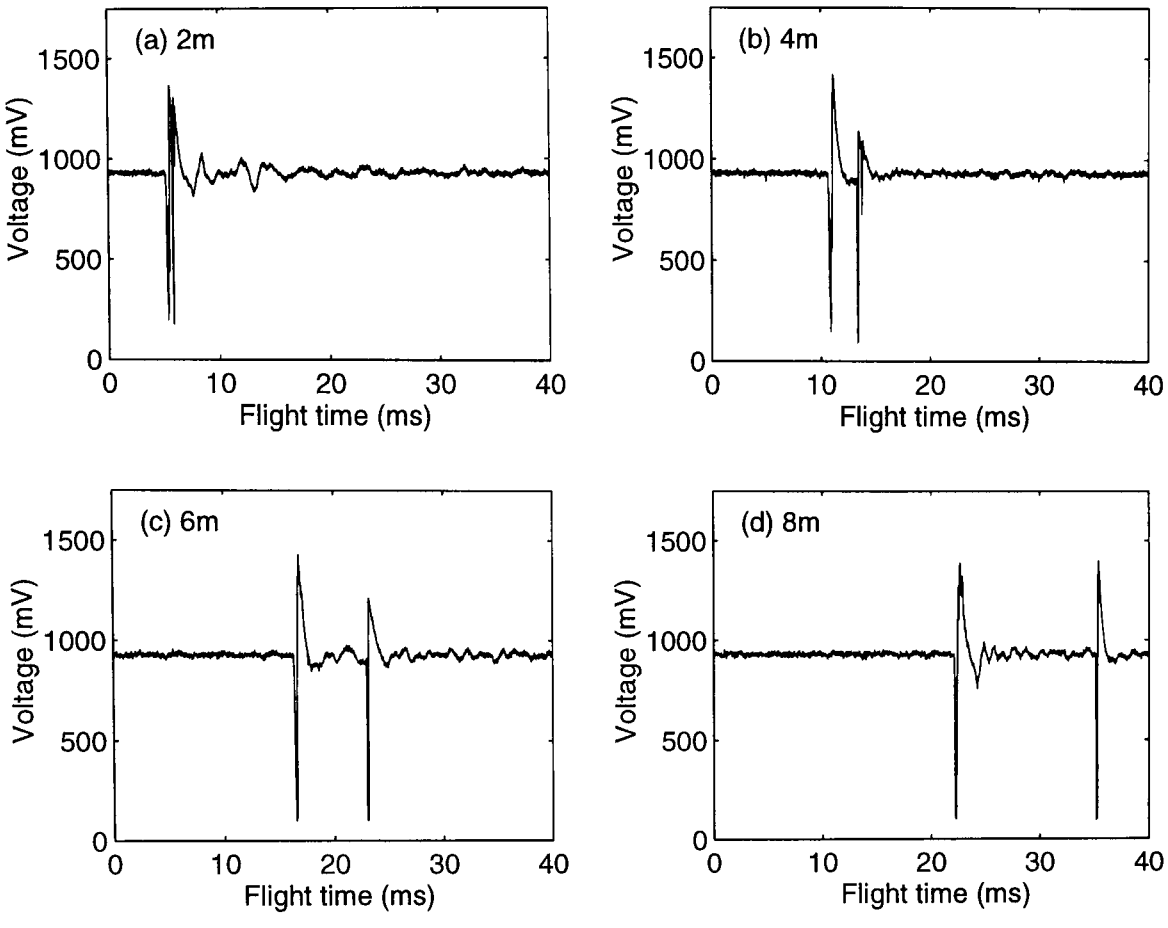

Figure 2.14 *The output waveforms from four skyscreens at 2, 4, 6 and 8m from the gun muzzle for a 36g load of #3 lead shot using a 0.030" choke.*

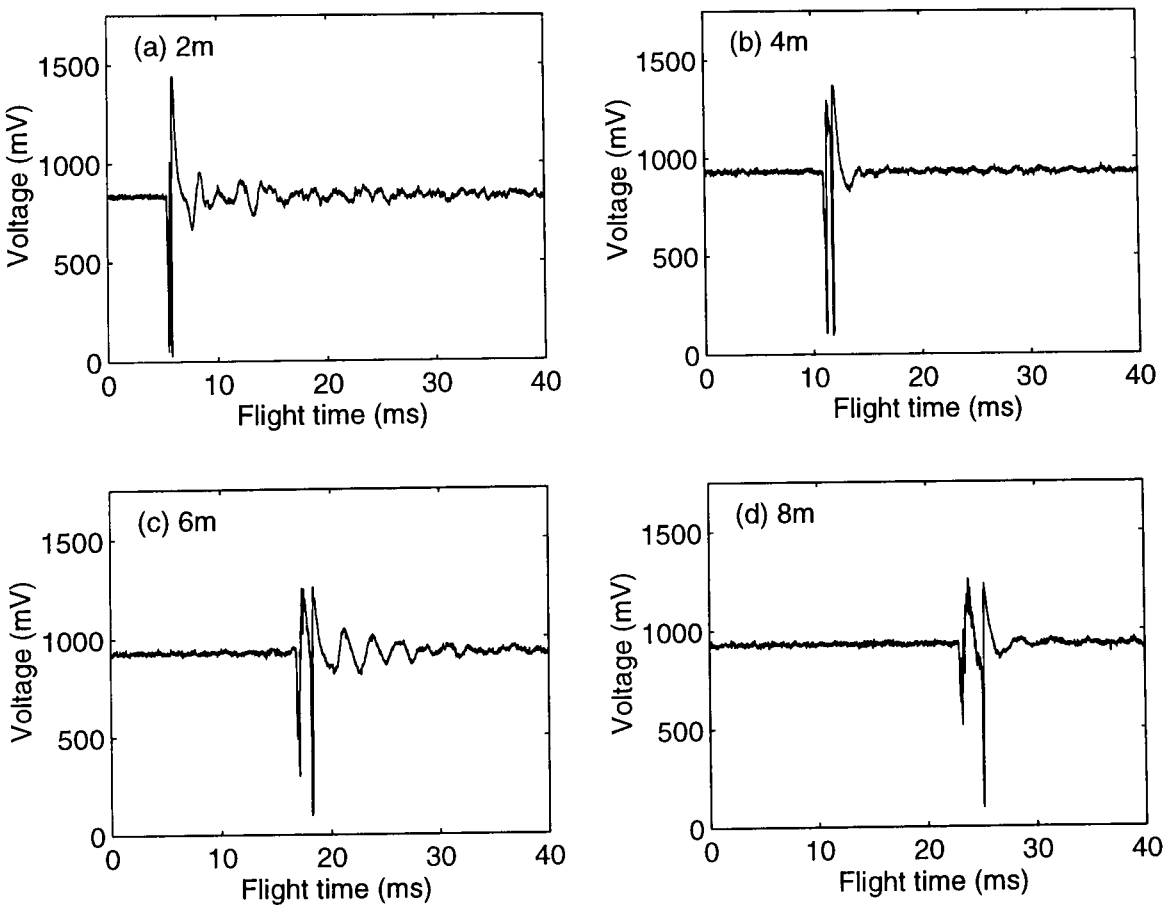

Figure 2.15 *Skyscreen output of a 32g load of #3 steel shot that has pellets imbedded in the plastic shot cup.*

2.4.3 Limitation of skyscreens

The skyscreens were initially tailored for single 5.56mm rifle rounds travelling around Mach 2-3. The lower velocity and larger mass associated with shot clouds near the muzzle generated a poor trailing edge transient response from the skyscreens. This is because the lower frequency representing the shot mass did not fall within the operational limits of the skyscreens. Expanding the output waveform from a skyscreen set at 4m (Figure 2.16) the poor transient response is translated as a large overshoot and slow decay time. This poor transient response is discussed and summarized in section 2.8.2 where the skyscreens were exposed to known pulses of light, from an LED connected to a pulse generator.

The skyscreens were also not designed to resolve the small lower velocity projectiles which make up the shot cloud. With the limitation in resolution there was a range when the shot cloud had dispersed to an extent that the individual pellets could not be reliably detected. This distance was dependent on the shot sizes and choke, but typically found to be 10m. Figure 2.17 shows the output waveform from a skyscreen placed at 11m when a 36g load of #3 lead shot passed through its beam.

The resolution limitation is shown in Figure 2.17 where the shot cloud is represented by a lot of small voltage spikes at 32ms that have no real shape, compared to Figure 2.16, making it difficult to locate any part of the cloud. Also at ranges greater than 10m the shot cloud becomes a diffuse object and the acceptance angle of the detection planes is too narrow to capture the whole spread of the pellets travelling 1m above the skyscreens. With these limitation the skyscreens were only used at ranges out to 8m were the pellets are travelling in close proximity to one another (at 2m ~ 0.2m in length dependent on choke) and at approximately Mach 1.

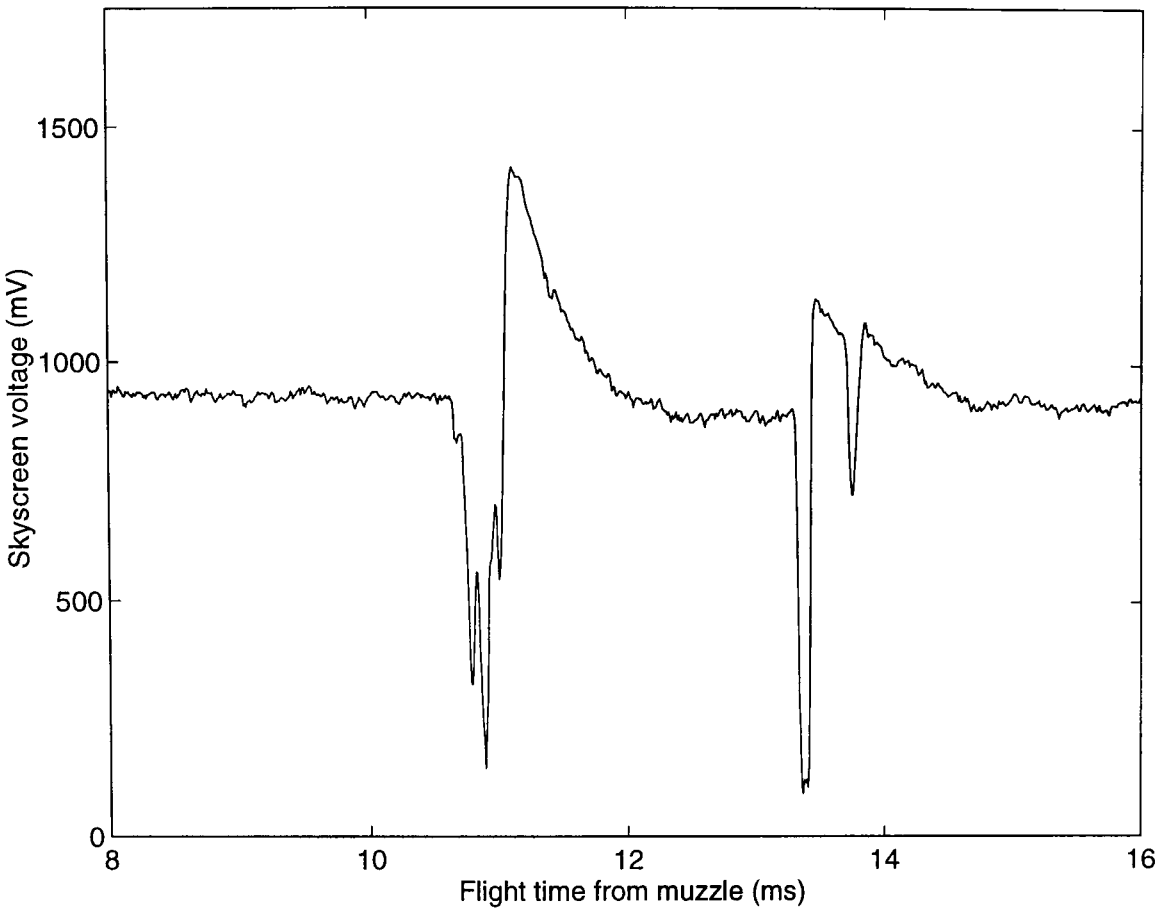

Figure 2.16 *Output waveform showing the poor transient response of the skyscreens (expansion of Figure 2.14(b)).*

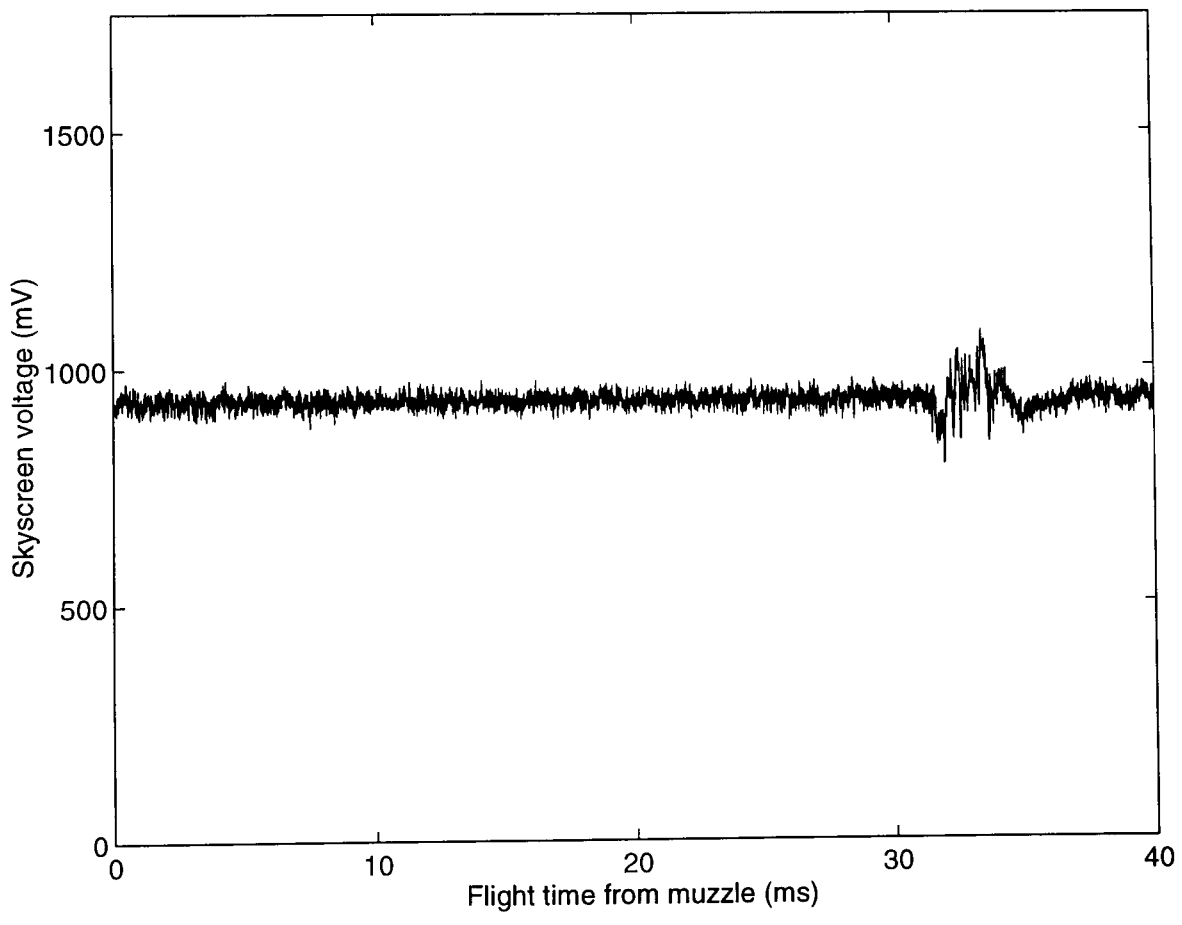

Figure 2.17 *The skyscreens output when reaching its operation limitation at 11m from the muzzle for a 36g load of #3 lead shot using a 0.000" choke.*

2.5 STRATEGY AND DESIGN OF BALLISTICS TARGET

2.5.1 Requirements of the ballistics target

The ballistics target was required to gather timing information on the distribution of spheres in a shot cloud. As the shot cloud is not a single projectile there are five distinct parts (shown in Figure 2.20) which were routinely measured for timing data. These are:

(a) Starting time (t_0) - The reference for other timing measurements and corresponds to the shot column's leading edge exiting the muzzle, discussed in section 2.3.

(b) Leading edge of the shot cloud (t_1) - Time for the first pellet to be intercepted by the target.

(c) Leading edge of the main cloud (t_2) - Time taken for the first pellet of the main section of the shot cloud to strike the target. This does not include the flyers which would register as t_1.

(d) Trailing edge of the main cloud (t_3) - Time for the last pellet of the main cloud to reach the target. This does not included any stragglers.

(e) Trailing edge of the shot cloud (t_4) - Time for the last pellet to reach the target and the reading must not include possible wad strikes.

Using the timing data measured over a set of distances from the gun muzzle to the target, the ballistics characteristics of a shot cloud can be found (described in section 4.2).

2.5.2 Design of the ballistics target

The ballistics target was designed around a modular grid with separate detection panels (Figure 2.18). The panels consisted of sandwiching a piezoelectric transducer between polycarbonate, rubber, and plywood. The polycarbonate stopped the pellets damaging the transducers and increased the area of sensitivity per transducer, whilst the plywood kept the target rigid. When the polycarbonate is struck, a signal is produced by the transducer; the rubber backing sheets (the black appearance in the panels) help to reduce the "ringing" of the panel. The rubber washers are used to isolate the metals screws from the plywood and impede the coupling between panels.

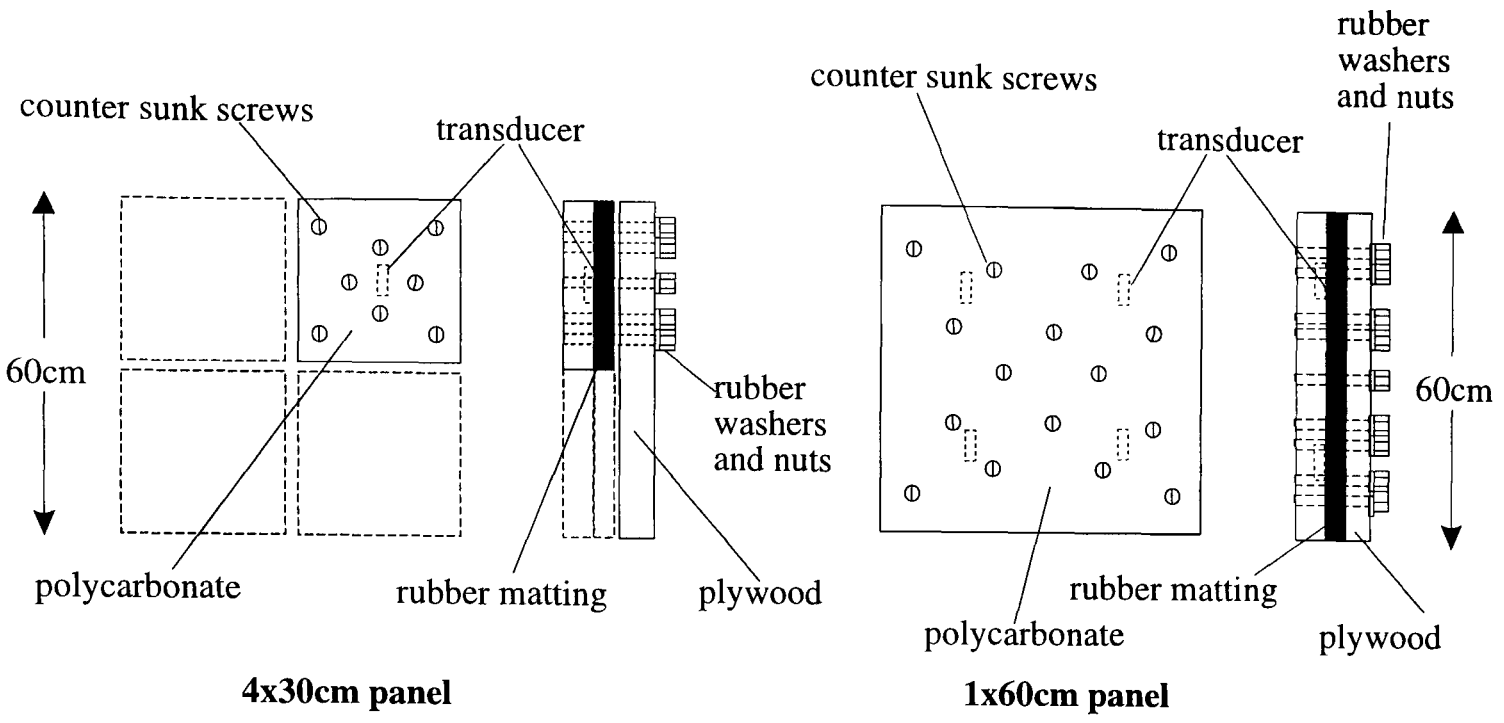

Figure 2.18 *The different types of configuration used for the 60cm square panels in the ballistics target.*

At distances over 20m the shot cloud has a wide spread, for example approximately 3m for lead shot and cylinder choke (the widest spread normally available) at 50m. For safety reasons and the ability to measure the whole shot cloud, the target was been built to 3.6m square with a six by six grid (36 panels) of 60cm square panels, as shown in Figure 2.19. Each panel could have been used either as a single impact detector (configuration of a 60cm panel) or as a set of smaller individual detector units which gave better positional information. The centre four plywood panels each typically had four 30cm square impact detector units with individual outputs, compared to the single output from a 60cm unit. If more than one transducer was placed behind a single piece of polycarbonate the ringing time, defined in section 2.5.3, was found to be degraded. The target was designed to have more transducer outputs in the centre where the pellet density is at its highest and information importance at its greatest. Under normal conditions of shooting and an accurately centred shot cloud, very few pellets struck the outer panels, which were there mainly to stop anything that went wayward. The target was mounted on a trolley which ran on a 2m gauge track, for ease of movement, and allowed extreme range variation of 15m to 60m from the firing point. Normal testing was carried out at ranges from 20m to 50m.

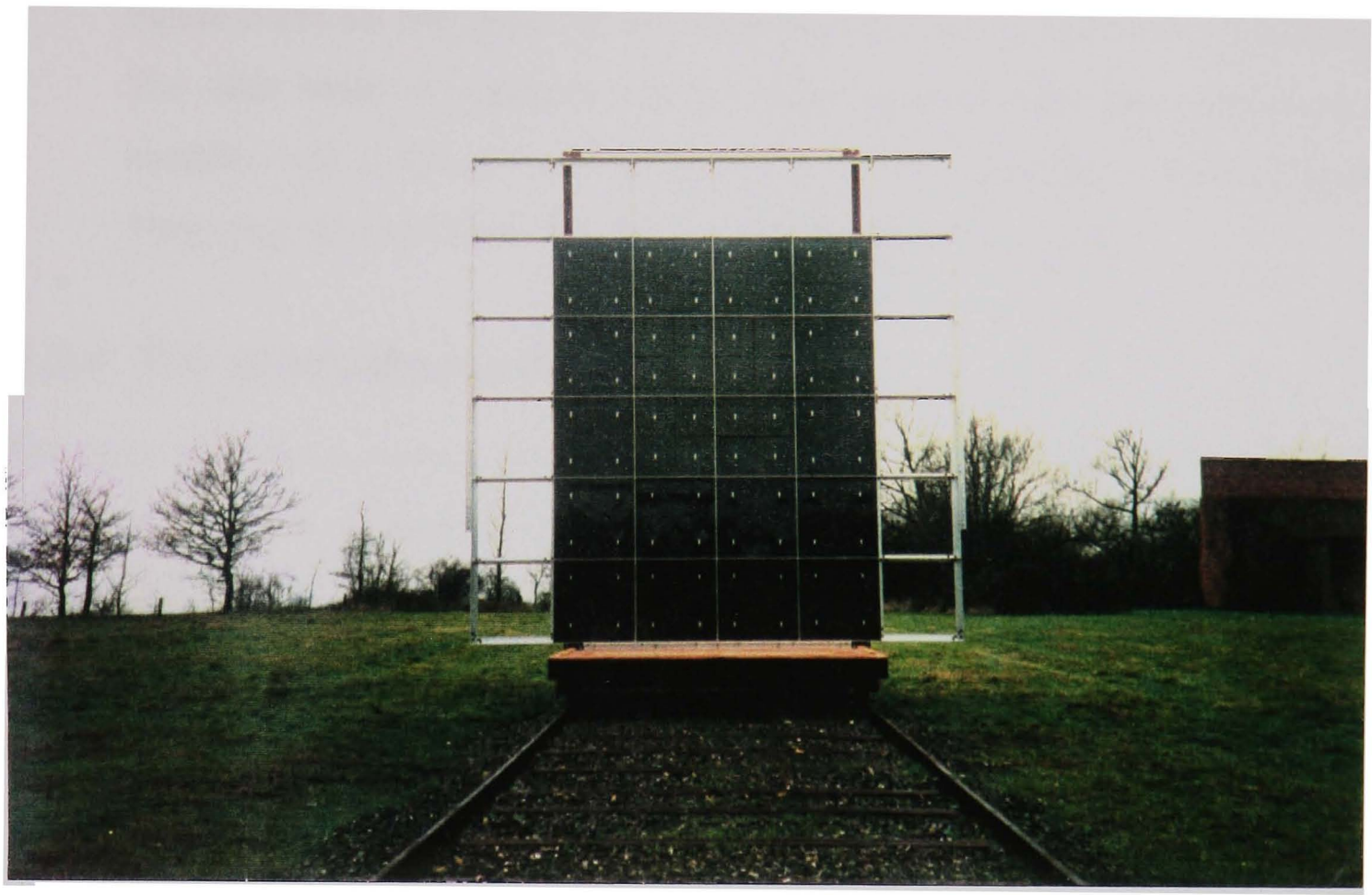

Figure 2.19 *The ballistics target with 20 of the 36 panels in place with the centre four configured for 30cm square units.*

2.5.3 Properties of the ballistics target

The two main concerns with the acousto-electronic target were the ringing time and coupling factor of the panels. The ringing is best defined as the undesired oscillation produced by a single impact and it characterizess the impulse response of the system. From this the dynamic response of multiple impacts (in a linear system) can be calculated. The coupling between panels degrades the single impact signals by the addition of unwanted breakthrough. These two properties are important as they effected the uncertainties in the timing information produced from the ballistics target and are defined as:

- RINGING TIME refers to the time taken for the voltage to decay to 10% of the initial peak impact signal. This extra undesired signal (shown in Figure 2.28) was caused by flexing in the panel and the impact signal reflecting at different material boundaries.

- COUPLING FACTOR was the peak output voltage received (shown in Figure 2.29) on one panel by an impact on an adjacent panel as a percentage. The main cause of coupling was by direct physical paths from one panel to another, such as the plywood in contact with all four panels on a 60 cm panel. There may also be some coupling via the air between the panels.

2.5.4 The shot cloud profile

The data acquisition system allows up to 32 impact detector outputs to either be recorded separately, or combined electronically. The separate recording of all the impact detector outputs gave positional as well as timing information about the impacts on the ballistics target and was used to obtain a general indication of the shapes of shot clouds at various ranges (section 3.5). The experimental procedure and set up for three-dimensional reconstruction is described in section 2.7.

Summing the outputs from the individual detector panels, via charge amplifiers, gave a more comprehensible overview of the "shot cloud profile". This was a unique feature of the measurement system and is best understood as the dynamic counterpart of the pattern, where:

- a pattern gives an overview of the pellet distribution across the *width* of the shot cloud.
- a "shot cloud profile" gives an overview of the pellet distribution along the *length* of the shot cloud.

Each shot cloud profile is the unique "signature" from one cartridge, at one range, as the pellets arrive at the target. Every trace is built up from a series of voltage measurements and Figure 2.20 shows three shot cloud profiles for three different 36g loads of #3 lead shot at ranges of 30, 40, and 50m. An individual pellet impact caused a spike of voltage (Figure 2.28) followed by a decaying oscillation lasting about 1ms, corresponding to the "ringing" of the target after being struck. Because there was nearly 200 impacts on the target occurring within a few tens of milliseconds, the individual pulses merge to form the shot cloud profile.

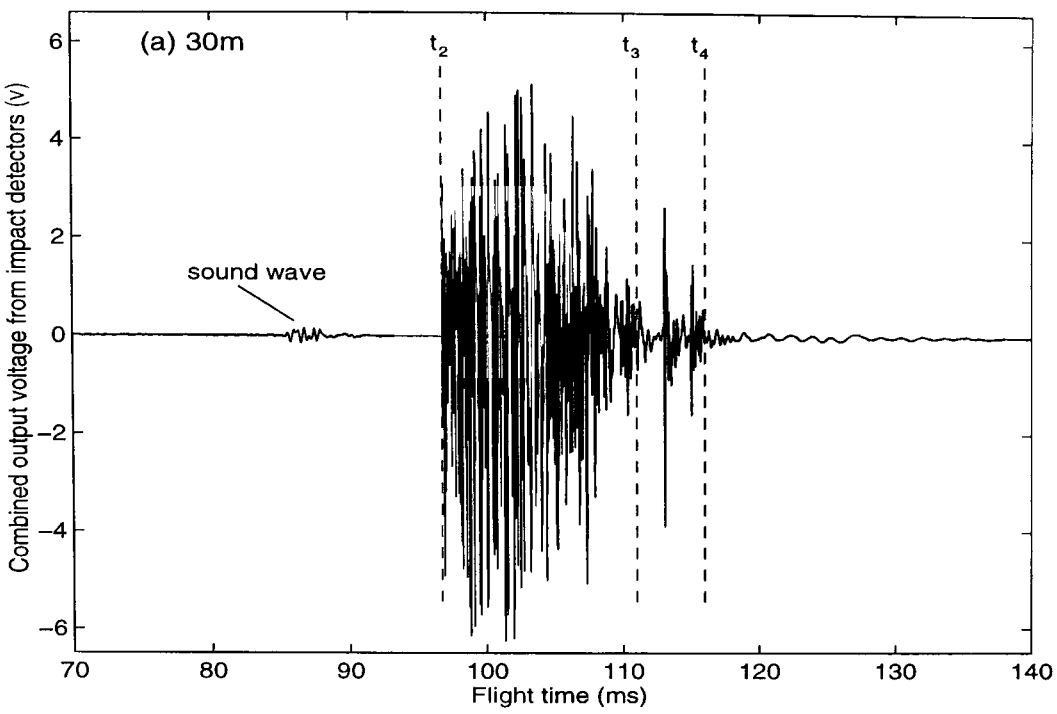

Figure 2.20 *Three "shot cloud profiles" from tests on a 36g load of #3 lead shot at 30, 40 and 50m from the gun muzzle using 0.030" choke. The earliest arrivals correspond to the left-hand side of each trace.*

The shot cloud is shown to gradually lengthen with range in Figure 2.20 upon which the appearance of more 'stray' impacts occur before and after the majority of pellets have reached the target. The ripple in trace (a) at about 88ms is due to the sound wave. From the shot cloud profile the main timing information can be extracted and in Figure 2.20(a) it can be seen that the first pellets (t_1 and t_2 are the same as there are no flyers) arrive at 30m after 96ms. The bulk of the remainder takes a further 14ms approximately, and the last impacts (t_4) arrive 115ms after firing. Thus the whole shot cloud arrives at the target within approximately 19ms at this range. As the shot cloud travels further downrange the profile at 40m Figure 2.20(b), shows a greater dispersion with impacts, or small groups of impacts, occurring before as well as after the "main" section of the cloud. The whole cloud takes about 26ms to arrive at this range. At 50m the cloud has evolved further, and the time interval from first to last pellets is about 48ms.

After studying thousands of such profiles for a wide range of shot types and loads, it has been found that the most consistent feature is the flight time (t_2) for the leading edge pellets of the "main section" of the shot cloud, this will be shown in section 3.2. The erratic nature of the stray impacts has led to a decision to concentrate on the flight times for the leading and trailing edge pellets in the main section of the shot cloud for contractual and research work.

The shot cloud profiles offer unprecedented detail in the quality control information they can give, particularly with regard to the pellet energy variation within the shot cloud.

2.6 ACQUISITION OF PELLET CO-ORDINATES

2.6.1 Requirements of the pattern analysis

The pattern has already been described as an overview of the pellet distribution across the width of the shot cloud. It has traditionally been a time-consuming process, involving firing at a large enough sheet of paper (or other suitable surface) to record the

impact points, estimating (perhaps inaccurately) the centre of the distribution, and manually counting the number of hits within various standard circles and sectors.

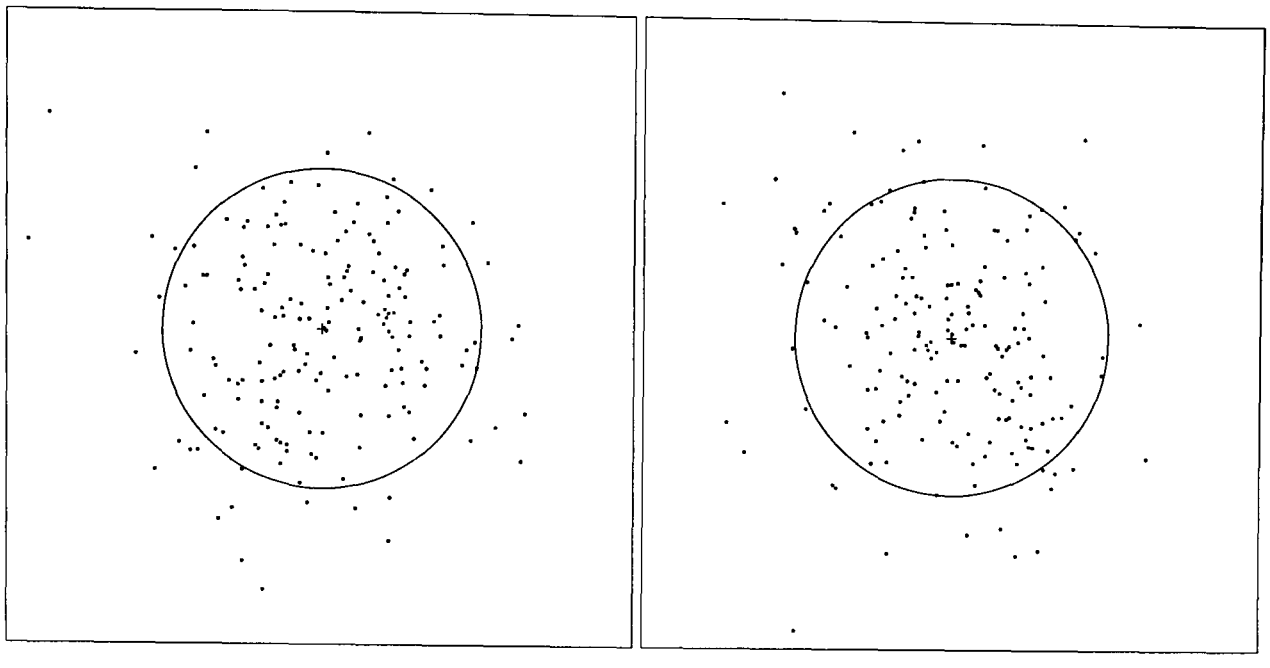

Figure 2.21 *Two reproduced pattern for a 36g load #3 lead shot using 0.030" choke at 40 yards. The traditionally standard 30" diameter circle is shown superimposed on the pellet distribution and the cross denotes the pattern centre. Both patterns are from the same production batch of ammunition.*

Figure 2.21 shows two representative shot distribution with the traditional 30" circle superimposed. The main requirement of the pattern was to acquire the pellet co-ordinates so statistical analysis on the lateral distribution could be performed.

2.6.2 Acquisition and analysis of pattern image

The shot patterns were recorded the traditional way on 1.5m square opaque black paper, backed by an absorbent material (soft plywood) which was mounted against the ballistics target (Figure 2.22). The recorded patterns were then placed in front of a light box (experimental set up shown in Figure 2.23) where the thick black opaque paper allowed the CCD camera, capable of recording images with up to 4416x3456 pixels, to store the points of light representing pellet holes into a Tagged Image File Format (TIFF) on the interfaced computer. With the camera set 3m away from the light box a field of view measuring 2m by 1.75m could capture the image of all the pellet holes on the pattern sheet. From the TIFF files, software analysis was used to generate the x and y co-ordinates of all the holes and from which the geometric pattern centre was found.

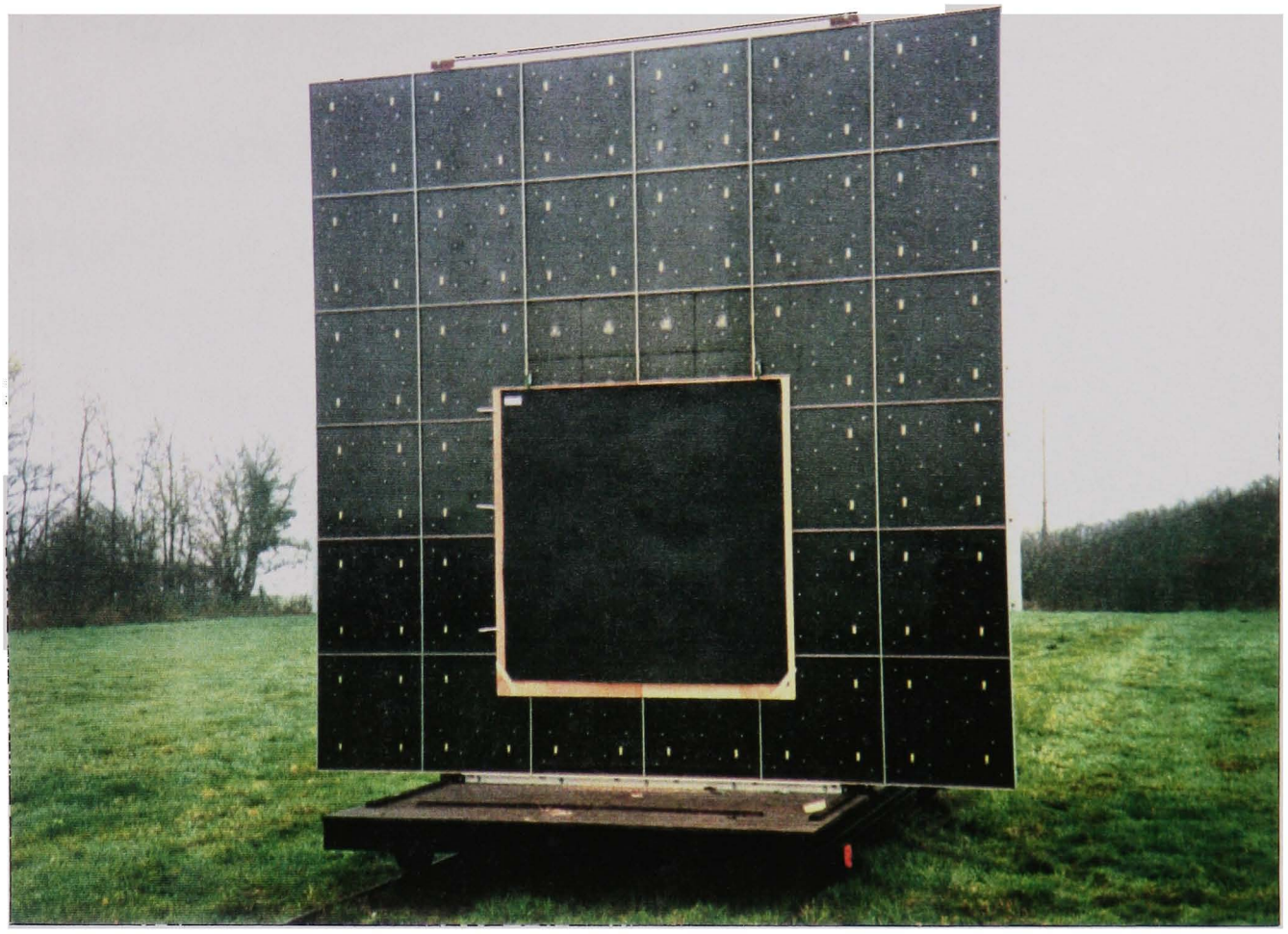

Figure 2.22 *The 1.5m square pattern paper mounted against the ballistics target using a backing of soft plywood. The polycarbonate target panels are still in place to intercept any wayward pellets.*

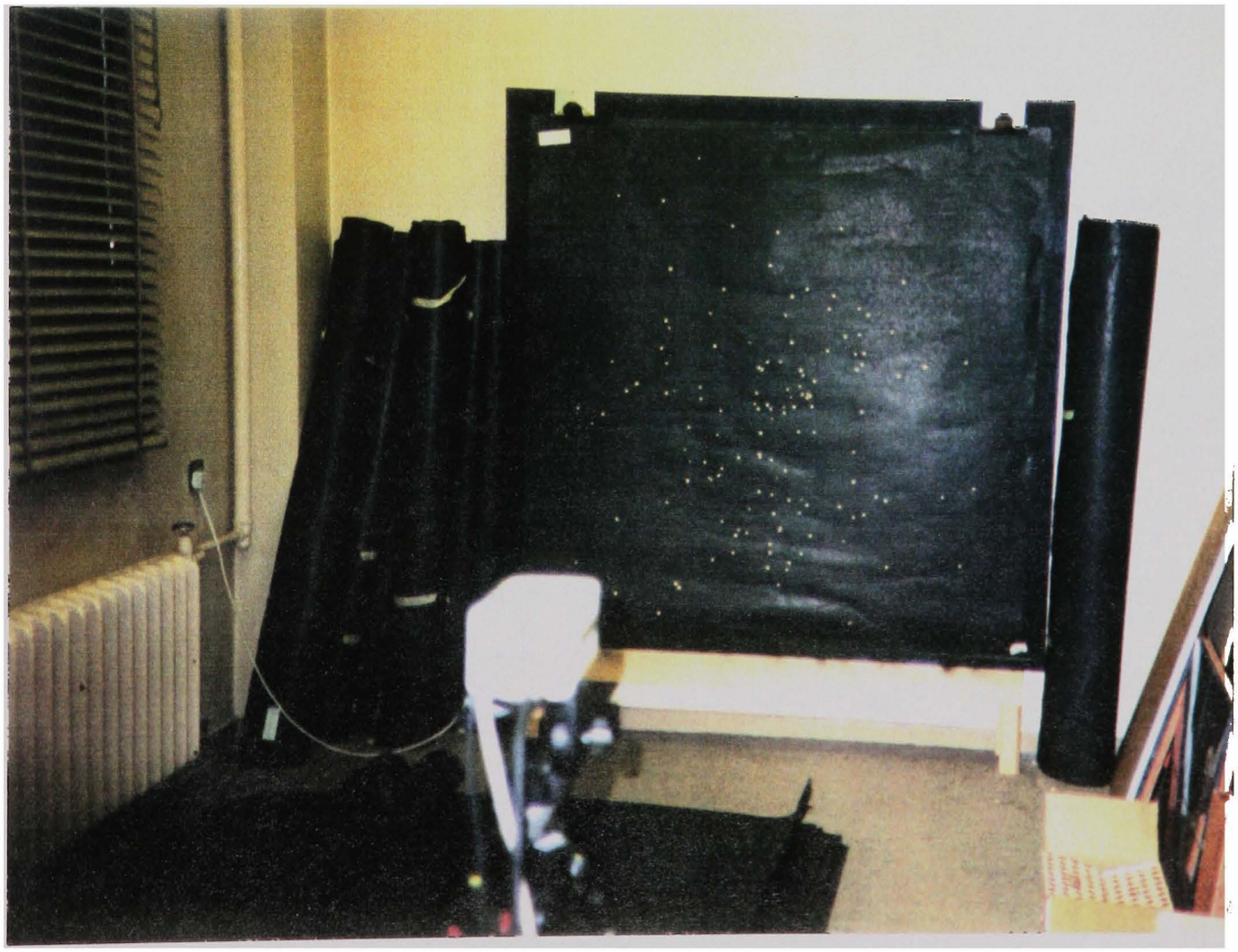

Figure 2.23 *The CCD camera in position facing the light box, where the pellet holes are seen as dots of light.*

2.7 THREE-DIMENSIONAL RECONSTRUCTION

2.7.1 Experimental procedure

Combining all the impact detector outputs, via an electronic summing unit, allowed the shot cloud profile to be recorded on one channel. This procedure did not give any positional information on the pellet distribution across the width of the cloud. Using the 32 recording channels (described in section 2.3.1) it was possible to combine the lateral (patterns) and longitudinal (shot cloud profile) pellet distribution, for one cartridge, to give a general indication of the shape of the shot cloud at one range. In obtaining the optimum impact detector configuration for three-dimensional outlines, consideration was given to the variation in the lateral spread of the shot cloud over the ballistics target distances, 20m to a maximum of 50m. The area covered by the 32 impact detector units had to receive the majority of the pellets from the shot cloud. The impact detectors also were required to be small to obtain the greatest spatial resolution. The chosen compromise was a 6x6 matrix of 30cm square detectors (allow a lateral spread of 1.8m and shown in Figure 2.24), the four corner units were disconnected to accommodate the 32 channels available.

A simpler configuration of the detector units was also used to observe the general outline of the shot cloud. This consisted of combining the detector panels into three rings, via separate summing units, with the centre four 30cm panels representing the inner ring, the next set of panels the middle ring and finally the outer ring with the corner panels included.

When combining the impact detector units via the summing units the single output is taken back to the instrumentation hut by a 100m coaxial cable. For the multiple channels work it was not practical to have 32 coaxial cables running back to the hut. Therefore the computer, which houses the data acquisition boards, was mounted behind the ballistic target and the impact detectors units connected direct via charge amplifiers. Ideally, for these 32 channels, and if more recording channels are to be added, a multiplexing procedure would be required to reduce the cabling. Figure 2.25 shows the colour coded cables used to prevent confusion in the set up.

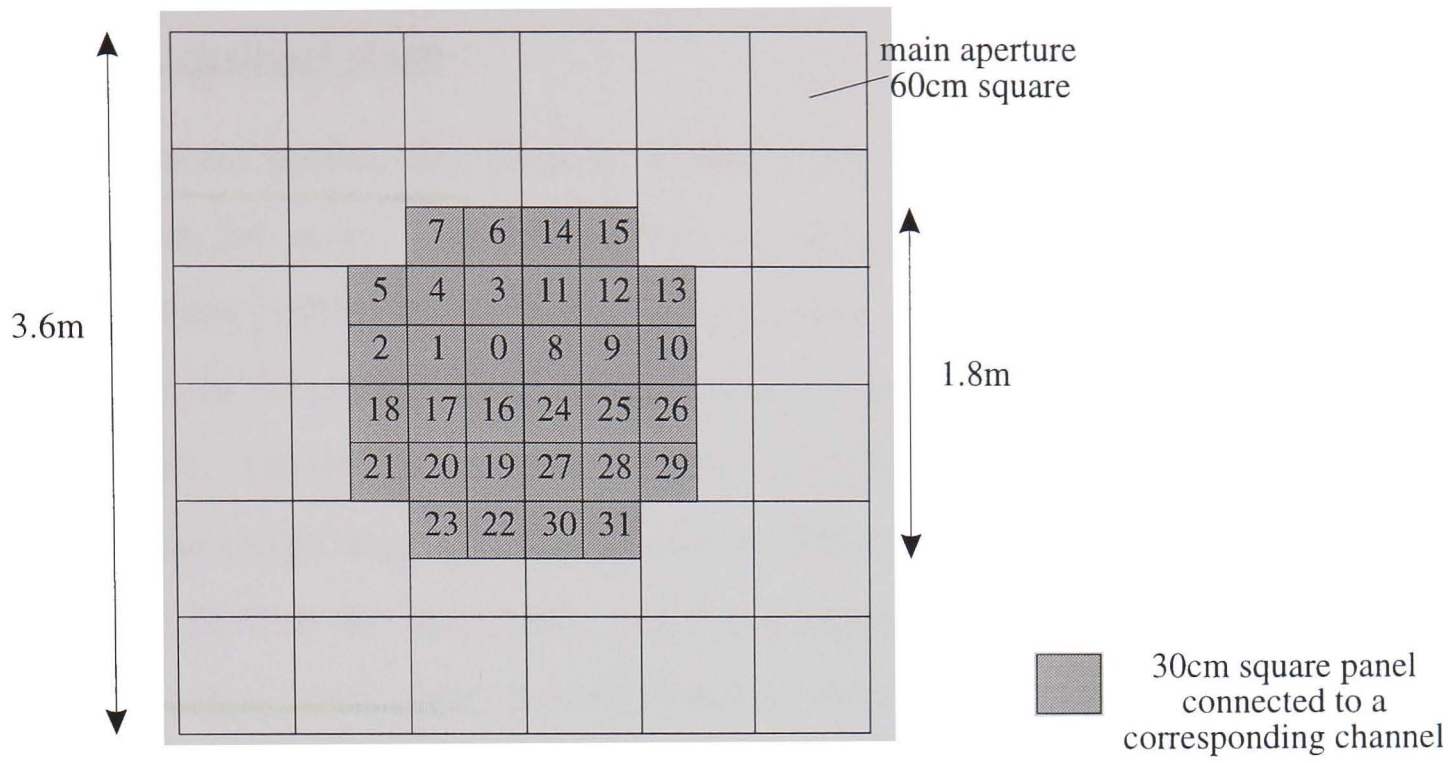

Figure 2.24 *The configuration of impact detector units for three-dimensional reconstruction of shot clouds.*

Figure 2.25 *The connection to the data acquisition boards for multiple-channel measurements.*

2.7.2 Acquired data

The shot cloud profile, described in section 2.5.4, represents the whole of the cloud impacting on the target. The outputs from the single impact detector channels gave their own shot cloud profiles which corresponded to their relative area. At close ranges (20m) the profiles for the central detection units were observed to be similar to the whole shot cloud profile. The profiles from the detector units further from the centre of the target, or when the target was moved downrange (50m), became more diffuse due to the dispersed nature of the shot cloud, and single impacts are then observed. Figure 2.26 shows the output from three detectors units in different parts of the ballistics target at 30m for a 36g load of #3 lead shot using a 0.030" choke. It can be seen that the central unit (channel 0) produced a waveform similar to the whole shot cloud profile (a), moving away from the centre of the target the arrival of individual pellets (b) and (c) could be detected and timed until no impacts occur (d). This is what would be expected for this type of load as its measured maximum lateral spread is less than 1m wide at 30m.

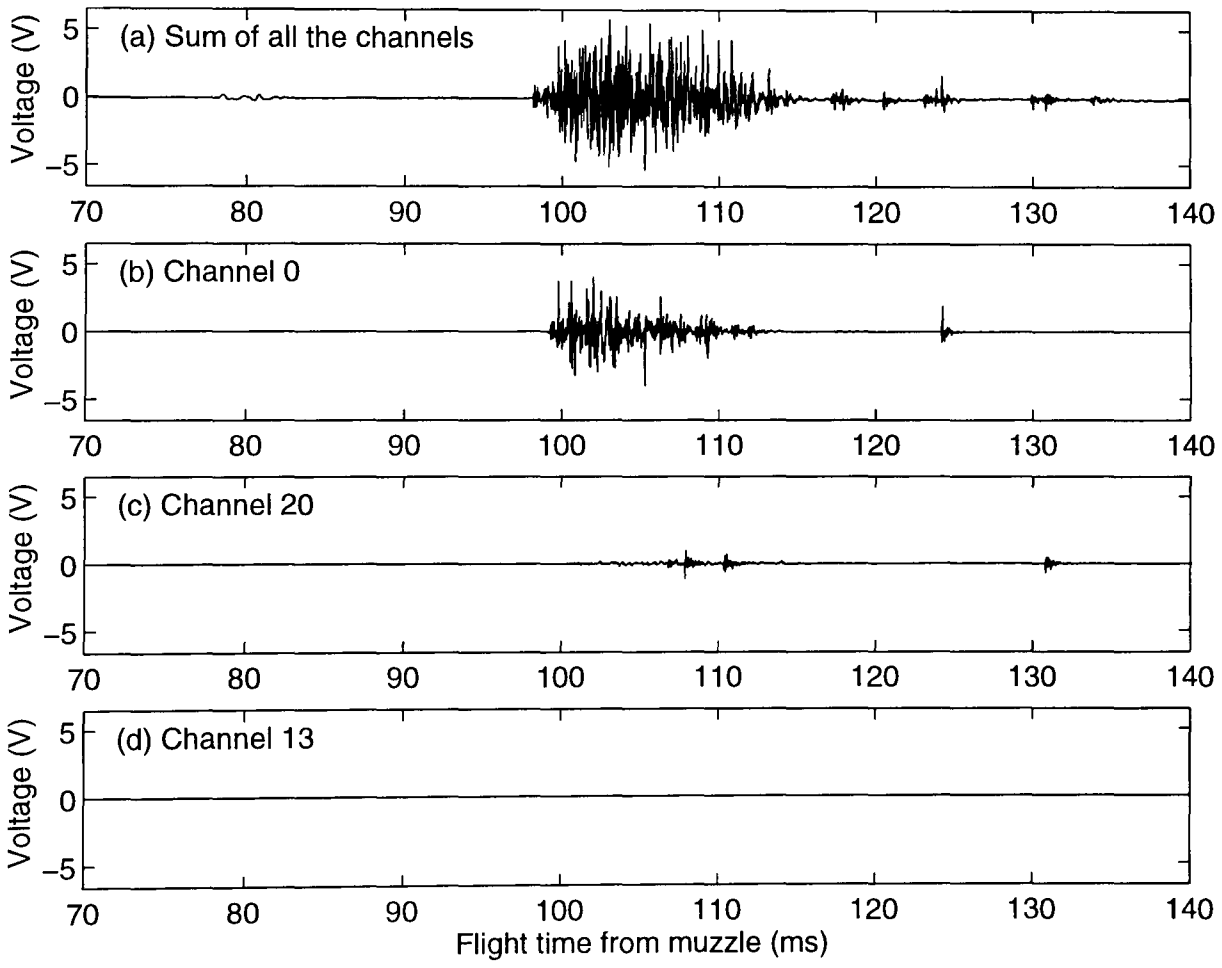

Figure 2.26 *Output waveforms from a selection of detector units showing the corresponding shot cloud profiles for three-dimensional outlines at 30m.*

From the individual shot cloud profiles for each unit it was possible to measure the time it took for the first and last pellet to arrive in that area. This gave a timing value of t_1 and t_4 for the 32 areas on the target. Summing all the channels together, Figure 2.26(a), t_2 and t_3 could be found for the whole shot cloud. The corresponding values for each channels were then obtained by finding the closest pellet arrival time within these limits.

2.8 PROPERTIES MEASURED AND ERROR ANALYSIS

2.8.1 Initiation of measurement system

The data acquisition system required a reliable trigger to provide accurate timing data from the skyscreens and ballistics target. The result from the high speed photography (Figure 2.12) showed that the wire was not broken by the blast wave and therefore not causing an early trigger. It was also necessary to find out what part of the shot column the wire broke on, starting the timer. Figure 2.12 shows that the wire was broken shortly after the leading edge and before the trailing edge of shot column exited the muzzle, producing a maximum uncertainty in t_0 of ±25μs for a compressed shot column of 2cm, travelling at a typically muzzle velocity of 400m/s.

This uncertainty in t_0 produced an error at 20m of approximately 0.05%, for a typically shot clouds flight time of 60ms, and has negligible influence due to the greater (1-2%) percentage variation, expressed by (3.1), associated with the flight times of cartridges from the same batch, see section 3.2. For measurements closer to the muzzle (1-10m) it has a greater influence and a timing uncertainty of 0.8% is produced, for a typically shot cloud flight time of 3ms at 1m, but this is still smaller than the variation within cartridges.

2.8.2 Skyscreen accuracy

The accuracy of the near-muzzle flight time measurements were dominated by the transient response of the skyscreens. It was known that they were originally designed for Mach 2 or 3 single 5.56mm rifle bullets which would take approximately 10μs to pass through the detector beam. Placing a green LED, connected to a pulse generator, in front of the skyscreens the transient response was obtained for the corresponding pulse widths

associated with the 5.56mm bullet and a shot cloud at 1m. For a pulse width of 10μs (rifle bullet) the skyscreens voltage output can be seen in Figure 2.27 to fall when the pulse goes to 0V and then rise when the pulse returned to 1000mV. Comparing this with the waveform produced from a pulse width of 500μs (time taken for a 20cm long shot cloud with a velocity of 400m/s at 1m) it can be seen that the fall off response is very sharp and distinct. However determining the rising edge (or trailing edge of the object) is more difficult as the slow upward decay, which corresponded to the rising edge of a 10μs pulse width, occurs before. In response to the rising edge of the pulse the skyscreens output sharply rose producing a large overshoot and decay time.

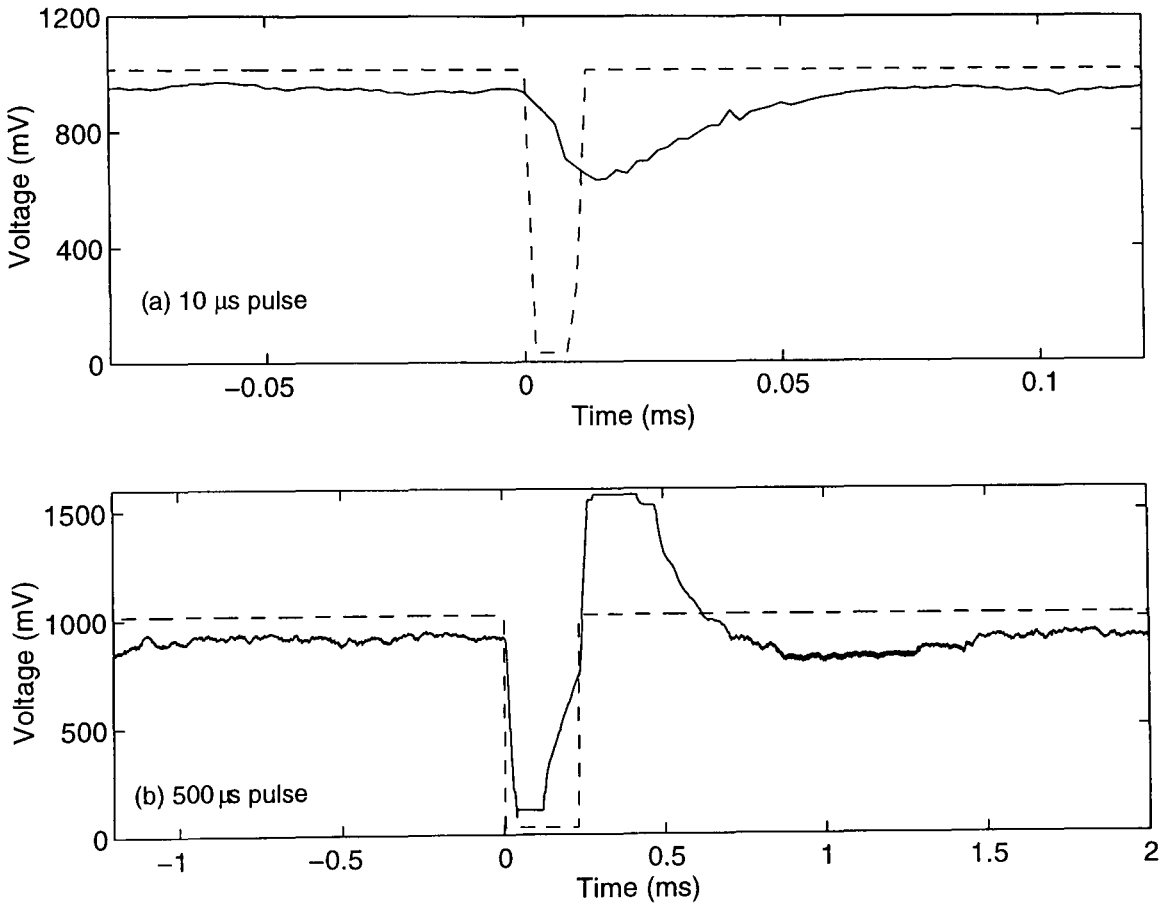

Figure 2.27 *Transient response of the skyscreens for a selection of pulse widths produced by connecting a LED to a pulse generator (--).*

It was decided to use only the leading edge data produced by the skyscreen as this was the most consistent and easily identifiable part of the shot column at near-muzzle ranges. The trailing edge uncertainty is much greater due to the poor low frequency response and was translated as the overshoot seen in Figures 2.17 and 2.27. It was hoped that the

skyscreen could be modified by altering the resistance and capacitance value, but this was not successful because their response was dominated by the photodetectors.

Another check on the accuracy of the leading edge data produced by the skyscreens was measuring the velocity of a .22 rifle bullet. This type of bullet was used as its ballistic behaviour is well known. The manufacturer quoted a velocity at 3m of 327m/s (this is dependent on the air density) and from 10 rounds fired over the skyscreens an average of 333 ± 2m/s was calculated, a discrepancy of less than 2%. In discussions with the manufacturer it was established that this was likely to be due to variation between batches.

2.8.3 Ballistics target (ringing and coupling)

The data acquired from the ballistics target was made up of range, voltage and timing measurements. The ranges, defined as the distance from the muzzle plane to the target plane, were measured using a surveyors tape and plumb line. This positioned the target to within 5mm of the correct mark and produced a 20μs timing error for the leading edge of a shot cloud at 20m with a velocity of 250m/s. Therefore this small discrepancy had negligible influence, due to the cartridge variation, on the flight time measurements. The voltage produced from the transducers was converted from analogue to digital by the data acquisition boards using 12 bit resolution. For routine tests the voltage settings were at ±10V, hence an uncertainty of ±2.5mV was obtained. The most important factor of the ballistics target system was the timing information, controlled by a crystal oscillator. Any uncertainties in this measurement would be inherited into future calculation and models. The main parameters which created these uncertainties in the acousto-electronic target were the ringing time and coupling factor.

The leading edge flight-time data produced by the ballistics target had an uncertainty dominated by the propagation delay of the acoustic wave across the polycarbonate panel. The maximum error occurred when there was a corner impact 0.2m away from the centred transducer on a 30cm square detection unit. The acoustic velocity through the polycarbonate is approximately 2000m/s, giving a delay of 0.1ms and a worst case

uncertainty at 20m of ±0.1% for a typical flight time of 60ms. This type of error is a factor of 10 smaller than the variation seen between cartridges from the same batch, so had negligible influence on the overall uncertainty.

The trailing edge data had a greater uncertainty and was controlled by the ringing time of the detection panels. From single impacts produced by air pistol pellets (Figure 2.28) and multiple channels recordings of a shot cloud, Figure 2.26(c), the ringing time was found to be approximately 1ms. This gave an uncertainty of ±0.75% at 20m and ±0.125% at 50m for their respective flight times of 60ms and 240ms. The trailing edge flight times themselves were seen in section 3.2.1 to have a greater variability than the leading edge, making this error much less significant. However, knowing these uncertainties it was possible to make corrections if it was thought necessary, making them a minor factor in the overall error of the system.

The coupling factor was investigated by firing an air pistol pellet at different areas of the detection panels and recording the signal breakthrough on another panel. Figure 2.29 shows the output signal when a neighbouring 30cm panels was struck by a single impact (Figure 2.28). It can be seen that the peak voltage is less than 10%, <1% energy, coupling on the neighbouring panels output. This was an important factor for multiple channel recordings as it allowed the sharp rise time of an impact to be seen above the breakthrough signals produced from the other panels. The impacts in Figure 2.26 are clearly visible and show no signs of any excessive breakthrough from the rest of the detection panels. It was found that these levels of ringing and coupling were a practical compromise as the improvement of one generally degraded the other. This was emphasized when experimenting with backing and construction of the target panels.

The ringing and coupling test showed the type of uncertainties generated by the ballistics target, which can now be allowed for if necessary in any future calculation. The leading edge flight time was shown to be the most accurate and consistent measurement and its uncertainty was ignored due to its relatively small effect compared to the variation in cartridge performance.

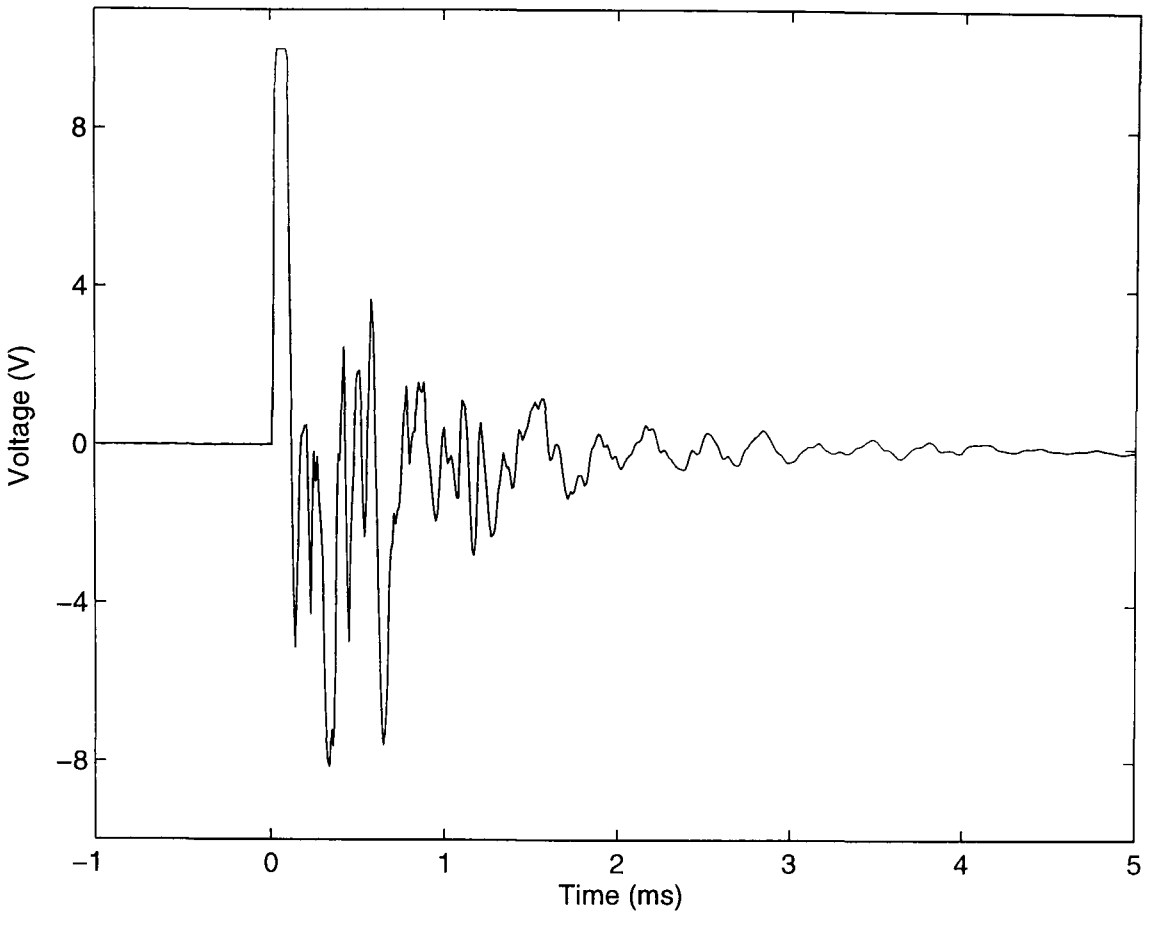

Figure 2.28 *A single impact from an air pistol .22 pellet showing the extra undesired signal produced by the targets oscillation.*

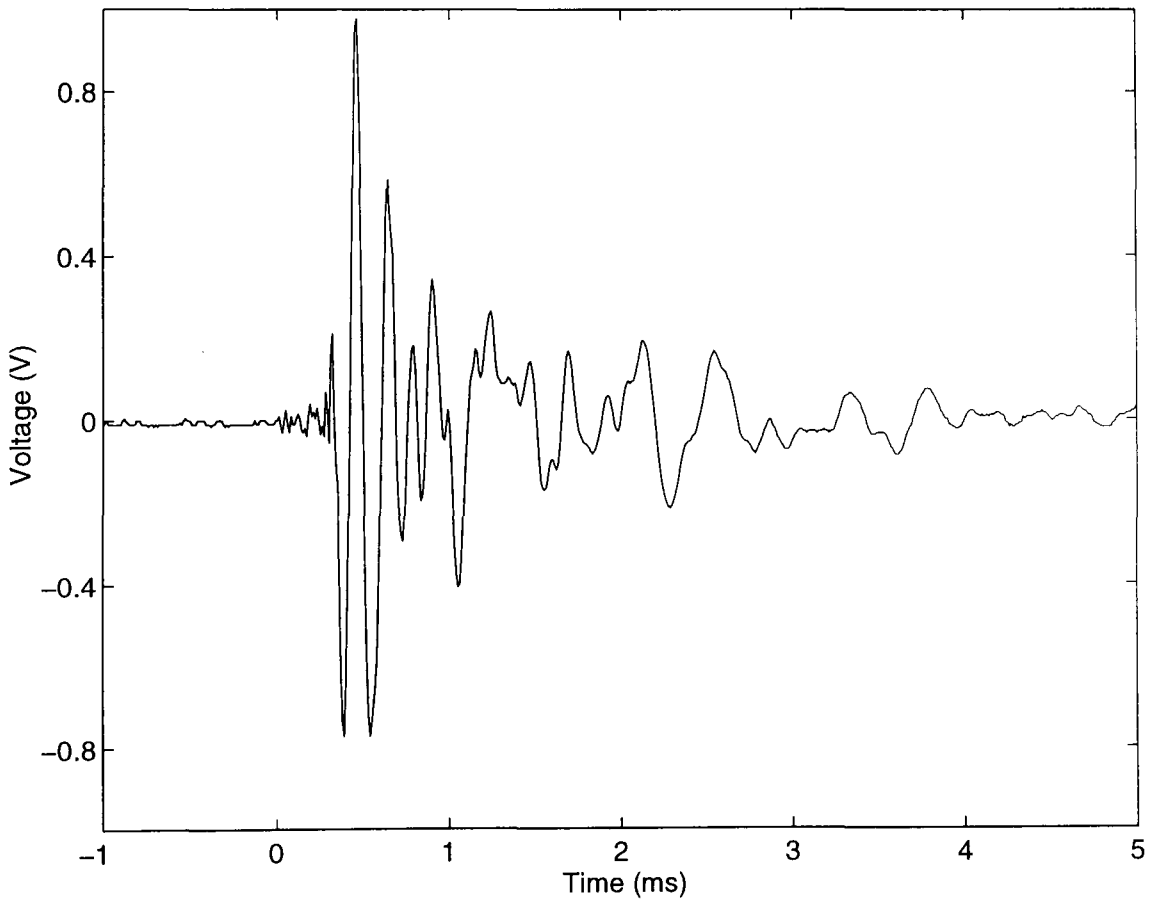

Figure 2.29 *The breakthrough produced by the single impact (Figure 2.28) on a neighbouring panel. Note that the voltage scale is different to that of Figure 2.28.*

Experiments were carried out after the construction of the ballistic target to find a way of reducing the ringing to such an extent that its effect could also be ignored. Rubber was bonded onto the back surface and the edges of the polycarbonate to reduce the oscillation and reflection waves produced. This method of construction reduced the ringing time from 1ms to 0.5ms and the coupling factor to 5%. A factor of 2 was not, however, thought to be a significant improvement to be implemented into the whole system because of the considerable extra expense incurred.

2.8.4 Pattern analysis

The camera was fixed at 3m from the light box obtaining a field of view of 2m by 1.75m. To examine the resolution capabilities of the camera (4416x3456 pixels) and its lens a test panel was placed on the light box with a range of hole diameters and spacings. The camera was able to detect holes >1mm in diameter anywhere in its field of view. This seemed to be ideal as the smallest possible pellets sizes to be used were 2mm, but the characteristics of the paper meant that the pellet holes closed slightly after penetration, causing a resolution problem. Therefore, it was essential to produce clean holes and special attention to paper quality was required for the smaller pellet diameters.

The holes on the test sheet were set at known distances apart to examine at what distance apart would the images of two holes merge. With each pixel representing 0.5mm it was found to be approximately 1mm or 2 pixels apart, but sensitive to the aperture settings. If the aperture allowed too much light in, the glare produced by each hole made them look bigger causing images to overlap. This meant that there was a compromise between the aperture settings required to acquire small holes (1mm) that did not produce much light and large holes (>3mm) in close proximity to one another.

From the holes on the test sheet it was also found that the pattern analysis system could generate pellet co-ordinates with an error less than 1mm in the middle of the field of view. At the corners and outer limits of the cameras field of view a hole had a maximum uncertainty of 5mm due to the lens distortion, where a mathematical correction algorithm could be implemented if thought necessary. From the pellet co-ordinates of the pellets

that struck the paper the pattern centre was calculated. One limitation of this part of the system was its sensitivity to the lateral spread of the shot cloud. Therefore when less than 100% of the pellets in the cartridge were intercepted by the paper an unknown error on the pattern centre was incurred. The majority of patterns taken at 40 yards showed at least 80% of pellet intercepted and at 30yds usually 100%. With the pattern also visually being fairly symmetrical the effects of these missing pellets are assumed to have negligible influence on the calculated pattern centre.

2.9 SUMMARY AND CONCLUSIONS

To produce comparative ballistics and reliable timing information the ballistics target and skyscreens have been shown to acquire leading edge data with a negligible uncertainty compared with the variation in the ammunition (section 3.2.1). The trailing edge data at 20m has a greater uncertainty dominated by the ringing time of 1ms which can be corrected for, but it is masked by the greater variation in ammunition. It is important to keep the timing errors much smaller than the variation in the ammunition to reduce the uncertainty in the results. From the timing information at various ranges the ballistic distribution of the pellets within a shot cloud was generated. The ballistics target also generated limited positional data which allowed three-dimensional reconstruction of the shot clouds outline. For greater positional accuracy on the lateral spread, the pattern analysis system obtained the pellet co-ordinates to within a few millimetres. This allowed the pellet distribution within the shot cloud to be calculated and analysed.

Due to the nature of the shot clouds dispersion it was not possible to construct a single measurement system which could obtain all the data. Ideally, it would have been better to follow a single shot cloud down range without interrupting its flight and show how it develops. Although this was not possible, the measurement system described in this chapter has produced timing and positional data on the distribution of pellets in a shot cloud to a accuracy which allows variation in results to be attributed to the ammunition. The ballistics system has been in full operation since mid-1994 for contractual use to help develop non-toxic alternatives to lead in shotgun cartridges.

Chapter 3

Shot cloud phenomena

3.1 INTRODUCTION

The measurement system described in the previous chapter produced voltage, time and range data from the ballistics target and lateral positional information on the pellets via the image processing equipment. In this chapter the raw data is analysed to determine the type of variation associated with the distribution and ballistic performance of pellets within a shot cloud. A consequence of the ballistic variation is a requirement to produce a representative result to describe the performance of a particular shot cloud. Therefore an optimum number of cartridges is necessary to generate a reliable averaged result whilst limiting the data acquisition time.

Using averaged flight time data for the leading and trailing edges of the shot cloud the longitudinal distribution of pellets is examined to ascertain the effects of altering the launch conditions (such as the internal ballistics of the barrel) and pellet properties. This approach produces the shot cloud length at any range between 20-50m. From the analysis of the shot cloud profile the pellet density along the shot cloud is calculated and this allows the nature of the longitudinal distribution of pellets to be found.

Traditionally, the lateral distribution of pellets has been determined by the pellet count within a 30" circle at 40 yards, but errors are generated from the inability of people to precisely place the circle on the pattern centre and count >10. In this investigation the lateral positions of the pellets are normalized about the pattern centre and the standard deviation of their x and y pellet co-ordinates are obtained. This gives a measure of the pellet dispersion and is used to examine the relationship between the lateral distribution of pellets and the internal ballistics of the barrel. A more in-depth investigation is then undertaken to determine the true nature of the lateral distribution of the pellets. It is then possible to examine the appropriateness of the traditional approximation that the average lateral pellet density distribution is a radial Gaussian. To conclude the analysis on the average lateral distribution of pellets, the Poisson process is shown to be an appropriate approximation for describing the hit probability distribution within small areas of the pattern.

The information generated on the longitudinal and lateral distribution of pellets in a shot cloud from the shot cloud profile and patterns only gives two-dimensional information. It is therefore not possible to determine whether , for example, the central pellets in the patterns are at the leading or trailing edge of the shot cloud. Finally, the combination of the lateral and longitudinal pellet distribution is assessed by the three-dimensional reconstruction of the shot cloud to resolve these questions.

3.2 SHOT CLOUD VARIATION

3.2.1 Construction of cartridge

The cartridge and barrel have a major influence on the downrange ballistic performance of a shot cloud because they set the launch condition for the pellets. To eliminate any unnecessary influence generated by the barrel on the launch conditions, a standardized proof barrel and chokes were used to produce a constant experimental set up between firings. The only experimental variations incurred between firings were in the atmospheric condition, which were found to alter <<1% over the typical period of a test, and the cartridge. A consequence resulting from the measurement system having to produce timing and pattern information between 20-50m at 5m increments and near-muzzle velocity measurements is that alike cartridges loaded to the same specification had to be used, such as the same production batch, and this was always done. The nature of the construction of a cartridge means that any small variation in its components will result in a different ballistic performance. For mass production cartridges components are loaded by volume, and therefore it is not possible to control the loading to a strict weight.

A convenient measure of the consistency within any sample is the ratio of the sample standard deviation (σ_s) to the average, or sample mean (m_s) as a percentage and is from now on referred to as the percentage variation (pv).

$$pv = \frac{\sigma_s}{m_s} \times 100 \qquad (3.1)$$

To establish the typical variation in the cartridge components and in order to produce ballistics reports, unfired cartridges were routinely opened and their contents measured. It was found that the typical percentage variation in the number of pellets was 1% for mass produced cartridges. This variation in the number of pellets along with the variation in pellet mass, which is controlled by the pellet diameter, affects the load weight of the cartridge and was seen to vary by 1% (Table 3.1). Changing the load weight alters the time/pressure curves associated with the pressure build up in the barrel, as a different amount of pressure is then required to start the load moving. The main property which controls the pressure is the amount of powder and the rate at which it burns. Another property which changes the pressure build up is the strength of the crimp on the cartridge case. The variation in pressures, created by the powder and crimp, and projectile weight alter the acceleration (a) of the projectile up the barrel (Newton's fundamental law $F=ma$, where force, F, is created from the pressure and mass, m, is the load weight). The different acceleration of the loads result in a variation of the muzzle varying and, therefore, different downrange ballistics of the shot cloud.

Material	Percentage variation (*pv*)			
	Load	Pellet count	Powder	Pellet diameter
Lead	0.9	1.0	0.7	2.7
Steel	0.9	1.0	0.9	1.8
Bismuth	0.9	1.0	0.6	2.8
Zinc	1.1	1.4	1.0	3.9
Hand loaded	0.2	0.4	0.4	2.5

Table 3.1 *The typical percentage variation (pv) in cartridge components for mass produced cartridges with different pellet material. Also included are the typical standards achieved by hand-loading.*

For cartridges which have been specially loaded by hand to achieve a certain performance, a greater control was obtained on the load weight, pellet count and powder weight with percentage variation smaller than that of the mass produced loads. The only component which cannot be controlled to the same high tolerance is the pellet diameter

(except by selection which is too time-consuming). Here the percentage variation is the same as seen in the mass produced cartridges, probably due to the pellets being supplied from the same source.

Once the pellets have left the barrel and the initial interaction between them is complete, they can be regarded as individual spheres in free flight. At this point, the drag force acting against them is modelled by (1.1) and for identical composite materials it is proportional to pellet diameter, assuming their velocities and shapes are the same. The variation in pellet diameter (Table 3.1) creates different deceleration effects on the pellet, whereby the smaller ones encounter a greater drag and take longer to reach the same distance as the large pellets, and a stringing-out process occurs.

An important property of the pellets is their shape. This alters the behaviour of the drag coefficient in (1.1) and therefore affects their deceleration. From measurement and observation of the unfired pellets it can be seen in Table 3.1 and Figure 3.1(a) that there is a percentage variation of 2.65% in the diameter and a visible variation in the shape of the lead pellets. The variation in the unfired pellets has only an effect on the weight of the load. It is more important to observe the true shape of the pellet when in flight, such as after firing when the pellets have been compressed together in the barrel and squeezed through a choke. To retrieve the fired pellets it was necessary to collect them in a given area where it was known that they have not encountered further damage. This was achieved by placing boxes filled with bubble wrap sheets on the target. When the pellets penetrated the sheets they were brought to a gentle halt without further deformation. From collecting the fired pellets it can be seen in Figure 3.1 that there is a greater variation in pellet shape and size compared to that of the unfired pellets. The result of this greater variation in shape will theoretically (shown later in the chapter) alter the deceleration of the pellets and generate a stringing-out effect.

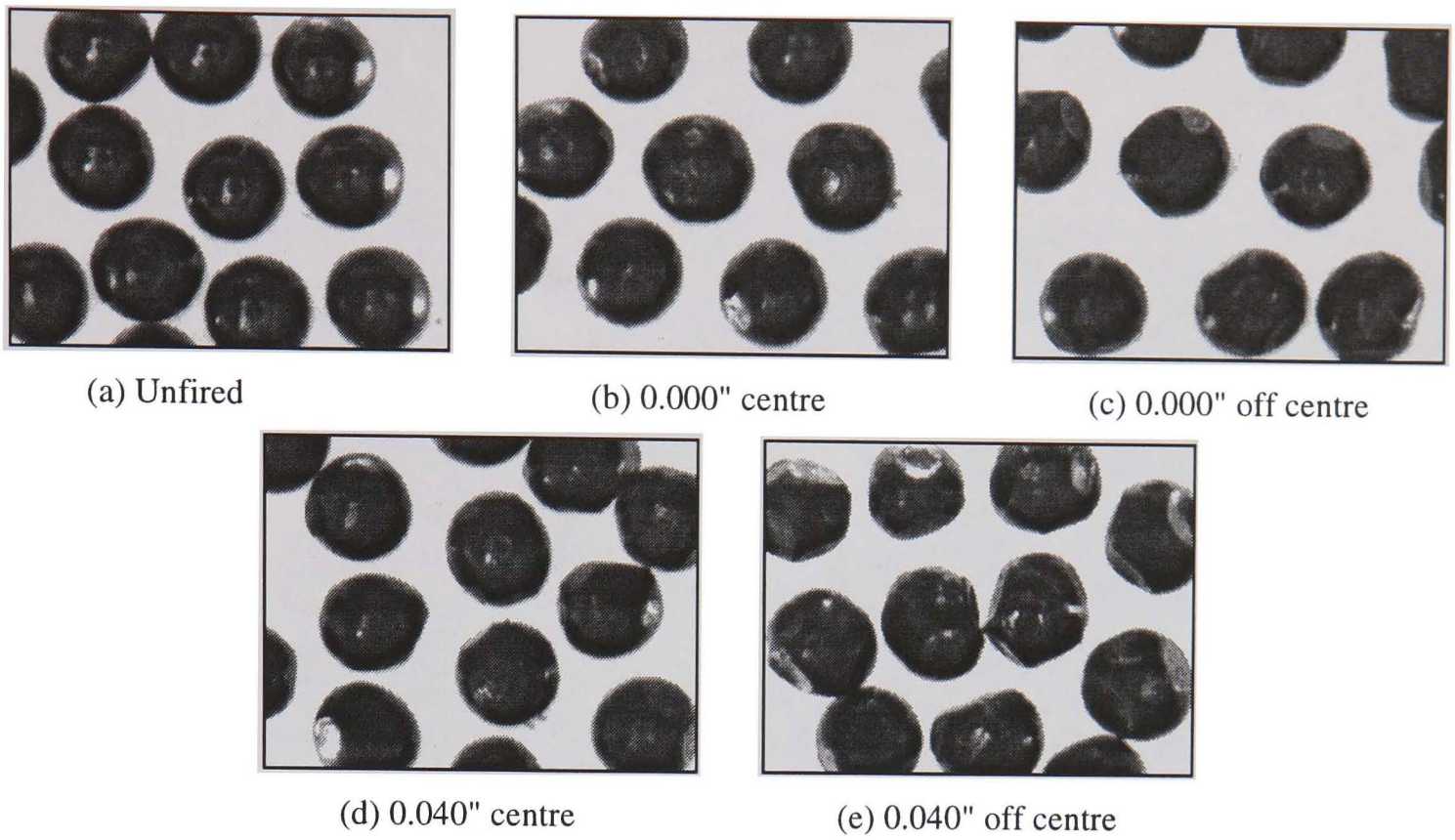

Figure 3.1 *The unfired pellets (a) for a 32g load of #4 lead shot. The pellets in (b)-(e) have been fired through either a 0.000" or 0.040" choke constriction and recovered in the pattern centre or 30" away from the pattern centre at 40yds.*

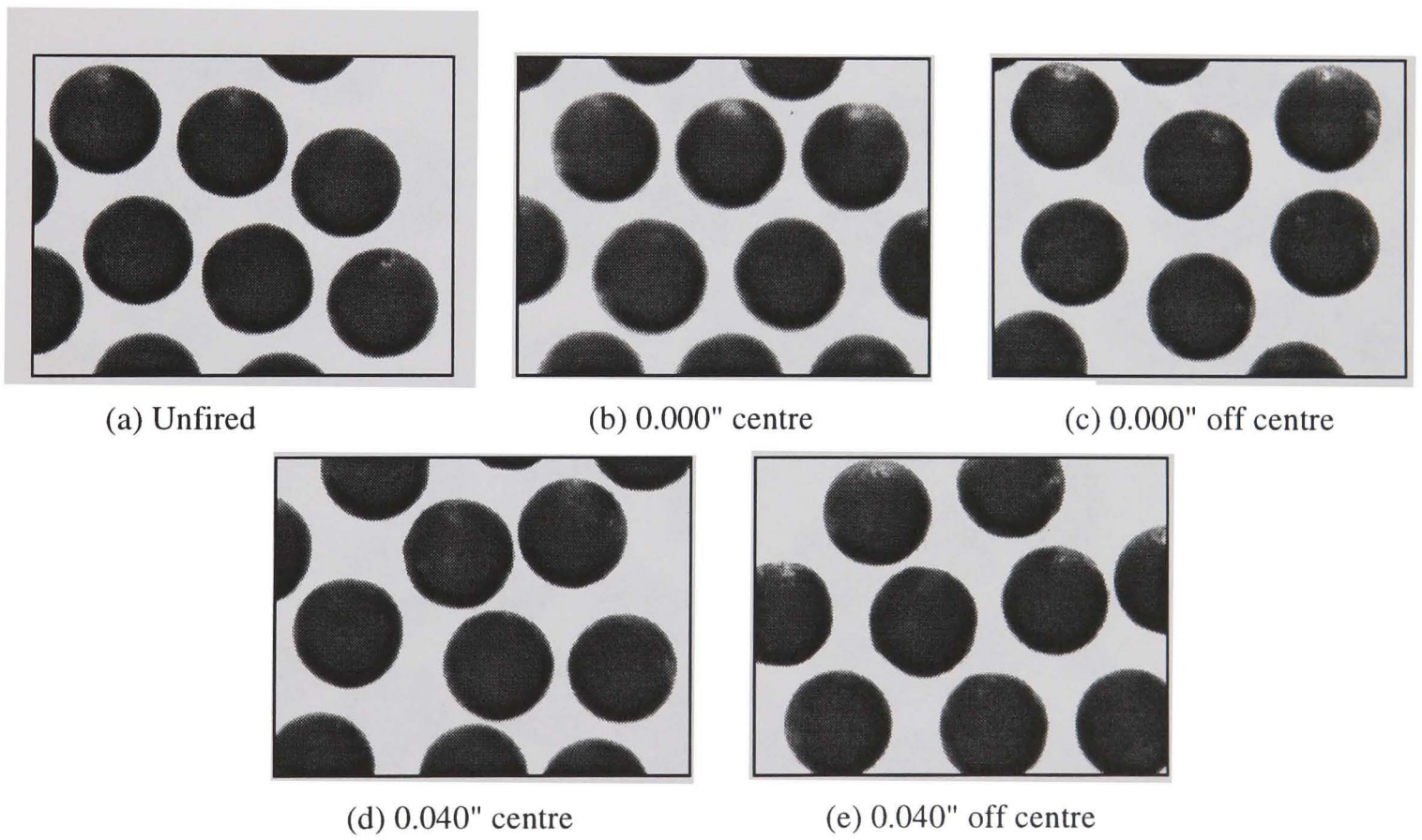

Figure 3.2 *The unfired pellets (a) for a 32g load of #4 steel shot which has been blackened. The pellets in (b)-(e) have been fired through either a 0.000" or 0.040" choke constriction and recovered in the pattern centre or 30" away from the pattern centre at 40yds.*

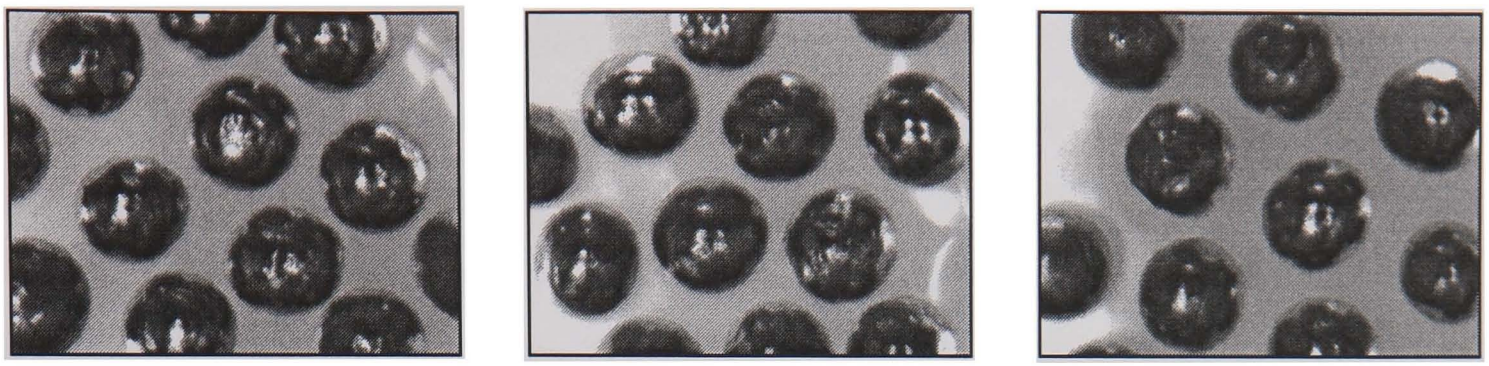

(a) Unfired (b) 0.000" centre (c) 0.000" off centre

(d) 0.040" centre (e) 0.040" off centre

Figure 3.3 *The unfired pellets (a) for a 33g load of #4 zinc shot. The pellets in (b)-(e) have been fired through either a 0.000" or 0.040" choke constriction and recovered in the pattern centre or 30" away from the pattern centre at 40yds.*

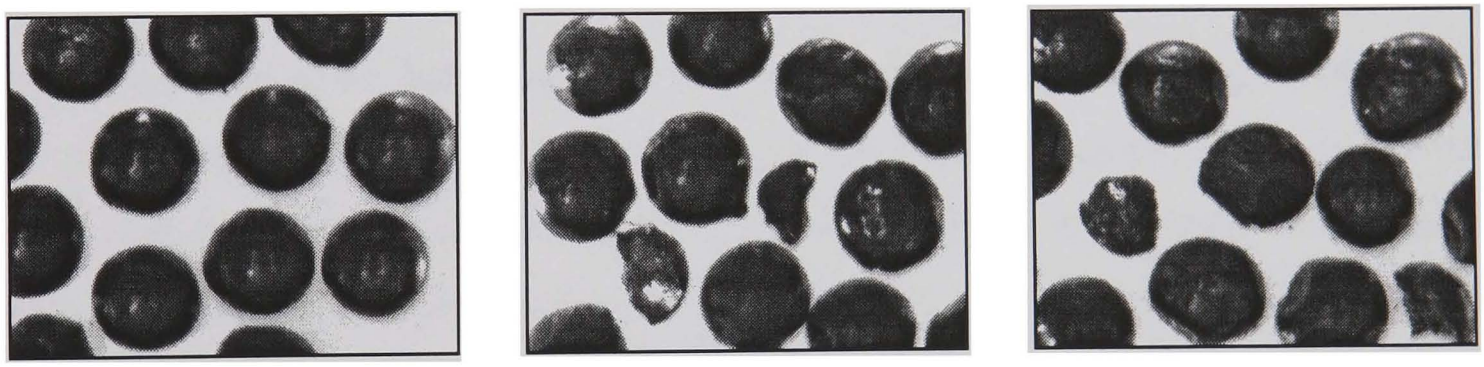

(a) Unfired (b) 0.000" centre (c) 0.000" off centre

(d) 0.040" centre (e) 0.040" off centre

Figure 3.4 *The unfired pellets (a) for a 32g load of #4 bismuth shot. The pellets in (b)-(e) have been fired through either a 0.000" or 0.040" choke constriction and recovered in the pattern centre or 30" away from the pattern centre at 40yds.*

The bubble-wrap test was carried out on several pellet materials and choke combinations. On inspection (Figure 3.2) it was found that steel pellets were approximately spherical and suffer little deformation when passed through the choke. This finding led to a decision that steel pellets would be used where possible for experimental data and theory that required single spheres in free flight. It was noted that for the softer materials, such as lead and zinc (Figure 3.3), the pellet deformation and shape variation was greater than that of steel. However, the zinc pellets had the worst percentage variation (3.85%) in their initial pellet diameter and from the observation of the unfired pellets there was a larger variation in shape seen than in any of the other materials. This made it difficult to determine the actual deformation of the pellets in flight. In the case of bismuth (Figure 3.4), a brittle material when pure but alloyed for shotgun applications, there were small pieces of the material found in the bubble wrap. This suggested that fragmentation had occurred on a small percentage of pellets that have been fired. The remaining fired bismuth pellets seem to experience the same deformation as encountered by the lead pellets.

On examination of the bubble wrap at the pattern centre and comparing it with that at 30" off centre, it was possible to locate where the worst shaped pellets travel. It was found that they, in general, were striking the outer section of the target, whereas the more spherical pellets were found in the pattern centre. However, for Bismuth an equal distribution of small fragments were located around the target, and for complete pellets the more deformed were located at the edges.

The effect of choke on the deformation of the fired pellet was studied. With the exception of steel pellets, it was found that the greater the constriction, the worse their shape became. This is shown in Figures 3.1, 3.3 and 3.4 for lead, zinc and bismuth pellets passing through 0.000" and 0.040" of choke constriction.

One component in the modern shotgun cartridge which has yet to be mentioned is the plastic wad. The wad holds the pellets, in theory, until a short time after exiting the muzzle, after which it falls away from the load, due to its inferior aerodynamic performance. Therefore the wad has the final influence on the pellets after they have

left the barrel. It has been noticed that within a batch of cartridges there was occasionally a variation in the appearance of the wads. They could be of different design, have different number of cushioning layers, different numbers of cuts in the wall of the wad, and can be inconsistent in the depth of the cuts. The variation in the wads had a great effect on the patterns because if the wad does not release the pellets consistently then the initial spread is altered, and therefore so is the final pattern. It has been observed that the wads do not open in the same way and fall away to different parts of the test range. They have been seen to travel with the shot for a long period of time (seen in the shot cloud profile and by the skyscreens), spin off at strange trajectories (visually), possibly spilling the pellets, or fall away quickly leaving the pellets to travel downrange.

The overall effects of the choke and cartridge components on the ballistic variation of a shot cloud is not being addressed here, but the inconsistency in the construction of the cartridges is given to show that it is not possible to produce identical cartridges.

3.2.2 Consistency in flight times

The skyscreens and ballistics target generate timing, range, and voltage data. The voltage data is of no relevance when determining the flight times of different parts of the shot clouds, as it is only an indicator of a pellet's arrival. In section 2.8.2 the near-muzzle measurements were shown only to produce reliable timing information for the leading edge of the shot column. The analysis of this raw flight time measurements for any material has indicated that the percentage variations on an average of ten cartridges (the reason for ten is explained later) over the eight skyscreens are very similar. It was observed, however, that each material had its own typical percentage variation and in Table 3.2 the average from all lead loads tested is shown to produce the smallest variation in the initial stages of flight (0-8m). For steel loads a double peak was detected which varied around 1.3% and 2.3%. The remaining percentage variations shown in Table 3.2 are for material which have been averaged over a smaller number of loads (<15), due to the limited supply obtained, making it more difficult to justify the assumptions.

Material	Percentage variation (*pv*)		
	Minimum	Maximum	Average
Lead	0.6	2.1	1.1
Steel	1.0	2.5	1.7
Bismuth	0.8	2.5	1.6
Zinc	0.6	1.7	1.2

Table 3.2 *The maximum, minimum and average percentage variation on the leading edge near-muzzle flight times for a selection of pellet materials.*

To obtain flight time information on shot clouds at ranges between 20 and 50 metres the ballistics target is used and from the output the shot cloud profile is generated. From the shot cloud profile (Figure 2.21) it is possible to identify and obtain timing information on four distinct parts of the shot cloud. As explained in section 2.5.1 the timing information t_1 and t_4 represent the leading and trailing edges of the whole shot cloud and include any pellets which travel in front or behind the main section. From routine measurements of these four timing points the percentage variation for t_1 and t_4 has been measured to be a least double that of the leading and trailing edge of the main section of the shot cloud t_2 and t_3. This is due to the erratic occurrence of the stray pellets (or 'fliers') shown in Figure 2.21.

An alternative approach considered for generating timing information on different section of the shot cloud was a calibration technique performed on the shot cloud profile (describe later in section 3.3.3). Timing data was produced that represents the arrival of a certain percentage of the total number of pellets at the target. Using this procedure the averaged flights times for 5% and 95% of the pellets reaching the target were found to have similar percentage variation to the observed values t_2 and t_3. In Table 3.3 the observed flight times and processed data representing several arrival percentages are shown for a 36g load of #3 lead shot. It was decided after examining a large selection of different cartridges (over 150 different batches) that the most consistent and easily identifiable flight time measurements produced by the ballistics target were t_2 and t_3 and of these, the leading edge of the main shot cloud, t_2, was the more consistent.

Range (m)	Percentage variation (*pv*)							
	Observed time		Percentage of pellets arrived at target					
	t_2	t_3	5	10	20	80	90	95
20	1.1	1.7	1.0	1.0	1.0	1.6	1.7	2.0
30	1.2	1.7	1.0	0.9	1.0	1.6	1.6	1.2
40	1.0	1.5	0.7	0.8	0.7	1.5	1.4	1.5
50	0.6	1.2	0.6	0.5	0.5	1.0	1.1	1.3

Table 3.3 *The percentage variation on the average flight times at a selection of ranges for a 36g load of #3 lead shot using 0.030" choke.*

The flight time data measured by skyscreens showed that the percentage variation on the average of 10 cartridges changed for different types of pellet material. The same relationship is observed when examining the percentage variation for t_2 and t_3. The most consistent part, on average, of a shot cloud containing lead pellets is shown in Table 3.4 and Figure 3.5 to be the leading edge t_2 with the trailing edge t_3 30% larger. Examining the limited flight time data on shot clouds containing either bismuth or zinc pellets a similar trend was also seen, but in these cases the percentage variations are greater.

Material	Percentage variation	
	t_2	t_3
Lead	1.2	1.5
Steel	1.8	1.5
Bismuth	1.5	2.0
Zinc	1.4	1.5

Table 3.4 *The typical average percentage variations in t_2 and t_3 over 20-50 metres for a selection of pellet materials.*

For shot clouds containing steel pellets the trailing edge flight times t_3 were found to be the most consistent part of the shot cloud. The reason for this is that the stray pellets are commonly observed to arrive before the main section of the shot cloud generating a greater variation. Therefore the most consistent edge of the shot cloud is dominated by the side with the least occurrence of stray pellets.

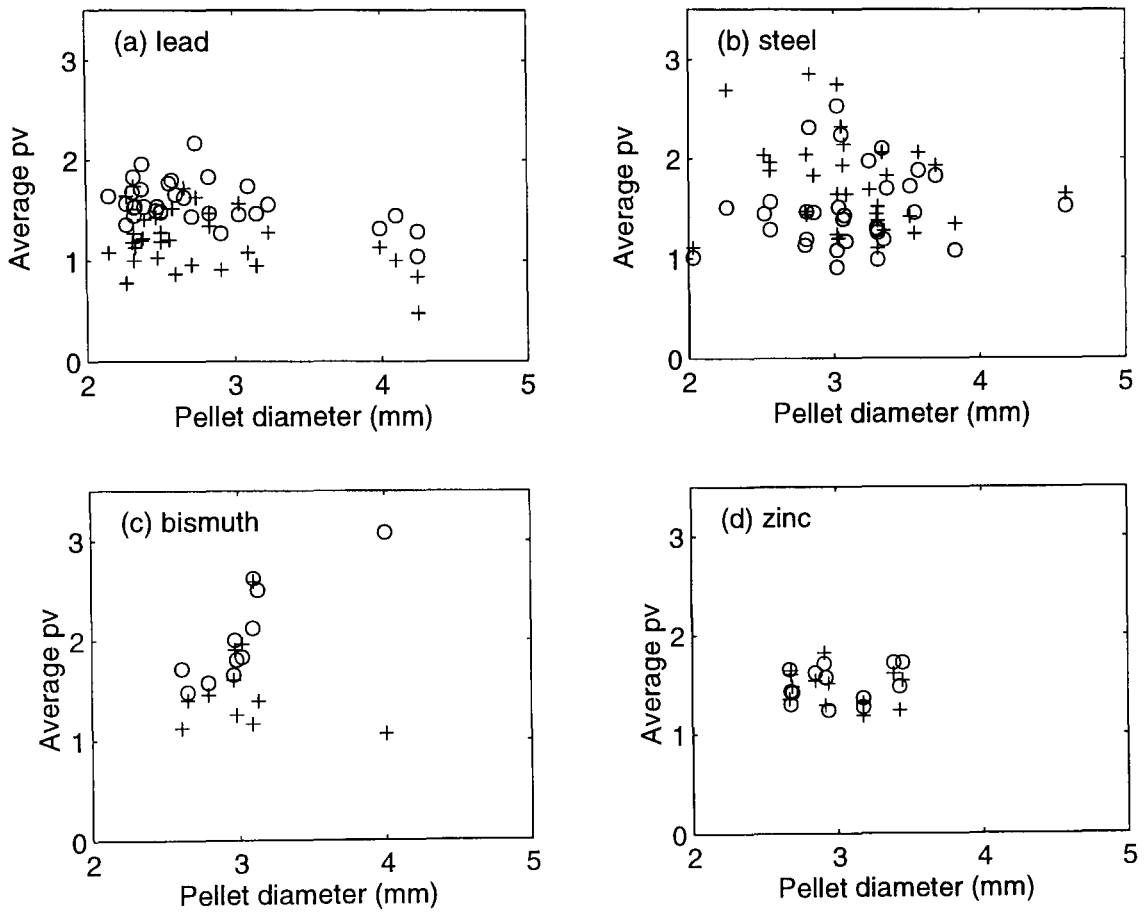

Figure 3.5 *The average percentage variation observed in t_2 (+) and t_3 (o) flight times over 20-50 metres for a selection of pellet diameters and materials.*

3.2.3 Lateral pellet distribution

The majority of data collated on the lateral distribution of pellets within shot clouds was produced from the pattering of shotgun ammunition sent for testing at the measurement facility. In these tests, patterns were taken at 30 and 40 yards to determine the pellet counts in a centred 30" diameter circle. The two counts are a traditional measurement in shotgun ballistics and the areas associated to these circles were taken simply as a matter of convenience. The custom was adopted in the last century when gun makers first began to investigate the patterning ability of their guns, and now has become so thoroughly established that any change would produce irrelevant or at least difficult to

interpret data for the shooting community. A more fundamental approach is used during this investigation into the lateral distribution of pellets which analysis the standard deviation of the x and y axis of the pellet co-ordinates, but the traditional 30" circle measures are still referred to for completeness.

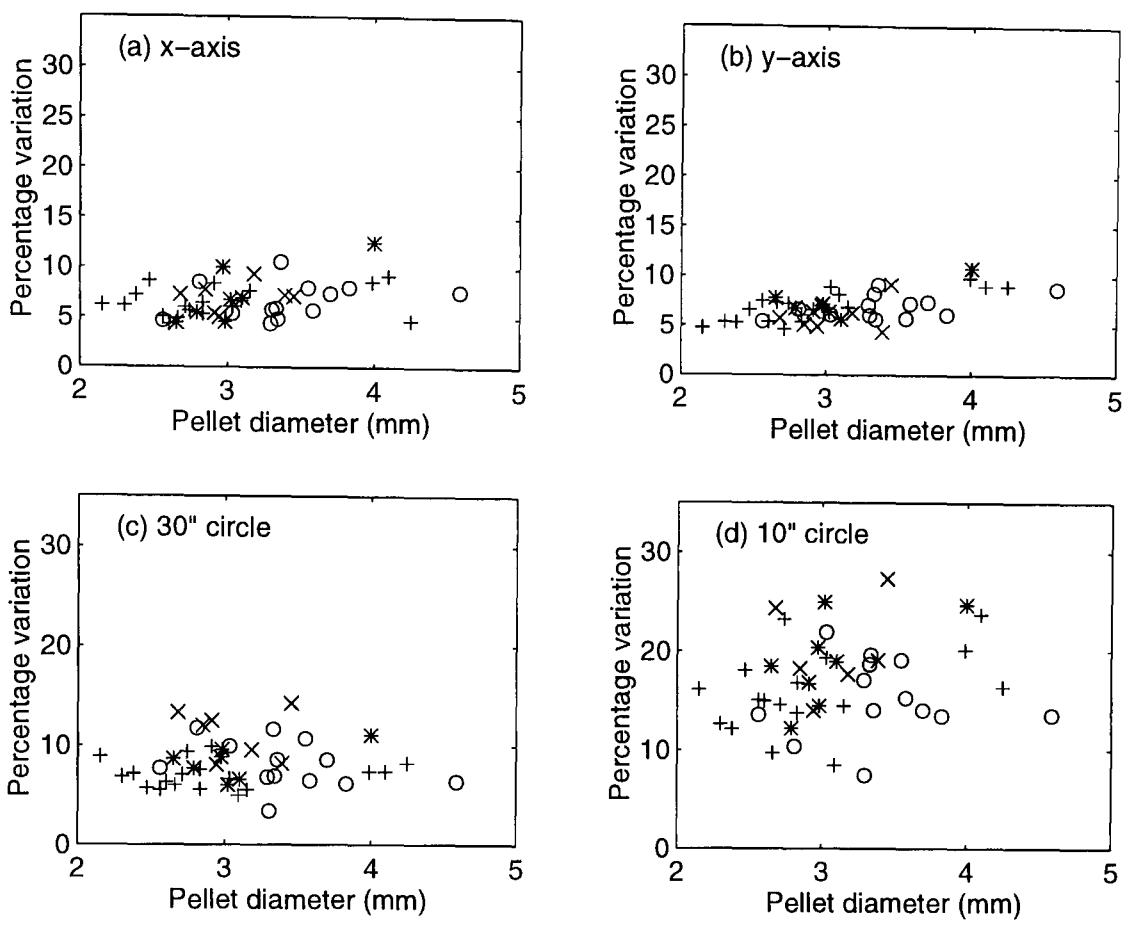

Figure 3.6 *The lateral percentage variation of the pellet co-ordinates in the x- and y-axis and the pellet counts in a 10" and 30" circle at 40 yards for lead (+), steel (o), bismuth (*) and (x) zinc loads.*

The results from the pattern tests have shown that the greatest variation associated with shotgun ballistics is in the lateral pellet distribution. It was found and can be seen in Figure 3.6 that the standard deviation of the pellet co-ordinates in either the x or y directions at a particular range, in this case 40yds, has a typical percentage variation between 5-10% for a sample of 10 patterns. This pattern variation was fairly constant between material and independent of choke and range, unlike that in the ballistics where the material density altered the typical variation. When analysing the traditional 30" circle measure, the pellet count in a 30" circle at 40yds was also found to produce the same order of percentage variation, but this measure is sensitive to the lateral spread of pellets and the size of the circle. If too large a circle is chosen all the pellets will be encompassed suggesting little variation occurs and the use of too small a circle gives a

larger variation, as seen in Figure 3.6(d).

3.2.4 Obtaining a reliable average

With the variation in ballistics, especially patterns, between cartridges from the same batch, a sufficient number should be tested at each range to obtain a reliable averaged result. When increasing the number of cartridges tested at a given range the average results start to converge. In Table 3.5 the average results for different number of cartridges and their corresponding percentage variations are shown for the leading edge flight times for the skyscreens at 8m, the ballistics target at 50m and patterns at 40yds. It is noted that the average obtained converges rapidly if more than five cartridges are used for all measurements. When averaging over 10 cartridges the results converge to a factor of ten less than the percentage variation seen in the corresponding measurement. It was therefore decided that a compromise of 10 cartridges at each range produces a practical optimum between a reliable average and an excessive acquisition time.

Averaged number of cartridges	Flight time to 8m		Flight time to 50m		Standard deviation in the *x*-direction	
	m_s (ms)	*pv*	m_s (ms)	*pv*	m_s (mm)	*pv*
1	22.17	-	223.2	-	324.7	-
2	22.21	0.04	221.1	2.12	301.5	7.69
5	22.25	0.20	220.6	1.47	292.8	7.06
10	22.25	0.83	219.9	0.95	287.3	7.28
20	22.27	0.81	220.0	0.78	287.4	6.76
40	22.28	1.03	219.9	1.86	286.6	5.82

Table 3.5 *The mean and percentage variation averaged over different numbers of cartridges for a 36g load of #3 lead shot flight time measurements at 8 and 50m, and the standard deviation of the x-axis pellet co-ordinates at 40yds for a 32g load of #3 steel shot.*

3.3 BALLISTICS : LONGITUDINAL SPREAD

3.3.1 Near-muzzle behaviour

The measurement system was primarily designed to gather data on shot cloud dispersion at ranges between 20-50m. The addition of the skyscreens enabled limited near-muzzle information to be obtained. As described in section 2.8.2, the skyscreens which were available for use in this investigation could only register the leading edge of the shot column reliably and information on the longitudinal and lateral spread of pellets near the muzzle could not be achieved. From the limited data, it was possible to observe the change in the leading edge flight time, and therefore the velocity, of the shot cloud for different internal shotgun characteristics. In Table 3.6 the average leading edge shot column velocities at 2.5m over 10 cartridges are given for a selection of pellet materials and choke constrictions. The range of 2.5m has been chosen as a convenient near-muzzle measurement as it is the new standard in shotgun cartridge regulation for steel.

To determine the accuracy of the averaged data points and therefore the relationship between choke constriction and the leading edge shot column velocities, the standard error on the mean of the sample is used,

$$SE = \frac{\sigma}{\sqrt{N}} \quad , \tag{3.2}$$

where N is the number of patterns and σ is the standard deviation of the sample. In this case, the sample is the leading edge shot column velocites for 10 cartridges. From (3.2) it can be seen that it is necessary for four times as many samples to be taken to obtain an average which is twice as accurate. This agrees with the intuitive idea that more cartridges are required to increase the confidence on the average.

The near-muzzle leading edge velocities measured using cartridges from the same production batch for choke constrictions less than 0.030" were observed (shown in Table 3.6 for 2.5m) to have similar averages at ranges below 4 metres. The small variations between the velocities for choke constrictions less than 0.030" are shown in

Table 3.6 to be within the standard errors of the measurements. For more constrictive chokes, such as >0.030", it was found that leading edge shot column velocity increased slightly (more than the associated standard errors on the measurements) compared to the less constrictive chokes. However with less than a 2% difference in the velocities of the extreme constriction, the choke is assumed to have a minor affect on the leading edge shot column velocity. Unfortunately it has not been possible to examine the behaviour of bismuth in these tests due to the limited supply available.

Material	2.5m leading edge velocities for different choke constriction and the *SE* in brackets. (m/s)		
	0.000"	0.020"	0.040"
32g load of #6 lead shot	409 (1.6)	411 (0.9)	413 (2.1)
28g load of #7$^1/_2$ lead shot	396 (1.7)	397 (1.9)	402 (1.6)
32g load of #3 steel shot	361 (0.8)	363 (2.2)	369 (1.8)
28g load of #1 steel shot	430 (1.1)	431 (2.4)	437 (1.5)
30g load of #3 zinc shot	389 (1.7)	390 (1.4)	397 (1.2)
28g load of #5 zinc shot	418 (1.4)	420 (1.5)	426 (1.0)

Table 3.6 *The averaged leading edge shot column velocity at 2.5m from 10 cartridges and its associated standard error (given in brackets) for a selection of pellet materials and choke constrictions.*

The chamber length of a barrel is designed to take the length of a fired cartridge case. As the barrel is fitted with interchangeable chamber sleeves the standard 2$^3/_4$" length cartridges were fired through different chamber lengths. In Table 3.7 the effects of altering the chamber length are shown to be minimal (standard errors) on the leading edge shot column velocity for all materials. Therefore the effects of altering the internal ballistics of the barrel, via choke constriction and chamber length, on the leading edge of the shot columns initial velocity are assumed to be negligible.

Material (all $2^3/_4$" cartridges)	2.5m leading edge velocities for different chamber lengths and *SE* in the brackets. (m/s)		
	$2^1/_2$"	$2^3/_4$"	3"
28g load of #$7^1/_2$ lead shot (0.000")	380 (1.3)	374 (1.4)	374 (0.9)
28g load of #$7^1/_2$ lead shot (0.030")	385 (1.3)	384 (1.2)	383 (1.3)
32g load of #3 steel shot (0.000")	362 (1.4)	358 (2.0)	360 (2.0)
32g load of #3 steel shot (0.030")	394 (0.9)	390 (1.6)	393 (1.4)
30g load of #4 zinc shot (0.030")	426 (1.0)	430 (2.2)	426 (2.6)

Table 3.7 *The average leading edge shot column velocity at 2.5m from 10 cartridges and associated standard error for a selection of pellet materials (all $2^3/_4$" cartridges) and chamber lengths.*

The skyscreens are unable to generate information on the longitudinal and lateral distribution of pellets in a shot cloud, but they do allow the wad to be observed as it separates away from the shot cloud. From the silhouette outlines generated by the skyscreens which represent the two entities, it was found that they are inseparable at 1m from the muzzle. The wad starts to become distinguishable from the shot cloud at 2m onwards and in Figure 3.7 the separation times and distances between the leading edge of ten shot clouds and their wads are given. The inconsistency in the separation distances in Figure 3.7a(ii) and b(ii) is clearly seen for both the lead and steel loads. This variation in separation must generate different interactive effects between the wad and the pellets, thus altering the initial spread of pellets. In Figure 3.7b(ii) it can be seen that for three of the steel cartridges fired, the wad separation is very gradual compared with the others. By retrieving the wads, some designs of steel cartridges have been discovered with pellet embedded in their base, thus giving them extra momentum. This would cause the wad to maintain its velocity and travel in a close proximity to the pellets, unlike the desired performance of the wad which falls away quickly so as to produce little interference with the shot cloud.

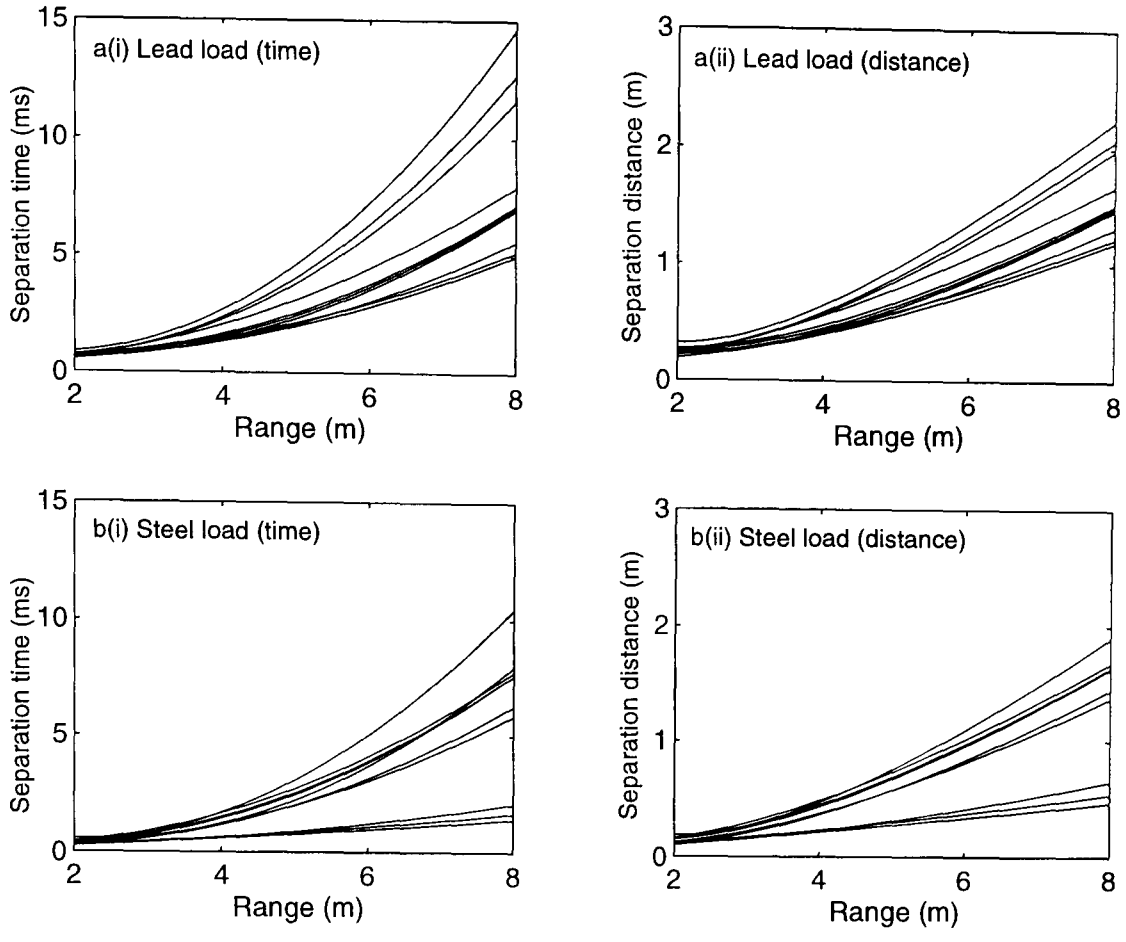

Figure 3.7 *The wad separations in time and distance from the leading edge of the shot column, for a 36g load of #3 lead shot (0.030" choke) and a 32g load of #3 steel shot (0.020" choke).*

The limited available data from the skyscreens has shown that the leading edge muzzle velocity is relatively unaffected by the choke constriction. It has also been possible to show that the initial conditions of the shot clouds are not identical since the influence of the wad on the pellet changes between loads. This information can only explain a small amount of the initial development of a shot cloud. In order to examine the full effects, the internal ballistics of a gun have on the distribution of pellets in a shot cloud it is necessary to investigate the near muzzle behaviour in much more depth. A possible tool for this would be high speed photography.

3.3.2 Changing the internal ballistics of the gun

A minimal effect was seen on the leading edge velocity of the shot column at ranges below 4m when the internal ballistics of the barrel were altered. At ranges between 20-50m more detailed information is obtained using the ballistics target. From the time-range data, velocities for the leading and trailing edges of the shot cloud and its length are obtained (see section 4.2 for more details on the analysis of flight time data). In

Figure 3.8 the leading edge velocities are given for several different material loads (where supplies allow) and it can be seen that altering the choke has an effect on the downrange ballistics of the shot cloud. For lead, steel and zinc loads which pass through a tighter constriction (solid line) a higher leading edge velocity is obtained at 20-50m, the trailing edges also increased but are not shown.

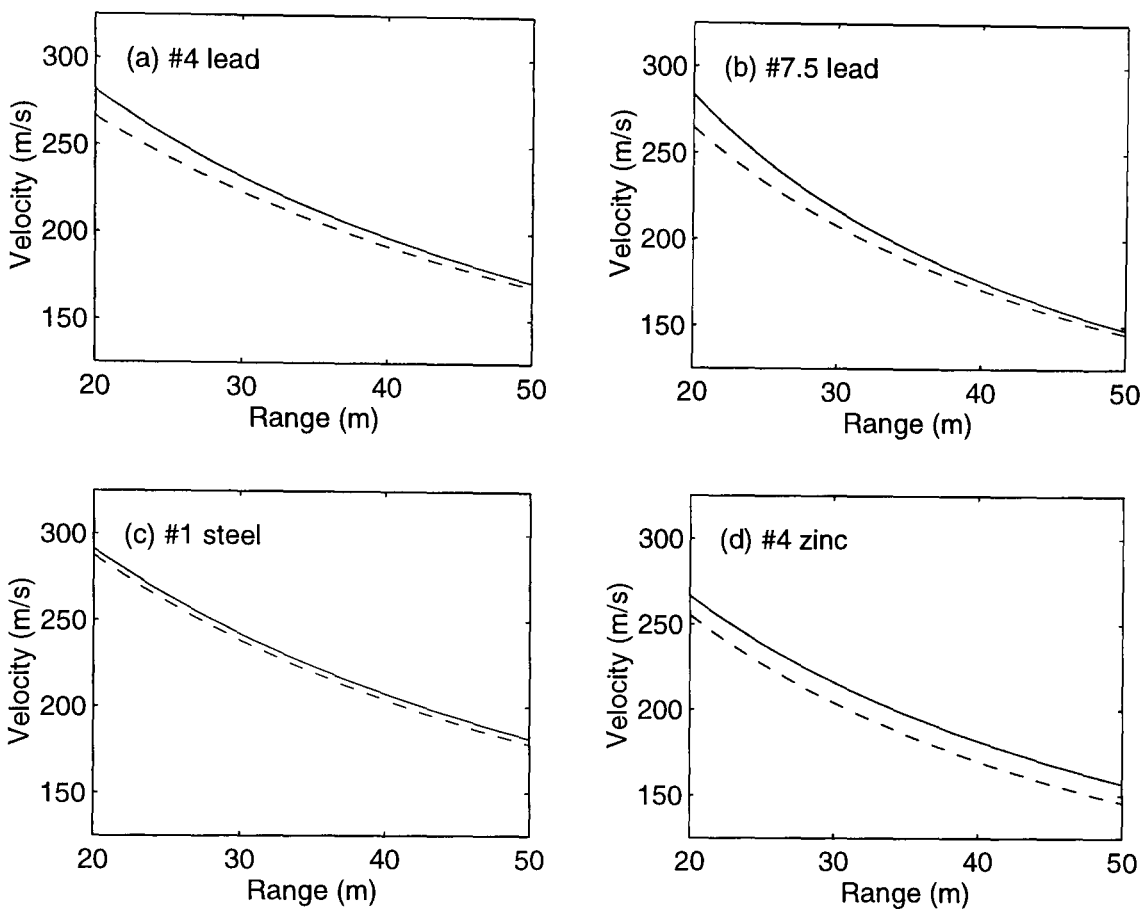

Figure 3.8 *The leading edge shot cloud velocities generated from choke constrictions of 0.000" (--) and 0.040" (solid line) for (a) a 36g load of #4 lead shot, (b) a 28g load of #7$^{1}/_{2}$ lead shot, (c) a 28g load of #1 steel shot and (d) a 30g load of #4 zinc shot between 20 and 50 metres.*

An explanation for the increase in velocity with a more constrictive choke is the pellets slip stream one another and generate a more aerodynamic shape for the shot column, thus maintaining their velocities for longer. The sparkshadow photographs (Figure 1.6) generated by Lowry in the 1970s established that an increase in choke constriction lengthens the initial longitudinal spread of pellets and reduces the lateral spread. He showed that for a load of #7.5 lead shot that at 18 feet (5.5m) the tighter full choked barrel produced a more compact cloud in the direction of the air flow. This smaller area in the direction of flow creates a more aerodynamic shape where the dispersion of the shot cloud takes longer, compared to the more diffuse cloud produced by the less

constrictive choke, for the pellets to become independent in free flight. Therefore pellets in a shot cloud produced by the tighter choke spend less time subject to the full force of the air resistance and achieve a greater velocity downrange. This is confirmed in Figure 3.8 where a negligible difference at the muzzle increases to, typically, 5% at ranges between 20-50m when the choke constriction is increased from 0.000" to 0.040". A consequence of a higher pellet velocities, if they are travelling in the transonic regime, is that they experience a greater drag. This results in the difference between the two sets of leading edge shot cloud velocities slowly reducing from the point when the more constrictive choked pellets become independent.

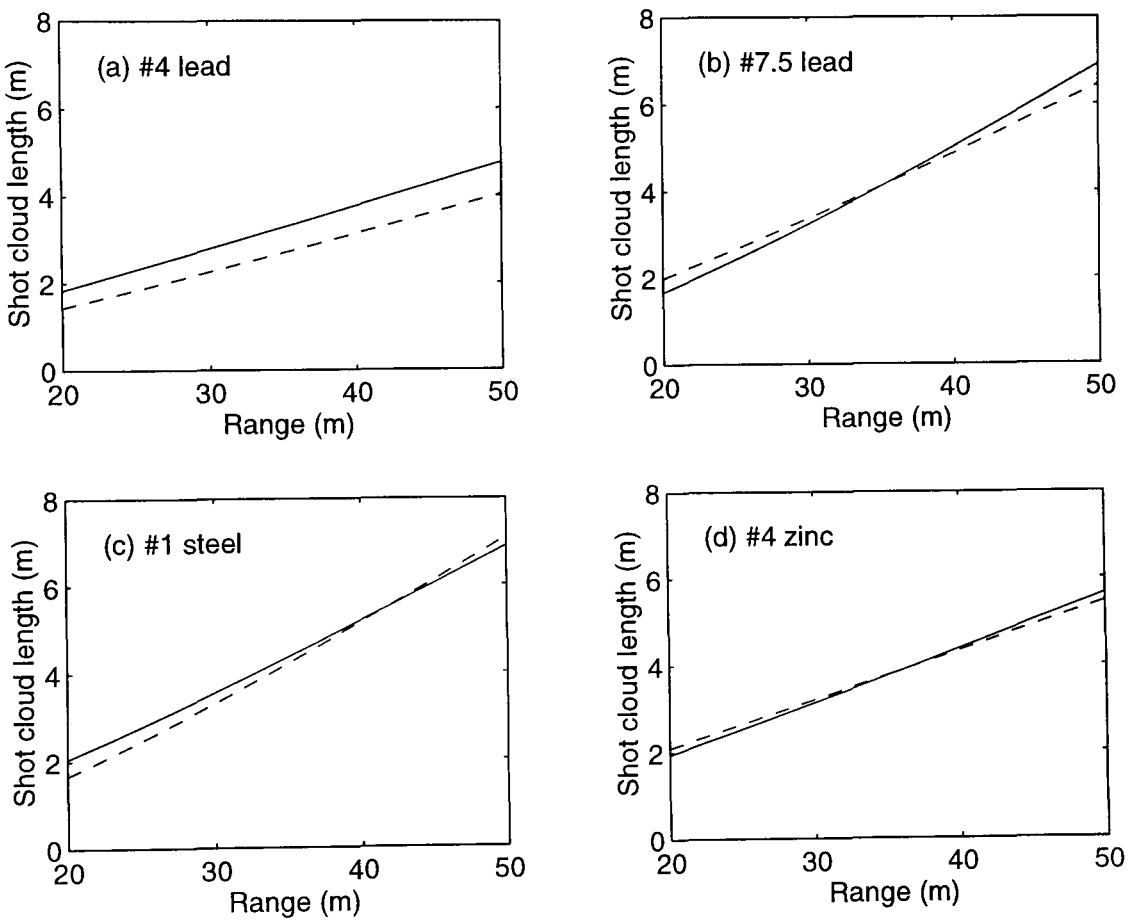

Figure 3.9 *The shot cloud lengths generated from choke constrictions of 0.000" (--) and 0.040" (solid line) for (a) a 36g load of #4 lead shot, (b) a 28g load of #7½ lead shot, (c) a 28g load of #1 steel shot and (d) a 30g load of #4 zinc shot between 20 and 50 metres.*

The shot cloud length is a measure for the maximum longitudinal distribution of pellets and is described in section 4.2.6 as the distance between the leading and trailing edges of the shot cloud when the leading edge is at a specified range. Over the period of this investigation a large ballistics database (150 batches) has been generated on different types of pellet materials, loads and chokes and from this no specific relationship has

been found between choke constriction and shot cloud length. Using the flight time data for the lead loads shown in Figure 3.8, the length dependence on choke constriction is illustrated to be very inconsistent in Figure 3.9.

The initial distribution of pellets in the longitudinal direction of the shot cloud has been shown by Lowry to increase with choke constriction. However, from his sparkshadow photographs (Figure 1.6) it was observed that this relationship between choke and shot cloud length changes at a certain range, in the case of the 28g load of #$7^1/_2$ lead shot it was 18 feet. Here the shot cloud produced by the more open cylinder choke becomes longer than the corresponding full choke cloud. Therefore the effects of choke on the longitudinal distribution of pellets diminishes, and the in-flight effects increase, the further from the muzzle the shot cloud travels. At 20-50m the shot cloud length for the more constricted choke would then be shorter, if the in-flight effects were the same, but in Figure 3.9 this is shown not to be the case, suggesting a more complex effect. It is known that the pellets stay compacted for longer in both the lateral and longitudinal direction when fired through the tighter choke, but the greater corresponding pellet deformation, as shown in section 3.2.1, generates an increase in their drag once they experience the full effects of air resistance. The variation in pellet shape could create a greater dispersion than the less deformed pellets associated with the more open choke. Therefore the longitudinal distribution of the shot cloud at the measurement ranges 20-50m is controlled more by the variation in aerodynamic performance of the pellets rather than the initial spread produced by the choke.

The shot cloud length behaviour, for any pellet material, at ranges between 20-50m has indicated that it has no relationship with the initial launch condition. However, a trend has been observed between different loads of pellet materials with the same diameter and load weight. In Figure 3.10 the shot cloud lengths are given for a selection of 32g loads containing either lead, steel, bismuth, or zinc #5 shot. It has been shown in general that the steel load produces the shortest length over the measurement range, whereas lead loads are of similar length at 20m but produce a much longer shot cloud at 50m.

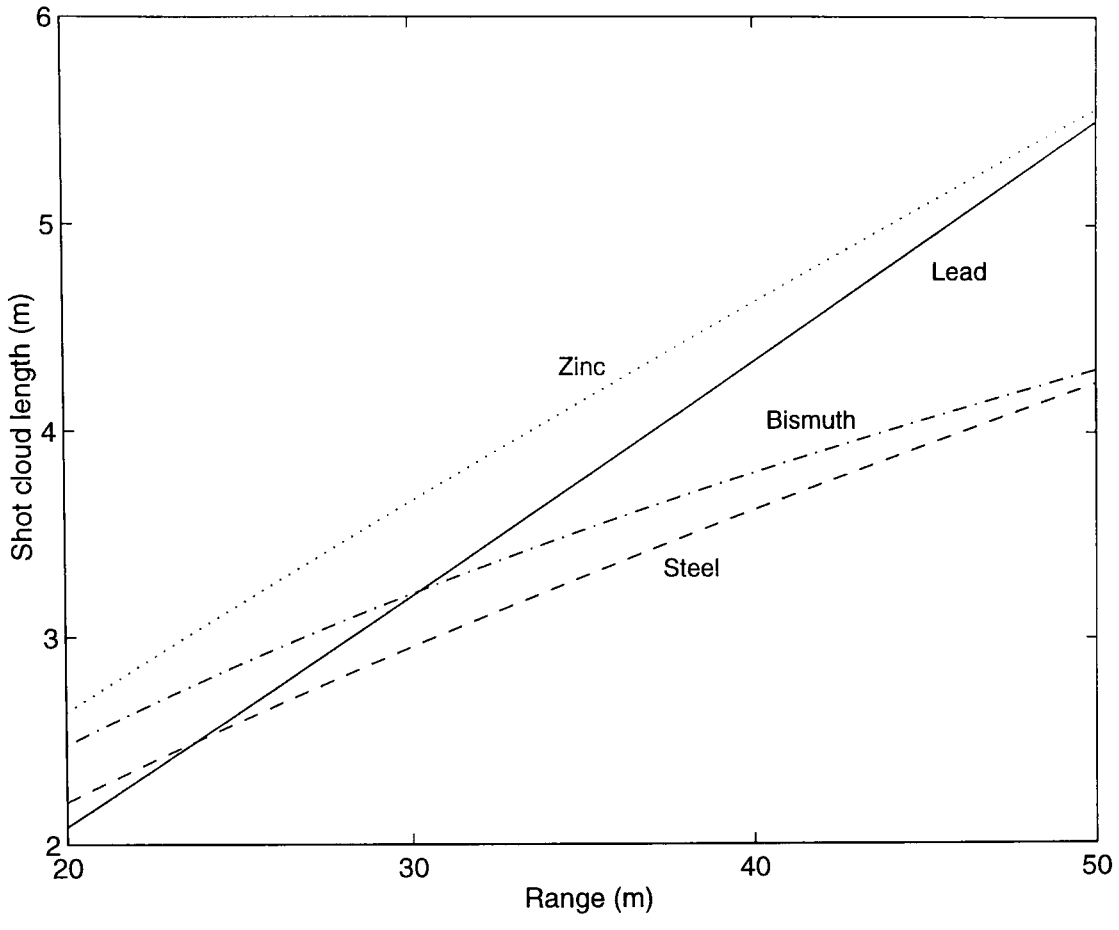

Figure 3.10 *The shot cloud length between 20 and 50m for a 32g load of #5 lead (0.030" choke), steel (0.020" choke), bismuth (0.030" choke) and zinc (0.030" choke) shot.*

The contrasting development rates in the length of the shot clouds for different pellet materials can be explained by their respective shot cloud profiles, as shown in Figure 3.11. From the characteristics of the lead profiles, the pellets are shown to slowly expand in the longitudinal direction with a few impacts breaking away at the trailing edge of the main section at a range above 35m (Figure 3.11(a)). This associated stringing out effect may be explained by the variation in the in-flight pellet shapes. For steel loads, the shot cloud profiles, Figure 3.11(b), are generally more compact over the measurement ranges, but with their greater volume of pellets in flight, the lengths at 20m for the same pellet diameters and load, are seen in Figure 3.10 to be longer than those for lead. However, with their associated smaller variation in steel pellet shape, and therefore in drag, the diffusion rate is less in the longitudinal direction and results in the shortest shot cloud length at 50m.

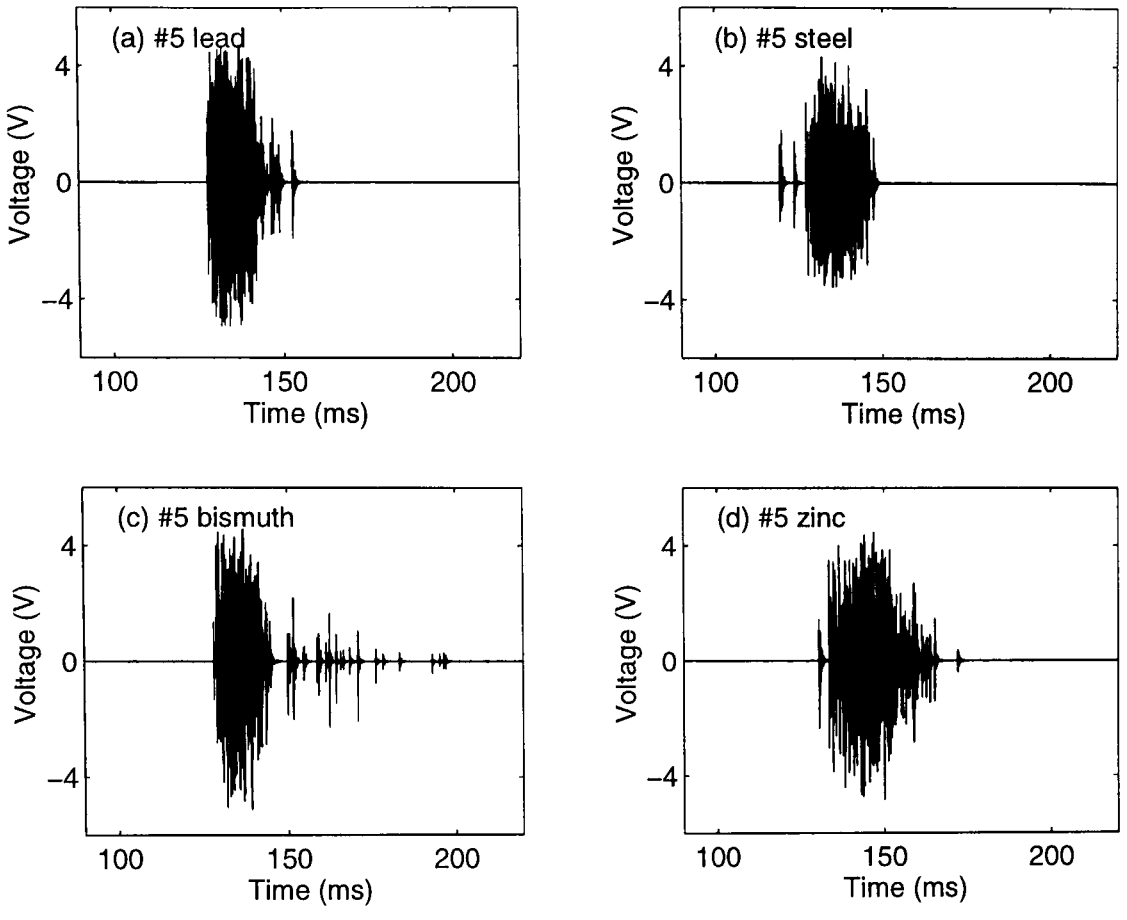

Figure 3.11 *The shot cloud profiles at 35m for a 32g load of #5 (a) lead (0.030" choke), (b) steel (0.020" choke), (c) bismuth (0.030" choke) and (d) zinc (0.030" choke) shot.*

For bismuth loads it was discovered in section 3.2.1 that a degree of fragmentation occurs on a small percentage of pellets after firing. This is confirmed by its shot cloud profile, Figure 3.11(c), where small impacts are observed to string out behind the main section of the shot cloud. At close ranges, such as 20m, these fragments have not fallen away sufficiently to be regarded as stray pellets and therefore are still part of the main section of the shot cloud. When the shot cloud has reached 35m, the inferior aerodynamics of the smaller fragments separates them, by several metres, away from the main shot cloud, thus producing a shorter shot cloud at 50m to that of lead (Figure 3.10). For the zinc loads with their variations in pellet shape, even before firing, and larger volume of pellets in flight it is seen in Figure 3.10 that they produce the longest shot cloud over the whole measurement range. Nevertheless, the effect of similar variation in pellet shape to that of lead is shown by the fact that the two loads have similar lengths at 50m.

The conclusions from investigating the effects of choke on the longitudinal distribution of pellets in a shot cloud are that the in-flight effects are dominant at the measurement

ranges 20-50m. With the uncertainties in pellet performance it has been decided that there is no satisfactory theory as yet that can render practical measurements superfluous.

3.3.3 Shot cloud profile in terms of pellet density

The voltage and time data generated by the ballistics target are combined together to produce the shot cloud profile (Figure 3.12(a)). The shot cloud profile is best translated as the cross section of the shot cloud in time at a particular distance, such as what might be observed from standing at the side of the shot cloud. It does not indicate what proportion of the pellets arrive at any point in time. Ideally, the impacts would be recorded and counted individually to obtain data on the pellet distribution along the cloud. However the maximum rate of arrival of the pellets (up to several hundred per millisecond) is too high for the single-impact response time of the detector array, and an alternative approach is required to determine the longitudinal pellet distribution.

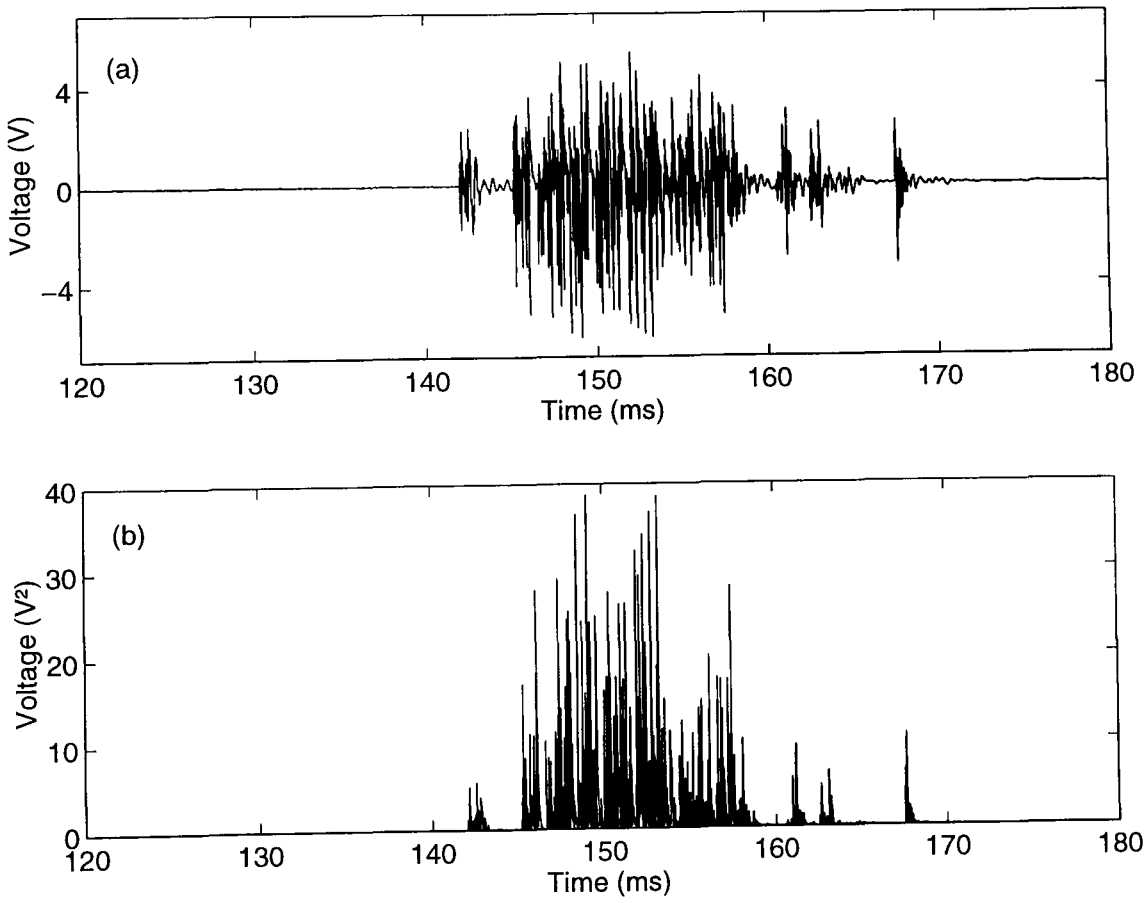

Figure 3.12 *(a) The shot cloud profile for a 36g load of #3 lead shot at 40m and (b) the square of its voltage readings representing the energy distribution along the shot cloud.*

If it is assumed that a constant proportion of the kinetic energy for any impact on the ballistics target is transferred as electrical power to the output of the system, then a plot of the square of the voltage readings, Figure 3.12(b), against time in Figure 3.12(a) represents the rate of delivery of energy to an output load. The area under the plot would then be proportional to the total kinetic energy in the shot cloud and the energy distribution along the cloud is obtained, and from this the pellet distribution can be estimated.

To test this assumption the target was fixed at a known distance from the muzzle, chosen so that the summing unit's output was not saturated, and the shot pattern centred on the target. Groups of detectors were then disconnected symmetrically in turn so that only a half, quarter, or three-quarters of the shot cloud were recorded. To allow for inaccuracies in centering the pattern and departures from radial symmetry in the shot clouds, alternate halves, quarters or three-quarters, respectively, were disconnected and the readings from 40 cartridges averaged in each case. The results in Figure 3.13 show the expected linear relationship between the rate of delivery of energy by the pellets to the target (percentage of shot cloud recorded via connected target area) and the total output power (percentage of maximum output power). If all the pellets in the cloud have the same kinetic energy then the squared values in Figure 3.12(b) would give the pellet distribution along the shot cloud, but in fact a correction is necessary to allow for the velocity distribution within the shot cloud and this can be estimated from the flight time data.

This method of determining the pellet distribution along a shot cloud can only work if the output from the ballistics target does not saturate the summing unit. It has been noticed that at ranges 25m and below the voltages produced by the impacts are often greater than the supply rails of the summing unit, therefore the total energy produced by the shot cloud cannot be estimated.

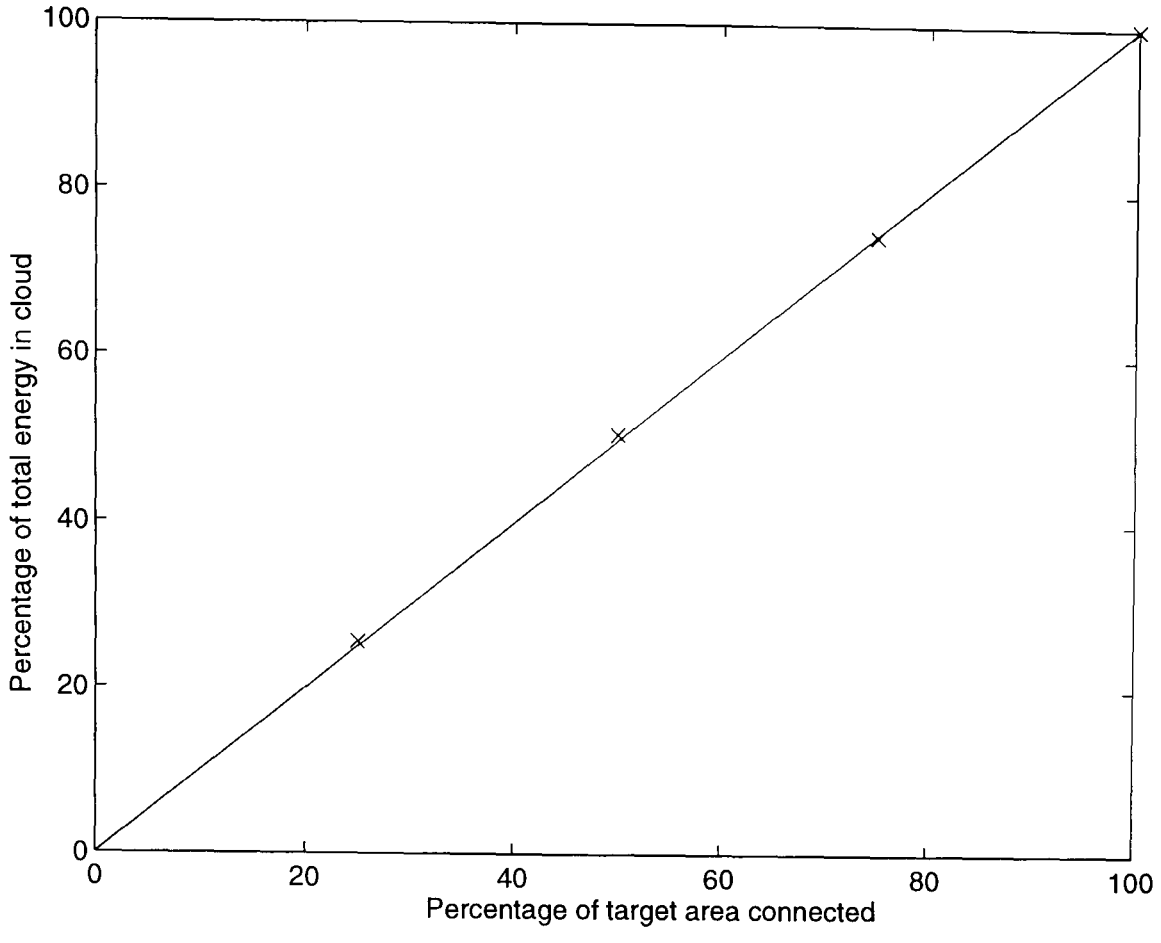

Figure 3.13 *The linear relationship between the rate of delivery of energy by the target and the total output power of the target when different percentages of the target are connected. The solid line represents the theoretical linear relationship.*

3.3.4 Distribution of pellets along the shot cloud

With an approximation for the pellet distribution along the shot cloud, using the method described in the previous section, it is desired to find the best probability density function which described the data. In order to obtain a reliable distribution, the pellet distribution in the longitudinal directions from 10 shot cloud profiles, starting at t_2 as this is the most consistent and easily identifiable point, were averaged. In Figure 3.14(a) the averaged calculated pellet density distribution along the shot cloud is given for a 36g load of #3 lead shot at 40m, whereby the total area under the curve represents the total energy delivered to the target, or the pellet distribution along the shot cloud.

Using a least squares fitting process to the approximated longitudinal pellet density distribution, for a range of shot clouds containing different pellet sizes and materials, to a variety of probability distributions including Gaussian, Rayleigh, and Maxwell-Boltzmann, it was found that the Rayleigh distribution,

$$p(t-t_2)=\frac{(t-t_2)}{\sigma^2}e^{-(t-t_2)^2/2\sigma^2} \quad , \tag{3.3}$$

produced the most appropriate fit, illustrated in Figure 3.14(b), where σ is the standard deviation and the maximum pellet density. Although the Rayleigh distribution visually gave the best fit to the data, the Gaussian distribution,

$$p(t-t_2)=\frac{1}{\sigma\sqrt{2\pi}}e^{-(t-t_2)^2/2\sigma^2} \quad , \tag{3.4}$$

produced the smallest normalized deviation d_n, Equation (4.13), by a factor of 10. This suggested that the Gaussian best describes the distribution (Figure 3.15(a)). However, the Gaussian probability density function produces a symmetrical curve about t_2, which is unlike the nature of the longitudinal distribution of pellets (Figure 3.14(a)).

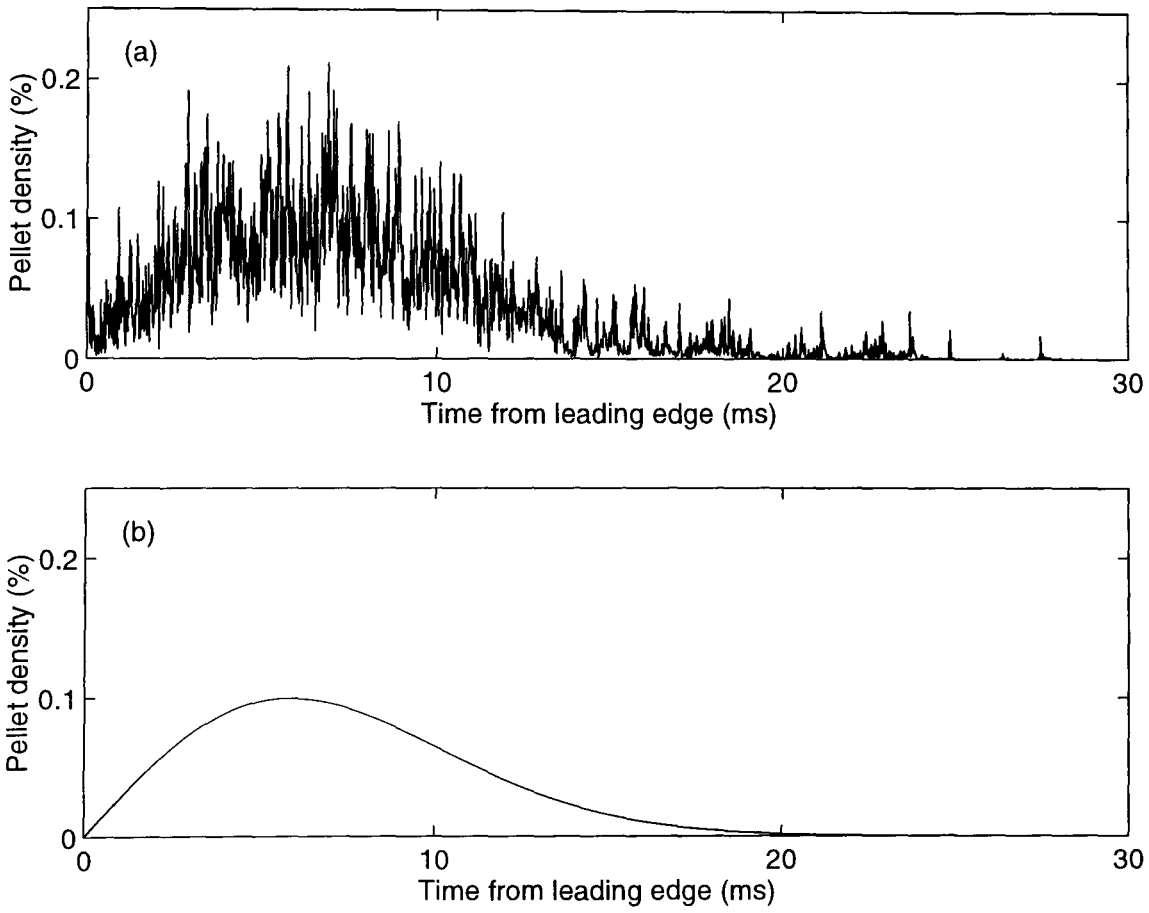

Figure 3.14 *(a) The average squared voltage readings of 10 shot cloud profiles starting at t_2 and the corresponding (b) fitted Rayleigh distribution to the data for a 36g load of #3 lead shot.*

Two other distributions based on the Gaussian distribution were tried. Firstly, in Figure 3.15(b) a Gaussian was multiplied by time, t, which reproduces the Rayleigh distribution and secondly the Gaussian was multiplied by t^2. Here the normalized deviation was a factor of 4 smaller than the Rayleigh distribution but the initial shape of the curve, Figure 3.15(c), was incorrect. When fitting to the Maxwell-Boltzmann distribution, Figure 3.15(a), it was also found to produce a smaller value of d_n with an inaccurate representation of the longitudinal pellet distribution.

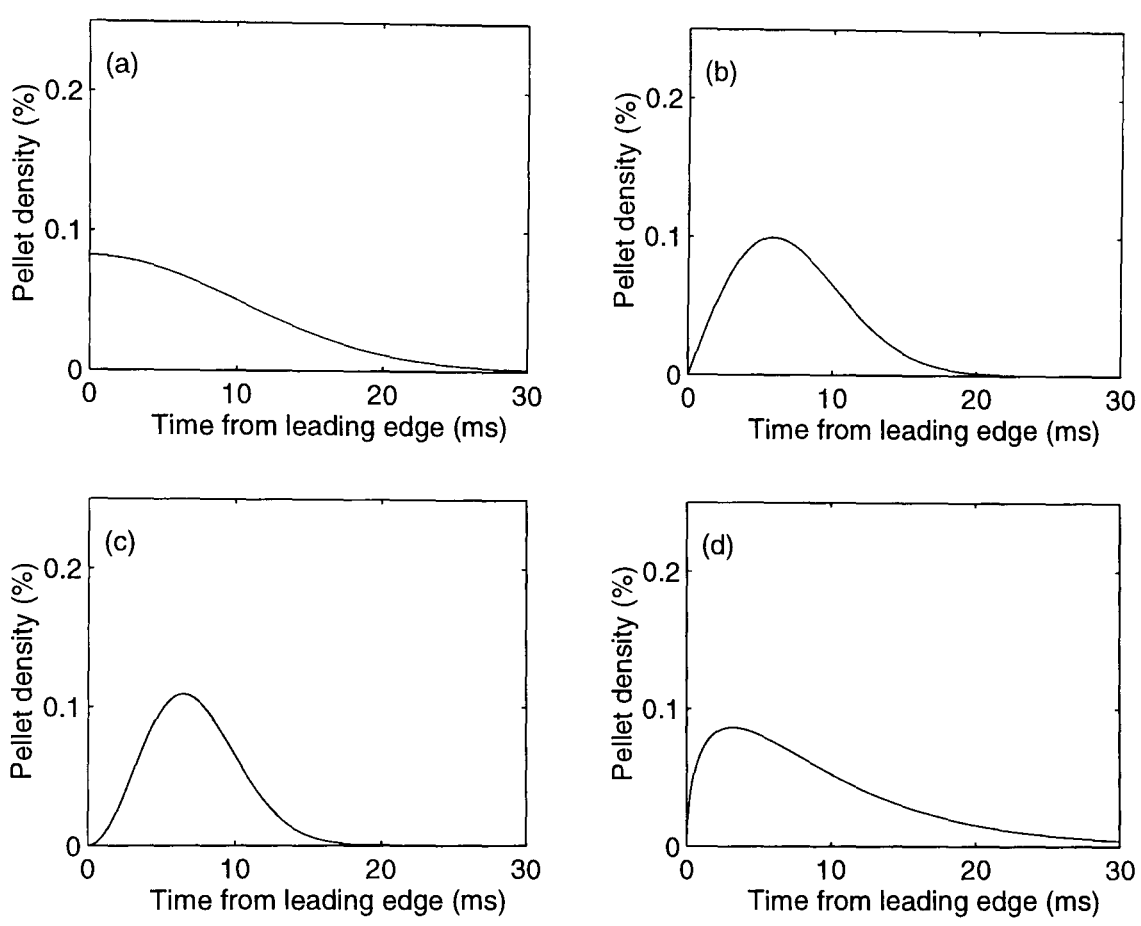

Figure 3.15 *A least squares (a) Gaussian, (b) Gaussian multiplied by t, (c) Gaussian multiplied by t^2 and (d) Maxwell Boltzmann fit to the longitudinal percentage pellet density distribution of a 36g load of #3 lead shot at 40m.*

A measure of the longitudinal pellet density distribution within a shot cloud is described by the standard deviation associated with the fitted Rayleigh, this also locates the maximum pellet density in time. Therefore for each range, the standard deviation represents the dispersion of the shot cloud and in Figure 3.16 it is seen to lengthen with range. Unfortunately this method of determining the longitudinal dispersion does not allow an accurate relationship between the longitudinal spread and range, or time, to be analysed, because of the saturation problems of the ballistics system. It has been noticed

that below 30m the typical energy delivered to the target saturates the amplifiers in the summing unit and an error is present in the estimation of the fitted Rayleigh distribution. The summing unit could be re-calibrated but then the system would than not be sensitive enough for the small shot at extreme range, therefore a compromise has been established. To conclude, the longitudinal distribution of pellets in a shot cloud is best described by a Rayleigh distribution and the effect of choke on it at the measurement range 20-50m is minimal.

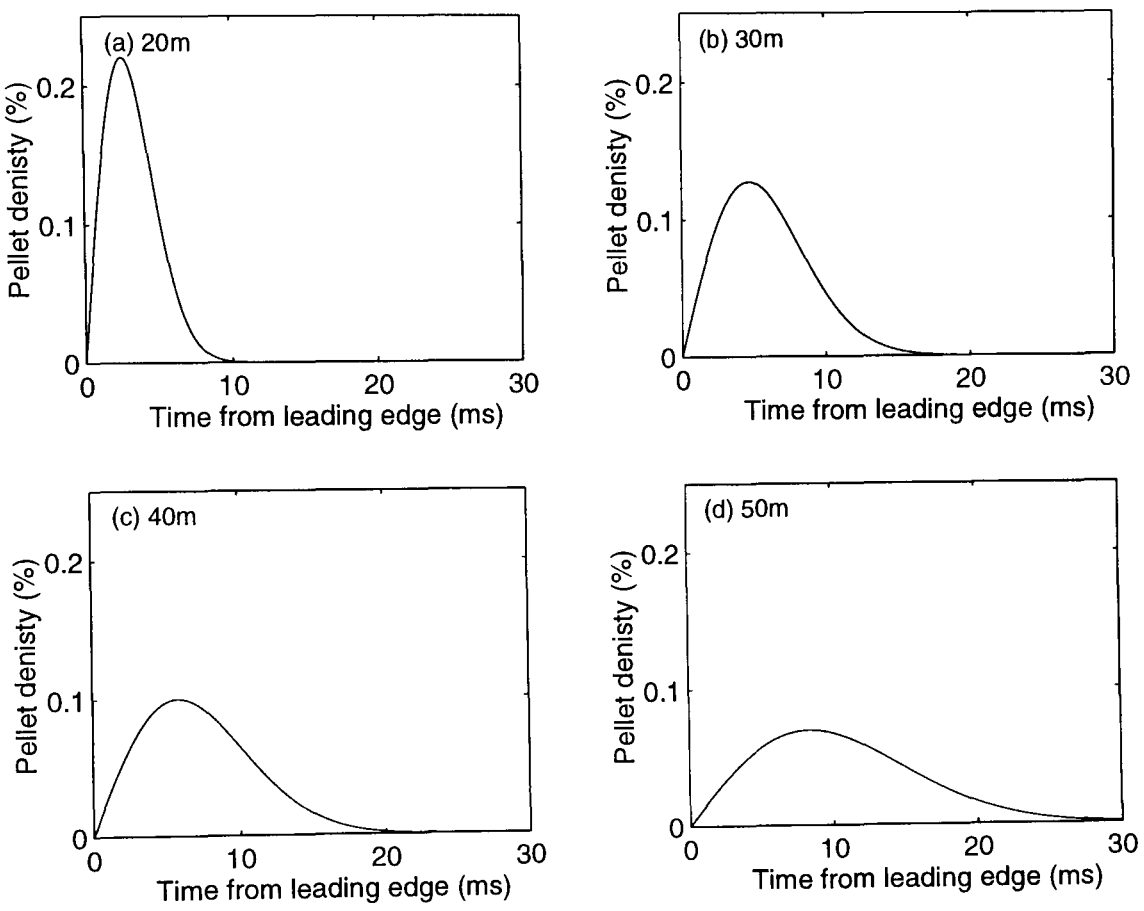

Figure 3.16 *The approximated least squares Rayleigh fit of the longitudinal percentage pellet density distribution for a 36g load of #3 lead shot at a selection of ranges.*

3.4 PATTERNS : LATERAL SPREAD

3.4.1 Effect of altering the internal ballistics of the gun

The internal ballistics of a gun, especially the choke, have been shown by Lowry's high speed photography experiments to affect the lateral and longitudinal spread of pellets. In general, near the muzzle, the more constrictive choke, such as the full choke barrel in Figure 1.6, produces a tighter shot cloud in the lateral direction. It is not possible to

verify these findings with the measurement techniques describe in Chapter 2, but the effects of the internal gun ballistics on the lateral distribution of pellets at greater ranges (20-50m) can be observed.

The proof barrel used in all experiments allows for a standardized means of launching the pellets. However it was possible to alter the constriction at the muzzle by ten choke tubes which have a $2^3/_4$" linear taper profile. There were also $^1/_2$" and 1" parallel section choke profiles in one choke constriction. Experiments were undertaken to examine the effect of choke on the lateral spread of the pellets, or patterns, downrange. The range chosen was 40 yards (36.6m) as it is the traditional range to measure patterns and combines contractual and research requirements. From the image processing procedure described in section 2.6 a two-dimensional pattern is obtained giving the x (horizontal) and y (vertical) co-ordinates of every pellet intercepted by the pattern sheet. From these pellet co-ordinates the statistical pattern centre is established by averaging the x- and y-components.

A convenient measure of the lateral dispersion is the standard deviation (σ) of the pellet co-ordinates as it represents a proportion of the total width (where 3.290σ contains 99.9% of the pellets) of the shot cloud. In general the standard deviation is preferred by scientists as it has the same units and dimensions as the data. The traditional measure of patterns in the shooting community is the percentage of pellets in a 30" circle at 40 yards and has been explained earlier to be the unit of area used for comparative measures on pellet density.

In Figure 3.17 the standard deviation of the x and y pellet coordinates and the percentage counts in a 30" circle at 40 yards are given for two loads of lead pellets using different choke constriction. The standard deviations in both cases are shown to decrease rapidly when the choke constriction is increase from 0.000" to 0.020", but any further increase in constriction seem to have little visible effect on the lateral distribution. It must be noted that the fitted curves are only there to help illustrate the trends and are not based on any known relationship between choke constriction and lateral dispersion. The data

points are again obtained by averaging over 10 patterns as a compromise between accuracy and acquisition time.

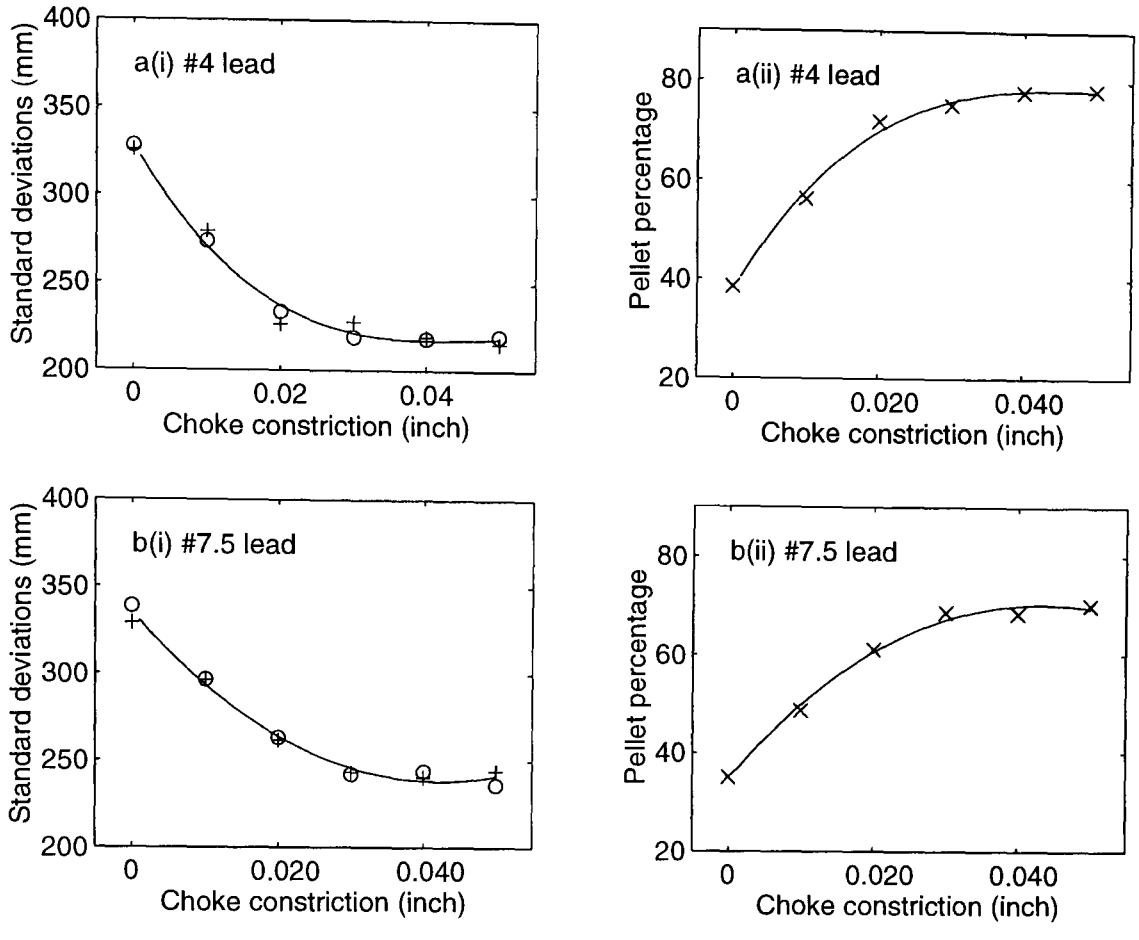

Figure 3.17 *The effect of linear tapered choke constrictions on (i) σ_x (+) and σ_y (o) of the lateral pellet co-ordinates and (ii) percentage pellet count in a 30" circle at 40 yards for a 36g load of #4 lead shot and 28g load of #7$^1/_2$ lead shot. The solid lines are only given as a guideline to the relationship.*

The calculated standard errors on the mean associated with the averaged standard deviation (σ_x and σ_y) of the pellet coordinates in the x and y directions have been found, from the analysis of hundreds of patterns, to be typically 1-2% for all loads. These errors are illustration in Table 3.8 where the standard error on the average σ_x, σ_y and the pellet percentage in a 30" circle are given for the 28g load of #7$^1/_2$ lead shot shown in Figure 3.17(b). Therefore with the small uncertainties (standard errors) associated to the averaged data points in Figure 3.17, the integrity of the relationship between choke constriction and lateral pellet distribution is validated.

Choke constriction (inch)	Distribution in the *x*-axis (mm)		Distribution in the *y*-axis (mm)		Pellets counts in a 30" circle	
	σ_x	*SE*	σ_y	*SE*	Percentage	*SE* (%)
0.000	329	3.6	339	4.0	35.1	1.0
0.010	296	4.9	297	4.1	48.6	1.4
0.020	262	3.7	263	4.2	61.0	1.5
0.030	243	3.8	242	2.8	68.6	1.1
0.040	240	3.6	244	5.4	68.4	1.1
0.050	244	4.3	236	2.2	70.1	1.0

Table 3.8 *The standard deviation and standard error associated with the lateral pellet co-ordinates in the x and y axis for a selection of linear tapered choke constrictions at 40 yards when using a 28g load of #7$^1/_2$ lead shot. Also given are the traditional percentage pellet count in a 30" circle and their corresponding standard errors.*

The effect of choke on the lateral distribution of lead pellets at 40 yards has been shown in Figure 3.17 to be insensitive once the constriction is above 0.030", where a levelling-off process occurs. When altering the material density of the pellets, a similar restriction on the ability to tighten the pattern is seen. In Figure 3.18 the relationship between the choke constriction and lateral pellet distribution are given for two steel loads, using σ_x, σ_y and the count in a 30" circle, and in Figure 3.19 the results for a bismuth and zinc load are shown. The reasons for this levelling-off characteristic of pellet distributions is not understood at present and further investigation is required. The first action to be taken is to establish the effect of choke on the near-muzzle lateral distribution. Unfortunately the result shown by Lowry only covered the extreme chokes effect on the shot cloud. If the lateral spread near the muzzle is found to tighten consistently with an increase in choke then the limiting effects at 40 yards can be put down to the in-flight effects of the pellet as they travel downrange. However, if the near-muzzle distribution levels off as well, the limiting factor is caused by the internal ballistics of the barrel.

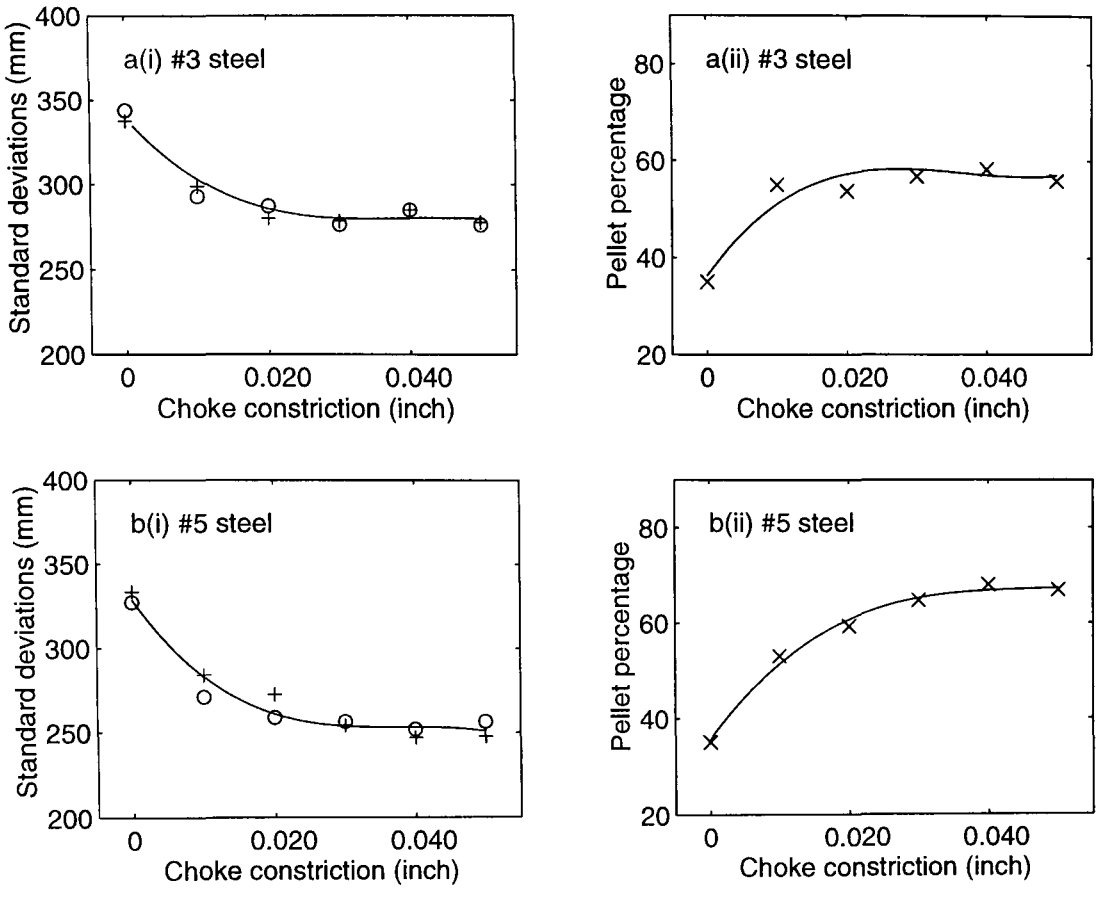

Figure 3.18 *The effect of linear tapered choke constrictions on (i) σ_x (+) and σ_y (o) of the lateral pellet co-ordinates and (ii) percentage pellet count in a 30" circle at 40 yards for a 32g load of #3 steel shot and a 28g load of #5 steel shot. The solid lines are only given as a guideline to the relationship.*

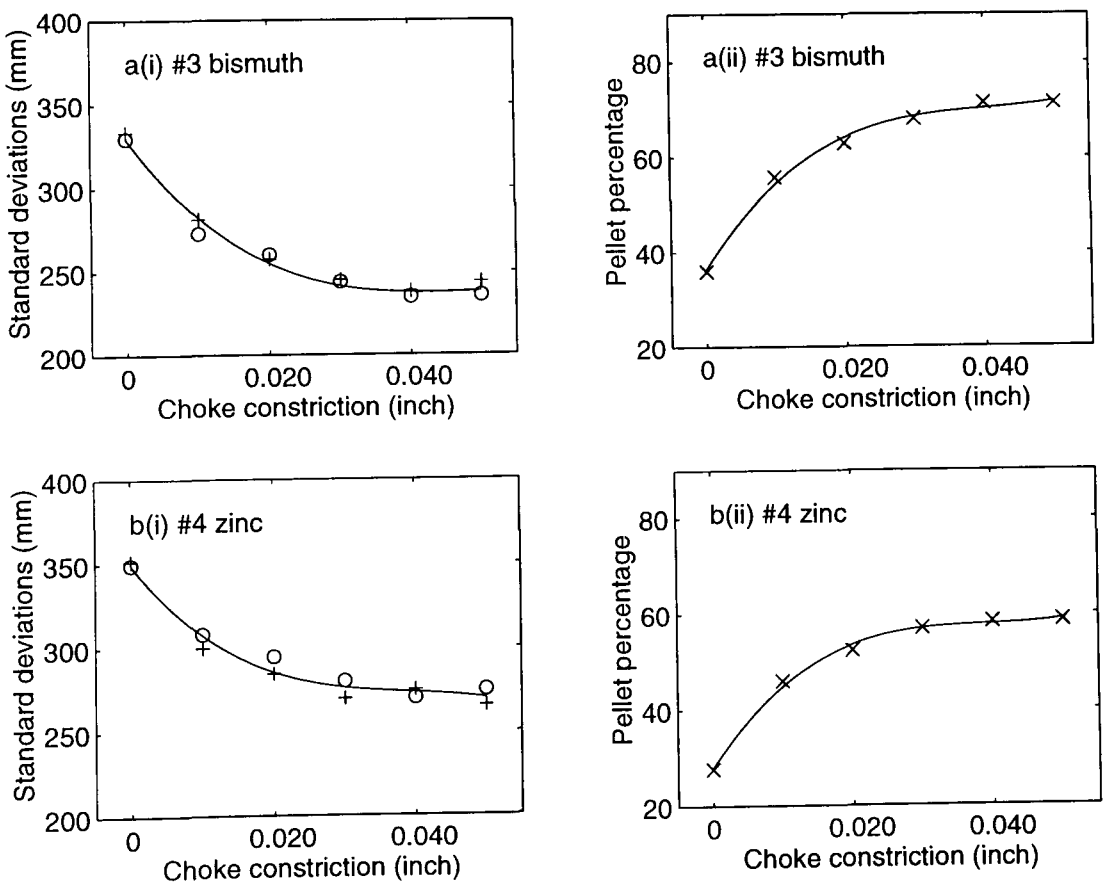

Figure 3.19 *The effect of linear tapered choke constrictions on (i) σ_x (+) and σ_y (o) of the lateral pellet co-ordinates and (ii) percentage pellet count in a 30" circle at 40 yards for a 36g load of #3 bismuth shot and a 30g load of #4 zinc shot. The solid lines are only given as a guideline to the relationship.*

The internal ballistics of the barrel, via choke constriction, have been shown to affect the downrange lateral pellet distribution, but not the longitudinal distribution. To limit the possible variation in the experimental set up of the measurement facility, all choke tubes from 0.000" to 0.050" constriction were produced with a linear taper profile. A separate 0.020" constricted choke tube was constructed with a 1" parallel section profile to examine the effect of choke profile on the lateral pellet dispersion. In Table 3.9 the averaged pellet counts in a 30" circle at 40 yards and their corresponding standard deviations are given for a selection of material loads. It was found that for the same constriction the 1" parallel section produced a slightly tighter distribution of pellets at 40 yards than the linear taper profile for every batch of ammunition tested. However, the standard errors associated with the distribution show that statistically there is no significant difference between the two profiles, expect for the one steel load tested where an improvement is seen when using the 1" parallel section profile. Here it has been established that there is little difference between the two 0.020" constricted choke profiles, but it has not been feasible to fully investigate the effect of choke profile on the lateral distribution of pellets, due to the lack of availability of specially prepared choke tubes for the test barrel and the research priorities.

Material	Linear taper 0.020" choke		1" parallel section 0.020" choke	
	Pellet percentage	*SE* (%)	Pellet percentage	*SE* (%)
36g load of #4 lead shot	71.8	1.6	72.3	1.3
28g load of #7.5 lead shot	61.0	1.5	63.6	2.5
28g load of #5 steel shot	59.3	1.5	65.2	1.2
36g load of #3 bismuth shot	62.9	1.6	63.6	1.4
30g load of #4 zinc shot	52.4	0.7	51.0	1.8

Table 3.9 *The percentage of pellets in a 30" circle at 40 yards for a selection of different loads when fired through 0.020" choke constriction with a linear taper or 1" parallel section profile.*

The other variable which can be altered in the test barrel to change the internal ballistics is the chamber length. In Table 3.10 the standard deviation and pellet counts at 40 yards are given for a 36g load of #4 lead shot loaded into a $2^3/_4$" cartridge cases which were fired through a selection of chambers lengths. The averaged results show a definite alteration to the lateral dispersion of the shot cloud large when using the wrong chamber length. These differences between the averages are greater than the expected standard error, so the chamber length can alter the lateral spread of pellets at 40 yards.

For this part of the investigation no attempt is given to explain these occurrence as the internal ballistics of a gun is its own science, but the tighter pattern generated by $2^1/_2$" chamber length may be caused by the restrictive crimp opening acting like an internal choke. It is not recommended to try these experiments with a standard shotgun as they are not design to withstand the extra pressured generated from restricting the opening of the crimp.

Chamber length (inch)	Distribution in the *x*-axis (mm)		Distribution in the *y*-axis (mm)		Pellet percentage in a 30" circle	
	σ_x	*SE*	σ_y	*SE*	Average	*SE*
$2^1/_2$	198.3	5.1	205.1	4.0	82.4	0.7
$2^3/_4$	218.7	4.6	223.5	5.1	75.3	1.6
3	203.1	4.2	211.7	4.4	79.4	1.4

Table 3.10 *The standard deviations and standard errors associated with the lateral pellet co-ordinates in the x- and y-axis for a selection of chamber lengths at 40 yards when using a 28g load of #$7^1/_2$ lead shot (0.030" choke) with a cartridge length of $2^3/_4$". Also given are the traditional average percentage pellet count in a 30" circle and their corresponding standard errors.*

From the choke and chamber length experiments it has been demonstrated that the internal ballistics of the gun contribute to the lateral distribution of pellets downrange. With the large number of possible combination and permutation in the configuration of shotguns (such as the chamber and choke profile, chamber length, choke constriction and ammunition) the feasibility of investigating, or generalizing all the combined effects

was not possible. However, it was established that altering the chamber length changed the lateral dispersion of pellets and increasing the constriction of linear tapered profile chokes over 0.030" has little effect on the lateral pellet distribution. These findings reinforce the attitude that many aspects of shotgun ballistics, especially patterns, have no satisfactory theory to predict or explain the effects of the internal ballistics of a gun on the downrange behaviour of a shot cloud.

3.4.2 Lateral pellet density distribution

The results from numerous patterns were used to examine the relationship between the lateral pellet dispersion in *x*- and *y*-axis. In Figure 3.20 the ratio of their standard deviations are shown for a variety of pellet diameters and materials at 40 yards. The majority of patterns are seen to lie above the theoretical dotted line (identical dispersion in both axis) suggesting a bivariate distribution. A similar relationship was observed between the lateral dispersions of pellets at 40yds with choke constriction (Figure 3.21) and with range (Figure 3.22).

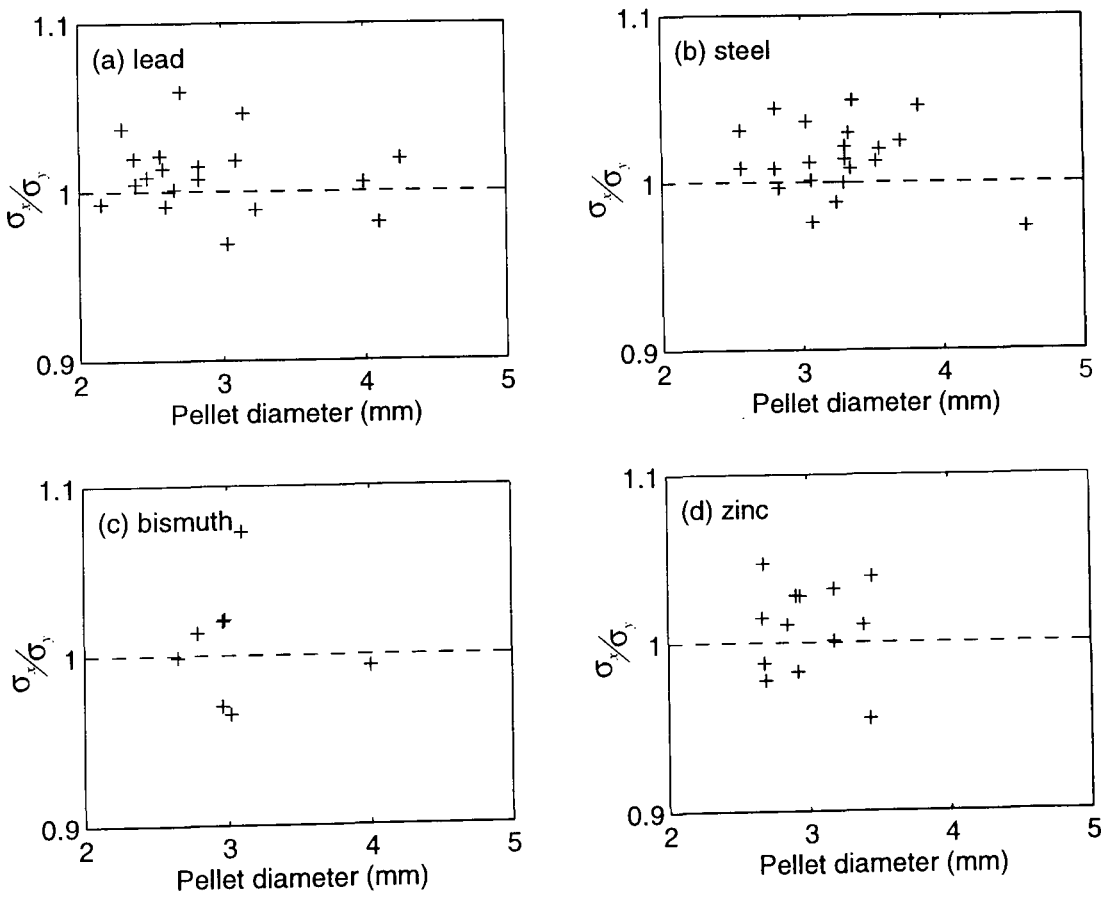

Figure 3.20 *The ratio of standard deviations, σ_x/σ_y, for the lateral dispersion of lead, steel, bismuth and zinc pellet at 40 yards.*

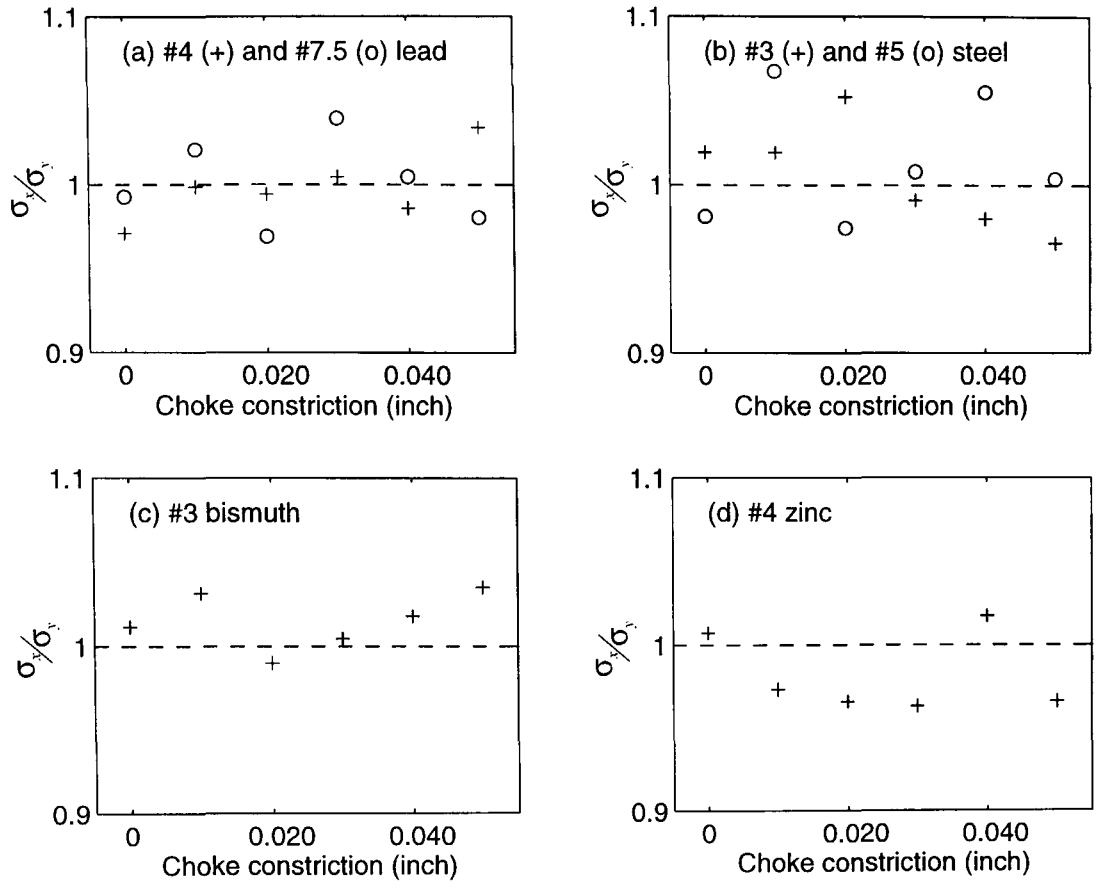

Figure 3.21 *The ratio of standard deviations, σ_x/σ_y, for the lateral dispersion of (a) a load of #4 (36g) and #7$^1/_2$ (28g) lead shot, (b) a 32g load of #3 and #5 steel shot, (c) a 36g load of #3 bismuth shot and (d) a load of #4 zinc shot with choke constriction at 40 yards.*

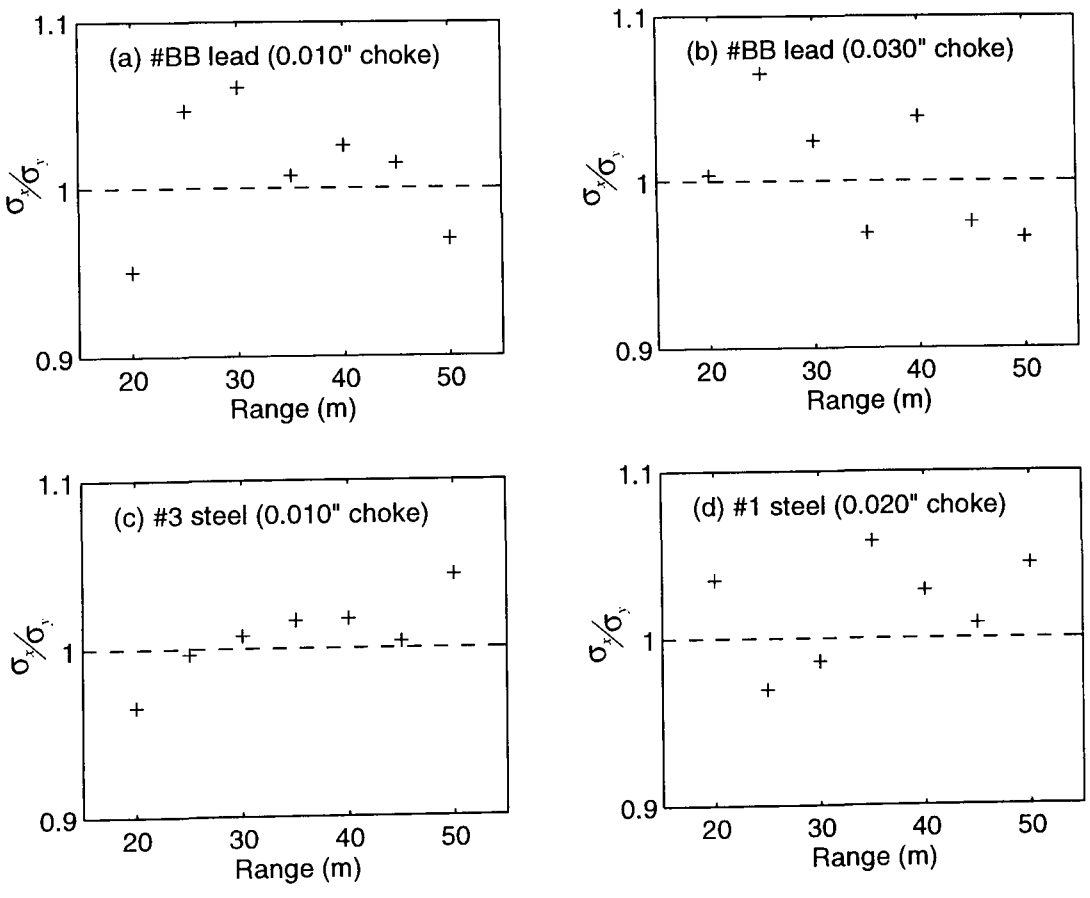

Figure 3.22 *The ratio of standard deviations, σ_x/σ_y, for the lateral dispersion of a 36g load of #BB lead shot (0.010" and 0.030" choke), a 28g load of #3 steel shot (0.010") and a 28g load of #1 steel shot (0.020" choke) with range.*

In general, the difference between the pellet dispersion in the *x*- and *y*-axis is 1%. This is of the same magnitude as the calculated standard error on the dispersions, shown in Table 3.8. Therefore with the small discrepancy between the lateral pellet distribution in the *x*- and *y*- axis it is assumed from now on that they are approximately equal.

$$\sigma_x = \sigma_y = \sigma \tag{3.5}$$

The assumption made in (3.5) agrees with the conclusion Journée [1] made on the lateral pellet dispersion in a shot cloud. However, Journée found a greater dispersion in the vertical axis that increased with range, this was not consistently observed, Figure 3.22, by this investigation. One problem associated with the cartridge design around the time of Journée's work was the occurrence of creux patterns, otherwise known as 'blown' or 'cartwheel'. At the centre of these patterns there are large regions devoid of pellets. This would cause a different lateral dispersion to that produced by the modern shotgun cartridge and explain the differences in his findings.

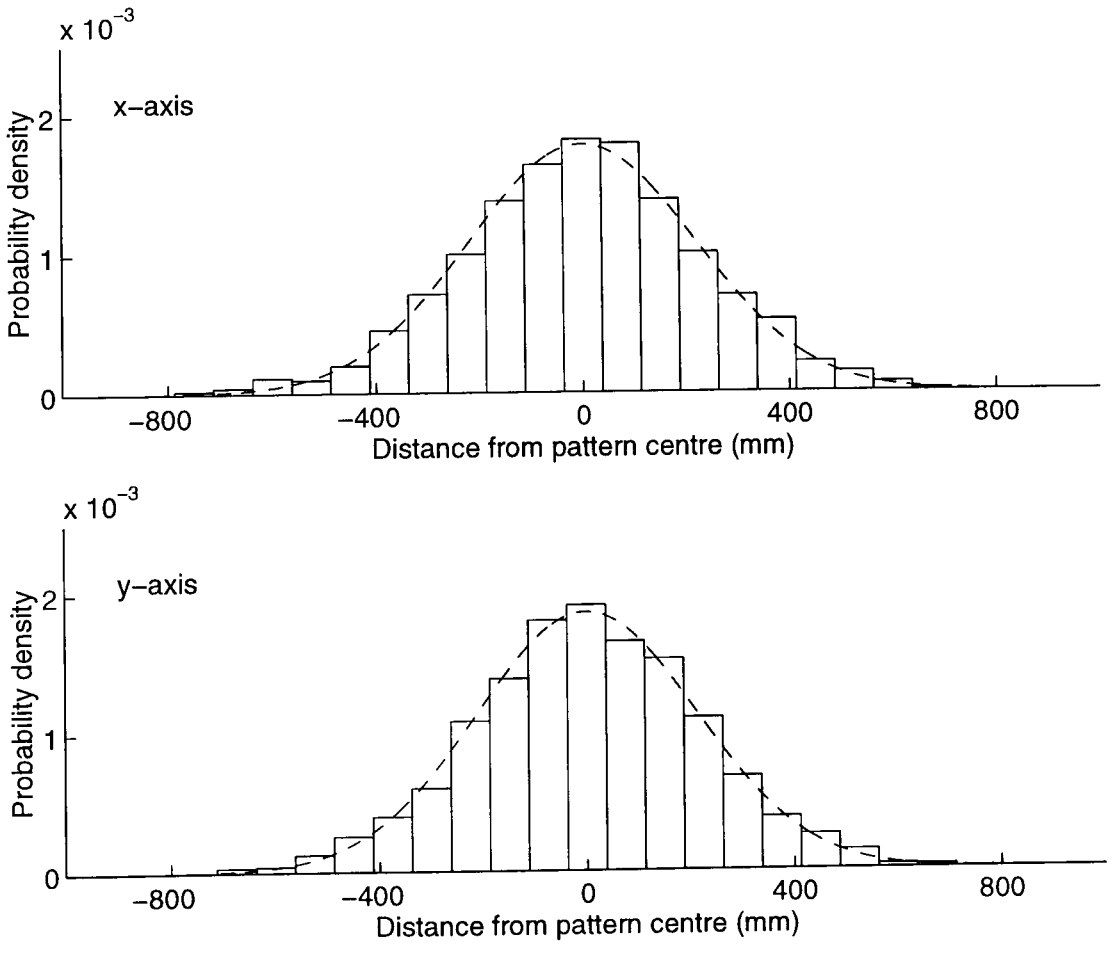

Figure 3.23 *The average probability densities for consecutive horizontal (x) and vertical (y) 75mm strips averaged about the centre of 10 patterns are given for a 36g load of #4 lead shot (0.030" choke) at 40 yards.*

Assuming identical standard deviation in the x- and y-axis it is then desired to determine the nature of their dispersions. In Figure 3.23 the average probability densities for consecutive horizontal and vertical 75mm strips about the centre of 10 patterns are given for a 36g load of #4 lead shot (0.030" choke). This method of analysis is known as the 'Winchester grid' and illustrates the Gaussian characteristics of both dispersions. From testing over 2000 patterns, a selection shown in Appendix B , the same relationship has been found for different pellet materials, chokes and ranges.

The Gaussian, or normal, probability distribution function,

$$\rho(r) = \frac{1}{\sigma\sqrt{2\pi}} e^{-r^2/2\sigma^2} \qquad (3.6)$$

is the most well known of all mathematical distributions. It has a bell shape curve, shown in Figure 3.23 as the overlaid plot, which is centred symmetrical about the origin. The width of the dispersion is controlled by the standard deviation and its peak at the pattern centre. The Gaussian probability density distribution in (3.6) can be converted to give the expected number of pellet in each strip width (P_c)

$$P_c = P_0 e^{-r^2/2\sigma^2} \quad , \qquad (3.7)$$

where P_0 is the pellet count in the centre strip, r is measured from the centre of a strip to the pattern centre and σ is the standard deviation. The strip, or bin, width, was chosen to encompass a sufficient number of pellets in the majority of the strips (>5 pellets) so that an accurate representation of the distributions was obtained. Therefore if the two distributions have a Gaussian nature, by taking logarithms of (3.7) we obtain

$$\frac{r^2}{2\sigma^2} = \ln(P_0) - \ln(P_c) \quad , \qquad (3.8)$$

and a plot of $-\ln(P_c)$ against r^2 should produce a straight line with a gradient $1/(2\sigma^2)$ where the standard deviation (σ) of the distribution can be determined. The intercept of

the plot in the *y*-axis will then give an estimate for the pellet count at the pattern centre (P_0). Additionally, the ratio of the two pellet counts (average over 10 patterns), representing the left and right sides of the horizontal distribution or top and bottom halves of the vertical dispersion, for each r^2 checks whether if the distributions are symmetrical about the pattern centre, another requirement of the Gaussian. In Figure 3.24 the symmetry of both the *x* and *y* distributions about the pattern centre can be seen until 4×10^5 mm (2σ) for a 36g load of #4 lead shot (0.030" choke) at 40 yards. The reduction in symmetry is reasonable as there is a greater variation associated with the fringes of the pattern (2σ) due to fewer pellets.

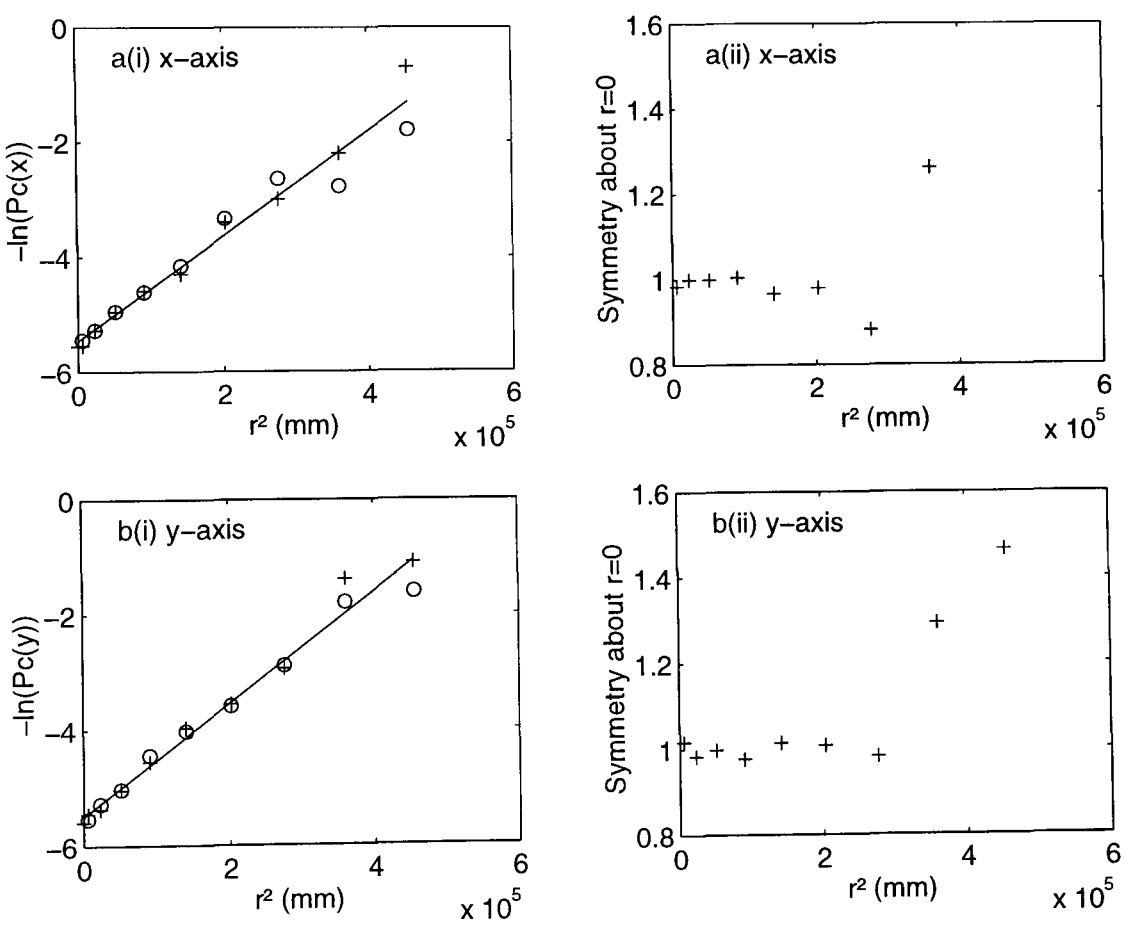

Figure 3.24 *(i) A plot of* $-\ln(P_c)$ *versus* r^2 *for the (a) left (o) and right (+) sides of the x-axis and (b) the (o) top and (+) bottom of the y-axis distribution with their (ii) corresponding ratios for a 36g load of #4 lead shot (0.030" choke) at 40 yards. These results where obtained by averaging over 10 patterns.*

The plots in Figure 3.24 give a simple visual check as to whether the *x* and *y* distributions are Gaussian. An alternative method which determines the suitability of the fitted distribution function *f(x)* to the data *y* is described by the χ^2 distribution (chi-squared). The quantity χ^2 is described [45] as the square differences between the

observed values and the theoretical predictions, suitably weighted by the errors of the measurement:

$$\chi^2 = \sum_i \frac{[y_i - f(x_i)]^2}{\sigma_i^2} = \sum_{i=1}^{N} \left(\frac{y_i^{actual} - y_i^{ideal}}{\text{expected error}} \right)^2 \qquad (3.9)$$

If the function agrees well with the actual values then χ^2 will be small but for an inappropriate function produces a large χ^2. To examine the goodness of the fit (χ^2) for the x and y distribution the average pellet count y_i and their corresponding standard deviation σ_i in each strip were calculated and compared with a least squares fitted Gaussian $f(x_i)$. To make judgements and decisions about the goodness-of-fit the probability distribution for χ^2, given by (3.10), assesses the probability of finding a function, described in a set of N data points, that produces a greater χ^2 and therefore worse fit. This function is controlled by the number of degrees of freedom $n=N-m$, where m are the number of parameters in the fit function including the overall normalization. The number of degrees of freedom adjusts the probability according to the number of fitted parameters involved. A look-up table is given in Appendix C for the χ^2 distribution.

$$P(\chi^2; n) = \int_{\chi^2}^{\infty} P(\chi'^2; n) d\chi'^2 \qquad (3.10)$$

When binning data, or taking pellet counts in specific areas of the patterns, attention is required to choose an area of a suitable size, or bin, for the number of data points, or pellets. If the bins are made too large this can obscure the goodness of fit and on the other hand if they are made to small the standard deviation, or errors, become a major influence which disguises the poor fit. It is also necessary to have sufficient data points to obtain a accurate representation of the distributions. The relatively low number of pellets associated with individual patterns produces a larger χ^2 and a higher probability of finding a better fit. This confirms the earlier established requirement of averaging over 10 patterns to obtain a reliable result.

Note the normalized deviation d_n, described by (4.13), is mainly used as a means of determining the most appropriate fit to the experimental data from a selection of models or functions.

For the averaged distributions shown in Figure 3.23, the x and y distributions were split into 19 equal bin widths 75mm wide. In assessing the suitability of the Gaussian to describe the distribution of pellets, a least squares Gaussian fit with 16 degrees of freedom was performed on the experimental data. The goodness of fit χ^2 was calculated to be 3 and 3.5 in the x- and y-axis with both corresponding χ^2 probabilities greater than 99%. This shows that the Gaussian is a good approximation for describing the radial distribution of pellets in the x and y directions as there is less than 1% chance of finding a better fit.

To emphasise the overall suitability of using a Gaussian distribution to describe the dispersion of pellets in both axis, the χ^2 probabilities are given in Tables 3.11 and 3.12 for a selection of chokes, materials and ranges (distribution shown in Appendix B) along with the calculated standard deviation from the pellet co-ordinates (calc.), a r^2 versus-ln(P) plot (fit 2) and a least squares fit to a Gaussian (fit 1). It can be seen that the probability of finding a better fit is less than 1%, with a typical χ^2 of 3, in the horizontal and vertical directions for patterns produced from choke constriction greater than 0.020" at 40 yards. A good visual representation of the classical bell shape Gaussian from the averaged distribution of pellets in the horizontal and vertical strips are also seen. Along with the plots of x^2 and y^2 versus -ln(P) generating the theoretical straight line and a standard deviation to within 5% of the measured, the Gaussian distribution is justified to be an appropriate description of the pellet distribution in the x and y axis for choke constriction greater than 0.020".

Material	*x*-axis				*y*-axis			
	$P(\chi^2,n)$	σ_x (mm)			$P(\chi^2,n)$	σ_y (mm)		
	(%)	calc.	fit 1	fit 2	(%)	calc.	fit 1	fit 2
Figure 3.23	99	228	234	221	99	219	227	213
28g load of #7$^1/_2$ lead shot (0.000" choke)	99	329	371	384	98	339	400	392
28g load of #7$^1/_2$ lead shot (0.040" choke)	99	240	239	250	99	244	242	239
32g load of #3 steel shot (0.000" choke)	98	338	402	408	99	344	426	406
32g load of #3 steel shot (0.040" choke)	99	278	290	259	98	276	263	280
36g load of #3 bismuth shot (0.000" choke)	99	334	402	406	99	329	392	391
36g load of #3 bismuth shot (0.040" choke)	99	238	229	234	99	235	248	227
30g load of #4 zinc shot (0.000" choke)	85	352	431	442	98	349	434	422
30g load of #4 zinc shot (0.040" choke)	99	265	266	274	99	275	283	281

Table 3.11 *The probability of χ^2 for a Gaussian, calculated pellet standard deviation (cal.), corresponding standard deviation parameter from a least square Gaussian fit of the data (fit 1) and the standard deviation associated with the gradient of a* -ln(*p*) *plot against r^2 (fit 2) of the pellet distribution in the x- and y-axis for a selection of loads average over 10 patterns at 40 yards.*

Range (m)	x-axis				y-axis			
	$P(\chi^2,n)$	σ_x (mm)			$P(\chi^2,n)$	σ_y (mm)		
	(%)	calc.	fit 1	fit 2	(%)	calc.	fit 1	fit 2
20	99	150	149	149	99	158	163	158
30	99	249	262	269	99	227	230	227
40	95	313	328	343	98	305	327	305
50	85	347	382	412	98	358	468	358

Table 3.12 *The probability of χ^2 for a Gaussian, calculated pellet standard deviation (cal.), corresponding standard deviation parameter from a least square Gaussian fit of the data (fit 1) and the standard deviation associated with the gradient of a* -ln(*p*) *plot against r^2 (fit 2) of the pellet distribution in the x- and y-axis for a 36g load of #BB lead shot (0.030" choke) at various ranges average over 10 patterns.*

A less defined Gaussian is observed (Appendix B) in the lateral distribution when chokes less than 0.020" constriction, especially cylinder at 40 yards, are used or when increasing the range (Table 3.12). Analysis of these more diffuse patterns reveals that the probability of χ^2 is more than 98% for the two distributions with their corresponding χ^2 at least a factor of 2 greater. Therefore the resemblance between Gaussian and the actual distribution of pellets slightly worsens the more diffuse the pattern becomes, but the probability of finding a better fit is still very low. The good qualitative agreement for these more diffuse patterns is due to the higher expected error associated to the fringes of their patterns. This is not seen in the averaged representation for their distributions (Appendix B), where a worse agreement is suggested. The extra variation associated with the diffuse patterns is also encountered in the $-\ln(P_c)$ plot where the data points are more scattered, reducing the accuracy of the estimated standard deviation (fit 2) to within 10% of the equivalent parameter generated from a least squares Gaussian fit (fit 1) to the data.

The suitability of describing the distribution of pellet in the x and y axis to a Gaussian has typically been found to be at least 95% probable. Even with the worst possible cases seen over this investigation of 80%, the good qualitative agreement between the theoretical and experimental distribution allows the lateral distribution of pellets in both axis to be regarded as Gaussian.

In Tables 3.11 and 3.12 the standard deviations obtained from the two fitting process are shown to be similar for the patterns with choke constriction. However, a large discrepancy is seen between the calculated standard deviations from the fitting processes and the measured standard deviations from the pellet co-ordinates for the more diffuse patterns. This is because the pattern paper does not retrieve all the pellets, thus underestimating the true standard deviation of all the pellets fired from the cartridges. As the fitting processes are less affected by this occurrence, they establish a more reliable means of determining the standard deviation.

During this section several assumptions are made from statistical analysis of the pellet co-ordinates and are found to agree with the findings of Journée [1] and Lowry [36].

Firstly, the standard deviation of the distribution in the x and y are equal and secondly, their distributions are Gaussian. Therefore the pattern is constructed of two independent variables x and y, each with a Gaussian distribution, variance σ^2, and zero mean. To examine the radial distribution (x, y) of pellets in the xy plane, the joint probability function is found from

$$p(x,y) = p(x)p(y) = \frac{1}{\sigma\sqrt{2\pi}} e^{-x^2/2\sigma^2} \frac{1}{\sigma\sqrt{2\pi}} e^{-y^2/2\sigma^2} \tag{3.11}$$

$$p(x,y) = \frac{1}{2\pi\sigma^2} e^{-(x^2+y^2)/2\sigma^2} \tag{3.12}$$

and described by $p(x,y)\mathrm{d}x\mathrm{d}y$, where $r^2=x^2+y^2$. In polar coordinates $p(x,y)\mathrm{d}x\mathrm{d}y$ transforms to $p(r,\theta)\mathrm{d}r\mathrm{d}\theta$,

$$p(r,\theta) = \frac{r}{2\pi\sigma^2} e^{-r^2/2\sigma^2} \quad , \tag{3.13}$$

where r and θ are independent variables with $0<r<\infty$ and $0<\theta<2\pi$. Writing

$$p(r,\theta) = p(r)p(\theta) \tag{3.14}$$

then, since the total probability in the angular direction is 1, for circular symmetry the total probability in any direction θ is $p(\theta)=1/2\pi$ as θ varies from 0 to 2π. Hence,

$$p(r) = \frac{p(r,\theta)}{p(\theta)} = \frac{r}{2\pi\sigma^2} e^{-r^2/2\sigma^2} 2\pi \tag{3.15}$$

giving

$$p(r) = \frac{r}{\sigma^2} e^{-r^2/2\sigma^2} \tag{3.16}$$

which is the Rayleigh distribution. By splitting the radial pellet distribution into a number *n* of annuli the pellet counts were obtained for equal increments of *r*, where the radius of the circles were multiplies of *r* (Figure 3.25), and the characteristic shape associated to the Rayleigh distribution observed (Figure 3.26).

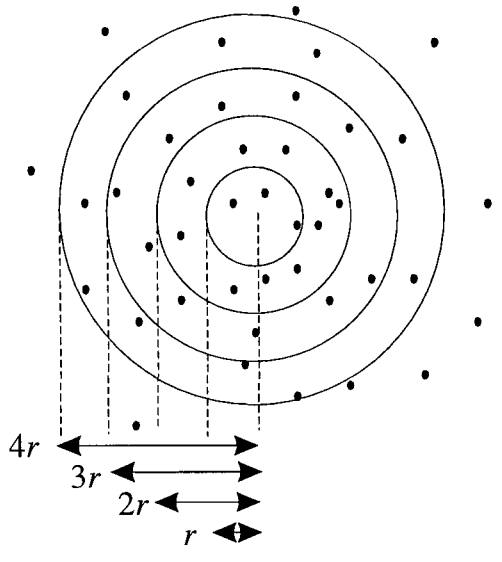

Figure 3.25 *The analysis procedure to determine the radial pellet distribution as a function of radius from the pattern centre, where the pellet counts are obtained in n number of annulii and the where circles radius at multiplies of r.*

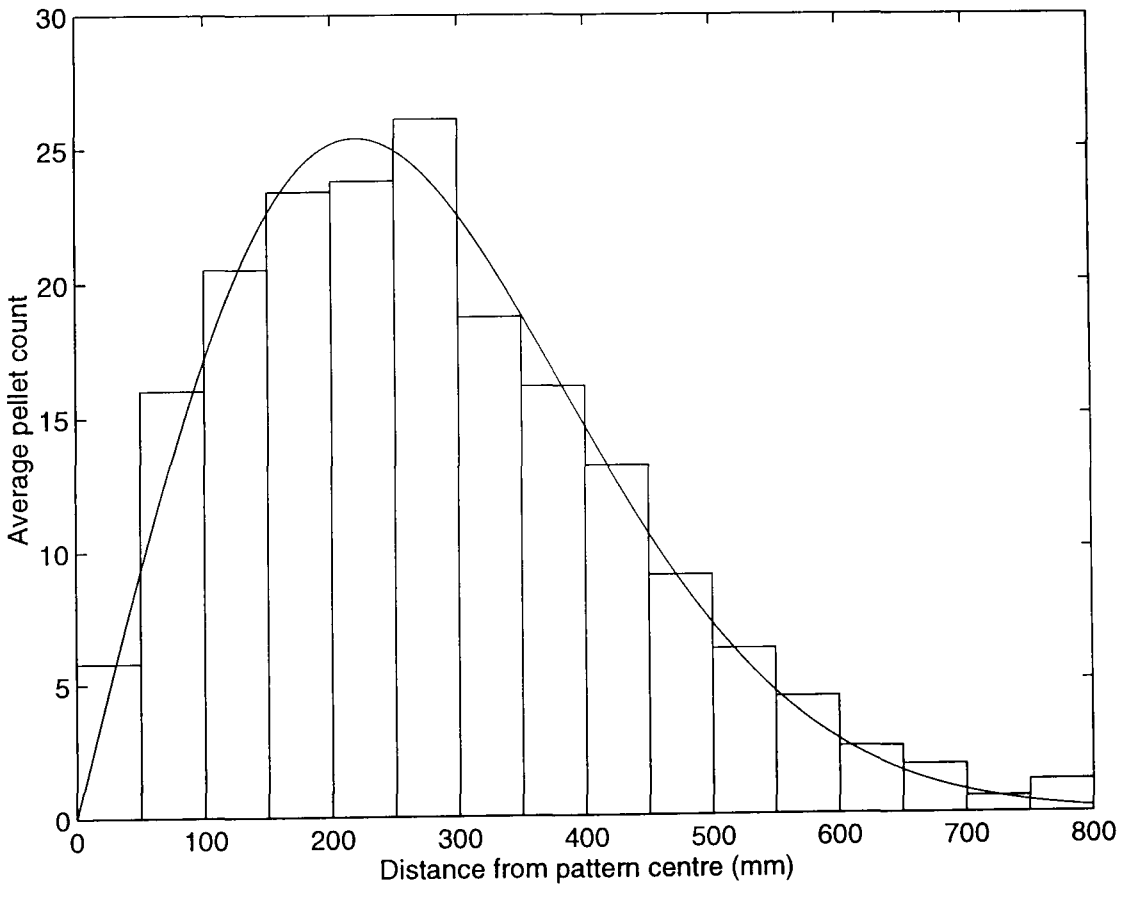

Figure 3.26 *The radial distribution as a function of radius for a 36g load of #4 lead shot (0.030" choke) at 40 yards. The histogram shows the average pellet counts in zones or annulii which have been incremented by multiples of r, and the curve is a fitted Rayleigh distribution.*

In Figure 3.26 the average pellet counts over 10 patterns for a 36g load of #4 lead shot are plotted against radial distance from the pattern centre. To check the suitability of the Rayleigh distribution a least squares fit with 14 degrees of freedom was applied to the data, producing a χ^2 of 2.41 and a 99% probability of χ^2. This excellent qualitative agreement confirms that the result of two independent Gaussians in the *x*- and *y*-axis, when observed in any annular direction as a function of radius, is the theoretical Rayleigh distribution.

The Rayleigh distribution expresses the radial pellet distribution in any annulus as a function of radius, where the areas change for different annulii. For ballistics it is desired to establish the pellet density per unit area (ρ), so the hit probability can be determined. The pellet density per unit area varies with distance r from the pattern centre and is determine from the Gaussian distribution in (3.6) and of the form

$$\rho = \rho_0 e^{-r^2/2\sigma^2} \quad , \tag{3.17}$$

where ρ_0 is the pellet density at the pattern centre. For this application the annuli must have equal areas, so the radii increments of the circles decrease from the pattern centre. In Figure 3.27 the pellet densities in 25 equal area annular zones are given for a 36g load of #4 lead shot (0.030" choke), and the radius, r, from the pattern centre is taken as the half area point for each annulus. Fitting (3.17) to the measured radial distribution with 18 degrees of freedom, χ^2 was calculated to be 2.42 with a 99% probability of not finding a better fit.

For the radial pellet density distribution in Figure 3.27 a good visual and qualitative agreement is established (with a probability of χ^2>99%) with (3.17). From the analysis of thousands of patterns during this investigation the probability of χ^2 has been observed to be greater than 99% for every combination of pellet size, material, range and choke. This reinforces the suitability of the Gaussian distribution as the best function which describes the radial pellet density distribution. In Table 3.13 the calculated χ^2 are given

for a selection of pellet sizes, materials and ranges (distribution shown in Appendix D) when fitting the data to (3.17).

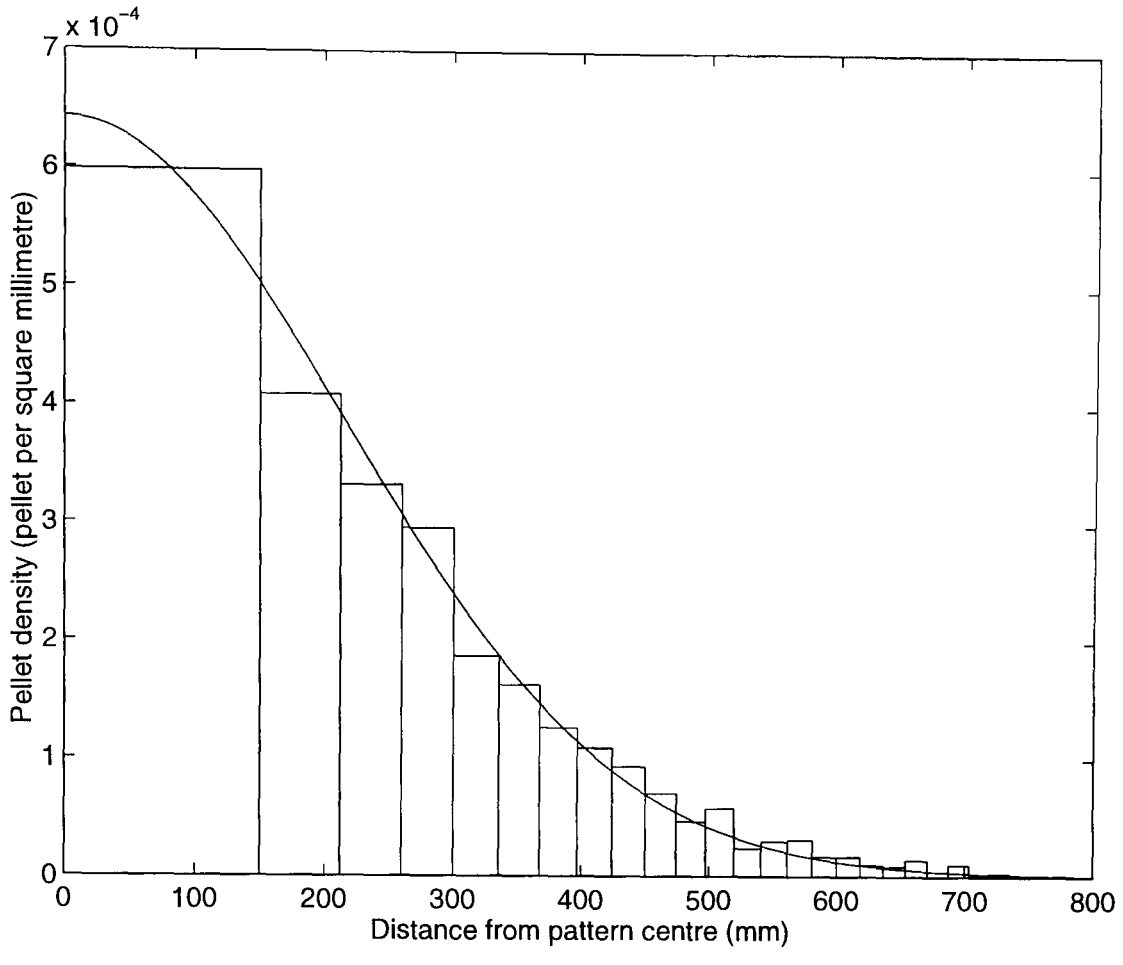

Figure 3.27 *The average radial distribution of pellet density averaged over 10 patterns for a 36g load of #4 lead shot (0.030" choke) at 40 yards. The histogram shows the calculated pellet densities in zones, or annuli, of equal area, and the curve is a fitted Gaussian.*

The results in Table 3.13 show that the goodness of fit becomes worst for the more diffuse patterns, but the increase in χ^2 has no significant effect on the probability of finding a better fit. From visual observation of the distribution produced by the more open chokes at 40 yards, shown in Appendix D, it suggests that they are starting to stray from the Gaussian, as Lowry [36] stated from his observations. However, the statistical analysis for the goodness of fit allows for the expected errors, especially large when there is only a few pellets in the outer annulus, and determines that the Gaussian distribution lies within these possible variation, therefore producing good qualitative agreement.

Material	χ^2	Radial standard deviation (mm)		
		Fit A	Fit B	30" circle
Figure 3.27	2.4	215	225	228
28g load of #7$^1/_2$ lead shot (0.000" choke) at 40 yds	5.1	389	410	402
28g load of #7$^1/_2$ lead shot (0.040" choke) at 40 yds	2.5	239	250	244
32g load of #3 steel shot (0.000" choke) at 40 yds	4.5	391	417	406
32g load of #3 steel shot (0.040" choke) at 40 yds	3.4	274	291	294
36g load of #3 bismuth shot (0.000" choke) at 40 yds	7.6	395	404	403
36g load of #3 bismuth shot (0.040" choke) at 40 yds	3.1	225	238	241
30g load of #4 zinc shot (0.000" choke) at 40 yds	7.7	440	442	473
30g load of #4 zinc shot (0.040" choke) at 40 yds	2.5	270	283	286
36g load of #BB lead shot (0.020" choke) at 20m	1.4	150	151	152
36g load of #BB lead shot (0.020" choke) at 50m	6.2	410	430	450

Table 3.13 *The Goodness of fit, χ^2, when fitting the measure pellet density distribution for a selection of pellet sizes, materials, chokes, and ranges to (3.17) and their corresponding associated radial standard deviation calculated from a least square fit (Fit A), a plot of r^2 versus* -ln*(1-p(n)), Fit B, and the pellet count in a 30" circle.*

The calculated radial standard deviation from the pellet coordinates were found to be the average of the individual standard deviations associated with x and y distributions. Earlier it was assumed that the standard deviation of the distribution in the x and y axis, thus the radial standard deviation are identical. In Table 3.13 this is validated by the calculated standard deviation generated from the least squares fit of a Gaussian to the radial pellet density data being within the expected standard errors of the (typically 5-10%) x and y distribution in Tables 3.11 and 3.12.

In establishing that the radial pellet distribution is best described by a Gaussian, an alternative method of calculating the standard deviation is achieved from (3.17) and the traditional pellet counts in a 30" circle. Firstly the total number of pellets, n_{total}, fired from the cartridge is obtained by integrating the density function, Equation (3.17), with respect to total area of the pattern. This is done analytically by considering a small area $rdrd\theta$ with pellet density $\rho(r)$ and integrating it over a circle with infinite radius,

$$n_{total} = \int_0^{2\pi}\int_0^{\infty} \rho_0 e^{-r^2/2\sigma^2} rdrd\theta$$

$$= 2\pi\rho_0\sigma^2 \qquad (3.18)$$

Similarly the number of pellets, n_r, in a centred circle with radius r can be found by

$$n_r = \int_0^{2\pi}\int_0^{r} \rho_0 e^{-r^2/2\sigma^2} rdrd\theta \qquad (3.19)$$

$$n_r = 2\pi\rho_0\sigma^2(1 - e^{-r^2/2\sigma^2}) \qquad (3.20)$$

and the proportion of pellets contained within it is given by

$$\frac{n_r}{n_{total}} = 1 - e^{-r^2/2\sigma^2}. \qquad (3.21)$$

Finally, re-arranging (3.21), the standard deviation σ for the radial distribution can be estimated from the percentage of pellets, $\%_r$, within any given radius circle r by

$$\sigma = \frac{r}{\sqrt{-2\ln(1 - \frac{\%_r}{100})}}. \qquad (3.22)$$

Conversely the percentage of pellets in any other circle can be determined from (3.21) a calculated standard deviation. In Table 3.13 it is shown that a good approximation (to within 5% of the fitted values) of the radial standard deviation is accomplished from the pellet count in a 30" circle.

A simple test for radial Gaussian is generated by plotting the logarithm of both sides of (3.21). The plot of r^2 against -ln(1-$P(n_r)$), where $P(n_r)$ is the average percentage of pellets over 10 patterns in a circle with radius, r, should produce a straight line with gradient $1/(2\sigma^2)$ which intercept the origin if the radial distribution is a true Gaussian. This method produces a good estimation of the standard deviation for diffuse patterns where all the pellets are not retrieved. From obtaining the percentage pellet counts in various circle sizes out to the traditional 30" measure the corresponding standard deviations (Fit B) calculated from the gradient of the slope are given in Table 3.13. From analysis it has been found that this method of determining the radial standard deviation also gives a good approximation to within 5% of the equivalent measure generated by the least squares fit (Fit A) to a Gaussian of the radial pellet density data.

In Figure 3.28 the r^2 versus -ln(1-$P(n)$) plots are given for a 28g load of #7$^1/_2$ lead shot at 40 yards using 0.000" and 0.040" choke, and a 36g load of #BB lead shot (0.030" choke) at 30 and 40 metres. These plots illustrate the relationships of the compact (Figure 3.28 a(ii) and b(i)) and diffuse (Figure 3.28 a(i) and b(ii)) lateral pellet distributions. The straight line fitted to the percentage of pellets measured in circles of diameters less than 762mm (30") generated an estimate for the radial standard deviation. It is noticeable that the measured pellet percentages in circles larger than 900mm, for the more compact distributions start to visually stray from the theoretical straight line produced by a Gaussian. For these circles with radii greater than 1.65σ, 2.3x10^5 in the vertical axis, at least 90% of the pellets are encompassed within them. When allowing for the expected errors, the standard deviation of the averages shown in Figure 3.28 as the error bars, it is then possible to establish that the measured distribution is still statistically within the expected radial Gaussian (straight line). Therefore by simply taking measurements of pellet counts in different diameter circles

centred on the pattern centre the radial distribution is shown to be approximately Gaussian for different types of pellet distribution.

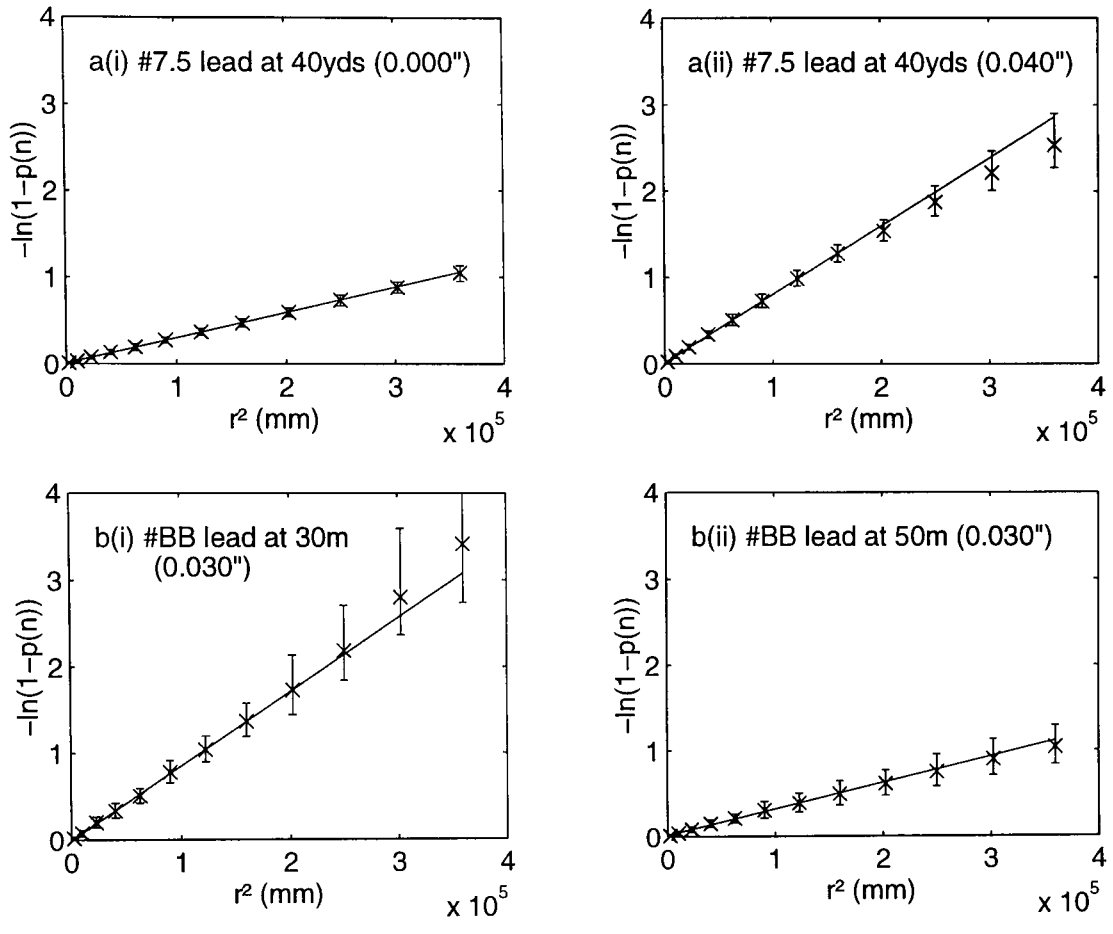

Figure 3.28 *A plot of r^2 versus -ln(1-p(n)), where p(n) is the pellet percentage in a circle of radius r for (a) a 28g load of #7$^1/_2$ lead shot at 40 yards using 0.000" and 0.040" choke. In (b) a 36 load of #BB lead shot is given for a 0.030" choke at 30 and 50m. The straight line is extrapolated from the best fit of the p(n) made in circles with diameter less than 762mm (30").*

3.4.3 Evolution of the lateral distribution

The lateral distribution of pellets in a shot cloud at any range has been shown in section 3.2.1 to be affected by the internal ballistics of a gun. An alternative method of altering the lateral spread of pellets without changing the properties of the gun is by adjusting the range. From tests using pattern plates it can be demonstrated that the width of lateral distribution of pellets increases with range. Therefore to determine the effect of range or flight time on the lateral distribution of pellets, the standard deviations were calculated from the pellet counts in a 30" circle for a limited selection of pellet sizes, material and chokes, at 5m increments between 20 and 50 metres.

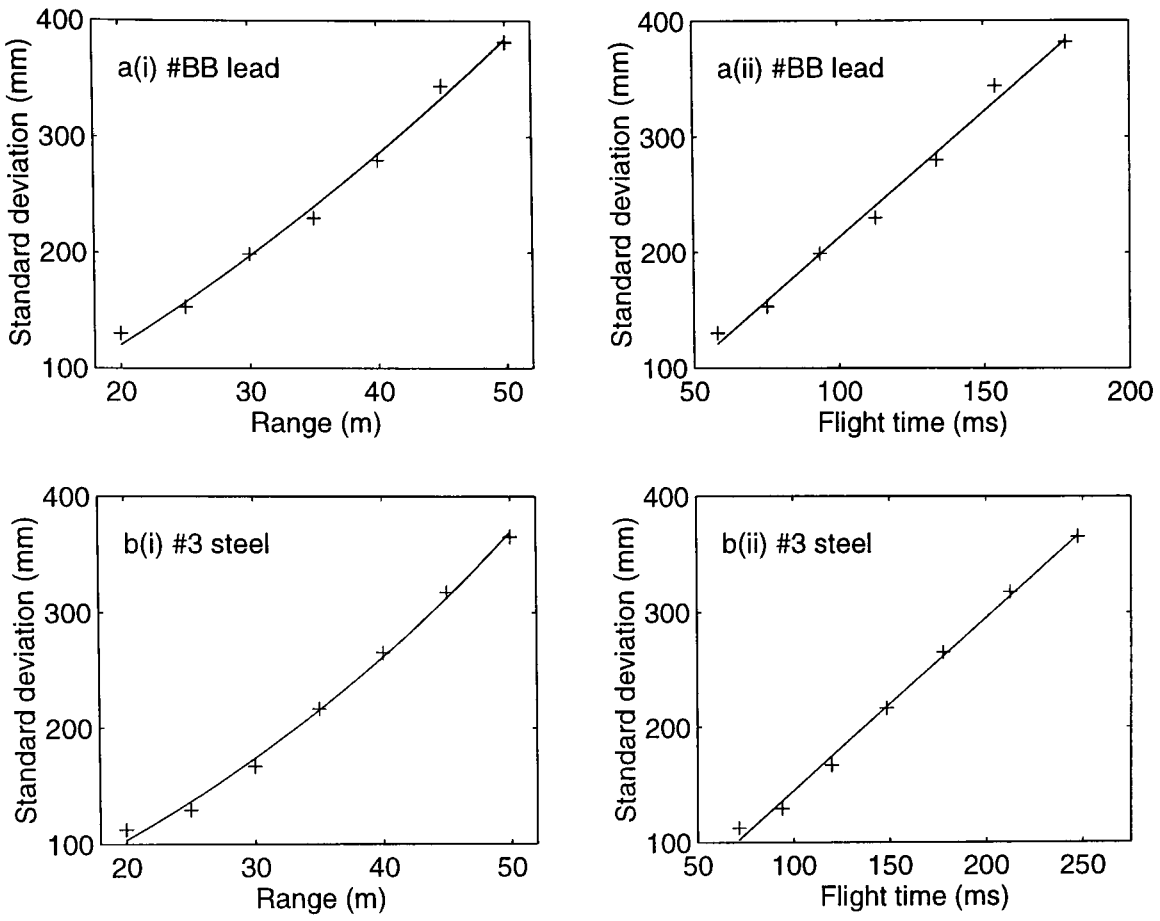

Figure 3.29 *The radial standard deviation (+) as a function of (i) range and (ii) leading edge flight time, t_2, for a 36g load of #BB lead shot (0.030" choke) and a 28g load of #3 steel shot (0.030" choke). The fitted curves are only there as an indicator of the relationships and the standard deviation were calculated from the average pellet counts in a 30" circle over 10 patterns.*

The visual indication shown in Figure 3.29 suggests that the lateral pellet dispersion, via the standard deviation, has a linear relationship with the leading edge flight time (t_2). By fitting a straight line to the calculated radial standard deviations and corresponding flight times for (a) 36g load of #BB lead shot (0.010" choke), (b) 36g load of #BB lead shot (0.030" choke) as shown in Figure 3.29(b), (c) 28g load of #3 steel shot (0.010" choke) and (d) 28g load of #3 steel shot (0.030" choke) as shown in Figure 3.29(a) the following expressions were obtained.

$$\begin{aligned} \sigma_a &= 2560t + 1.2 \\ \sigma_b &= 2180t - 5.5 \\ \sigma_c &= 1440t + 10.3 \\ \sigma_d &= 1500t - 4.98 \end{aligned} \qquad (3.23)$$

The nature of the fitted expressions in (3.23) shows that the relationship between the lateral pellet distribution and flight time passes close to the origin. With the negligible

influence of the additional terms on the lateral distribution, at the corresponding flight time between 20-50m, they can be ignored. Therefore the radial standard deviation is assumed to be proportional to flight time, where C_p is the pattern coefficient, σ is in millimetres and time t is in seconds. Note, the pattern coefficient will alter for the same ammunition when the choke is changed.

$$\sigma = C_p t \tag{3.24}$$

To assess the appropriateness of (3.24), a goodness of fit tests was applied to the data and found to be typically 1.5. With a corresponding 5 degrees of freedom, the high probability of χ^2 >95% establishes its suitability.

The linear relationship between lateral spread and flight time, describe in (3.24), has not been found to be affected by velocity and therefore is appropriate for pellets either obeying, as described in section 4.2, a cube or square of law of air resistance. Hence, the radial standard deviation with respect to range will be proportional to the time-range data. It is shown in section 4.2 that the majority of conventional shotgun cartridges are best modelled by a cube law of air resistance, therefore placing (4.7) into (3.24), the relationship (3.25) between radial standard deviation and range (R) is obtained, where k_3 is the deceleration constant and v_0 the initial velocity of the pellets. However, there are situations when the square law is a more appropriate model and expression (3.26) is obtained with its own deceleration constant, k_2.

$$\sigma_{cube} = C_p\left(\frac{1}{v_0}R + \frac{k_3}{2}R^2\right) \tag{3.25}$$

$$\sigma_{square} = C_p\left(\frac{1}{k_2 v_0}(e^{Rk_2} - 1)\right) \tag{3.26}$$

In Chapter 4, the initial velocities (v_0) and deceleration constants (k) of the pellets are shown to control their flight times. The deceleration constant is shown in (4.26) and

(4.29) to be inversely proportional to the pellets diameter (d), and material density (ρ_m) at the standardized atmospheric density (ρ_a), section 2.2.2. Hence, from section 4.4.3 the deceleration constants for a pellet travelling in the standard atmosphere are,

$$\frac{1}{k_3} = 450.8\rho_m d \tag{3.27}$$

$$\frac{1}{k_2} = 2.08\rho_m d \tag{3.28}$$

By placing (3.27) into (3.25) and (3.28) into (3.26), the theoretical pattern coefficients (3.29) and (3.30) are obtained for pellets obeying a cube or square law of air resistance.

$$C_{p_{cube}} = \frac{\sigma_R}{\left(\frac{R}{v_0} + \frac{R^2}{901.6\rho_m d}\right)} \tag{3.29}$$

$$C_{p_{square}} = \frac{\sigma_R}{\frac{\rho_m d}{v_0 2.08}\left(e^{2.08R/\rho_m d} - 1\right)} \tag{3.30}$$

In Figure 3.30 the theoretical pattern coefficients are given for the radial standard deviation, σ_R, associated with a 70, 60, 50, and 40% pellet count in a 30" circle at 40 yards, where the pellets, $d\rho_m$, have an initial velocity of 400m/s under standardized atmospheric conditions and obey a cube law of air resistance. From the calculated pattern coefficients, the evolution of the lateral distribution of pellets as a function of time, Equation (3.24), and range, Equation (3.25), can be determined for this pellet specification.

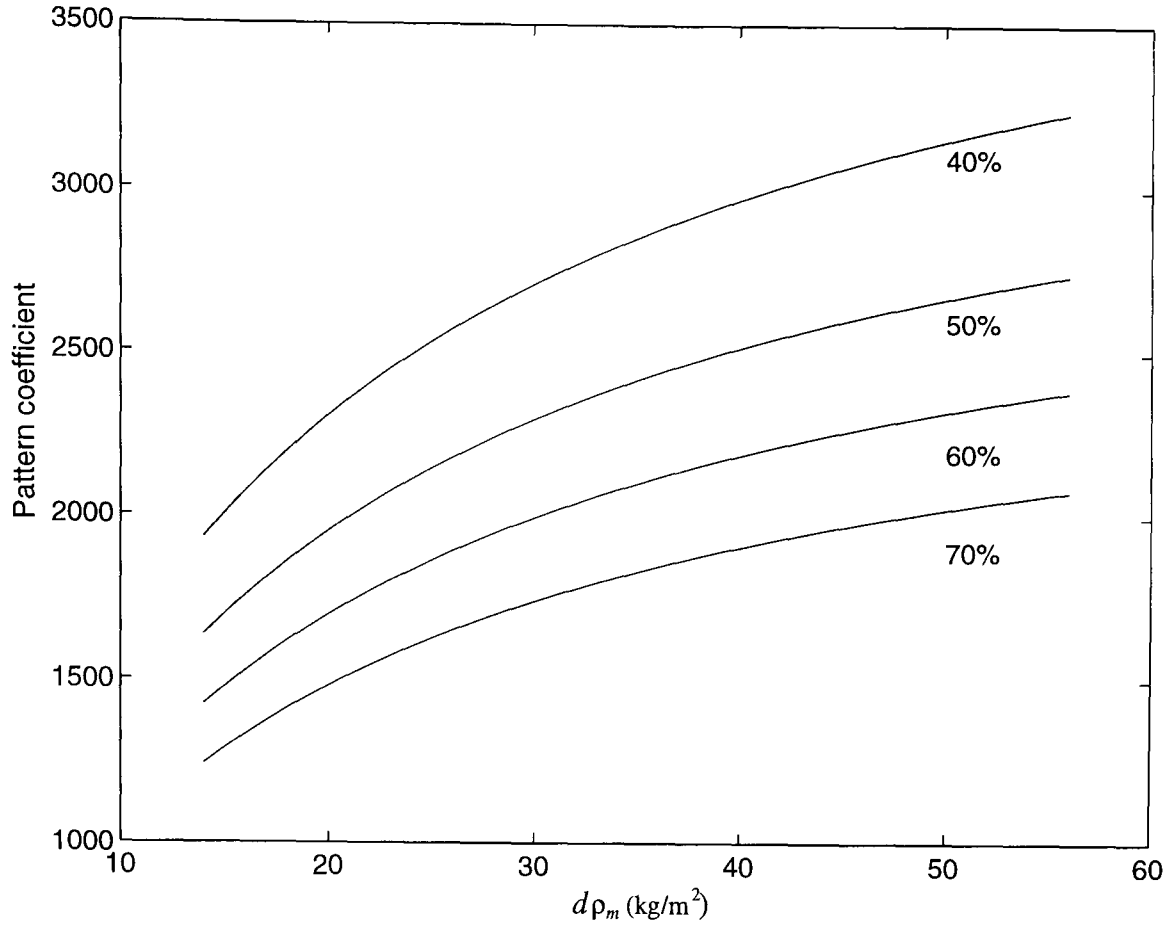

Figure 3.30 *The corresponding theoretical pattern coefficients for the radial standard deviations associated with a 70, 60, 50, and 40% pellet count in a 30" circle at 40 yards, where the pellets, $d\rho_m$, have an initial velocity of 400m/s under standardizes atmospheric condition are obeying a cube law.*

3.4.4 Hit probability

The consistency in the lateral pellet distribution, described by the percentage variation of measured standard deviation of the x and y pellet coordinates was shown in section 3.2.3 to be typically between 5-10% for a sample of 10 patterns. The variation causes a further reduction in the pellet density consistency associated with areas that are relatively smaller than the total area of the distribution. This is illustrate in Figure 3.6 and Table 3.14 where the percentage variation in the pellet counts increase, typically by a factor of three, when reducing the circles diameter from 30" to 10", i.e. as the area of interest. Therefore the variation in pellet density associated with smaller areas becomes an important factor when calculating the hit probability distribution on a given target area.

Circle diameter (mm)	Pellet count for 10 patterns										Mean	Standard deviation	*pv*
	1	2	3	4	5	6	7	8	9	10			
127 (5")	9	14	6	10	9	9	8	6	18	3	9.2	4.02	43.7
254 (10")	27	39	39	24	29	42	26	27	43	30	32.6	6.92	21.2
762 (30")	154	147	156	149	134	141	147	123	149	137	143.7	9.56	6.64

Table 3.14 *The pellet counts in 5", 10" and 30" circles for a 36g load of #4 lead shot using a 0.030" choke at 40 yards along with their mean, standard deviation and percentage variation (pv).*

For events which have a large number of possibilities (the number of pellets in the total area of a pattern) and a small number of outcomes (the pellet counts in areas much smaller than the total distribution) the statistical process described by the Poisson distribution and derived by (for example) Barlow [45] is applicable. This means the hit probability distribution $P(H)$ of the pellets on a given area will follow a Poisson distribution, which is described by (3.31). This process gives the probability $P(H)$ of obtaining exactly H pellets in a given target area with an average number of pellets $\overline{H}$.

$$P(H) = \frac{\overline{H}^{H} e^{-\overline{H}}}{H!} \tag{3.31}$$

For the Poisson distribution to be valid in this context, it is required that the pellet density (ρ) over the area of interest (A) is approximately constant so that

$$\overline{H} = \rho A \quad . \tag{3.32}$$

The probability of exactly H pellets in a given area is of no practical interest in the ballistics field, except where H=0. Therefore the probability for at least x pellets is actually the probability of all the pellet counts in A less than x, subtracted from 1, and given by

$$P(\geq x) = 1 - e^{-\overline{H}} \left[\sum_{k=0}^{x-1} \frac{\overline{H}^k}{k!} \right] \quad . \tag{3.33}$$

The nature of the Poisson distribution means that there is always a finite probability of zero pellets in the area of interest A, and therefore in the ballistics sense there is always a possibility that a shooter centres a target in the pattern but still misses. A graphical representation of the Poisson distribution is given in Figure 3.31, this shows the probability of finding at least x pellets in a given target area. For example if at least 5 pellets are required in a given target area A, for at least 90% of the time, it is necessary on average to obtain 8.

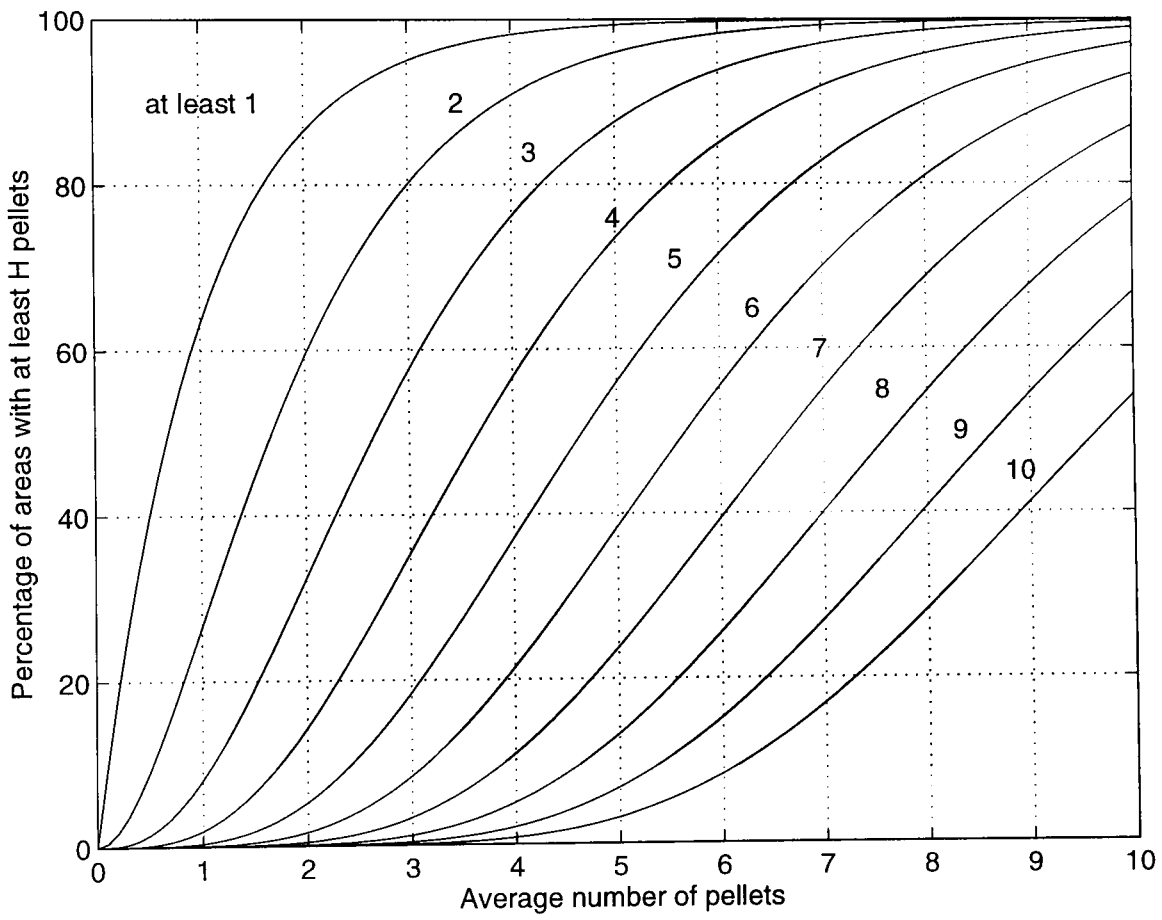

Figure 3.31 *The variation in the percentage of target areas A receiving at least H pellets with average number of pellet. In the graph H varies from 1 to 10.*

To illustrate the appropriateness of the Poisson distribution on the lateral dispersion of pellets in a shot cloud, a linear relationship should result from

$$\overline{H} = \ln\left[\frac{\overline{H}^{H}}{H!P(H)}\right] , \qquad (3.34)$$

which is the logarithm of (3.31). The average number of pellets ($\overline{H}$) and the probability of H number of pellets can be found by examining small areas (A) in the lateral distribution that have equal pellet densities (one of the requirements for a Poisson distribution). With the associated radial Gaussian distribution the pellet density in an area A will be on average the same on any given circumference from the pattern centre. To achieve practical measurements on $P(H)$ over a range of average pellet counts, $\overline{H}$, the lateral pellet distributions were split into 5 equal area annuli within a 774mm diameter circle. Each annulus was then divided into 12 equal segments (shown in Figure 3.32) with area equivalent to a 100mm diameter circle. By averaging over 10 patterns the average number of pellets associated to the segments in each annulus were obtained along with the corresponding probabilities of finding 0, 1, 2 and 3 pellets. As the pellet density decreases from the pattern centre the five calculated values of $P(H)$ were different. To produce more variation in $P(H)$, annuli with different pellet densities and therefore average pellet counts, in each segment were also produced by altering the choke constriction.

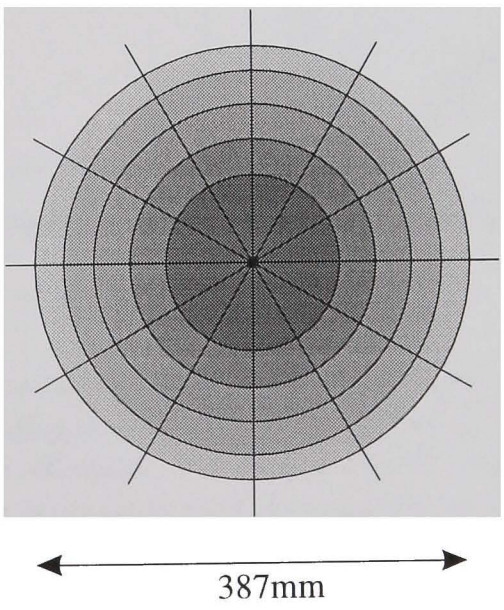

Figure 3.32 *The lateral pellet distribution within a 774mm diameter circle split into 5 equal area annuli and 12 equal segments. Each segments has the equivalent area of a 100mm diameter circle.*

The expected linear relationship associated with the Poisson distribution is demonstrated in Figure 3.33 between the probability of finding H pellets, in a given area A with an average pellet count of $\overline{H}$ for a 36g load of #4 lead shot (0.000" - 0.050" choke), where A is the equivalent area of a 100mm diameter circle. This same relationship has also been generated during the investigation from the lateral pellet distribution produced by different pellet sizes, materials and at different ranges and several other examples given in Appendix E. Therefore it is concluded that the Poisson distribution is applicable in the analysis of the lateral distribution of pellets in a shot cloud, and especially in the ballistics application of hit probability on a target.

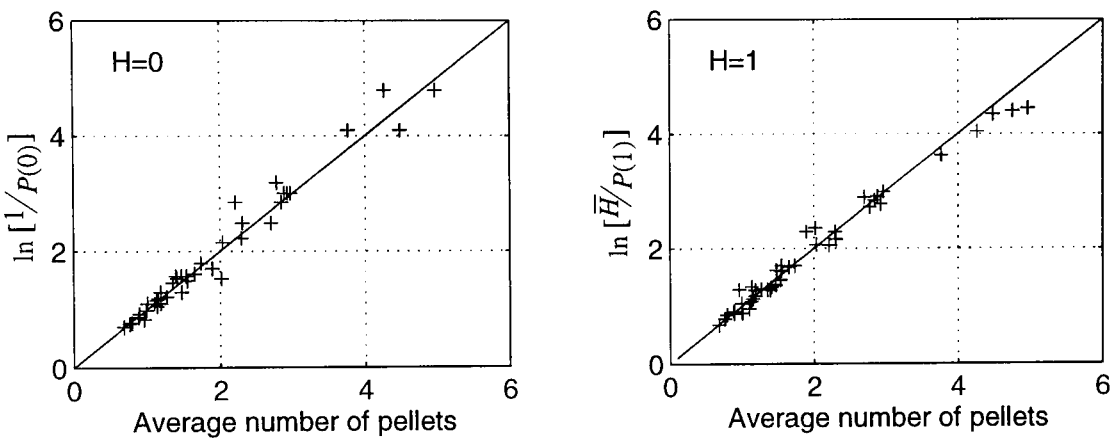

Figure 3.33 *The relationship between the measure average pellet counts ($\overline{H}$) in areas, A, of similar pellet densities and the corresponding probabilities of finding 0, 1, 2 and 3 pellets for a 36g load of #4 lead shot (0.000" - 0.050" choke) at 40 yards. The area A chosen in that of a 100mm diameter circle and the solid line represents the theoretical Poisson distribution.*

3.5 THREE-DIMENSIONAL REPRESENTATION

3.5.1 Implementation of shot cloud reconstruction

The investigation into the pellet density distribution within a shot cloud has established that the longitudinal and lateral distributions are best described by Rayleigh and Gaussian distributions, respectively. However, their combined effect on the overall distribution is unknown. For example what is the true separation between two pellets 2cm apart laterally, they could actually be 2m apart longitudinally? From the limited positional information generated by the ballistics target this overall pellet distribution of the shot cloud can be observed by the reconstruction of the shot cloud outline (Figure 3.34).

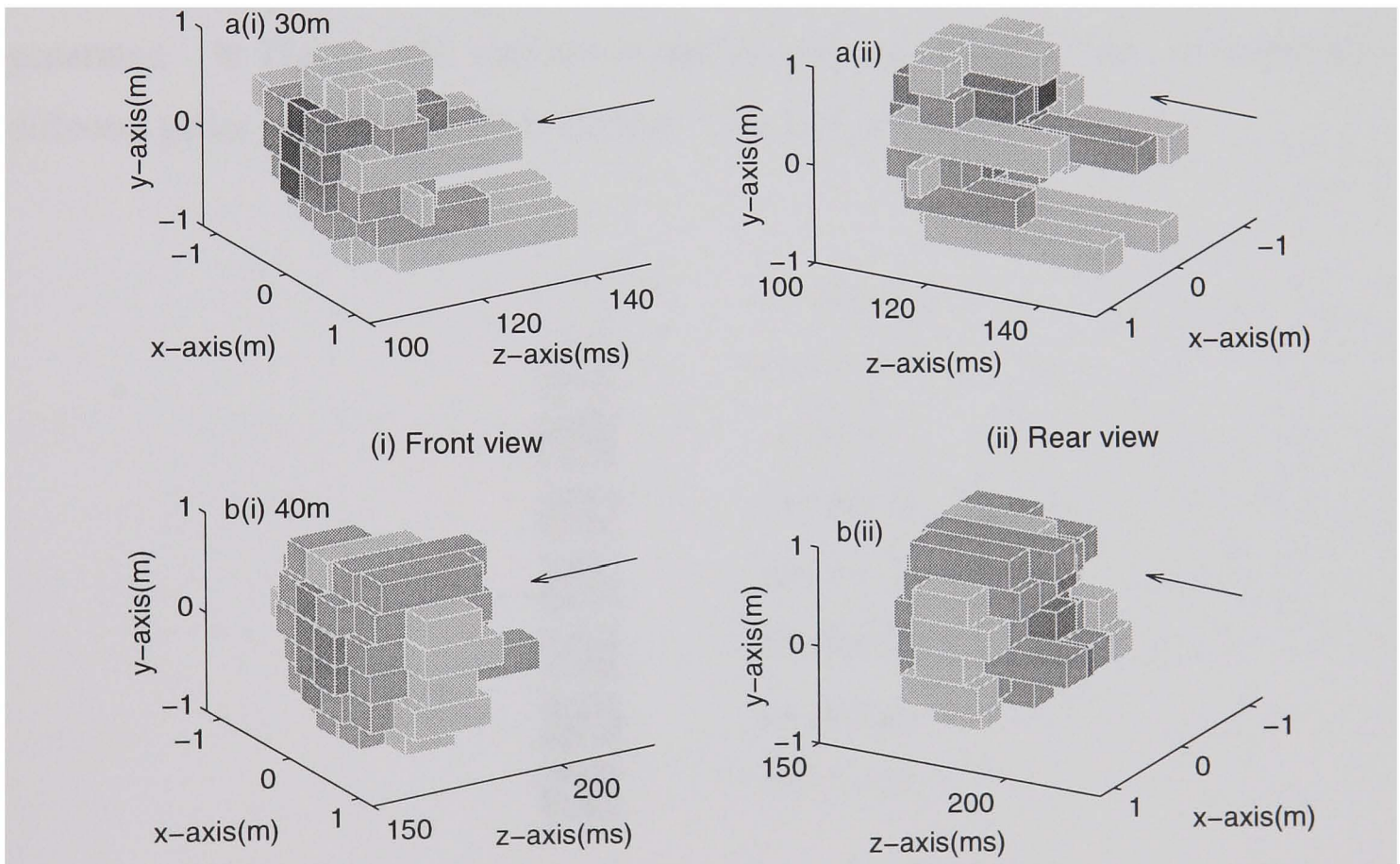

Figure 3.34 *The reconstruction of a shot cloud viewed from the (i) front and (ii) rear as it reaches the target at (a) 30 and (b) 40 metres for a 28g load of #9 lead shot (0.010" choke). The gray shades indicate the pellet density associated with that particular area of the shot cloud and the z-axis is the longitudinal direction in milliseconds. The arrows indicate the direction of flight.*

For the reconstruction of shot clouds at one range, between 20-50m, the ballistics target is split into 32 smaller individual impact areas (30cm square detector panels). These

smaller areas were recorded separately and enabled the corresponding flight times for the first and last impact in different regions of the shot cloud. The full description of the experimental set up is given in section 2.7. From the flight time data for each individual impact area and their spatial co-ordinates an outline of the shot cloud was built up. In Figure 3.34 the front (i) and (ii) rear view outlines for a 28g load of #9 lead shot using 0.010" choke are given at (a) 30 and (b) 40 metres.

In section 3.3.3 it was shown that it is possible to calibrate the shot cloud profile in terms of pellet density by the proportion of the sum of squared voltages in a given area to the sum of total square voltages produced by the whole shot cloud profile. Introducing this concept to each of the impact areas, by calculating the percentage of their combined square voltages to the sum of the total square voltages produced by all the impact areas, an indication of the pellet density throughout the shot cloud was generated. In Figure 3.35 various shades of grey are given which are associated to different pellet percentages (P) in Figures 3.34, 3.36 and 3.37.

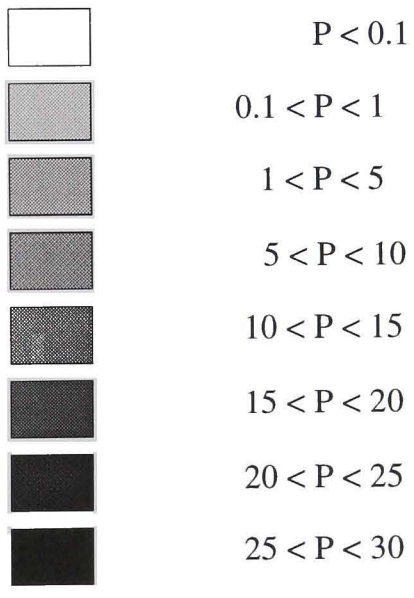

Figure 3.35 *The associated shade of grey representing pellet percentage* P *in a given area.*

The three-dimensional reconstruction of the pellet arrival times at the ballistics target in small impact areas has shown that no one shot cloud is the same as another, therefore emphasizing the inconsistency in pellet distribution between identical loads. However, from the reconstruction of several hundred shot clouds, a trend was discovered

irrespective of shot size, material, choke or range. The general shape of the shot cloud revealed that the pellets arriving first (leading edge) are located in the centre of the pattern, as seen in Figure 3.34, and the trailing edge pellets appear at the outer regions.

The results from the reconstruction of the shot clouds and the bubble-wrap tests (recovery of fired pellets in section 3.2.1) indicate that the deformed pellets, collected at the outer parts of the pattern, travel at the trailing edge shot cloud. The well formed pellets, associated with the pattern centre, are to be found at the leading edge of the shot cloud. The same conclusion can be made indirectly from Journée's [1] experimental work on pellets cartridge to pattern location. For these experiments he colour coded different parts of the unfired cartridge load, these pellets then produced coloured marks on the white pattern plates after firing. He determined that the pellets loaded at the rear of the cartridge were predominately found in the outer regions of the pattern, and the corresponding front pellets produced marks in the pattern centre. Therefore with the greater associated deformation on pellets at the rear of the load, caused by the pressure in the barrel compressing them into the pellets above, a similar relationship between the pellets deformation and location in the shot cloud is seen in both experiments.

3.5.2 Three-dimensional outlines

The importance of reconstructing the shot cloud in this investigation was to demonstrate the general relationship between the pellet position in the lateral (pattern) and longitudinal (shot cloud profile) distributions. After discovering that there is a large variation in the shapes of the shot clouds, which makes interpretation of any relationships difficult, it was decided that no further useful information could be obtained from measurement technique. Therefore the main interests in the three-dimensional reconstruction is in the measurement and instrumentation aspect of the research.

For a true three-dimensional outline, all the axes should be in the same units, and therefore it is required to change the time units in Figure 3.34 into range. Using data produced by the standard ballistics tests, the leading and trailing edge velocities can be

generated for any given range. Although the extreme velocities are known, the actual distribution within the shot cloud is not determined due to the impact response limitation of the ballistic target. Therefore it is assumed, as a first approximation, that the velocity distribution between the leading and trailing edges is linear with time. Therefore a linear distribution of velocities along the shot cloud is used to associate a velocity with a relative impact time and hence a distance from the leading edge. The distance for the first and last impact on each detector are represented as a solid block at their appropriate position in the cloud. This is shown in Figure 3.36 where three-dimensional outlines for a 28g load of #9 lead shot at 30m and 40m illustrates the pellet density increasing at the pattern centre for a tighter choke or shorter range. With regard to the pellet material, the shot cloud lengths of steel loads are confirmed in Figure 3.37 to be the shortest of any material tested.

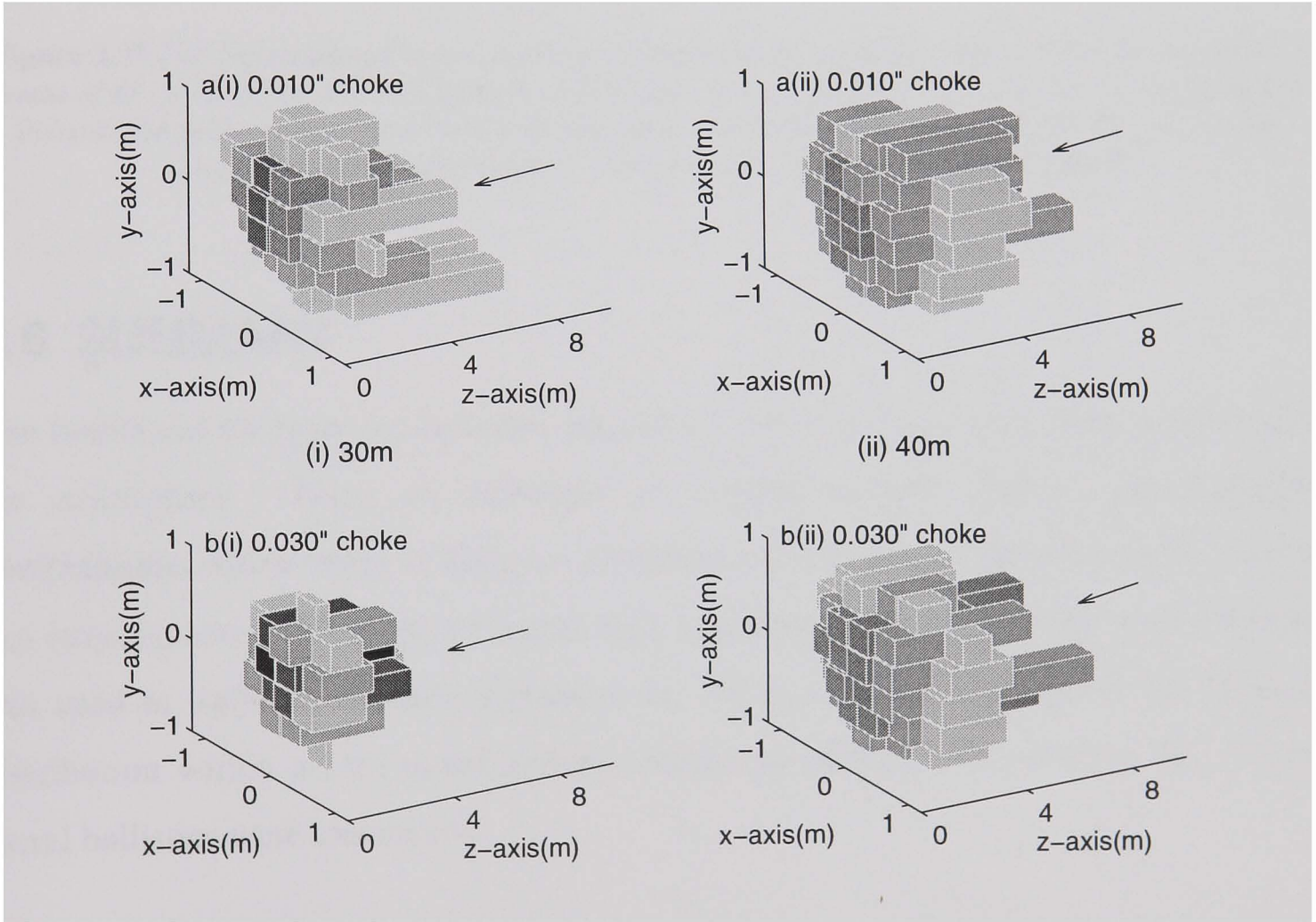

Figure 3.36 *The 3-dimensional reconstruction, viewed from the front, of a shot cloud at (i) 30 and (ii) 40 metres for a 28g load of #9 lead shot when using (a) 0.010" and (b) 0.030" choke. The grey shades indicate the pellet density associated with that particular area of the shot cloud and the z-axis is the longitudinal direction in metres. The arrows indicate the direction of flight.*

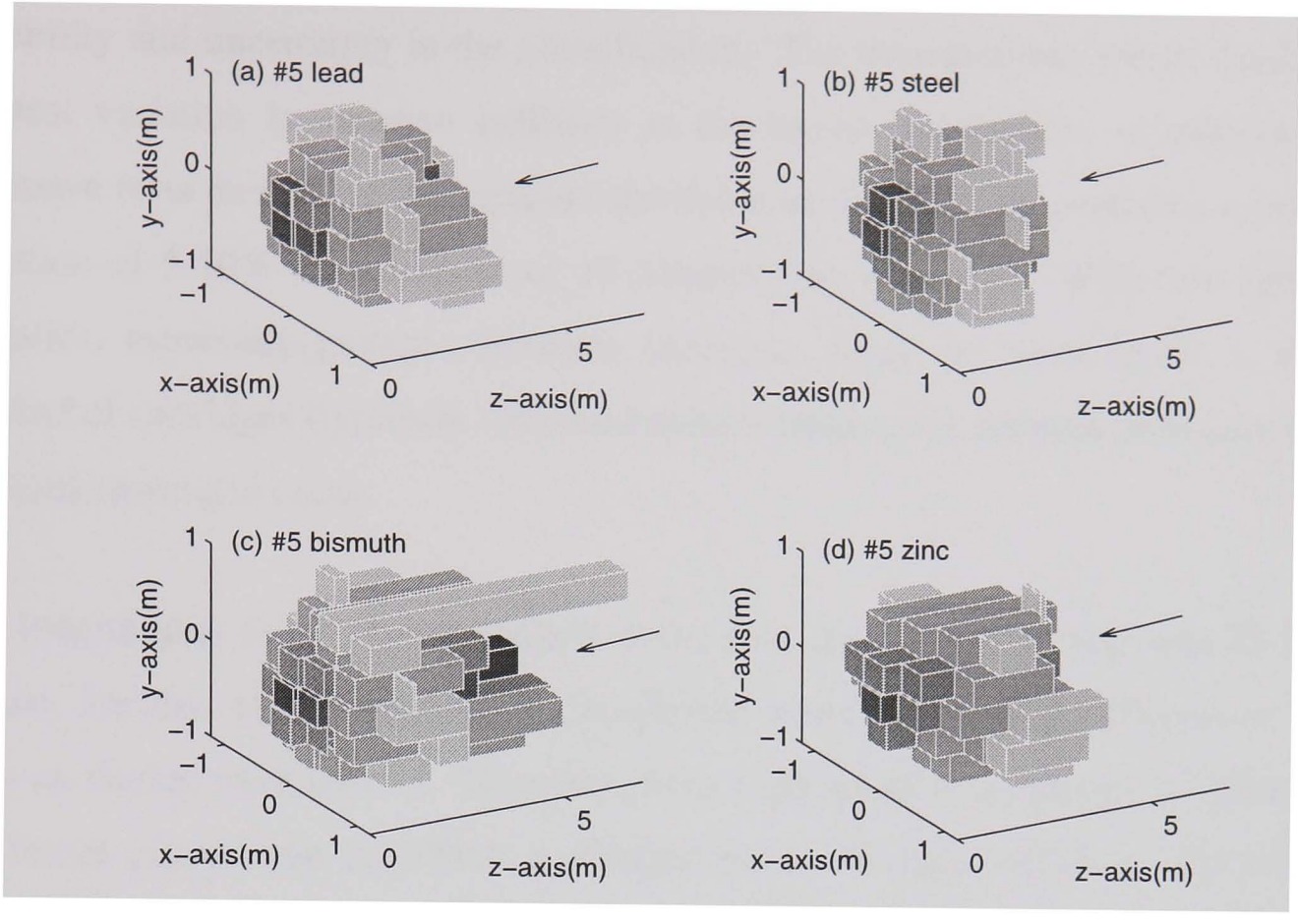

Figure 3.37 *The 3-dimensional reconstruction, viewed from the front, of a shot cloud at 40 metres for a loads of #5 (a) lead, (b) steel, (c) bismuth and (d) zinc shot when using 0.030" choke. The grey shades indicate the pellet density associated with that particular area of the shot cloud and the z-axis is the longitudinal direction in metres. The arrows indicate the direction of flight.*

3.6 SUMMARY

The traditional shotgun and cartridge are used in this investigation to launch pellets into the atmosphere. There are hundreds of internal shotgun ballistic and cartridge combinations which result in different distributions of pellets in the shot cloud. During this investigation a standardized barrel with interchangeable choke tubes and chambers was used to limit the number of unknowns. With a standardized barrel the different distribution within a shot cloud and the associated effects when altering the internal barrel ballistics were examined.

Tests on a large selection of shotgun ammunition have shown that from a batch of cartridges there is a variation in their ballistic performance. The leading edge flight times of the shot clouds, ignoring stray pellets, were found to be the most consistent and easily identifiable measurement of the system. They have a typical percentage variation of 1-2% compared to the 2-4% for the trailing edge, where there was a greater

variability and uncertainty in the identification. The measurement which displayed the greatest variation in shotgun ballistics is the lateral distribution, or pattern. From extensive tests measuring the standard deviation of the pellet co-ordinates a percentage variation of 5-10% for a sample of 10 patterns was observed. With this variation in ballistics, especially patterns, between cartridges from the same batch, a sufficient number of cartridges (typically 10) tested at each range were deemed necessary to obtain a reliable averaged result.

The longitudinal distribution of pellets in the shot cloud at ranges between 20-50m was shown, via shot cloud length, to be unaffected when the internal ballistics of the gun, such as choke, were altered. However, from high speed photography it is known that the initial distribution of pellets is affected by the internal ballistics. Therefore it is assumed that the in-flight effects of the pellet become the more dominant factor, thus masking the internal ballistics effect, at ranges greater than 20m. Far more informative, and a unique feature of the measurement facility described in section 2.5.4, is the shot cloud profile which gives an overview of the pellet distribution along the length of the shot cloud. From the analysis of the shot cloud profiles it was established that the longitudinal pellet distribution is best described as a Rayleigh distribution.

Analysing the lateral distribution of pellets in the shot cloud it was established that there are two independent distributions, that is the horizontal (x) and vertical (y) pellet distributions. These two distributions were shown, for the data generated over this investigation, to be best described as Gaussian distributions with zero means and equal standard deviations. Combining the two independent Gaussians the characteristics of a radial Gaussian density distribution about the pattern centre was justified. With the lateral spread following a Gaussian distribution, it was confirmed that the Poisson process was applicable for describing the probability of finding a given number of pellets in a small area of the pattern.

It was concluded that an acceptable method of measuring the radial standard deviation associated with the lateral distribution of pellets at any range, could be obtained from the pellet count in a given circle. Experiments were undertaken to determine the effect

of choke on the lateral distribution of pellets. The results of increasing choke constriction at a fixed range (40yds) showed that the standard deviation levelled off, therefore lateral pellet distribution did not reduce, after 0.030". These results were obtained using a linear tapered choke profile and further experiments are required on different choke profiles to verify this relationship between lateral distribution and choke constriction. It is known from earlier work by Lowry that choke alters the initial lateral and longitudinal spread of pellets near the muzzle. However, he did not establish whether these limiting effects on the lateral distribution of pellets occur at the muzzle, because he only used a small selection of choke constrictions. Therefore it would be recommended to examine these near-muzzle initial stages of the shot cloud development to determine if it is the in-flight effects of the pellets which cause this limiting on pattern width at ranges over 20m.

The inconsistency in pellet distribution in similar shot clouds, such as the cartridges from the same batch, was emphasized when reconstructed in three dimension. The combination of the variation seen in the shot cloud profile, and especially the patterns, produced outlines which altered dramatically. However, a general trend in the shape of shot cloud was found and indicated that the trailing edge pellets in the shot cloud profile are located in the outer regions of the pattern. Combining this information with the findings of the bubble-wrap tests, the recovery of fired pellets, it is concluded that the worst deformed pellets travel at the rear of the shot cloud in outer regions of the pattern, and the well-shaped pellets travel at the leading edge in the centre of the pattern.

It has emerged clearly from this work that it is not possible to produce a satisfactory theory which can predict the downrange behaviour of shot clouds from the muzzle condition in sufficient detail to render practical measurement superfluous. Ballistics therefore have to remain very much an experimental science. Also further work is required to understand the full effects of choke constriction and choke profile on shot clouds. This is probably best investigated using high speed photography over the first 10 metres of flight, together with conventional pattern tests.

Chapter 4

Modelling shot cloud ballistics with single sphere theory

4.1 INTRODUCTION

The work presented in this chapter is concerned with condensing and summarizing the experimental time-range data to obtain the ballistic characteristics of shot clouds. The data is summarized by being fitted to an appropriate model, whereby the muzzle velocity, velocity and energy per pellet, shot cloud length and the deceleration characteristics of the pellets are calculated. It is also shown how comparative ballistics are made by correcting the experimental data to a standardized atmosphere.

An assumption used throughout the chapter is that the shot cloud has dispersed sufficiently at the measurement range (>20m) so each individual pellet is travelling relatively freely. Using the equation of motion for a single sphere in free flight, two types of fit are derived and correspond to the individual pellets obeying a cube or square law of air resistance. To ascertain the suitability of the models a measure of the deviation of the fitted data to the experimental data is used to show the best fit.

In order to standardize the ballistic characteristics of the shot cloud, the deceleration characteristics of the pellets are analysed. From a scaling relationship between the pellet's diameter and its deceleration characteristics, comparative ballistics are obtained for different pellet densities. The standardized ballistics for lead, steel, bismuth and zinc are given in a contract report for the Department of the Environment [13] and were presented to the shooting community [40].

The measurement facility has generated a large amount of data on a variety of pellet diameters and densities which take the format of shot clouds. A method is described which condenses all the data into a normalized plot and shows the consistency of the results obtained.

The final aim of the chapter is to use a synthesis procedure to predict the downrange ballistics of a shot cloud. Using the drag force equation for a single sphere in free flight the synthesis model is compared with experimental data to assess its validity.

4.2 CURVE FITTING TO AN APPROPRIATE MODEL

4.2.1 Behaviour of the pellets

The ballistics measurements consist of time-range data for different shot materials and pellet diameters. These results are to be condensed and summarised by fitting to an appropriate model. The pellets obey different laws and trends through their flight and it is assumed that they have dispersed sufficiently, at the measurement ranges of 20-50m, to be flying independently. Therefore, each pellet's aerodynamic performance, at the measurement ranges may be approximated as a single sphere travelling in free flight.

4.2.2 Single sphere drag coefficient

The main forces experienced by a sphere when in free flight, described in section 1.4.1, cause it to decelerate. The force of air resistance is dependent on four parameters: the sphere's cross sectional area, the atmospheric conditions, the sphere's instantaneous velocity and the drag coefficient. The drag coefficient was described early as a non-dimensional coefficient dependent on Mach Number, shape and Reynolds number. Experiments by Charters and Thomas [4], Bailey and Hiatt [5] and others [10,24] show that, for the Reynolds numbers (calculated in section 1.4.1) associated with shot clouds, the drag coefficient has three main stages, subsonic, transonic or supersonic. These stages have already been shown in Figure 1.7, where the drag coefficient is fairly constant below Mach 0.5 and above Mach 1.4 and approximately proportional to Mach number between the two constant levels.

The typical combination of shotgun and cartridge launches the pellets at velocity around 400m/s (Mach number ~1.2) and therefore a pellet in free flight would experience the transonic and subsonic stages of the drag coefficient curve. Although there are three distinct regions the drag coefficient curve has a smooth transition between the regions and would involve a more complex model. Therefore the following assumptions have been used to represent the drag coefficient (C_D) characteristics for the free flight pellets in a shot cloud. Firstly, as mentioned earlier, the pellets at the measurement ranges behave like smooth single spheres in free flight and the drag coefficient is only a

function of Mach number. For pellets at velocities below the critical value (M_C) and above the upper velocity, M_U, (this region above M_U is not encountered for most shotgun pellets in free flight) the drag coefficient is constant (shown in Figure 4.1). At velocities between the critical velocity (M_C) and an upper velocity level (M_U), the drag coefficient on a pellet can be approximated as directly proportional to the Mach number.

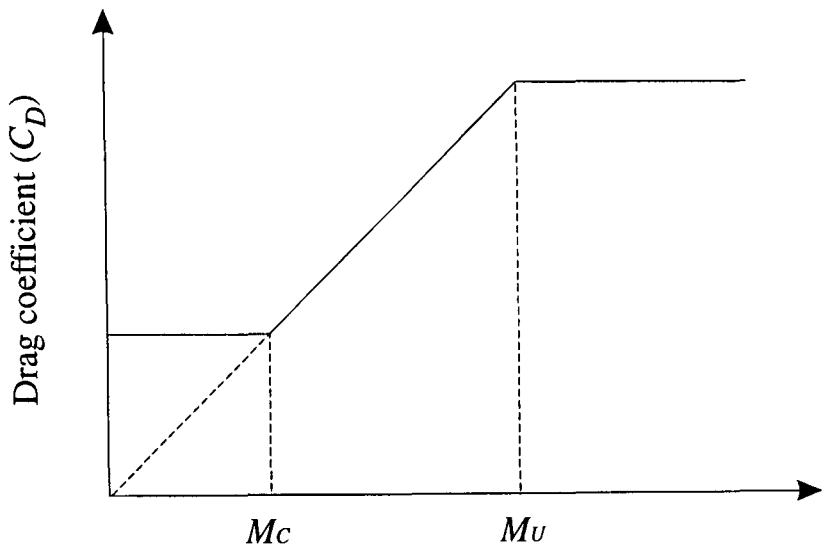

Figure 4.1 *The assumed shape for the drag coefficient versus Mach number for a single pellet in free flight.*

4.2.3 Deceleration of a pellet

The drag coefficient affects the force acting on the pellet, as given in (1.1), and therefore its deceleration. Using the assumptions in section 4.2.2 along with Newton's fundamental law of dynamics

$$F_D = m\frac{dv}{dt} \quad , \tag{4.1}$$

the deceleration of a pellet can be calculated

$$\frac{dv}{dt} = -\frac{\rho_a A v^2 C_D(M)}{2m} \quad . \tag{4.2}$$

In combining the constant ρ_a, A, and m (4.3) represents the general law of air resistance, where n is a function of velocity and k is the deceleration constant.

$$\frac{dv}{dt} = -k_n v^n \tag{4.3}$$

If the drag coefficient (C_D) is constant, i.e. a pellet's velocity is above M_U or below M_C in Figure 4.1,

$$\frac{dv}{dt} = -k_2 v^2 \tag{4.4}$$

so that a single pellet experiences a square law of air resistance. If a pellet is travelling at a velocity between M_U and M_C, i.e. in the transonic region, then C_D is assumed to be proportional to velocity and a cube law of air resistance is obtained, so that

$$\frac{dv}{dt} = -k_3 v^3 \quad . \tag{4.5}$$

It should be noted that k_2 and k_3, though they are both deceleration constants, have different dimensions.

4.2.4 Fitting time-range data

When a pellet is travelling in the transonic region it is assumed to follow a cube law of air resistance represented by (4.5). To obtain a flight time model (4.5) is integrated with respect to velocity and time, giving

$$v = \frac{v_0}{\sqrt{1 + 2k_3 v_0^2 t}} \quad , \tag{4.6}$$

writing $v=dR/dt$ and integrating again leads to

$$t = \frac{1}{v_0} R + \frac{k_3}{2} R^2 \quad . \tag{4.7}$$

The solution of (4.5) is a second-order polynomial expression of flight time, given by (4.7), as a function of range, R, where v_0 (initial velocity) and k_3 can be found from the experimental flight time data by a least squares fitting process [46]. It should be noted at this stage that the curve fitting is used only over the measured range 20-50m. This is because it is not good practice to extrapolate back to get the muzzle velocity, as the assumption of a pellet in free flight cannot hold for the region close to the muzzle where pellet interaction has been shown in Figure 1.6 to exist. This will be discussed in more depth later.

If a square law of air resistance is assumed for the free flight of a pellet a non-linear model for flight time is obtained with two constants v_0 and k_2 in (4.8). Once again these constants are found by a least squares fit process [46]. A weighted least square fit was not thought necessary in this application because the standard deviation on the average flight times were found to be similar over the measurement range. Therefore the weighting factor would be similar for each data point.

$$t = \frac{1}{k_2 v_0}\left(e^{-k_2 R} - 1\right) \tag{4.8}$$

4.2.5 Derivation of the velocity and energy per pellet

To obtain an expression for the velocity as a function of range for a cube law of air resistance,

$$\frac{dt}{dR} = \frac{1}{v} \tag{4.9}$$

and therefore (4.7) is differentiated with respect to time and range to give

$$v = \frac{v_0}{1 + k_3 v_0 R} \quad . \tag{4.10}$$

Differentiating (4.8) by time and range (4.11) is obtained for the corresponding expression of velocity representing a square law of air resistance.

$$v = v_0 e^{-k_2 R} \tag{4.11}$$

To obtain the kinetic energy (E) for both the cube and square law of air resistance all that is required is to use the equation of kinetic energy, given in (4.12), where m is the mass of the pellet.

$$E = \frac{1}{2} m v^2 \tag{4.12}$$

4.2.6 Shot cloud length

From the averaged leading and trailing edge flight time data it is possible to estimate the length of the shot cloud as a function of range, where the length at a particular range is arbitrarily defined as the distance between the leading and trailing edges of the shot cloud when the leading edge is at the specified range.

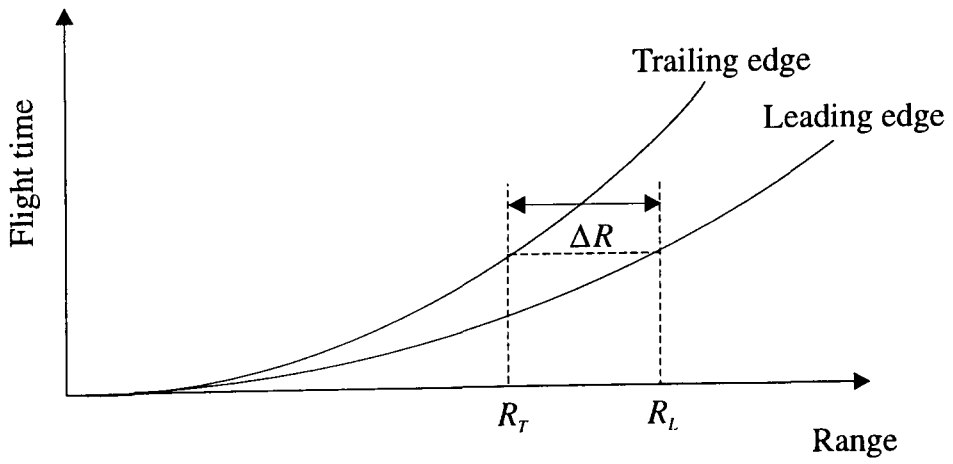

Figure 4.2 *Shows the relationship between the flight time and range for the leading edge R_L and the trailing edge R_T of the main shot cloud. The distance ΔR denotes the main shot cloud length.*

In Figure 4.2 it can be seen that the shot cloud length (ΔR) is defined to be the difference between the leading edge range (R_L) and the trailing edge range (R_T) when the leading and trailing edge flight times are the same.

4.2.7 Best model for data

Experimental flight time data from the measurement facility, described in Chapter 2, was used to obtain the fitted values for the initial velocity v_0 and the deceleration constant (k_2 or k_3) by a least squares fit of the time-range formula for either the square law result or the cube law of air resistance. This was routinely done for the leading (t_2) and trailing edges (t_3) of the main section of the shot cloud. From the two constants representing the initial velocity and the deceleration constant the velocity and energy per pellet and the length were obtained for shot clouds consisting of pellets with velocities that lay within one of the velocity regimes. This type of information was produced for every batch of ammunition tested and sent to the supplier along with the equivalent data in tables (see Appendix F for a typical ballistics test report).

In Figure 4.3 the leading, (i), and trailing edge, (ii), average flight time data from 10 cartridges per range are show for shot clouds with pellet velocities in (a) the cube law regime, or (b) square law regimes and the corresponding least square fits to (4.7) or (4.8), respectively. The cube law pellets were generated by a 36g load of #BB (4.25mm) lead shot using 0.030" choke and had a percentage variation (pv) of 1.2% and 2.1% for the leading and trailing edge. The square law pellets were generate by a 28g load of #4 (3.02mm) steel shot using 0.020" and had a percentage variation of 1.8% and 1.5% for the leading and trailing edges. The percentage variation (pv), as described in section 3.2.1, represents the standard deviation as a ratio of the average flight times. Therefore when averaging over 10 cartridges the standard error is less than 1% of the average flight times. With this small expected error associated to the averaged flight times it is of no visual benefit to plot error bars on Figure 4.3.

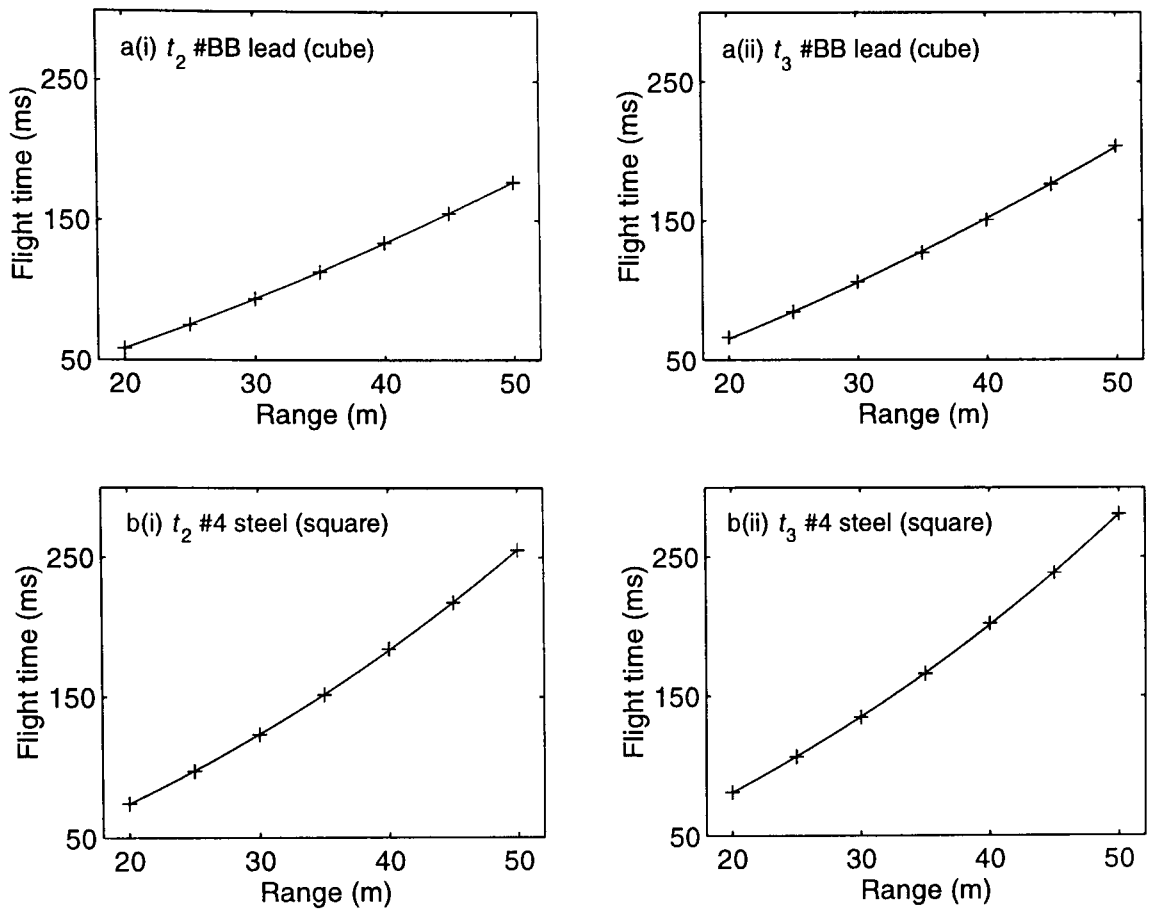

Figure 4.3 *The average (i) leading edge, t_2, and (ii) trailing edge, t_3, time-range data for pellets with velocities in the (a) cube law or (b) square law regime and their corresponding least square fits to (4.7) or (4.8). The cube and square law pellets were obtained from a 36g load of #BB (4.25mm) lead shot (0.030" choke) and a 28g steel load of #4 (3.02mm) steel shot (0.020" choke), respectively.*

The time-range curves in Figure 4.3 show excellent fit to the experimental data. As a measure of this agreement, the normalized deviation, d_n, of the fit from the experimental data is calculated and given by

$$d_n = \frac{1}{7}\sum_{n=1}^{7}\frac{(f_n - d_n)^2}{f_n^2} \quad , \tag{4.13}$$

where f_n are the fitted values obtained from the least square fit and d_n are the experimental data points. The values of d_n vary between 0 and 1, if the fit agrees well with the actual values then d_n will be small and if it is 1 the fit is very poor. The values of d_n obtained are typically of the order of 10^{-5} (see Table 4.1) for both the cube and square law fits shown in Figure 4.3.

In order to examine the effects of fitting the experimental data using either a square law or cube law of air resistance, the data from the square law experimental results were

used to attempt a fit to the cube law model. Similarly the square law fit was fitted to the cube law experimental data. The appropriateness of the fit was measured by the normalized deviation d_n and found to increase by a factor of 10 for all cases (shown in Table 4.1). This was found for any shot cloud that travelled downrange obeying either a square law of a cube law of air resistance over the ranges studied.

Material	Normalized deviation d_n			
	Cube law fit		Square law fit	
	Leading edge (t_2)	Trailing edge (t_3)	Leading edge (t_2)	Trailing edge (t_3)
36g load of #BB (4.25mm) lead shot (pellets obeying a cube law of air resistance)	2.2×10^{-6}	5.1×10^{-5}	1.1×10^{-5}	2.4×10^{-5}
28g load of #4 (3.02mm) steel shot (pellets obeying a square law of air resistance)	1.2×10^{-4}	8.7×10^{-5}	5.4×10^{-5}	3.5×10^{-5}
(a) 36g load of #4 (3.09mm) lead shot (mainly cube law)	4.4×10^{-5}	2.2×10^{-5}	6.6×10^{-4}	3.8×10^{-5}
(b) 30g load of #4 (3.33mm) steel shot (spends time in both laws between 20-50m)	2.8×10^{-5}	2.3×10^{-5}	5.9×10^{-5}	2.3×10^{-5}
(c) 24g load of #7.5 (2.32mm) lead shot (spends time in both laws between 20-50m)	1.8×10^{-5}	3.4×10^{-4}	5.8×10^{-5}	4.2×10^{-4}
(d) 28g load of #8 (2.19mm) zinc shot (mainly square law)	3.6×10^{-4}	4.6×10^{-4}	2.7×10^{-5}	5.1×10^{-6}

Table 4.1 *The normalized deviation, d_n, of the cube law and square law least squares fits to experimental data. The cube and square law pellets are the same are in Figure 4.3 and also shown are a selection of other loads with their corresponding velocities given in Figure 4.5.*

The drag coefficient characteristics have been shown in Figure 1.12 to become constant at velocities below M_C. The value of M_C is approximately Mach 0.5 and corresponds to 170m/s depending on air density. From fitting data to both square law and cube law least square fits, it has been found for the majority of shot clouds made from large diameter, high density pellets (i.e. >3mm lead pellets), the leading and trailing edge

velocities, shown in Figure 4.4(a), do not fall below M_C until 45-50m. This suggests that the pellets spend the majority of their measured flight time travelling in the transonic region. For shot clouds consisting of small diameter low density pellets, such as <2.5mm steel or zinc pellets shown in Figure 4.4(d), they travel for a shorter period (20-25m) above M_C and spend the majority of their measured flight time in the square law region. The shot clouds made up of small diameter high density or large diameter low density pellets are shown to travel below M_C for approximately a third (35-50m) of the measured flight time in Figure 4.4(b) and (c).

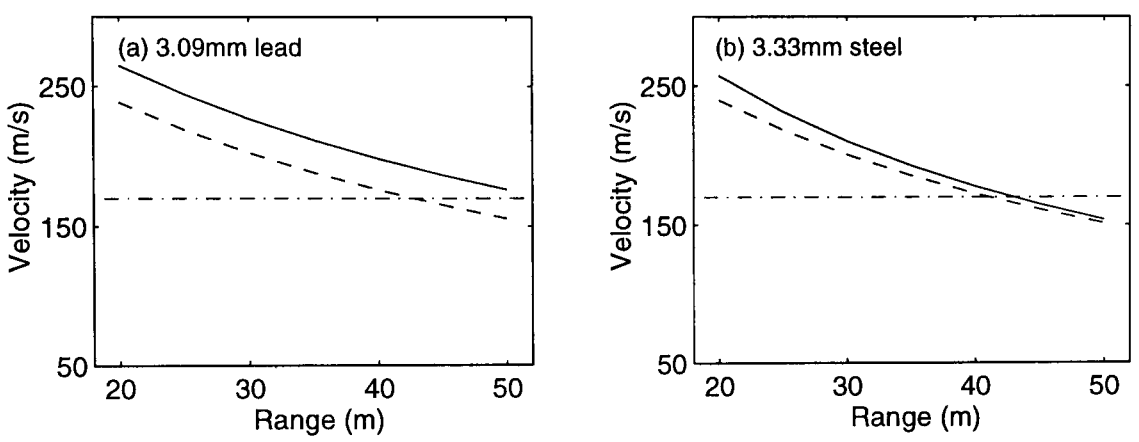

Figure 4.4 *Velocity distribution for the leading and trailing (--) edges of the shot cloud for (a) a 36g load of #4 (3.09mm diameter) lead shot, (b) a 30g load of #4 (3.33mm diameter) steel shot, (c) a 24g load of #7.5 (2.32mm diameter) lead shot and (d) a 28g load of #8 zinc shot (2.19mm diameter). The horizontal line corresponds to ~ Mach 0.5.*

The results in Table 4.1 shows that the deviation d_n of the fitted data to the experimental data supports the case for the cube law of air resistance being better than the square law fit for shot clouds that spend the majority of the measurement ranges above M_C. This model has been used in tests for contractual work to fit the leading and trailing edge flight time data to a second-order polynomial, Equation (4.7), which is a statistically

robust model with 7 data points and only 2 unknowns. The square law model is still used for the lower velocity loads, which are found to spend the majority of time below M_C in the square law regime over the measured ranges.

4.2.8 Muzzle velocity

The flight time data for the leading edge of the shot cloud is measured at 1m increments out to 8m from the muzzle, as described in section 2.4. From the flight times over a known distance, the instantaneous velocity at the mid-point between two skyscreens can be estimated. To obtain the muzzle velocity, the near muzzle flight times for each shot cloud were fitted to a time-range curve. Due to the complexity of a shot cloud near the muzzle there is no known model which summarizes its behaviour. It was found that a least squares second-order polynomial gave the best fit with the smallest d_n. As there were eight flight time data points it was considered that there is a high confidence level in extrapolating back from the 1m skyscreen and obtaining the velocity at the muzzle or out by say 1m to 9m if necessary. It is explained by Farrar and Leeming [47] that projectiles can slightly accelerate for a distance, equivalent to several calibres, after exiting the muzzle due to the high pressure gases mixing with the ambient air and changing the atmospheric condition near the muzzle. This has been recognized and ignored as it is a small relative effect.

The extrapolated muzzle velocity from the skyscreen data was compared with the theoretical value obtained from the fitted 20-50m flight time data. In Table 4.2 it can be seen that if the shot cloud spends the whole of its flight time over the measurement range in either the square law or cube law regimes the corresponding fitted value representing v_0 is within 5% of the measured muzzle velocity. For shot clouds that travel down the measurement range (20-50m) in both the regimes, (b) and (c), the theoretical and extrapolated muzzle velocities differs by >10%. It is clear from these differences that experimental data from the measurement range cannot be used to obtain a reliable measure of the muzzle velocity. Therefore it is not recommended to extrapolate back from 20-50m flight time data or out from the measured muzzle velocity. This is because models fitting data at the muzzle or the measurements ranges

(20-50m) cannot hold for other stages of the shot cloud development, due its dispersive nature.

Material	Muzzle velocity (m/s)	
	Extrapolated	Theoretical
36g load of #BB (4.25mm) lead shot (pellets obeying a cube law of air resistance)	393	399
28g load of #4 (3.02mm) steel shot (pellets obeying a square law of air resistance)	322	330
(a) 36g load of #4 (3.09mm) lead shot (mainly cube law)	391	399
(b) 30g load of #4 (3.33mm) steel shot (spends time in both laws between 20-50m)	393	428
(c) 24g load of #7.5 (2.32mm) lead shot (spends time in both laws between 20-50m)	402	472
(d) 28g load of #8 (2.19mm) zinc shot (mainly square law)	393	396

Table 4.2 *The extrapolated and theoretical muzzle velocity for the shot cloud loads given in Table 4.1. The extrapolated value is obtained from the skyscreen data and theoretical value was generated by the least square fit of the flight time data over the measurement range (20-50m) to the appropriate model of air resistance, either (4.7) or (4.8).*

4.3 CORRECTION FOR ATMOSPHERIC CONDITION

4.3.1 Properties of the atmosphere

A pellet will experience a different deceleration rate when the atmospheric conditions change. From (4.2) and (4.3) the deceleration constant, k_n, for the general law of air resistance is given by

$$k_n = \frac{\rho_a A C_D(M)}{2m} \quad , \tag{4.14}$$

where it can be seen that the air density (ρ_a) controls the deceleration of identical pellets travelling in different atmospheres. The density of the air is dependent on three properties, air pressure, air temperature and humidity. The perfect gas equation, described by

$$\rho = \frac{GK}{p} \quad , \tag{4.15}$$

relates the first two parameters to density, where p denotes the pressure in pascals, K the absolute temperature in degrees Kelvin, ρ the density in kg/m^3, and G is the gas constant. From (4.15) a rise in pressure creates an increase in density, but a rise in temperature decreases the density. Therefore, changing atmospheric condition can allow the pellet to travel more easily on a hot day when the pressure is low.

The perfect gas equation, (4.15), is only appropriate for the air density when the humidity is zero. The humidity is a measure of the percentage of water vapour present in the air and therefore alters the air pressure and density. To allow for this effect, de Mestre [21] shows that the pressure of the moist air (p),

$$p = p_a + p_w \quad , \tag{4.16}$$

is the combination of the water vapour (p_w) and air pressure (p_a). From (4.15) and (4.16) an expression for the density of moist air (ρ_{ma}) is thus given by

$$\rho_{ma} = \frac{p_w}{R_w K} + \frac{(p - p_w)}{R_a K} \quad , \tag{4.17}$$

where R_w and R_a are the respective gas constants for water and air, with ρ_a and ρ_w denoting the corresponding density contributions. The pressure p is what is measured and the pressure of the water vapour is found from (4.18) which is dominated by the

relative humidity of the air, where p_o is the pressure of the water vapour at temperature K and can be found in the chemistry tables [50].

$$p_w = \frac{RH}{100} p_o \tag{4.18}$$

From routine recording of the weather condition at the outdoor measurement facility (see section 2.2.2) the extreme air density variation found all year round was 6% (1.18-1.25 kg/m^3). With this type of variation it is necessary to standardize the atmospheric condition for comparative ballistics.

4.3.2 Pellets obeying a cube law of air resistance

It is evident from (4.14) that the deceleration constants (k_3) for identical cube law pellets, given in (4.5), travelling in different atmospheres are controlled by the air density (ρ_a). In relating a small change in air density, $\delta\rho_a/\rho_a$, to the small change in flight time, ($\delta t/t$), (G.6) shows that for small R the air density does not have a great influence on the flight time. As R becomes larger (shown in Figure G.1) the increase in flight time ($\delta t/t$) levels off to a point where it become approximately constant. Furthermore, the nature of (G.6) indicates that $\delta t/t$ is always less than $\delta\rho_a/\rho_a$.

$$\frac{\delta t}{t} = \frac{\delta\rho_a / \rho_a}{1 + 2/k_3 v_0 R} \tag{G.6}$$

It has already been stated that the variation in air density measured all year round was between 1.18-1.25kg/m^3. With the international standard for air density being 1.225kg/m^3, as shown in section 2.2.2, the extreme correction required for comparative ballistics is 4%. To show the effect air density has on the flight time experimental data for a 28g load of #6 (2.56 mm) lead shot was taken when the air density was 1.18 kg/m^3 and then fitted to (4.7) to find k_3 (7.4x10^{-5}) and v_0 (440m/s). In Figure 4.5 the increase in flight time with range is shown for the corresponding increase in k_3 when the air

density rises by 1, 2, 3 and 4%. It can be seen that the flight time is influenced more the further from the muzzle the pellets travel, but over the measurement ranges (out to 50m) the effects are less than 50% of the corresponding increase in air density. The deceleration constant used in this example is typically the maximum value for a pellet which obeys a cube law of air resistance over all the measurement range (20-50m), and therefore shows the extreme effects.

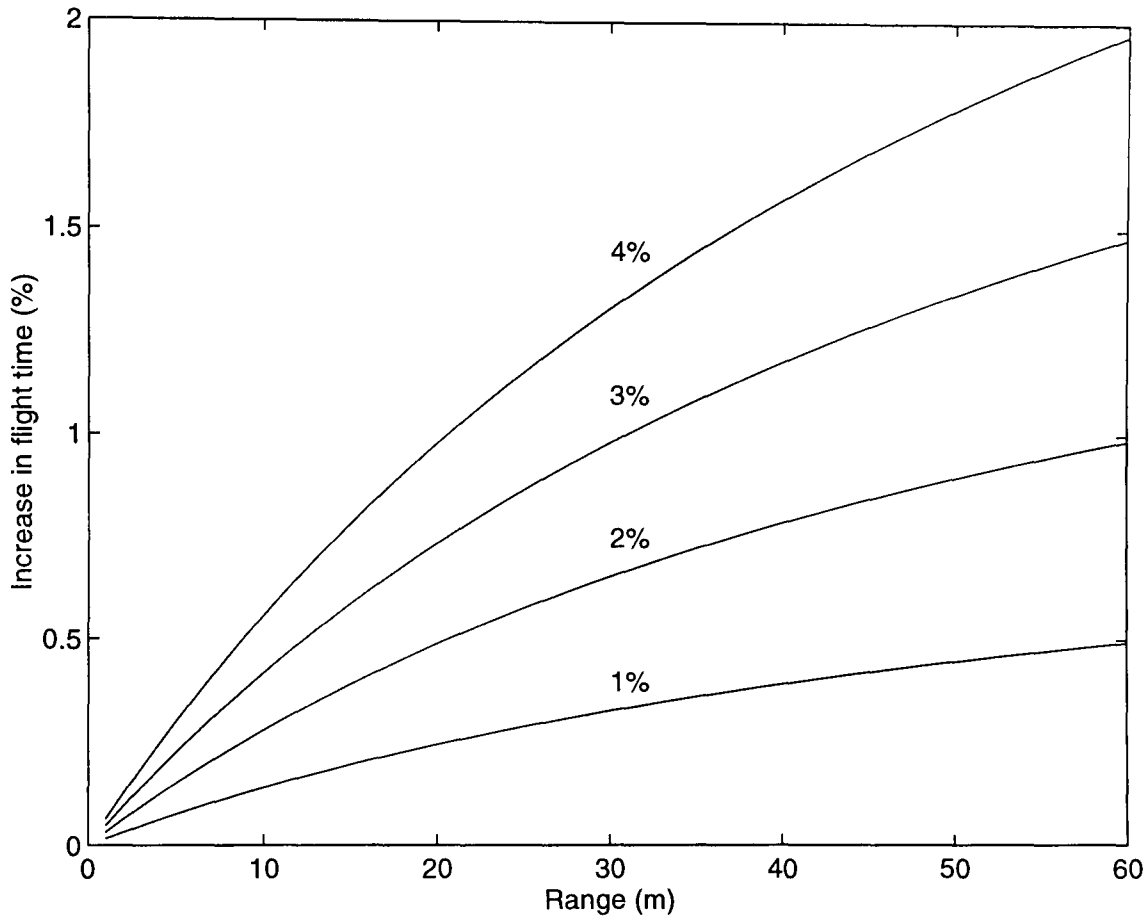

Figure 4.5 *Percentage increase in flight time with range for a increase in air density of 1, 2, 3 and 4%. The initial value for k_3 was obtained from the time-range data of a 28g load of #6 (2.56mm) lead shot being fitted to a cube law of air resistance with an air density of 1.18 kg/m^3.*

Using cartridges from the same batch, measurements were carried out on a different days when the atmospheric conditions met the standardized air density of 1.225 kg/m^3. Table 4.3 shows the standard deviation of the leading edge flight times over the measurement ranges for the two different atmospheric conditions. It can be seen from the standard deviation of both sets of data that the average flight times can be expected to vary by 1%. This means that for an increase in 4% in air density and with a theoretical maximum effect of 2% on the flight time, the standard deviation of both sets of data are within each others possible variation so mask the effects of air density.

Therefore the effects of air density cannot be reliably determined from the time-range data.

Range (m)	Air density 1 (1.178 kg/m^3)		Air density 2 (1.225 kg/m^3)	
	Average flight time (ms)	Standard deviation (pv in brackets)	Average flight time (ms)	Standard deviation (pv in brackets)
20	61.26	0.60 (1.0)	61.23	0.84 (1.4)
25	80.80	0.90 (1.1)	81.30	0.76 (0.9)
30	102.34	0.91 (0.9)	101.54	1.64 (1.6)
35	124.99	1.29 (1.0)	125.22	1.54 (1.2)
40	149.30	2.03 (1.4)	150.75	1.58 (1.0)
45	177.82	1.10 (0.6)	178.34	2.00 (1.1)
50	208.05	2.14 (1.1)	209.92	2.39 (1.1)

Table 4.3 *The average flight time (over 10 cartridges) and standard deviation of 28g load of #6 (2.56mm) lead shot for different air densities (1) 1.178 kg/m^3 and (2) 1.225 kg/m^3. The cartridges were from the same production batch.*

Fitting the data to the cube law of air resistance, given in (4.7), it was found that the corresponding values for k_3, $7.4\text{x}10^{-5}$ and $7.7\text{x}10^{-5}$ with similar initial velocity of 440m/s, have the same 4% difference as the corresponding measured air densities (1.18 and 1.225 kg/m^3). This shows that the effect of air density is seen in the fitting process but not in the raw measurement data, so correction for air density should be applied to the deceleration constant k_3 in (4.7).

4.3.3 Pellets obeying a square law of air resistance

When a pellet is obeying a square law of air resistance it is established from (G.13), which is derived in Appendix G.2, that a small increase in air density, $\delta\rho_a/\rho_a$, has a little effect on the flight time, $\delta t/t$, when R is small. As the range increases $\delta t/t$ also increases until it becomes linear with range at large R (shown in Figure G.2). Therefore over a

certain range the increase in flight time ($\delta t/t$) becomes greater than the increase in air density ($\delta\rho_a/\rho_a$). However, the behaviour of $\delta t/t$ for large R is not relevant for this investigation (and lies outside the range of validity of the models).

$$\frac{\delta t}{t} = \frac{\delta \rho_a}{\rho_a}\left[\frac{k_2 R}{1 - e^{-k_2 R}} - 1\right] \qquad \text{(G.13)}$$

The effect of air density on the flight time are shown in Figure 4.6 using data obtained on a typical square law load (over the measurement ranges) which when fitted to (4.8) produces a deceleration constant (k_2) of 0.022 and an initial velocity of 350m/s.

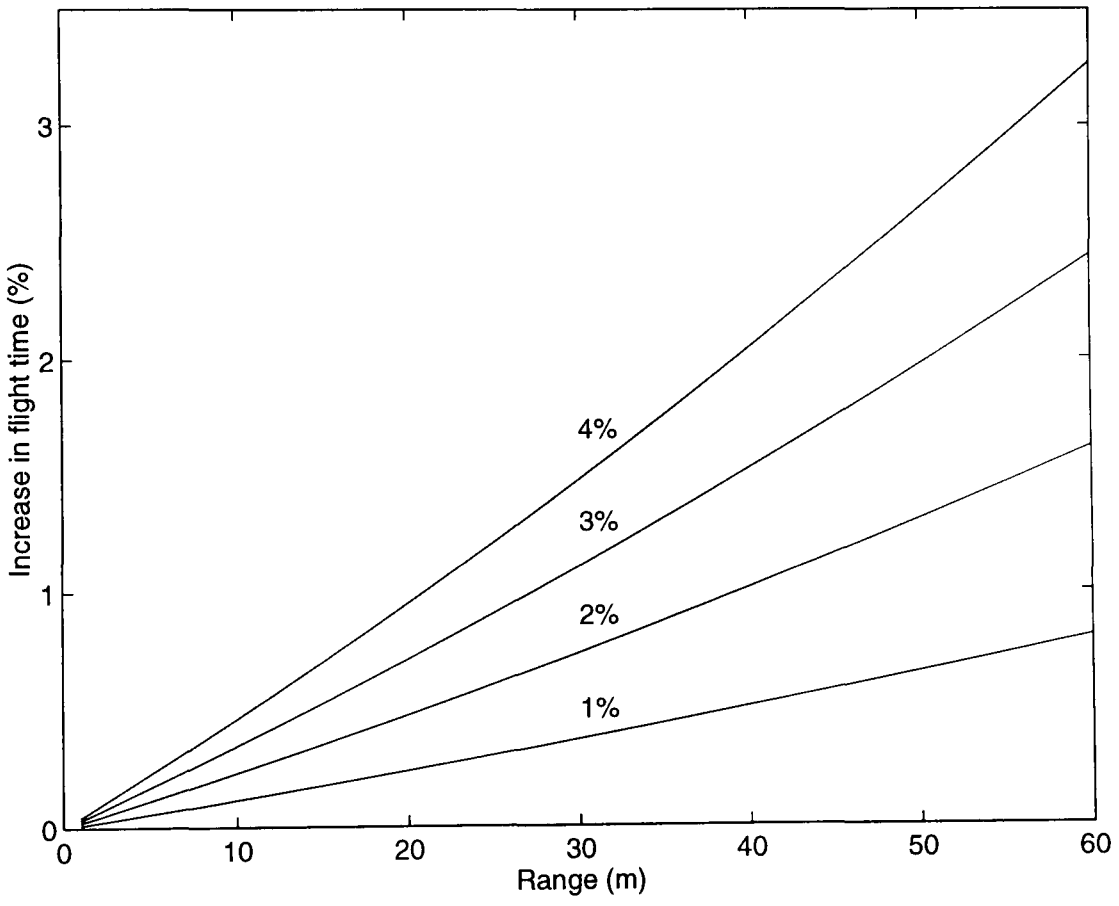

Figure 4.6 *Percentage increase in flight time with range for an increase in air density of 1, 2, 3 and 4%. The initial value for k_2 (0.022) was obtained from the time-range data of a typical load of pellets obeying a square law of air resistance over the measurement ranges.*

At measurement ranges greater than 40m the flight time increases shown in Figure 4.6 for a 4% air density difference starts to become larger than the variation seen in the leading edge flight time data. However, it is still not possible to see the true effect of the change in air density because the observed variations of the average flight times are

too great. The correction of the experimental flight time data for either a pellet obeying a cube of square law of air resistance is therefore not straightforward, due to the variation seen in the leading edge flight time. If correction for air density is thought necessary it is recommended that the fitted k_n values from (4.7) and (4.8) are corrected.

4.4 MEASUREMENTS ON DECELERATION CONSTANTS

4.4.1 Scaling of deceleration constant with pellet diameter

The property that affects a pellet travelling downrange is the opposing force generated by the air resistance. Substituting $m=\pi/6 d^3 \rho_m$ and $A=\pi/4 d^2$ into (4.14) the general deceleration constant is found to be

$$k_n \propto \frac{\rho_a}{\rho_m d} \quad , \tag{4.19}$$

where it can be seen to be inversely proportional to the pellets diameter (d) and relative density (ρ_m) and directly proportional to the atmospheric density (ρ_a). The main objective in this method of shot cloud analysis is to measure the deceleration characteristics of the individual pellets over the measurements range (20-50m), using the assumption that they are single spheres in free flight. From the deceleration characteristics it is then possible to standardize the shot cloud ballistics using the expressions in section 4.2.4-4.2.6. This is necessary to make comparative ballistics and has been completed in the contract report for the Department of the Environment [13].

The majority of shot clouds measured spend most of their flight time over the measurement ranges at velocities greater than Mach 0.5. To calculate the deceleration constant (k_3) for these types of loads the time-range data for the leading and trailing edges of the shot clouds were fitted to (4.7), a cube law of air resistance model. From the least squares fit, two constants were obtained for every pellet diameter and correspond to ($1/v_0$) and ($k_3/2$). From (4.19) a graph of $1/k_3$ versus d should produce a

straight line through the origin. Figures 4.7, 4.8 and 4.9 show the least squares best fit lines through the data, of the form

$$\frac{1}{k_n} = H + Id\,. \tag{4.20}$$

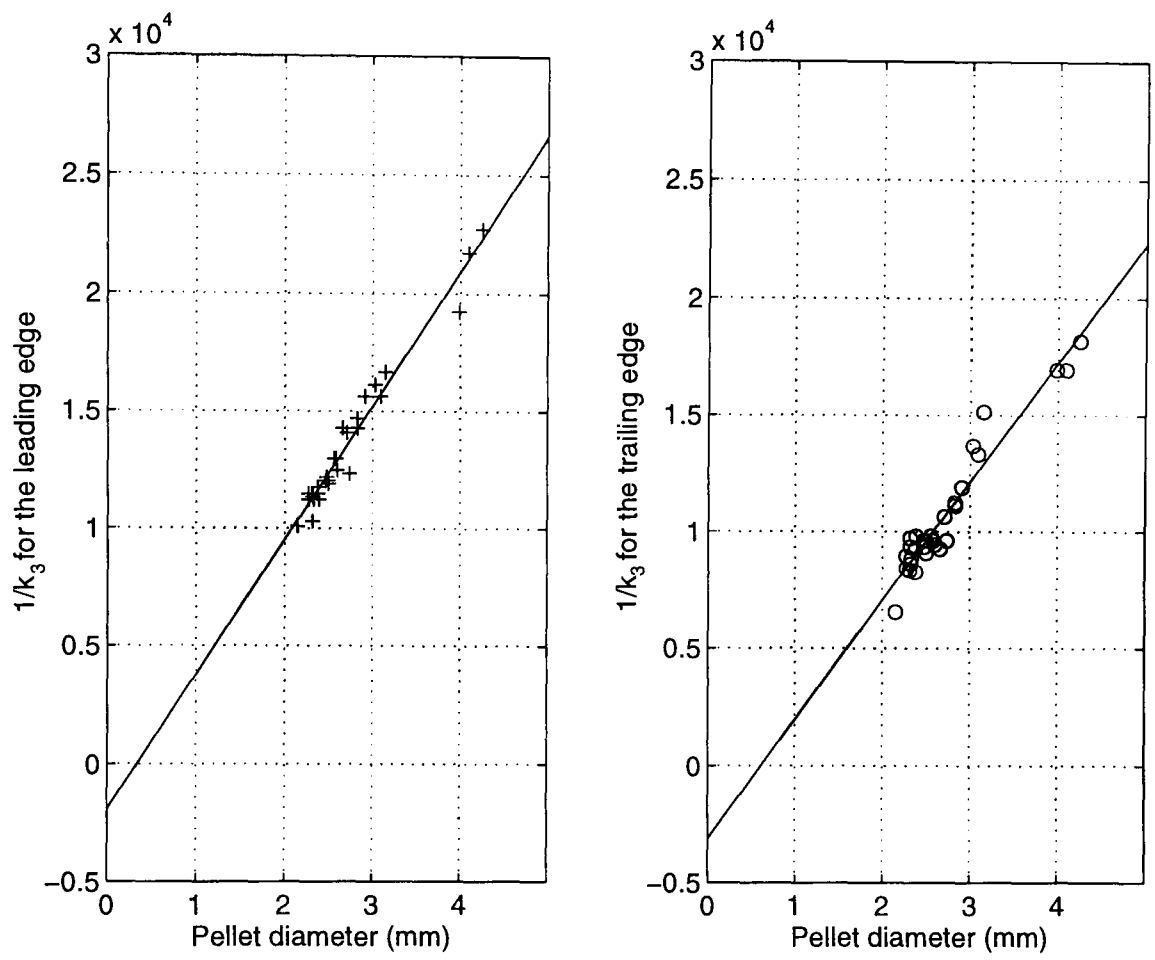

Figure 4.7 *Least squares fit of $1/k_3$ versus pellet diameter for all leading (+) and trailing (o) edge lead data points. The deceleration constants were obtained from fitting the time-range data to (4.7).*

The cube law model is shown in section 4.2.7 to be the better fit for the majority of loads tested, even though the pellets may not retain velocities greater than Mach 0.5 for all the measurement range. At ranges where the velocities have fallen below M_C the pellets experience a greater drag coefficeint value (C_D) than if cube law model is still assumed, due to the drag coefficient becoming constant (Figure 4.1). This results in a greater drag on the pellet which produces a longer flight time over the measurement range than if the drag coefficient stayed proportional to velocity for all velocities, as it would in a cube law model. With velocities falling below M_C at the longer ranges (40-50m) and the corresponding effects on the drag, the fitted gradient ($k_3/2$) associated with

R^2 of (4.7) increases as it is pulled up to the flight time data points. The smaller diameter pellets (<3mm) are more likely to have data points with velocities below Mach 0.5, due to their greater deceleration characteristics which incur a greater calculated deceleration constant (k_3) and pulls the fitted $1/k_3$ versus d curves below the origin. These effects are shown in Figure 4.7 where both the leading and trailing edge fits for lead pellets do not pass through to the origin.

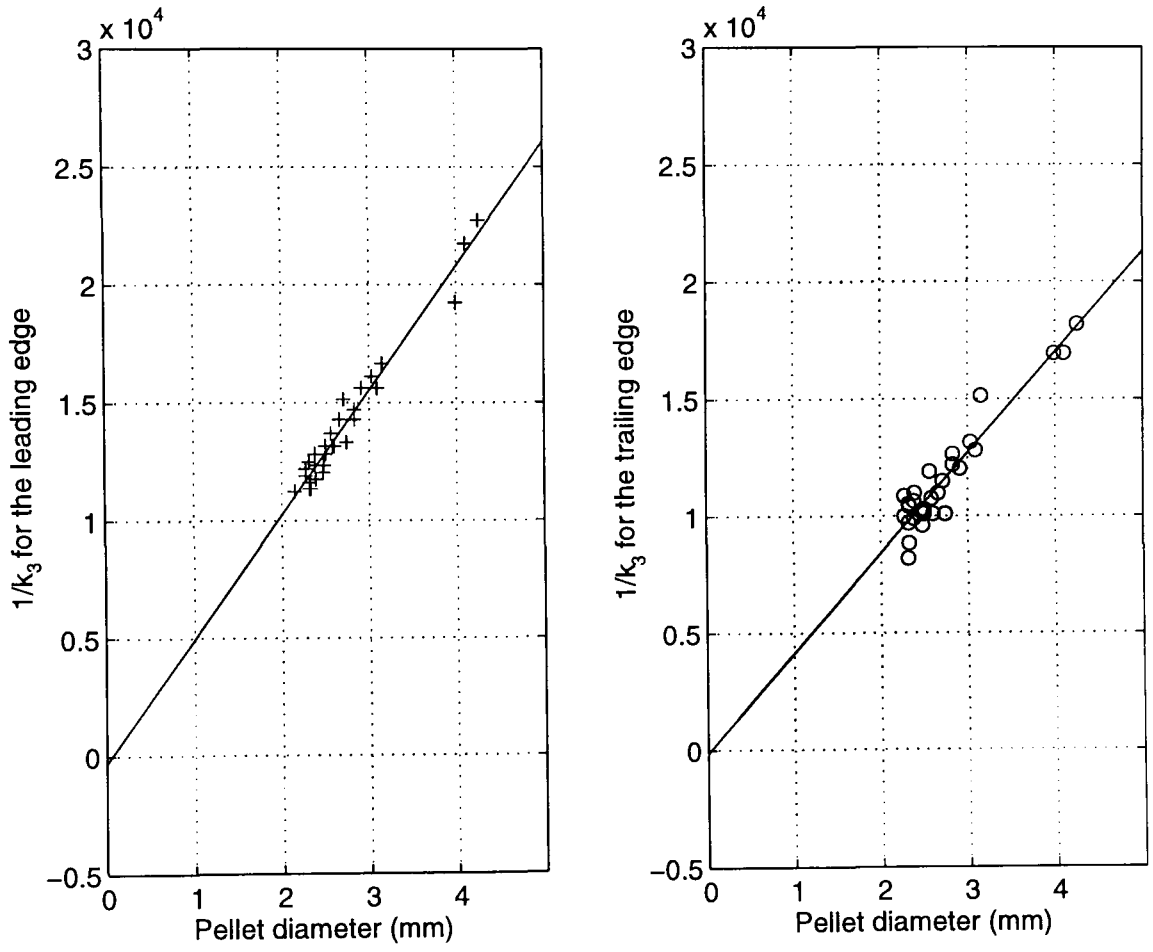

Figure 4.8 *Least squares fit of $1/k_3$ versus pellet diameter for only the leading (+) and trailing (o) edge lead data points that have velocities greater than M_C.*

To show the relationship between deceleration constant (k_3) and diameter (d) for pellets obeying a cube law of air resistance, flight time data points were only used if their corresponding velocities were greater than M_C. Figure 4.8 shows the calculated leading (+) and trailing (o) deceleration constants for a range of lead pellet diameters. Using the least square fit, described in (4.20), on this data the (4.21) represents the deceleration constant relationship with pellet diameter for the leading edge (k_l) and trailing edge (k_l) lead pellets, where d is the diameter of the pellet in millimetres.

$$\frac{1}{k_{l(lead)}} = 5280d - 310$$

$$\frac{1}{k_{t(lead)}} = 4280d - 140 \qquad (4.21)$$

It can be seen in Figure 4.8 and (4.21) that the trailing edge has a lower gradient line, which translates into a higher deceleration constant and therefore drag. The higher drag is confirmed by the poor shape of the fired pellets at the edge of the patterns (corresponds to the trailing edge) compared to the centre (corresponds to the leading edge) shown in section 3.2.1. It can also be seen that both the leading and trailing edge fits still do not pass through the origin but are a lot closer than Figure 4.7. Also the fits lack data on pellet diameters less than 2mm which would weight the fit in this region.

4.4.2 Effects of material density on the deceleration constant

To analyse the effect of material density on the deceleration constant measured cube law data flight time data from steel loads are fitted to (4.20). Figure 4.9 and (4.22) show the relationship between the diameters of steel pellets and their deceleration constants. It can be seen that the trailing edge gradient of slope is approximately the same as the leading edge. This suggests that the steel pellets experience the same drag force independent of their position in the shot cloud, at ranges between 20-50m. The lack of deformation of the fired steel pellet and their constant shape within the pattern, shown in section 3.2.1, confirms that the deceleration constant should be approximately the same for all the pellets.

$$\frac{1}{k_{l(steel)}} = 3780d - 70$$

$$\frac{1}{k_{t(steel)}} = 3790d - 690 \qquad (4.22)$$

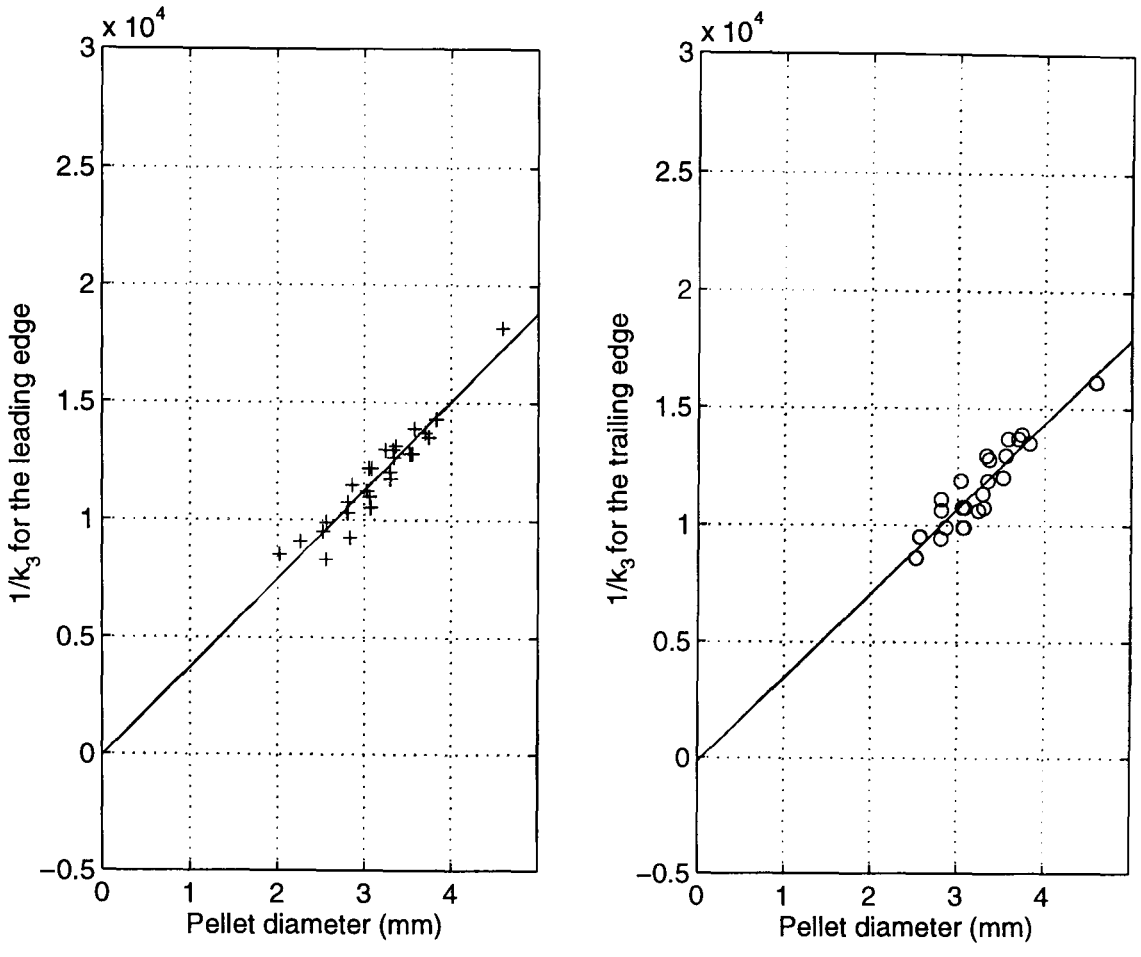

Figure 4.9 *Least squares fit of $1/k_3$ versus pellet diameter for only the leading (+) and trailing (o) edge steel data points that have velocities greater than M_C.*

There has been a good range of pellet diameters (2.0 to 4.6mm) for lead and steel shot, giving confidence in the relationship with deceleration constant. For the newer alternative shot there has been a much more limited range of shot sizes available, mainly being around 3mm. It has been decided that there are insufficient data points for these newer materials at present to obtain a reliable relationship at present but they are given in (4.23) for bismuth and zinc.

$$\frac{1}{k_{1(bismuth)}} = 4760d - 540$$

$$\frac{1}{k_{1(zinc)}} = 3470d - 470 \qquad (4.23)$$

The ratio in the leading edge deceleration constants (k_3) between lead and steel pellets of the same diameter can be seen in (4.21) and (4.22) to be the inverse of their densities. This is also confirmed by the limited data from the other materials in (4.23), which

correspond to the relationship in (4.19). The deceleration constants for the trailing edge do not follow the same relationship because of their tendency to have different pellet shapes and therefore drag after firing.

4.4.3 The combined effect on the deceleration constant

The deceleration constant has been shown in (4.14) to be affected by the density and diameter of the pellet and the air density. The combination of these effects can be used to summarize any given pellet's deceleration characteristics in a shot cloud. An analytical estimate of k_2 or k_3 can be found from the least square fits of the experimental data to (4.7) or (4.8), and from (4.14) a theoretical estimate for k_n can be calculated. If a cube law of air resistance is assumed the drag coefficient is modelled as

$$C_D = S\frac{v}{v_c} \quad , \tag{4.24}$$

where S is the gradient of the curve between M_U and M_C in Figure 4.1. Combining (4.23) and (4.24) the velocity component v disappears to make up the cube term in (4.5) and the constant representing the speed of sound (v_c) remains. Therefore for a pellet obeying a cube law of air resistance with a diameter d and density ρ_m the following deceleration constant is obtained

$$k_3(M) = \frac{3S}{4}\frac{\rho_a}{d\rho_m v_c} \quad . \tag{4.25}$$

From the analytical estimate of k_3 and the theoretical estimate of $\rho_a/(d\rho_m v_c)$, obtained from measurements on the pellets and the atmospheric condition, a plot of $d\rho_m v_c/\rho_a$ versus $1/k_3$ is shown in Figure 4.10. Once again this plot should produce a straight line that passes through the origin and from the least square fit of (4.20) an expression is generated for this relationship, given by 4.26, where an estimate of the gradient of the drag coefficient slope, S, can be obtained.

$$\frac{1}{k_3} = 1.622 \frac{d\rho_m v_c}{\rho_a} + 127.8 \tag{4.26}$$

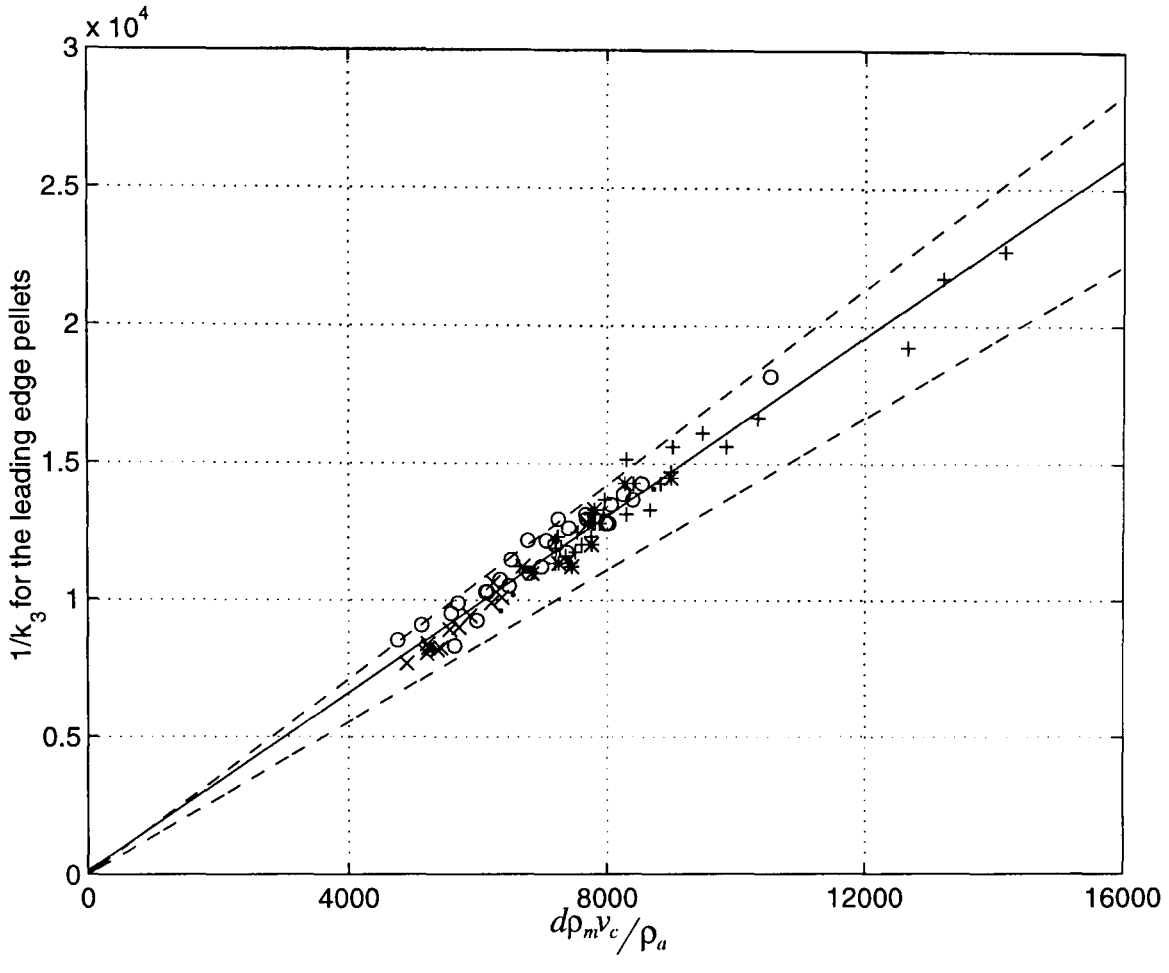

Figure 4.10 *The least square fit (solid line)of $1/k_3$ versus $d\rho_m v_c/\rho_a$ for the leading edge lead (+), steel (o), bismuth (*), and zinc (x) data with calculated constraining limits (--) for S. The solid line represents the least squares fit of (4.20) to the data and described by (4.26).*

To validate the time-range data for the leading edge pellets which are thought to be obeying a cube law of air resistance, a plot of their $d\rho_m v_c/\rho_a$ versus $1/k_3$ values should lie close to the straight solid line which represents (4.26). Therefore using the first approximation that $C_D \propto M$, there must be a limit on the value of S. The actual drag coefficient curve (Figure 1.12) shows that the slope in the transonic regime curls off at both ends and pellets at these limits will incur a different value of S. With the maximum velocity for a pellet of $1.4M$ (M_2) and the minimum $0.5M$ (M_1) to obey a cube law, the limits are set between the gradient of the line which goes from the origin to each of the points, as shown in Figure 4.11. The actual limits of S are calculated from values which were taken from Braun's data [24], as shown Figure 1.7, where C_{D1}=0.48

and C_{d2}=1.10 giving S_1=0.96 and S_2=0.75. These limits are plotted in Figure 4.10 to emphasise any data points which may not be truly obeying a cube law of air resistance.

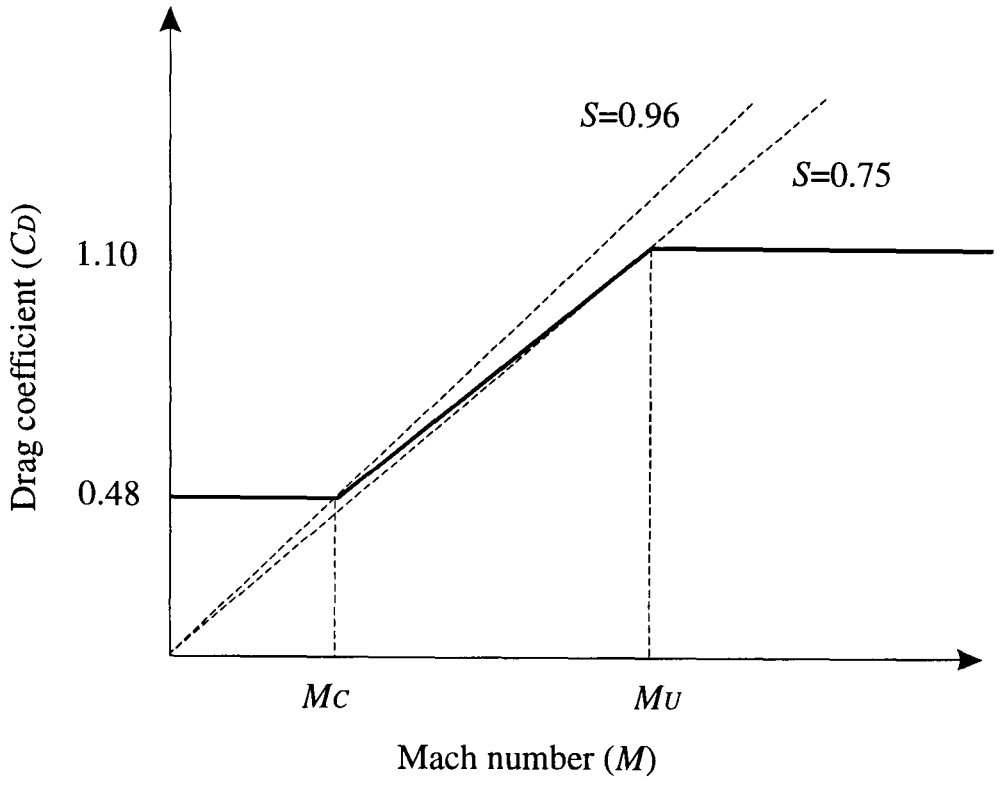

Figure 4.11 *The limit place on S for pellets obeying a cube law of air resistance.*

The majority of loads tested have obeyed a cube law of air resistance and from the data the deceleration characteristics on any pellet can be estimated from (4.26). However, these characteristics will not be the same for pellets obeying a square law of air resistance. An analytical value for the square law deceleration constant is obtained from (4.8) and the theoretical value is calculated when the drag coefficient is below M_C (Figure 4.1)

$$C_D = D \quad , \tag{4.27}$$

where D is a constant. Combining (4.14) and (4.27) an expression is obtained for the deceleration constant of a pellet with diameter d, density ρ_m and obeying a square law of air resistance.

$$k_2 = \frac{3D}{4}\frac{\rho_a}{d\rho_m} \tag{4.28}$$

In Figure 4.12 a plot of $d\rho_m/\rho_a$ versus $1/k_2$ is shown for pellets which obeyed a square law of air resistance over the measurement ranges (20-50m) and their corresponding least squares fit. From the fitting (4.20) to the data (4.29) and an estimation of the constant D is obtained.

$$\frac{1}{k_2} = 2.548\frac{d\rho_m}{\rho_a} - 0.015 \tag{4.29}$$

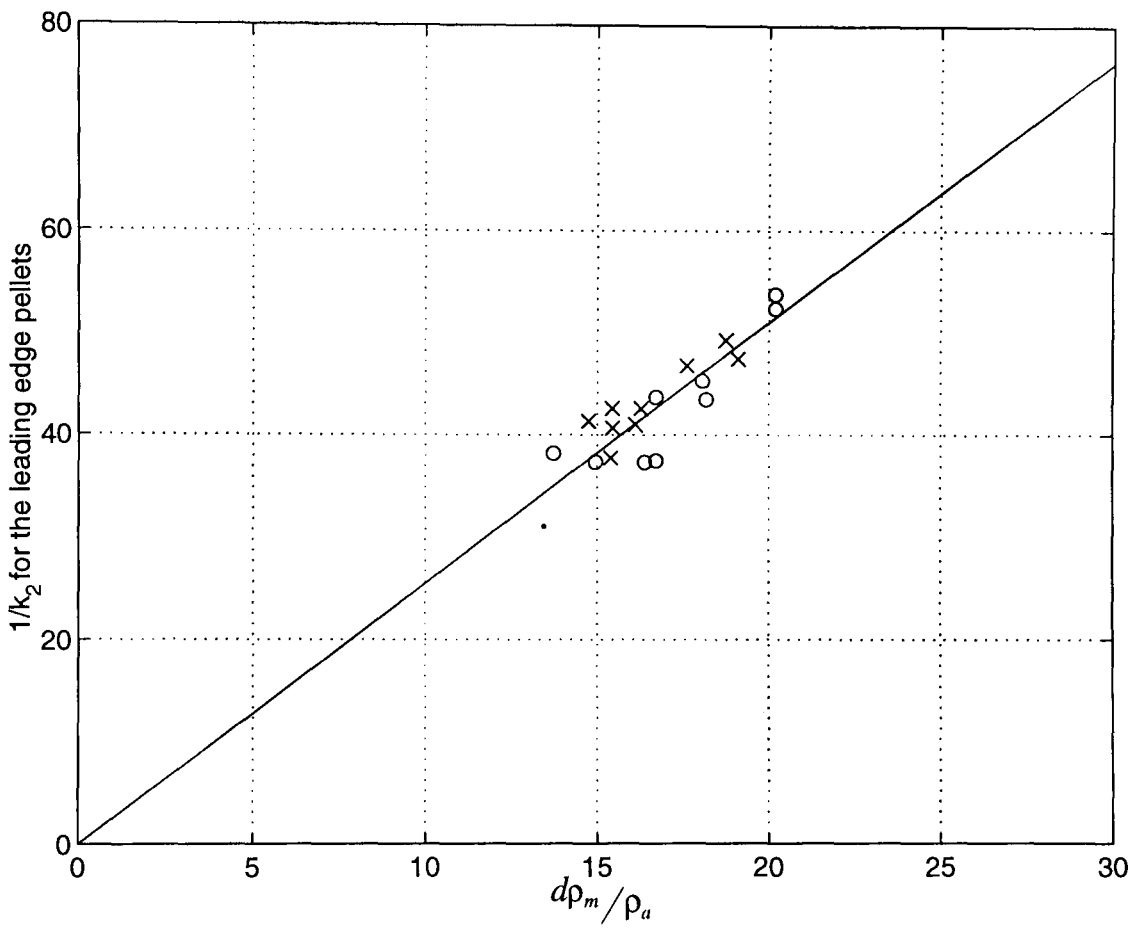

Figure 4.12 *The relationship between the deceleration constant ($1/k_2$) and $d\rho_m/\rho_a$ for leading edge steel* (o)*, and zinc* (x) *pellets obeying a square law of air resistance. The solid line represents the least squares fit of (4.20) to the data and described by (4.29).*

Expressions (4.29) and (4.26), which correspond to either square or cube law velocity regime, have been used to summarize the deceleration characteristics of any leading edge pellet. From the two basic assumptions that the drag coefficient is constant for pellets in the square law region and proportional to velocity in the cube law, Figures 4.10 and 4.12 show that the data seems to follow these trends. Using the fitted parameters representing S and D from (2.29) and (2.26) the constant part of the drag coefficient below M_C was found to be 0.52 and above the gradient of the slope equals

0.82. Combining these results Figure 4.13 shows that from the analytical and theoretical fits the actual value for M_C is0.63. As there have been no tests on pellets travelling at supersonic velocities over the measurement range (20-50m) it has not been possible to find the corresponding M_U value for pellets in a shot cloud.

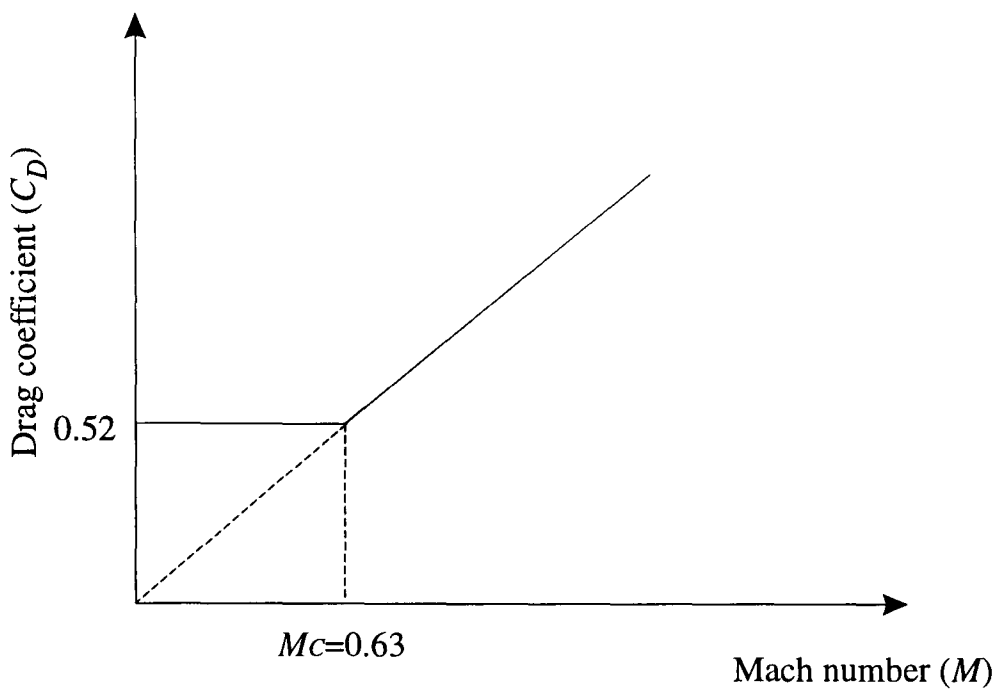

Figure 4.13 *Simplified approximation of the drag coefficient for a pellet obtained from the deceleration characteristics.*

4.5 SYNTHESIS MODEL BASED ON A SINGLE SPHERE

4.5.1 Synthesis process

During this chapter different methods have been used in analysing the measured time-range data to produce the ballistics characteristics of a shot cloud and its pellet distribution. Using the parameters found by a least square fit on the experimental data, the deceleration characteristics were calculated for pellets obeying either of the two separate laws of air resistance and an approximation of M_C was calculated. With the basic approximation on the drag coefficient characteristics and the measured pellet parameters and surrounding atmospheric condition, the drag force can be calculated for any given pellet velocity.

A synthesis procedure is now presented that models the behaviour of a pellet downrange from the equation of motion for a single sphere in free flight. This is achieved by deriving expressions for flight time and range as a function of velocity. Using a non-analytical approach a numerical integration is then performed on both expressions. The integration process initializes both expressions at the same specified initial conditions R_s, t_s, and v_s (they do not have to correspond to the muzzle condition) and then integrates by the same velocity increments. This generates flight time and range data for any given pellet velocity and the combination of these two predictions can be compared with the experimental time-range data to judge its validity. The synthesis model then shows that the downrange ballistics can be predicted by measurements made at one range (where the pellets are regarded as independent).

4.5.2 Flight time expression

The first part of the synthesis model is to determine the pellets flight time behaviour as a function of velocity or Mach number. From (1.1) and (4.1) the deceleration on the pellet is determined by,

$$\frac{dv}{dt} = -\frac{\rho_a A}{2m} v^2 C_D(v) \quad . \tag{4.30}$$

Normalizing (4.30) we obtain

$$\frac{1}{v_c}\frac{dv}{dt} = -\frac{\rho_a A v_c}{2m}\frac{v^2}{v_c^2} C_D\left(\frac{v}{v_c}\right) \quad , \tag{4.31}$$

and using

$$k_s = \frac{\rho_a A v_c}{2m}, \quad k_s t = T, \quad M = \frac{v}{v_c} \tag{4.32}$$

an expression is obtained in terms of Mach number, this being the major parameter which the drag coefficient (C_D) is dependent upon, and given as

$$\frac{dM}{dT} = -M^2 C_D(M) \quad . \tag{4.33}$$

After the integration of (4.33) M and T are transferred back to real time using (4.32) along with the two initial conditions of the synthesis model v_s and t_s.

$$\int_M^{M_s} \frac{dM}{M^2 C_D(M)} = -T + T_s \tag{4.34}$$

4.5.3 Range expression

To calculate the range as a function of velocity (4.35) is applied to (4.30) and by following the same process as shown in the time model (4.36) is obtained.

$$\frac{dv}{dt} = v\frac{dv}{dR} \tag{4.35}$$

$$\frac{dv}{dR} = -k_s \frac{v}{v_c} C_D(v) \tag{4.36}$$

Normalizing the velocity to Mach number and dividing by k_s, which is the same as in (4.32),

$$\frac{dM}{dX} = -MC_D(M) \tag{4.37}$$

where

$$X = \frac{k_s R}{v_c} . \tag{4.38}$$

Integrating (4.37) by the same velocity steps, or Mach number increments, as in (4.34), range data can be obtained after X and M are transferred back into real time.

$$\int_{M}^{M_s} \frac{dM}{MC_D(M)} = X - X_s \tag{4.39}$$

The expression of flight time and range in (4.34) and (4.39) are both dependent on M. Using the same initial constants (R_s, t_s and v_s) it is then possible to step both integration along at the identical intervals to produce a plot of range versus time. An advantage in this synthesis process is the ease in which any of the pellet parameters, atmospheric condition or the drag coefficient characteristics can be changed to observe their effects.

4.5.4 Comparison with experimental data

A numerical integration program was designed to model the downrange ballistics of a shot cloud using the derived expressions (4.34) and (4.39) from the single sphere theory. This was achieved by writing a program where the pellet's and atmospheric parameters (d, m, ρ_a, and v_c) are entered along with the initial condition (R_0, t_0 and v_0). A simplified approximation (Figure 4.13) was also generated for the drag coefficient using the data obtained from the deceleration characteristic work (section 4.4). The program takes the value of C_D from Figure 4.13 and therefore automatically alters the model from a cube law to a square law of air resistance when the pellet velocity falls below M_c. In both expressions velocity integration are necessary and the program starts at v_s calculating, by means of Simpson's rule, the area under the time-velocity expression and the range-velocity expression in the same velocity increments.

The outputs from (4.34) and (4.39) give the velocity as a function of time and range, as the program steps through at the same velocity increments for both expressions, time-range data is also obtained. This time-range model is compared to actual raw data taken at the measurement facility (Chapter 2), where the pellets parameters are routinely measured along with the atmospheric conditions, to show its accuracy. From the skyscreen measurements a value for the muzzle velocity was used, whereby t_s and R_s=0,

as the initial condition for the synthesis model. Entering these initial conditions into the expression for a selection of leading edge shot cloud pellets obeying different laws of air resistance, Figure 4.14 shows the output time-range curve compared to the raw flight time-range data. It can be seen that the model does not agree with the measured data, proving that it is not possible to accurately predict the development of a shot cloud from the muzzle velocity using the assumption that the pellets are in free flight.

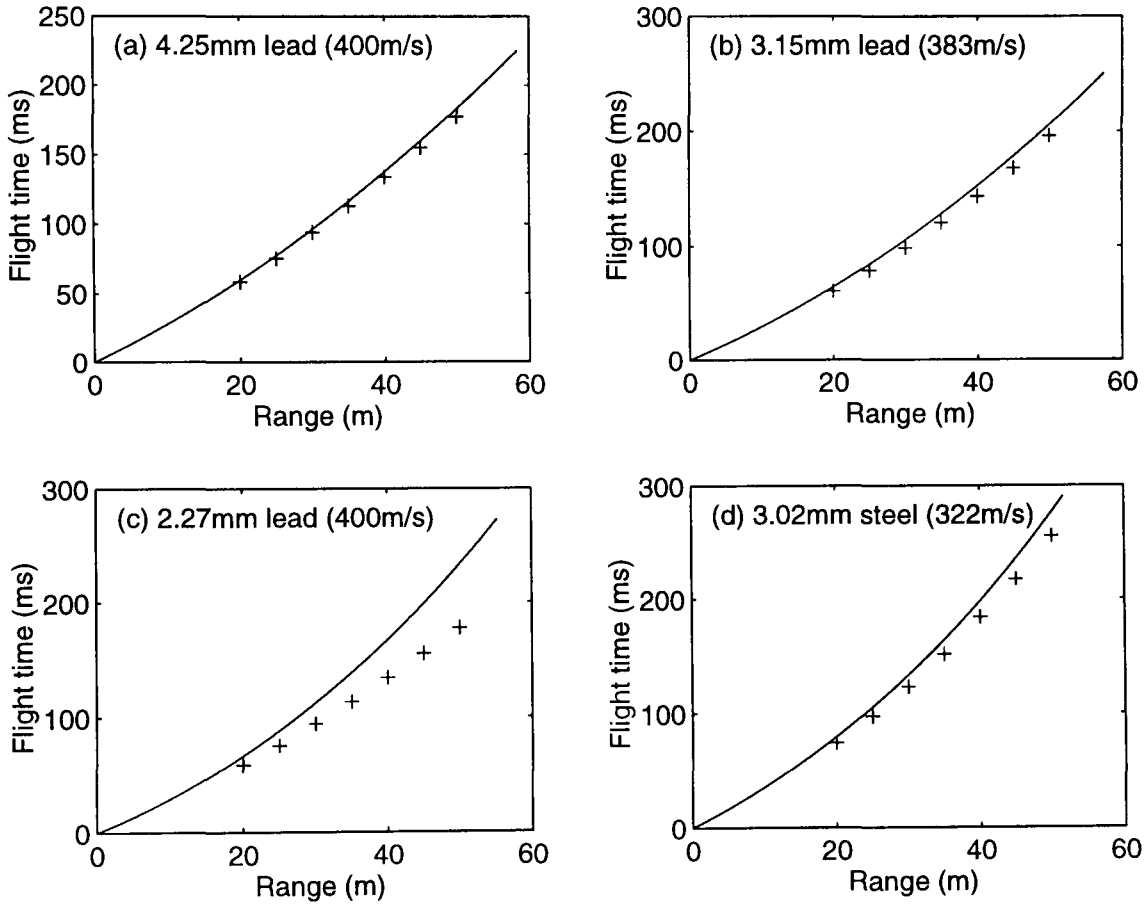

Figure 4.14 *The combination of expressions (4.34) and (4.39) to predict the downrange ballistics of the leading edge pellets from the initial velocity v_0 (given in the brackets) for (a) a 36g load of #BB lead shot (cube law), (b) a 36g load of #3 lead shot (transitional between cube and square law), (c) a 28g load of #7.5 lead shot (transitional between cube and square law) and (d) a 28g load #4 steel shot (square law), where (+) represent the measured flight time range data.*

A more appropriate method of modelling the development of the leading edge pellets in a shot cloud is to start the expression at a velocity where the pellets have dispersed sufficiently to be independent of one another. In Lowry's [48] and Bearman's [49] opinions the pellets have separated sufficiently at ranges >10m and therefore can be regarded as single spheres in free flight. With the skyscreens operational range limited to 8m it is best to acquire the initial condition from the ballistics target, which starts at

20m, to be sure this assumption is correct. Using the averaged time-range data measurements a value for t_{20} at R_{20} is obtained. The velocity is not measured, but using the appropriate law of air resistance, expressions (4.7) or (4.8), a theoretical value is generated for v_{20} from the flight time data over the measurement range (20-50m). Placing these parameters into the expression it can be seen in Figure 4.15 that the synthesis models fits the raw data better if started from 20m instead of the muzzle.

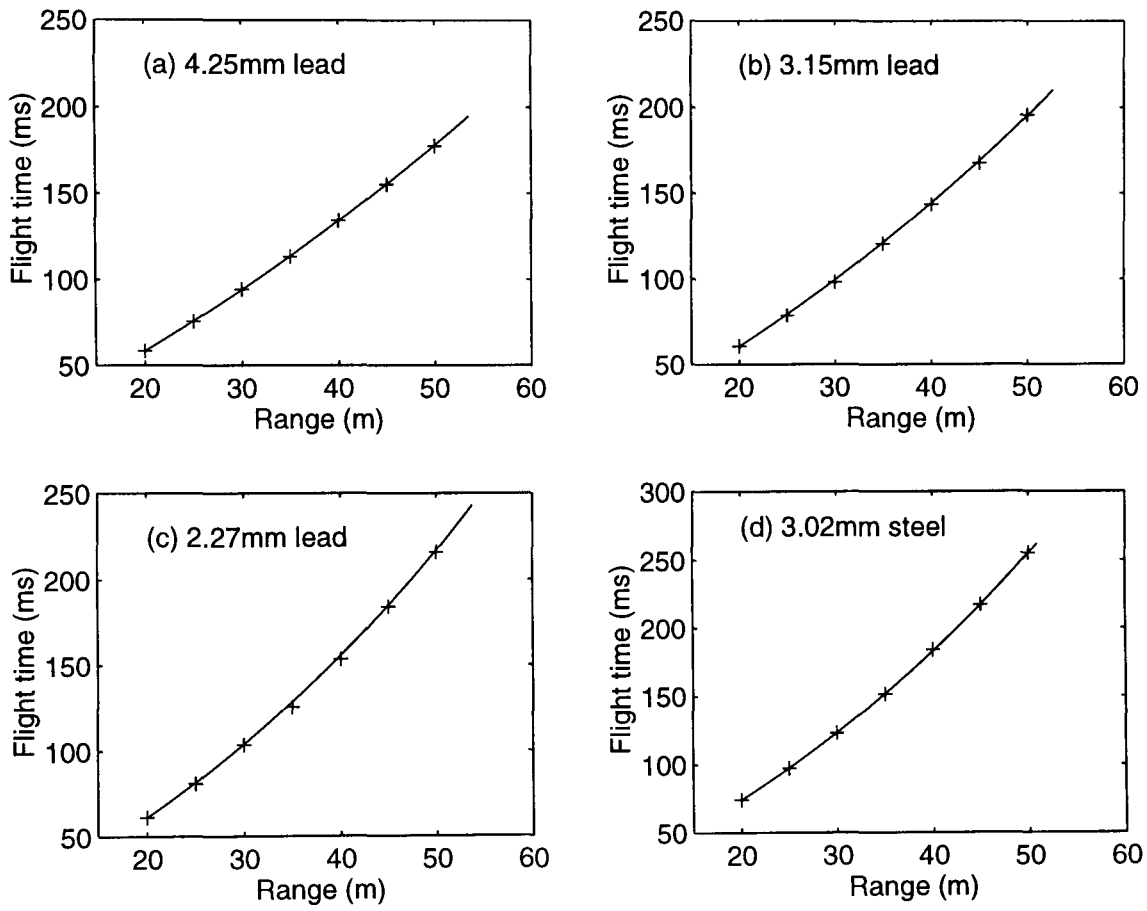

Figure 4.15 *The combination of expressions (4.34) and (4.39) to predict the downrange ballistics of the leading edge pellets starting from the velocity v_{20}, and time t_{20} for (a) a 36g load of #BB lead shot (cube law), (b) a 36g load of #3 lead shot (transitional between cube and square law), (c) a 28g load of #7.5 lead shot (transitional between cube and square law) and (d) a 28g load #4 steel shot (square law), where (+) represent the measured flight time range data which is also the same in Figure 4.14.*

The synthesis model derived from the drag force equation of a single sphere in free flight has been shown to give good quantitative agreement with the downrange ballistic measurement of the leading edge pellets of a shot cloud. A requirement for this type of model was that the initial condition parameters had to correspond to the pellets being in free flight. From the selection of shot cloud shown in Figure 4.15 it can be assumed, from the good quantitative agreement between the synthesis prediction and the experimental data, that the pellets are in free flight at ranges greater than 20m.

An approximation of the range where the pellets become independent is obtained by extrapolating the synthesis model back towards the muzzle until it intercepts the curve generated by extrapolating the near muzzle velocity out towards 20m. This interception is shown in Figure 4.16 for two loads of pellets and their corresponding synthesis prediction using the initial synthesis condition measured at 8m.

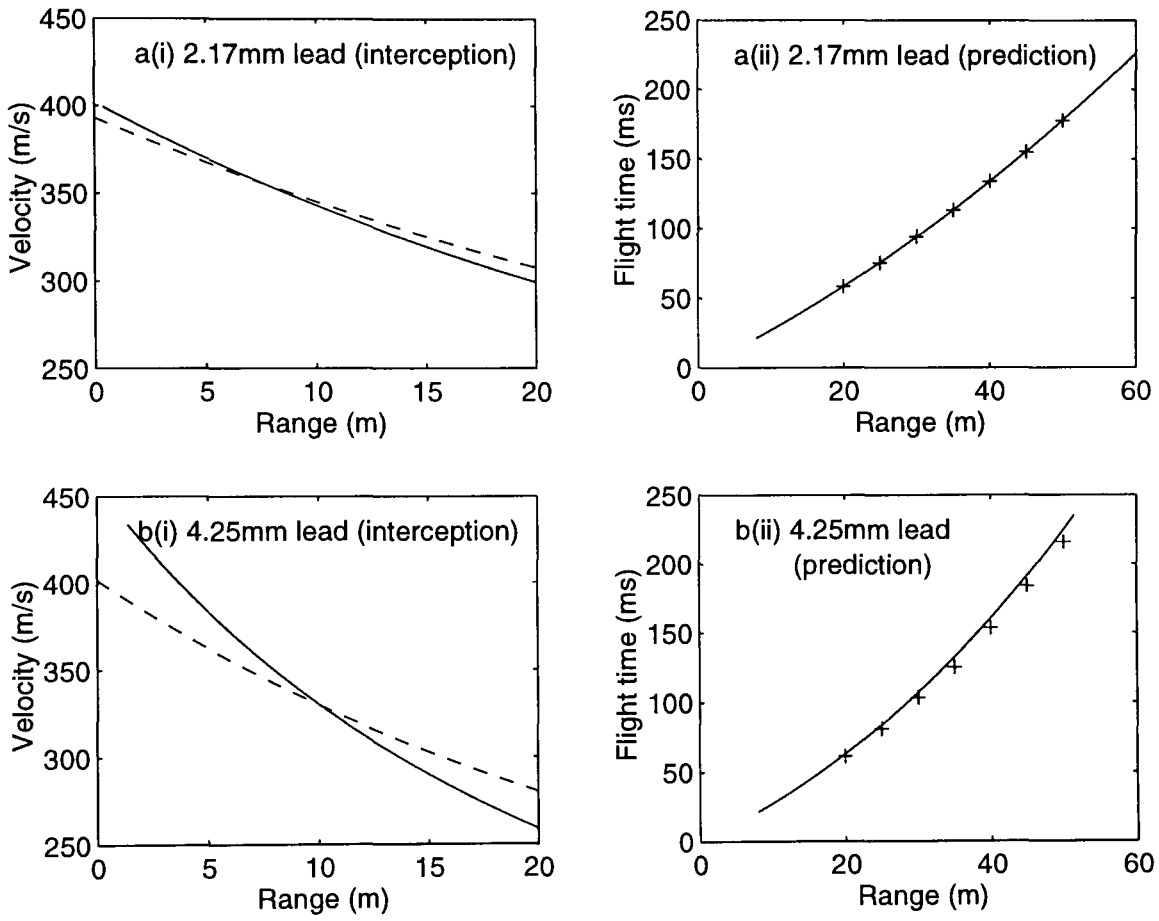

Figure 4.16 *The interception point between the extrapolation of the synthesis model back to the muzzle and the skyscreen data out to the measurement range for (a) a 36g load of #BB lead shot (cube law) and (b) a 28g load of #7.5 lead shot (transitional between square and cube law). The combination of expressions (4.34) and (4.39) are given in (ii) to predict the downrange ballistics for the leading edge pellets starting from the velocity* v_8 and time t_8 *for the same loads.*

In Figure 4.16a(i) it can be seen that the two extrapolated curves intercept at approximately 7m and b(i) at 10.5m. Starting the synthesis model at 8m it can be seen in a(ii) that the predicted data shows good agreement to the experimental flight time data, unlike in b(ii). This trend has been observed in every set of measurements carried out, whereby if the synthesis model is started anywhere after the interception point the model shows good agreement to the experimental data. However, if the initial condition for the synthesis model correspond to before the interception point a poor prediction is

acquired. From this approach it has been noted that there is no one range where the pellets become independent as this seems to be determined by the load, pellet diameters and choke. Although there was constant range for the interception between shot clouds, it was found that the pellets become independent typically between the ranges of 5-15m. Therefore at the ballistics measurement ranges (20-50m) the pellets can be assumed to be in free flight.

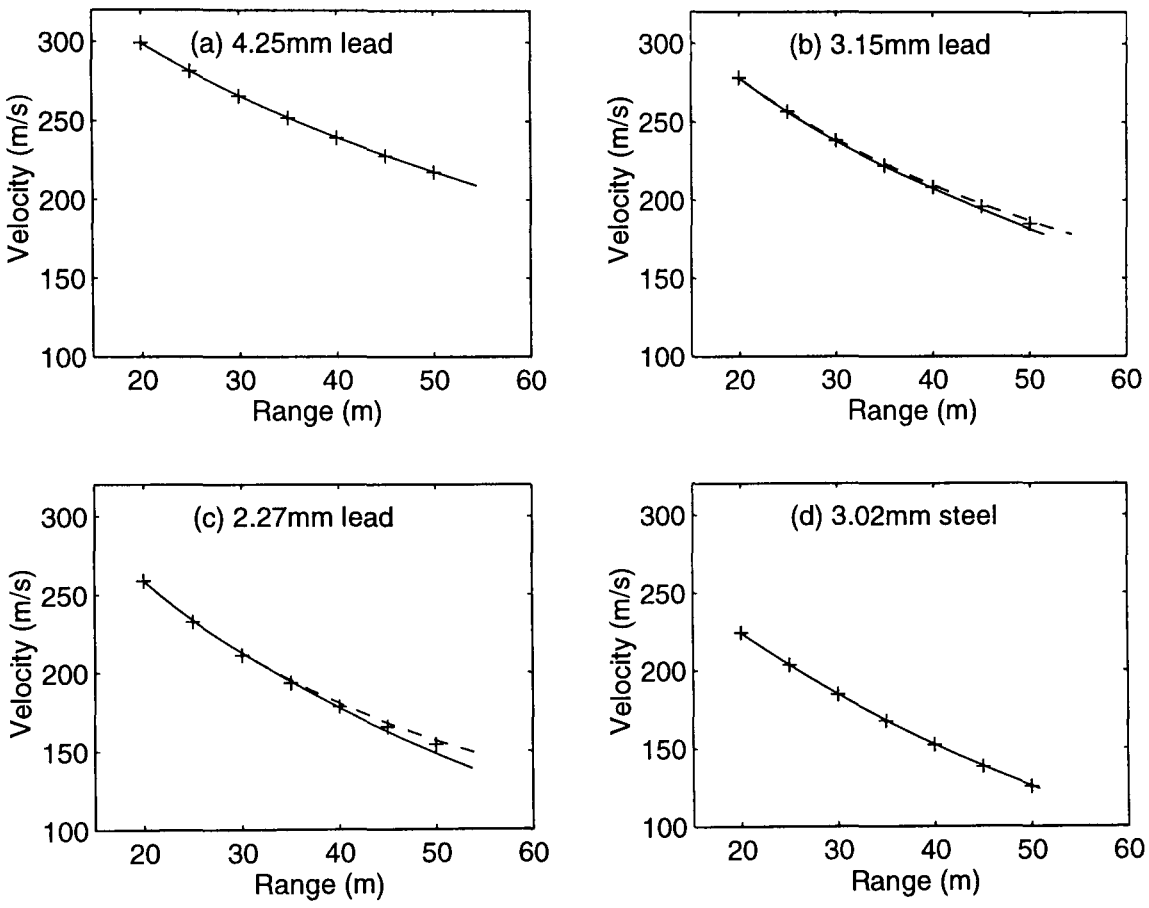

Figure 4.17 *The predicted velocity produced by the synthesis model for the leading edge spheres of (a) a 36g load of #BB lead shot (cube law), (b) a 36g load of #3 lead shot (transitional between cube and square laws), (c) a 28g load of #7.5 lead shot (transitional between cube and square laws) and (d) a 28g load of #4 steel shot (square law), where (+) represents the velocities obtained by fitting the raw data to the appropriate cube or square law of air resistance. Also shown are the predicted velocities when the drag coefficient function in the synthesis model is set to be always proportional to velocity (--).*

The expression (4.39) gives the velocity as a function of range for a pellet in free flight. Figure 4.17 show the synthesis model's prediction compared with the appropriate velocity fit in (4.8) or (4.10) for a selection of pellet loads. It can be seen that if the pellets only obey one of the laws of air resistance over the measurement ranges, such as above or below $0.65M$ as in Figure 4.17(a) and (d), the fitted and predicted data are similar. However, if the pellets travel between the two regimes over the measurement range it is shown in Figure 4.17(b) and (c) that the predicted data is lower at velocities

below $0.65M$. These discrepancies occur because the fitted function models a lower drag, due to the continuous assumption that the drag coefficient is proportional to velocity, instead of changing to a constant below $0.65M$. Changing the drag coefficient model in the synthesis model so it is always proportional to velocity, shown as the dotted lines in Figure 4.17(b) and (c), confirms the agreement between the predicted and fitted data. Therefore the fitted function in section 4.2 is confirmed to only produce accurate data when the pellets are travelling in one or other velocity regimes over the measurement ranges.

The preliminary work on the synthesis model has been predicting the downrange ballistics for the leading edge pellets of a shot cloud. In modelling the trailing edge of a shot cloud attention is required to the pellets deceleration characteristics. From (4.22) it was shown that the leading and trailing edge steel pellets experience the same deceleration characteristics and therefore drag coefficient. Using the simplified drag coefficient curve (Figure 4.13), calculated from the deceleration characteristics, for both the leading and trailing edge pellets the synthesis prediction are shown in Figure 4.18(a) and (b) to have good qualitative agreement to the measured time-range data when the initial conditions of the model are taken at 20m.

The trailing edge lead pellets in a shot cloud have been shown in (4.21) to experience a greater deceleration. This difference in deceleration (a factor 1.234) alters the assumed drag coefficient curve by reducing the value of S in (4.25) by the same factor as the air density, the speed of sound and material density are constant for the leading and trailing edge pellets. This reduction in S increases the gradient of the simplified drag coefficient curve representing the cube law of air resistance to 1.01, whereby M_U=0.51 if the constant value below M_C is 0.52. Using the two drag coefficient approximations for the leading and trailing edge pellet, Figure 4.18(c) and (d) shows the synthesis model prediction for the variation in the leading and trailing edge flight time with range and the experimental data for two lead and steel loads.

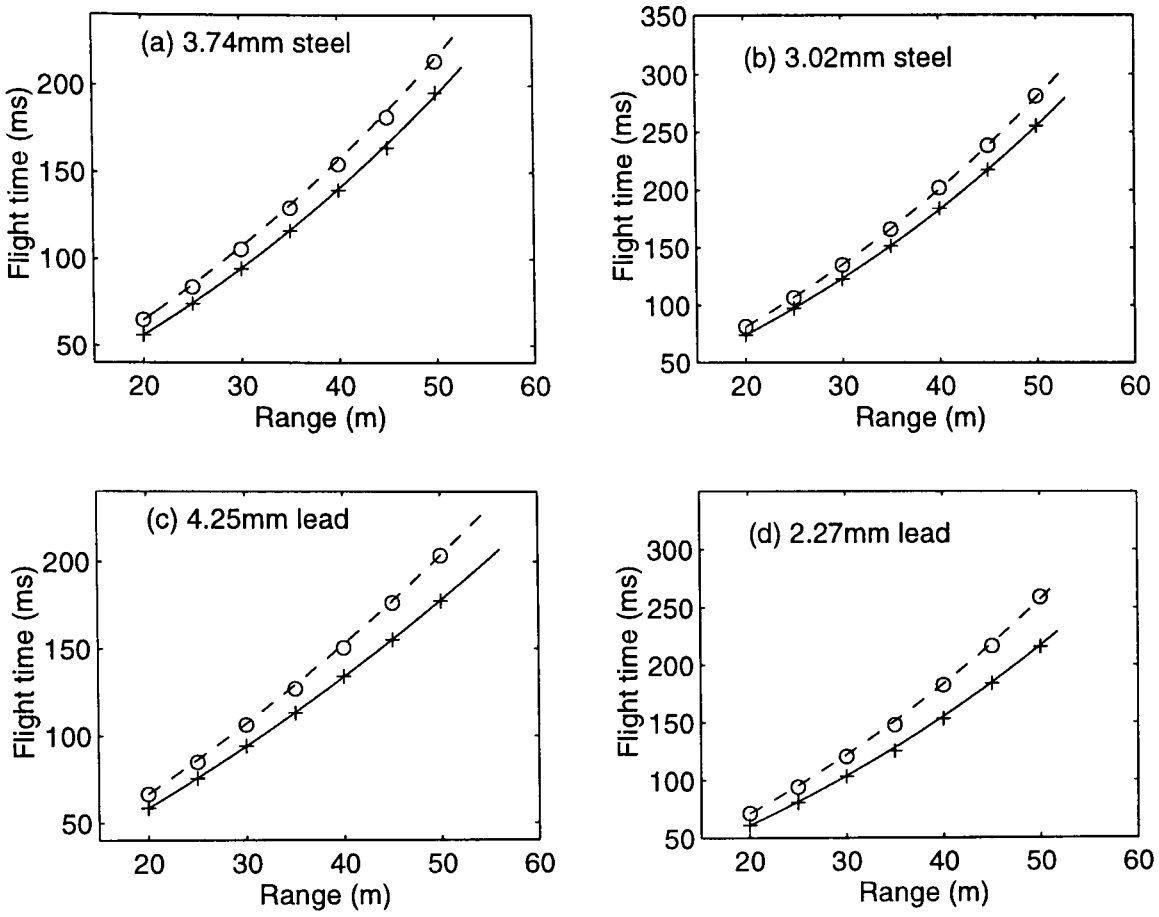

Figure 4.18 *The predicted variation in flight time with range for the leading (solid line) and trailing edge (--) pellets when the synthesis model is initialized at 20m. The leading (+) and trailing edge (o) measured data points are also shown for (a) a 28g load of #1 steel shot (cube law), (b) a 28g load of #4 steel shot (square law), (c) a 36g load of #BB lead shot (cube law) and (d) a 28g load of #7.5 lead shot (transitional between cube and square).*

The change in shape of the trailing edge pellets (as shown in section 3.2.1) has an effect on the drag. In using the synthesis process it is necessary to choose the appropriate drag coefficient behaviour for a particular material, to enable a correct prediction on the downrange ballistics of the shot cloud. With the correct drag coefficient characteristics the synthesis model produces a prediction on the variation of flight time (Figure 4.18) and velocity (Figure 4.19) with range for the leading and trailing pellets of the shot cloud along with its length (Figure 4.20). This has been shown to give good qualitative agreement when compared with experimental data. However, this approach requires reliable velocity data and it is difficult to input accurate leading and, especially, trailing flight times and velocities at 20m without making actual measurements.

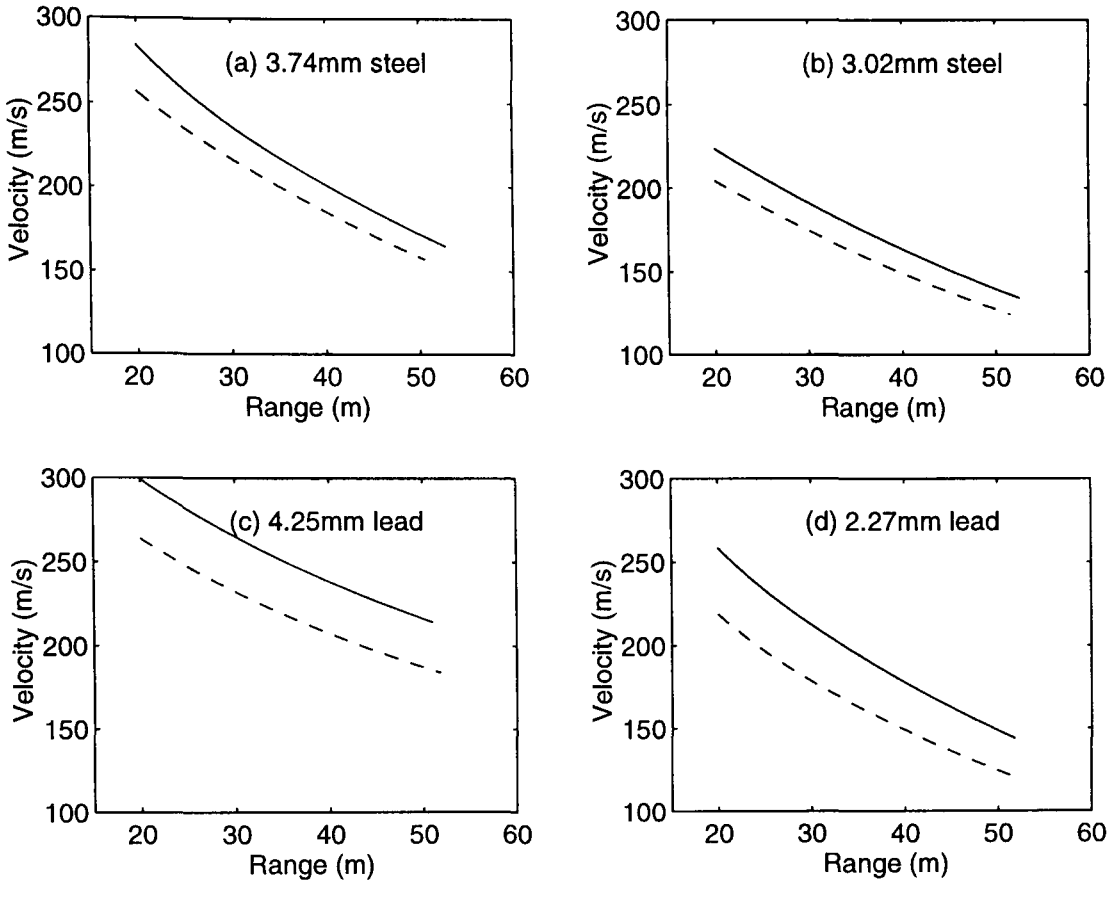

Figure 4.19 *The predicted variation in velocity for the leading (solid) and trailing edge (--) pellets when the synthesis model is initialized at 20m. (a) a 28g load of #1 steel shot (cube law), (b) a 28g load of #4 steel shot (square law), (c) a 36g load of #BB lead shot (cube law) and (d) a 28g load of #7.5 lead shot (transitional between cube and square).*

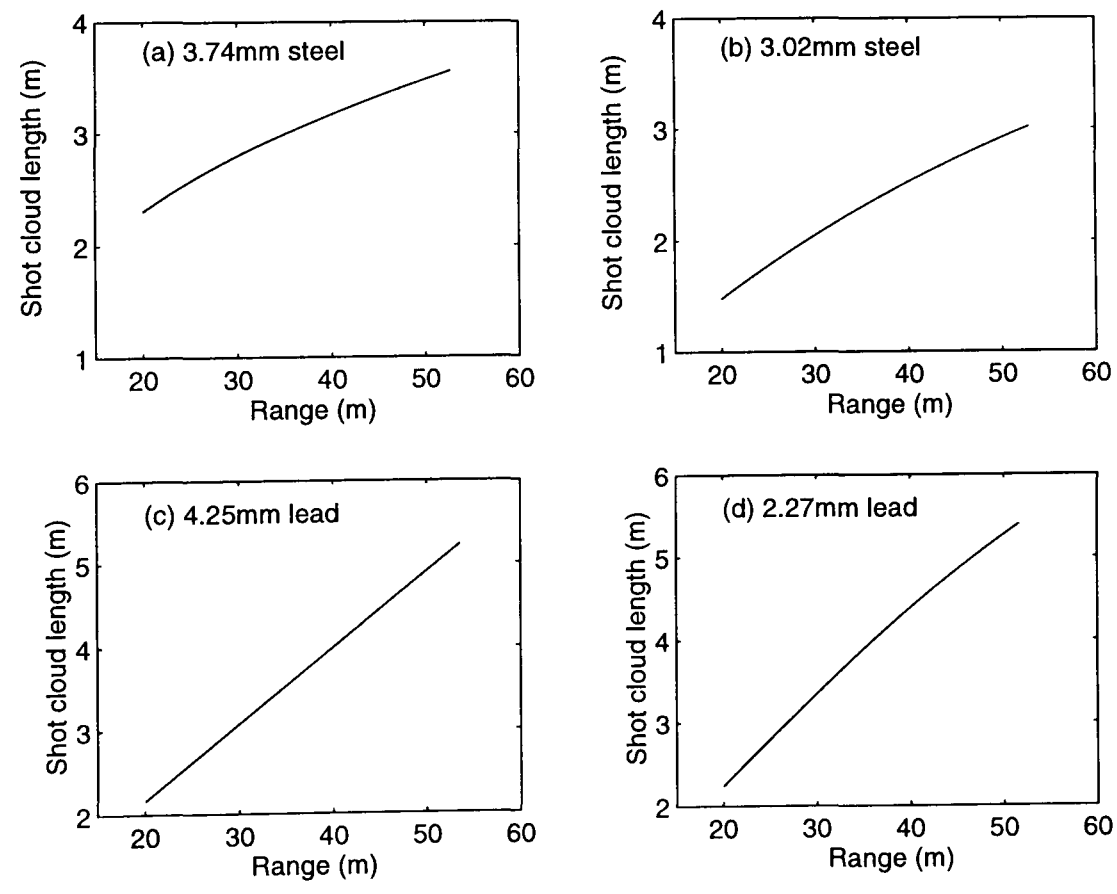

Figure 4.20 *The predicted variation in shot cloud length with range for (a) a 28g load of #1 steel shot (cube law), (b) a 28g load of #3 steel shot (square law), (c) a 36g load of #BB lead shot (cube law) and (d) a 28g load of #7.5 lead shot (transitional between cube and square) when the synthesis model is initialized at 20m.*

4.6 SUMMARY

In this chapter the ballistic characteristics of shot cloud have been analysed using the drag force equation of a single sphere in free flight. This has required several assumptions to be made about the behaviour of the pellets in the shot cloud. Firstly, the pellets were required to be independent of one another in flight and, secondly, the drag coefficient characteristics were constant below Mach 0.5 and above Mach 1.4; in between the drag coefficient is well modelled as being proportional to velocity. From these assumptions two expressions were determined that represented a pellet obeying a cube law or square law of air resistance. Manipulating the expression models were obtained for the flight time, velocity and shot cloud length. It was found from the normalized deviation of square and cube laws fits that the cube law of air resistance was appropriate for describing pellets that spent the majority of their measured flight time in the transonic regime. From the expressions a fitted value representing the deceleration constant and muzzle velocity were obtained. Along with the measured muzzle velocity by the skyscreen it was shown that it is not good practice to extrapolate from the muzzle to the measurement range or vice versa.

The least squares fit of the derived flight time-range equations produced a parameter which represents the deceleration constant of the pellets. From theoretical and analytical measures a relationship was shown between the deceleration constant and the pellet diameter, density and atmospheric condition for pellets obeying a cube law and square law of air resistance. The gradient of these two relationships enabled a better approximation of the boundaries of the assumed drag coefficient characteristics to be generated. It was also possible to show the effect that deformed pellets have on the drag coefficient, as the trailing lead pellet had a higher deceleration constant for the same diameter. This produced a steeper gradient in the cube law regime and altered the boundaries again.

Finally, a synthesis model was derived from the single sphere equation to predict the downrange ballistics of a shot cloud. It was shown that good quantitative agreement was obtained between the predicted and experimental data, on the variation in flight

time with range, when the synthesis model was initialized after the pellets became independent. The model also required the correct drag coefficient characteristics for the leading and trailing edge pellets, this was obtained from the deceleration work. Using muzzle conditions or corresponding data, where pellet interaction still occurs, produced very poor predictions, thus reinforcing that it is not good practice to extrapolate data to areas where the pellet behaviour is different.

Chapter 5

Stochastic model of a shot cloud

5.1 INTRODUCTION

5.1.1 Statistical aerodynamics

Experimentalists have been interested in the motion of a sphere for many years. As explained in Chapter 1, spheres were extensively used for the calibration of turbulence in wind tunnels until it was found that the small variation in the shape caused appreciable differences in the results [7,8,25,27,28]. From these calibration tests an interest has developed in the drag on a sphere moving through a fluid. There have been studies of the aerodynamic performance of single spheres in the transonic velocity range, but there is very little published work on the dynamics of an ensemble of spheres [1,2,10,11,16]. It is believed that this is partly due to the lack of military interest in this class of projectiles and the special problems associated with this type of measurement.

This investigation has been concerned with the statistical aerodynamics of ensembles of spheres, otherwise known as shot clouds. In order to study the aerodynamics of a shot cloud, the proof barrel was used to launch the projectile which consists of a large number of spherical pellets. The experiments carried out by Lowry [16] have shown, Figure 1.5, that the pellets leave the muzzle as a single semi-fluid object, the mass of which is not spherical and has no constant shape. The drag force of air resistance, the interaction between the pellets and the effects of irregularities cause a gradual separation of the pellets over the time of flight.

The mechanisms involved in the dynamic behaviour of shot clouds can be studied indirectly from the measurements in Chapter 3 showing how their dispersion changes with time while they are in flight. In this section several methods are presented to model the dispersion of pellets within a shot cloud as it develops in flight. The preliminary work involves the motion of a single sphere, described by (1.1), in free flight and the method for treating the problem of a shot cloud can be built upon an understanding of this motion. From these simple models, approximate analytic expressions are obtained for the shot cloud width and length at ranges of practical interest (typically 20 to 50m from the muzzle). Thus the models are not concerned with

a detailed treatment of the various processes involved in the dispersion of the pellets. The pellets have velocity components in each of the three Cartesian directions with the component along the axis defined by the barrel being much greater than the others. The effect of gravity is neglected and it is assumed that the distribution of pellets in the shot cloud is symmetric and statistically identical in each of the transverse directions. This is supported by the measurements in Chapter 3 which indicate Gaussian distributions in the transverse direction with standard deviations typically within 8% of each other. Apart from air resistance, which is modelled by one or other of the force-laws described in section 4.2, the forces on pellets arising, for example, from turbulence and from deviations of the shape from a perfect sphere are random in nature and are included by the addition of a random force term to the appropriate equation of motion. Further, this random force is modelled as a simple Markovian process with delta-function correlation (section 5.1.2). Also included is the effect of the launch conditions which depend upon the degree of choke used and are characterised by the initial variance of either the transverse velocity components (when calculating the width of the shot cloud) or the longitudinal velocity components (when calculating the length). Thus in each part of the model there are two parameters which arise from processes of a random nature. One is the variance associated with the launch conditions, determined by the choke, and the other is the rate of diffusion caused by the random force while the shot cloud is in flight. These may be used to achieve a two-parameter fit to the experimental width data and a second such fit to the length data.

Within these models, the time-dependent width and length of the shot cloud are found by calculating the variances of the displacements of pellets, that is, an average is taken over all pellets. The variance of the transverse co-ordinates of the pellets at a particular time is a measure of the width of the shot cloud at that time, whilst the variance of the displacements in the direction defined by the barrel is a measure of the shot cloud length.

5.1.2 Markovian process

The theory of stochastic processes deals with systems which develop in time or space in accordance with probabilistic laws. A stochastic (random) process applies to systems which evolve in time whilst undergoing chance fluctuations, for example the associated pellet fluctuations in a shot cloud over the flight time. There are many stochastic process which involve complex mathematics, but the Markovian process is one of the simplest. For this application, it models the forces arising from turbulence, collisions and other irregularities affecting the motion of the pellets in flight and is assumed to have zero mean. The nature of the Markovian process means it is ergodic, which means that the random forces acting on one pellet at different times during its flight are uncorrelated, or, equivalently, that the forces acting on two different pellets at any one time are uncorrelated.

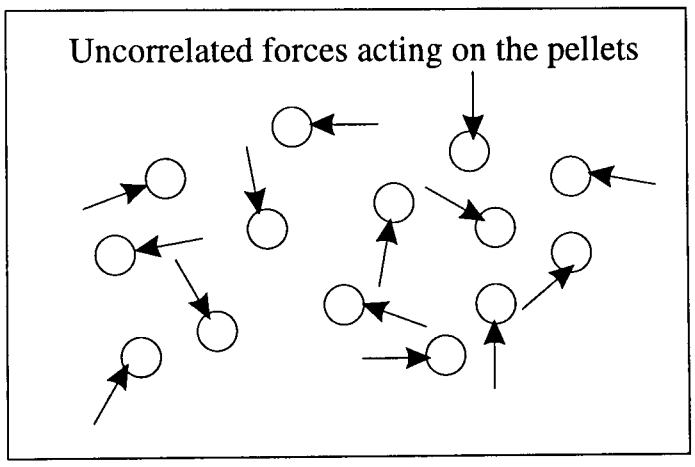

Figure 5.1 *Diagram to illustrate the random forces acting on the pellets.*

5.1.3 Initial equations

To begin the development of the models, to describe the dynamics of the cloud of spherical projectiles, the motion of an independent single pellet is reviewed. As explained in the section 1.1.1 and 4.2.1, the retardation force of air resistance is well-modelled by a force proportional to either the square or the cube of the magnitude of the velocity, v, depending upon the velocity range involved. It is assumed that over the distances and times of interest the pellets remain in a velocity range corresponding to only one of these force laws.

Consider first the case of the deceleration force due to air resistance having a magnitude proportional to the square of the magnitude of the velocity. The equation of motion for a single pellet can then be written

$$\dot{\underline{v}} = -k_2 v^2 \hat{\underline{v}} \ , \tag{5.1}$$

where $\hat{\underline{v}}$ is a unit vector in the direction of the velocity $\underline{v}$ of the pellet and k_2 is a constant depending on air density for a particular pellet. At the point of projection (on leaving the barrel), a pellet has a large velocity component in the direction of the barrel (defined here to be the z-direction). In the transverse x- and y-directions, the pellet will have small velocity components, and it is assumed for simplicity that there is no distinction between these transverse directions, the effects of gravity being neglected. Therefore, without loss of generality, only the x- and z-directions are considered. Consequently, writing $\underline{v}=(v_x, v_y, v_z)$, it is assumed that $v \approx v_z$ since $v_z >> v_x$ and $v_z >> v_y$. Hence $v^2 \hat{\underline{v}} = (v_z v_x, v_z v_y, v_z^2)$. Resolving (5.1) in the x- and z-directions we obtain

$$\dot{v}_z = -k_2 v_z^2 \tag{5.2}$$

$$\dot{v}_x = -k_2 v_x v_z \tag{5.3}$$

Integrating (5.2) with the initial condition $v_z(0)=v_0$ gives

$$v_z = \frac{v_0}{(1 + k_2 v_0 t)} \tag{5.4}$$

and integrating again gives the range travelled in the z-direction as

$$R(t) = \frac{1}{k_2} \ln(1 + k_2 v_0 t) \ . \tag{5.5}$$

Using (5.4), it is straightforward to integrate (5.3) with the initial condition $v_x(0)=v_{x0}$. In a similar way, if the force of deceleration due to air resistance is proportional to v^3, the equation of motions are

$$\dot{v}_z = -k_3 v_z^3 , \qquad \dot{v}_x = -k_3 v_x v_z^2 , \tag{5.6}$$

where k_3 is a constant, and integration of the first of these gives

$$v_z = \frac{v_0}{\sqrt{1+2k_3 v_0^2 t}} \tag{5.7}$$

and the corresponding range

$$r(t) = \frac{1}{k_3 v_0}\left\{(1+2k_3 v_0^2 t)^{1/2} - 1\right\}. \tag{5.8}$$

Note that R and k_2 refer to the square-law of air resistance whereas r and k_3 refer to the cube-law, and that k_2 and k_3 have different dimensions.

5.2 RANDOM FORCE MODEL

5.2.1 Addition of a random force term

While in flight, the motion of each pellet in the shot cloud may be influenced by collisions, by slip-stream effects and turbulence, by changes in air density, and by deviations of the shape from a perfect sphere. For a randomly distributed shot cloud, it is reasonable to model these influence as an additional random force $\underline{F}(t)$ acting on a pellet at time t. As a first attempt at modelling these effects the random force $\underline{F}(t)$ is added to the single sphere equation with square-law deceleration (5.1) so that the equation of motion for a single pellet becomes

$$\dot{\underline{v}} = -k_2 v^2 \hat{\underline{v}} + \underline{F}(t) \quad . \tag{5.9}$$

Taking components of (5.9) and using the same arguments as before in section 5.1.3, the expressions for the longitudinal and lateral velocity components are found to be

$$\dot{v}_z = -k_2 v_z^2 + F_z(t) \quad , \tag{5.10}$$

$$\dot{v}_x = -k_2 v_x v_z + F_x(t) \quad , \tag{5.11}$$

respectively, where F_x and F_z are the x- and z-components of $\underline{F}$. These random functions are assumed to have zero mean in the sense that at any time their average taken over all the pellets in the shot cloud is zero. To indicate such an average, angled brackets are used so that $\langle F_x(t)\rangle = \langle F_z(t)\rangle = 0$. If the displacement of $z(t)$ and $x(t)$ can be found in terms of F_x and F_z, then the square roots of the variances of $x(t)$ and $z(t)$ will be proportional to the length and width, respectively, of the shot cloud. In order to obtain analytic formulae for these, two approximations are used. Firstly, v_z is written as

$$v_z = \langle v_z \rangle + U(t) = \frac{v_0}{(1 + k_2 v_0 t)} + U(t) \quad , \tag{5.12}$$

where $\langle v_z \rangle$ is the solution of (5.10) in the absence of the random force term given by (5.4) and $U(t)$ is assumed to be a small perturbation from this mean value. Substituting the form (5.12) into the first term of (5.10),

$$\dot{U} = -\frac{2k_2 v_0}{(1 + k_2 v_0 t)} U + F_z(t) \tag{5.13}$$

is obtained, where it is assumed that $|U| << \langle v_z \rangle$ and consequently the higher powers of U can be neglected. When making comparisons of the model with experimental data, it must be verified that this approximation is valid over all times and ranges of interest. Secondly, when integrating (5.11), it is assumed that the effect of U on v_x is small

compared to the other terms in the equation, so that v_z in (5.11) is replaced by $\langle v_z \rangle$. Hence

$$\dot{v}_x = -\frac{k_2 v_0}{(1+k_2 v_0 t)} v_x + F_x(t) \quad . \tag{5.14}$$

Similarly for a deceleration force due to air resistance that is proportional to the cube of the magnitude of the velocity, the longitudinal velocity component is found to be

$$v_z = \frac{v_0}{\sqrt{1+2k_3 v_0^2 t}} + u(t) \tag{5.15}$$

and the equations of motion

$$\dot{u} = -\frac{3k_3 v_0^2}{(1+2k_3 v_0^2 t)} u + F_z(t) \tag{5.16}$$

and

$$\dot{v}_x = -\frac{k_3 v_0^2}{(1+2k_3 v_0^2 t)} v_x + F_x(t) \quad . \tag{5.17}$$

Equations (5.12) and (5.14) for the square-law of air resistance and (5.15) and (5.17) for the cube-law of air resistance form the basis of the analysis in the next sections.

5.2.2 The width of the shot cloud

In order to obtain the width of the cloud of pellets, the variance is calculated in the x-components of the displacements of the pellets from the axis defined by the direction of the barrel. For the square-law velocity dependence of the force due to air resistance, Equation (5.14) is integrated twice to obtain $x(t)$ in terms of $F_x(t)$. A first integral is easily achieved using the integrating factor method and it is found that

$$v_x(t) = \frac{v_{x0}}{(1+k_2 v_0 t)} + \frac{1}{(1+k_2 v_0 t)} \int_0^t (1+k_2 v_0 t') F_x(t') dt' \quad , \qquad (5.18)$$

where v_{x0} is the initial velocity component transverse to the barrel axis. It is assumed that the shot cloud is statistically symmetric so that $\langle v_{x0} \rangle = 0$. Integration of (5.18) gives

$$x(t) = \frac{v_{x0}}{k_2 v_0} \ln(1+k_2 v_0 t) + \int_0^t \frac{dt''}{(1+k_2 v_0 t'')} \int_0^{t''} (1+k_2 v_0 t') F_x(t') dt' \quad , \qquad (5.19)$$

where it has been assumed that $x(0)=0$, so that any small initial displacement from the z-axis is ignored. Note that $\langle x(t) \rangle = 0$ since $\langle v_{x0} \rangle = \langle F_x \rangle = 0$, so that the shot cloud remains statistically symmetric. Hence the variance of the transverse displacements is simply given by $\langle x^2(t) \rangle$. Squaring (5.19) and taking the ensemble average over all the pellets we obtain

$$\left\langle x^2(t) \right\rangle = \frac{\left\langle v_{x0}^2 \right\rangle}{k_2^2 v_0^2} \left[\ln(1+k_2 v_0 t) \right]^2$$

$$+ \int_0^t \int_0^t \frac{dt'' d\tau''}{(1+k_2 v_0 t'')(1+k_2 v_0 \tau'')} \int_0^{t''} \int_0^{\tau''} (1+k_2 v_0 t')(1+k_2 v_0 \tau') \left\langle F_x(t') F_x(\tau') \right\rangle dt' d\tau' \quad . \qquad (5.20)$$

The cross-terms involving $\langle v_{x0} F_x \rangle$ in (5.20) vanish since the initial velocities and the random force are uncorrelated giving $\langle v_{x0} F_x \rangle = \langle v_{x0} \rangle \langle F_x \rangle = 0$. In order to proceed further analytically, an expression is needed to represent the two-time correlation function $\langle F_x(t') F_x(\tau') \rangle$. The simplest model of the random force is chosen in which F_x is a Markovian random process (that is, a process without memory) having delta-function correlation [51]

$$\left\langle F_x(t') F_x(\tau') \right\rangle = D_x \delta(t' - \tau') \quad , \qquad (5.21)$$

where D_x is a diffusion constant. The random forces acting on the pellet can then be thought of as a series of independent impulses in random directions, and with random magnitudes of a certain variance. This model leads to the conventional diffusion process in the description of Brownian motion [52]. The constant D_x and $\langle v_{x0}^2 \rangle$ are, at this stage, two free parameters in the model. Using (5.21), it is shown in Appendix H.1 that (5.20) can be evaluated in closed form with the result that

$$W^2(t) = \langle x^2(t) \rangle = \frac{A}{k_2^2}\left[\ln(1+k_2 v_0 t)\right]^2$$

$$+ B\left[(1+k_2 v_0 t)^3 - 1 - 3\ln(1+k_2 v_0 t) - \frac{9}{2}\left[\ln(1+k_2 v_0 t)\right]^2\right] , \quad (5.22)$$

where $A = \langle v^2{}_{x0} \rangle / v_0^2$ is a non-dimensional measure of the initial spread of the transverse velocities, and $B = 2D_x / 27 k_2^3 v_0^3$. Of course, the last term on the right-hand side of (5.22) could be combined with the first, but it is preferred to leave the form unchanged and refer to the first term as that arising from launch effects and the remainder as arising from the in-flight effects. The square root of $\langle x^2(t) \rangle$ is proportional to the width $W(t)$ of the shot cloud at time t, and the constant of proportionality can be absorbed into the constants A and B when fitting (5.22) to experimental data. Using (5.22) and (5.5), the width $W(R)$ of the shot cloud in terms of the mean distance R travelled in the z-direction is given by

$$W(R) = \left\{ AR^2 + B\left(e^{3k_2 R} - 1 - 3k_2 R - \frac{9}{2}(k_2 R)^2 \right) \right\}^{1/2} . \quad (5.23)$$

In the case of the cube-law velocity dependence of air resistance, integration of (5.17) by the integration factor method gives

$$v_x(t) = \frac{v_{x0}}{(1+2k_3v_0^2t)^{1/2}} + \frac{1}{(1+2k_3v_0^2t)^{1/2}} \int_0^t (1+2k_3v_0^2t')^{1/2} F_x(t')dt' \quad , \tag{5.24}$$

and a further integration results in

$$x(t) = \frac{v_{x0}}{k_3v_0^2}\left[(1+2k_3v_0^2t)^{1/2} - 1\right] + \int_0^t \frac{dt''}{(1+2k_3v_0^2t'')^{1/2}} \int_0^{t''} (1+2k_3v_0^2t')^{1/2} F_x(t')dt' \quad . \tag{5.25}$$

The variance, by a similar argument to that used before, is given by

$$\left\langle x^2(t)\right\rangle = \frac{\left\langle v_{x0}^2\right\rangle}{k_3^2v_0^4}\left[(1+2k_3v_0^2t)^{1/2} - 1\right]^2 + \int_0^t\int_0^t \frac{dt''d\tau''}{(1+2k_3v_0^2t'')^{1/2}(1+2k_3v_0^2\tau'')^{1/2}}$$

$$\int_0^{t''}\int_0^{\tau''} (1+2k_3v_0^2t')^{1/2}(1+2k_3v_0^2\tau')^{1/2}\left\langle F_x(t')F_x(\tau')\right\rangle dt'd\tau' \quad . \tag{5.26}$$

Again, a closed form expression can be obtained if the correlation function, given by (5.21), is inserted. The method follows the same procedure as was used previously and the evaluation is given in Appendix H.2. From this lengthy calculation it is found that

$$W^2(t) = \left\langle x^2(t)\right\rangle = \frac{A}{k_3^2v_0^2}\left[(1+2k_3v_0^2t)^{1/2} - 1\right]^2$$

$$+C\left\{24(1+2k_3v_0^2t)^{1/2} + (1+2k_3v_0^2t)^3 - 15(1+2k_3v_0^2t) - 10\right\} \quad , \tag{5.27}$$

where $A = \left\langle v^2{}_{x0}\right\rangle / v_0^2$, as before, and $C = D_x/60k_3^3v_0^6$. Substituting (5.8) into (5.27) an expression for the width in terms of the range $r(t)$ in obtained:

$$W(r)=\left\{Ar^2+C(k_3v_0r)^3\left(20+15(k_3v_0r)+6(k_3v_0r)^2+(k_3v_0r)^3\right)\right\}^{1/2}. \quad (5.28)$$

Note that, as expected, the first terms of (5.23) and (5.28) give contributions to the width which vary linearly with range, this being the launch effect of the initial transverse velocity components on the width. It can also be seen directly from (5.28) and by expansion of the exponential in (5.23) that the remaining terms arising from the in-flight effects are, of course, positive and that for sufficiently small ranges they vary as the cube of the range. This confirms that launch effects are initially greater in magnitude than those which develop in flight.

5.2.3 The length of the shot cloud

The shot cloud length can be determined by calculating the variance in the z-components of the displacements of the pellets in the direction of the barrel. For the square-law dependence of air resistance the integrating factor method is used to solve (5.13). It is found that

$$U(t)=\frac{U_0}{(1+k_2v_0t)^2}+\frac{1}{(1+k_2v_0t)^2}\int_0^t(1+k_2v_0t')^2F_z(t')dt' \quad , \quad (5.29)$$

and hence, from (5.12), v_z is given by

$$v_z(t)=\frac{v_0}{(1+k_2v_0t)}+\frac{U_0}{(1+k_2v_0t)^2}+\frac{1}{(1+k_2v_0t)^2}\int_0^t(1+k_2v_0t')^2F_z(t')dt' \quad . \quad (5.30)$$

Integrating (5.30) with respect to t, the displacement in the direction of the barrel is given by

$$z(t)=\frac{1}{k_2}\ln(1+k_2v_0t)+\frac{U_0t}{(1+k_2v_0t)}+\int_0^t\frac{dt''}{(1+k_2v_0t'')^2}\int_0^{t''}(1+k_2v_0t')^2F_z(t')dt' \quad , \tag{5.31}$$

where the initial length of the shot cloud has been ignored so that all the pellets have displacements of zero at t=0. The variance of the displacements, obtained as before by averaging over the pellets and assuming that $\langle U_0\rangle$=0, gives

$$\left\langle z^2(t)\right\rangle-\left\langle z(t)\right\rangle^2=\left\langle z^2(t)\right\rangle-R^2(t)=\frac{\left\langle U_0^2\right\rangle t^2}{(1+k_2v_0t)^2}$$

$$+\int_0^t\int_0^t\frac{dt''d\tau''}{(1+k_2v_0t'')^2(1+k_2v_0\tau'')^2}\int_0^{t''}\int_0^{\tau''}(1+k_2v_0t')^2(1+k_2v_0\tau')^2\left\langle F_z(t')F_z(\tau')\right\rangle dt'd\tau' \quad . \tag{5.32}$$

Using the delta-function correlation

$$\left\langle F_z(t')F_z(\tau')\right\rangle=D_z\delta(t'-\tau') \quad , \tag{5.33}$$

where D_z is the diffusion constant, the square of the length of the shot cloud can be obtained in (5.34), where $\alpha=\left\langle U_0^2\right\rangle/v_0^2$ and $\beta=D_z/30k_2^3v_0^3$ by evaluating the variance in closed form (solution given in Appendix H.3).

$$L^2(t)=\frac{\alpha(k_2v_0t)^2}{k_2^2(1+k_2v_0t)^2}+\frac{\beta(k_2v_0t)^3}{(1+k_2v_0t)^2}\left(10+5k_2v_0t+(k_2v_0t)^2\right) \quad . \tag{5.34}$$

To obtain the shot cloud length in terms of the mean range it is necessary to substitute (5.5) into (5.34) to give

$$L(R)=\left\{\frac{\alpha}{k_2^2}(1-e^{-k_2R})^2+\beta\left(e^{3k_2R}+15e^{-k_2R}-6e^{-k_2R}-10\right)\right\}^{1/2} . \qquad (5.35)$$

For the cube-law velocity dependence of air resistance, integration of (5.16) yields

$$u(t)=\frac{u_0}{(1+2k_3v_0^2t)^{3/2}}+\frac{1}{(1+2k_3v_0^2t)^{3/2}}\int_0^t(1+2k_3v_0^2t')^{3/2}F_z(t')dt' , \qquad (5.36)$$

so that, using (5.15), v_z is given by

$$v_z(t)=\frac{v_0}{(1+2k_3v_0^2t)^{1/2}}+\frac{u_0}{(1+2k_3v_0^2t)^{3/2}}+\frac{1}{(1+2k_3v_0^2t)^{3/2}}\int_0^t(1+2k_3v_0^2t')^{3/2}F_z(t')dt' . \qquad (5.37)$$

Integrating (5.37) with respect to t and again ignoring the initial length of the shot cloud gives

$$z(t)=r(t)+\frac{u_0}{k_3v_0^2}\left[1-\frac{1}{(1+2k_3v_0^2t)^{1/2}}\right]+\int_0^t\frac{dt''}{(1+2k_3v_0^2t'')^{3/2}}\int_0^{t''}(1+2k_3v_0^2t')^{3/2}F_z(t')dt' , \qquad (5.38)$$

where $r(t)$ is given by (5.8). The variance in the displacements in this case is found (shown in Appendix H.5) by the same procedure used previously with the result that

$$L^2(t)=\frac{\alpha}{k_3^2v_0^2}\left[1-\frac{1}{(1+2k_3v_0^2t)^{1/2}}\right]^2$$

$$+\gamma\left\{(1+2k_3v_0^2t)^3-28+48(1+2k_3v_0^2t)^{-1/2}-21(1+2k_3v_0^2t)^{-1}\right\} , \qquad (5.39)$$

where $\alpha=\left\langle u_0^2\right\rangle/v_0^2$ and $\gamma=D_z/168k_3^3v_0^6$. In terms of the mean range $r(t)$ in (5.8), the length can be expressed as

$$L(r)=\left\{\frac{\alpha r^2}{(1+k_3 v_0 r)^2}+\gamma\left[(1+k_3 v_0 r)^6-28+48(1+k_3 v_0 r)^{-1}-21(1+k_3 v_0 r)^{-2}\right]\right\}^{1/2} . \tag{5.40}$$

5.2.4 Comparison with experimental data

The expressions derived in sections 5.2.2 and 5.2.3 for the shot cloud width and length appropriate to either a square law or cube law of air resistance were compared with experimental results obtained using the measurement facility described in Chapter 2. In order to check their appropriateness, measurements were taken using specially prepared loads of pellets the velocities of which lay within one or other of the velocity regimes over the measurement range (20-50m). Two types of steel pellets were therefore used in the primary experiments due to the spherical shape after firing, one obeying a square law (28g load of #4 steel (3.02mm) shot using 0.030" choke) and the other a cube law of air resistance (28g load of #1 (3.74mm) steel shot using 0.020" choke). The experimental width data was obtained by taking the average of the radial standard deviations of ten patterns, as in section 3.4, at seven ranges from 20m to 50m at 5m intervals. The length was obtained by a similar average of the flight-time data at the same ranges. The width and length were calculated in this way at each of the seven ranges for the two different types of loads.

The leading edge flight-time data were used to obtain the initial velocity v_0 and the deceleration constant (k_2 or k_3) by a least-squares fit of the time-range formula for either the square law result (5.5) or that for the cube law given by (5.8). Then the expressions (5.22) and (5.23) or (5.27) and (5.28) were used to generate a two-parameter least-squares fit to the width data, and expression (5.34) and (5.35) or (5.39) and (5.40) were used to make a similar fit to the length data.

In Figure 5.2(a) the average radial standard deviation data points are shown for the width of the shot cloud measured for pellets with velocities in the square law regime and the corresponding theoretical curves obtained from (5.22) in Figure 5.2a(i) and (5.23) in Figure 5.2a(ii). In Figure 5.2(b) the length data is given together with the theoretical

curves generated from (5.34) and (5.35). Figure 5.3 shows the corresponding results for the width and length of the shot cloud with pellet velocities lying in the cube law regime.

A visual inspection of Figure 5.2 and 5.3 indicates that there is excellent qualitative agreement between theory and experiment. To measure this agreement the normalized deviation d_n, given as (4.13), of the fits from the experimental data are calculated. The values of d_n obtained were typically of order 10^{-4} for the width data and 10^{-5} for the length data, proving that statistically there is a small deviation of the experimental data from the theory.

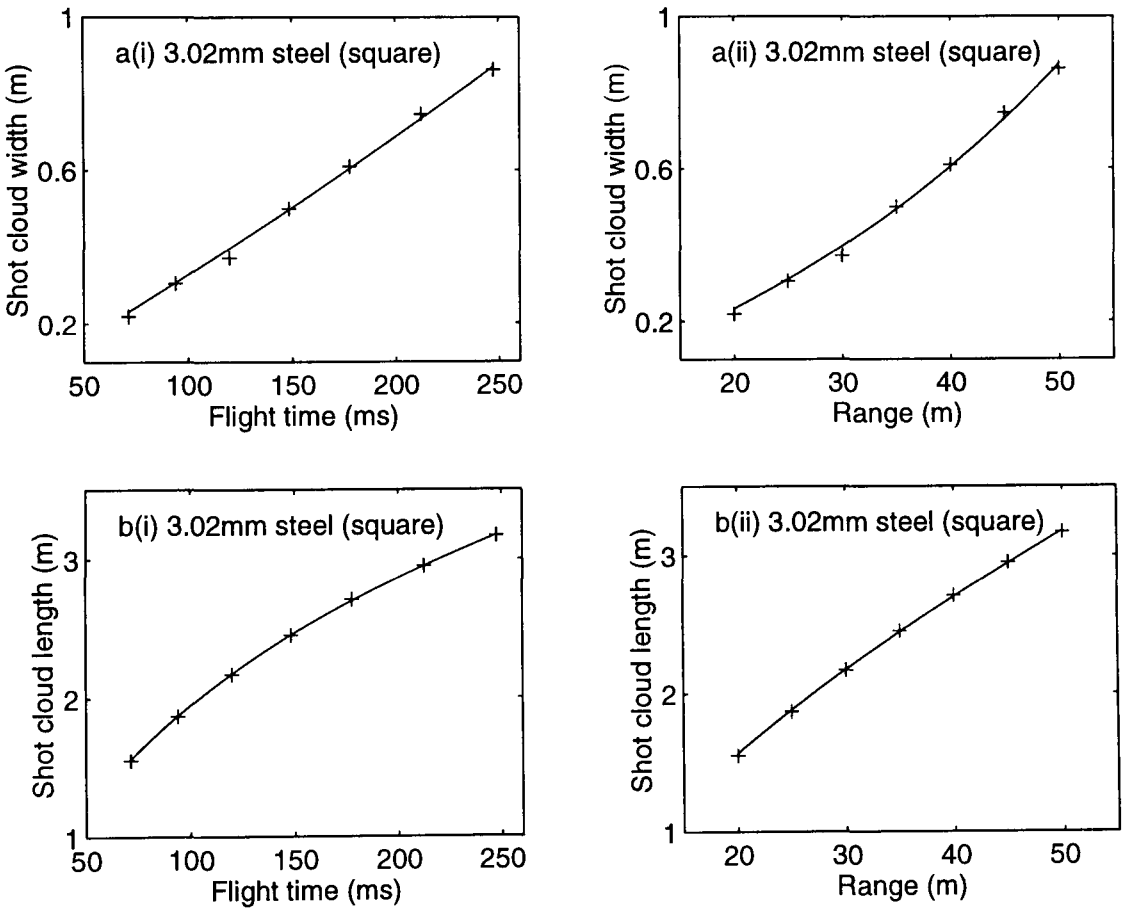

Figure 5.2 *The shot cloud (a) width and (b) length in metres for steel pellets (28g load of #4 steel shot using 0.030" choke) obeying a square-law of air resistance as a function of (i) flight time and (ii) range. The crosses represent average data points and the theoretical curves are obtained by a least-squares fit of the corresponding expression in section 5.2.*

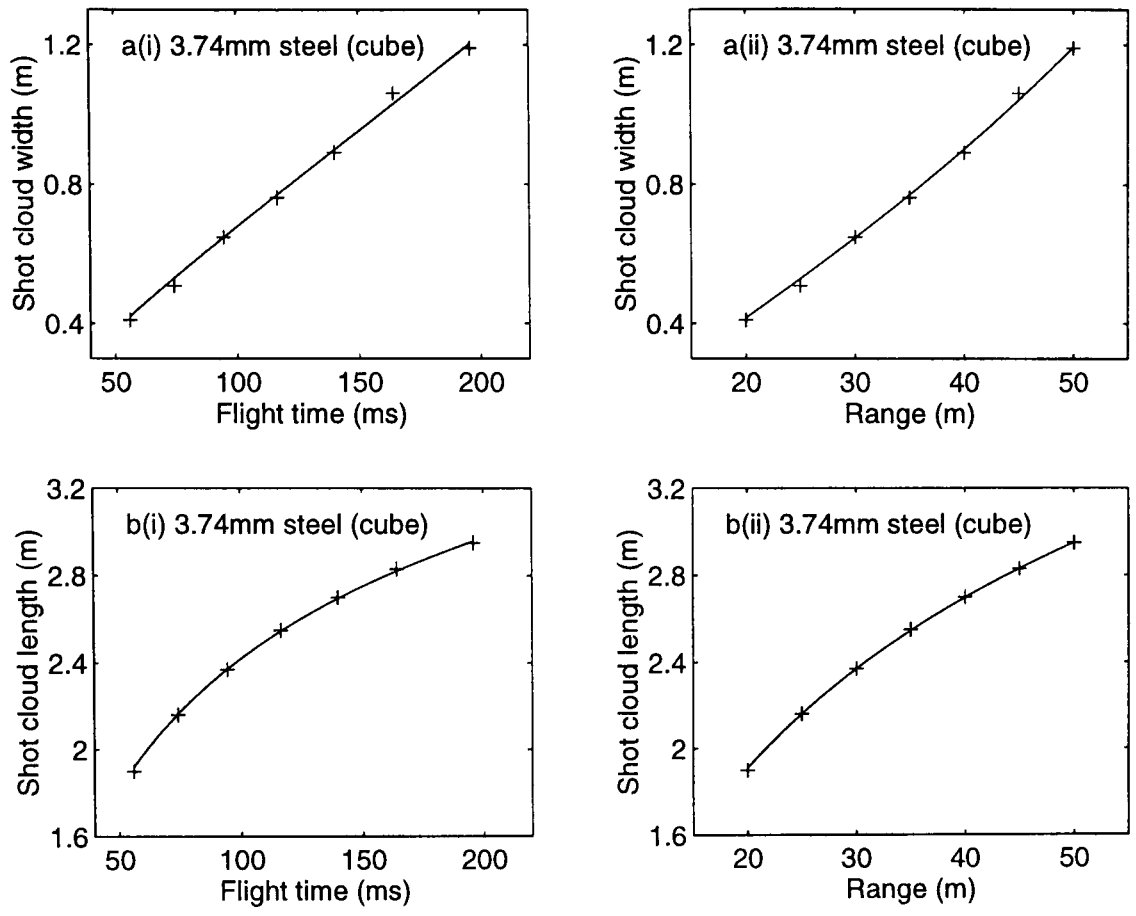

Figure 5.3 *The shot cloud (a) width and (b) length in metres for steel pellets (28g load of #1 steel shot using 0.020" choke) obeying a cube-law of air resistance as a function of (i) flight time and (ii) range. The crosses represent average data points and the theoretical curves obtained by a least-squares fit of the corresponding expression in section 5.2.*

In order to examine the effects of modelling the length and width using either a square law or cube law of air resistance, the square law experimental results were fitted to the cube law theory. Similarly the square law theory was fitted to the cube law experimental data. For the predicted length thus obtained, the deviation d_n increased by an order of magnitude and furthermore the theoretical curves predict an unrealistic contraction of the shot cloud in some cases (Figure 5.4(a)). The predicted widths, however, were found not to be sensitive to the choice of air resistance and little change in d_n was seen. This is because the basic equations (5.3) or (5.6) governing the transverse velocity component v_x of a pellet are both linear equations, moreover, the magnitudes of the multiplying factors $k_2 v_z$ in (5.3) and $k_3 v_z^2$ in (5.6) are very similar in value within the experimentally observed times (corresponding to ranges from 20m to 50m). This is shown in Figure 5.4(b) where the ratio of $(k_2 v_z)_{square} / (k_3 v_z^2)_{cube}$ is plotted against the corresponding flight times for the cube and square law experimental data.

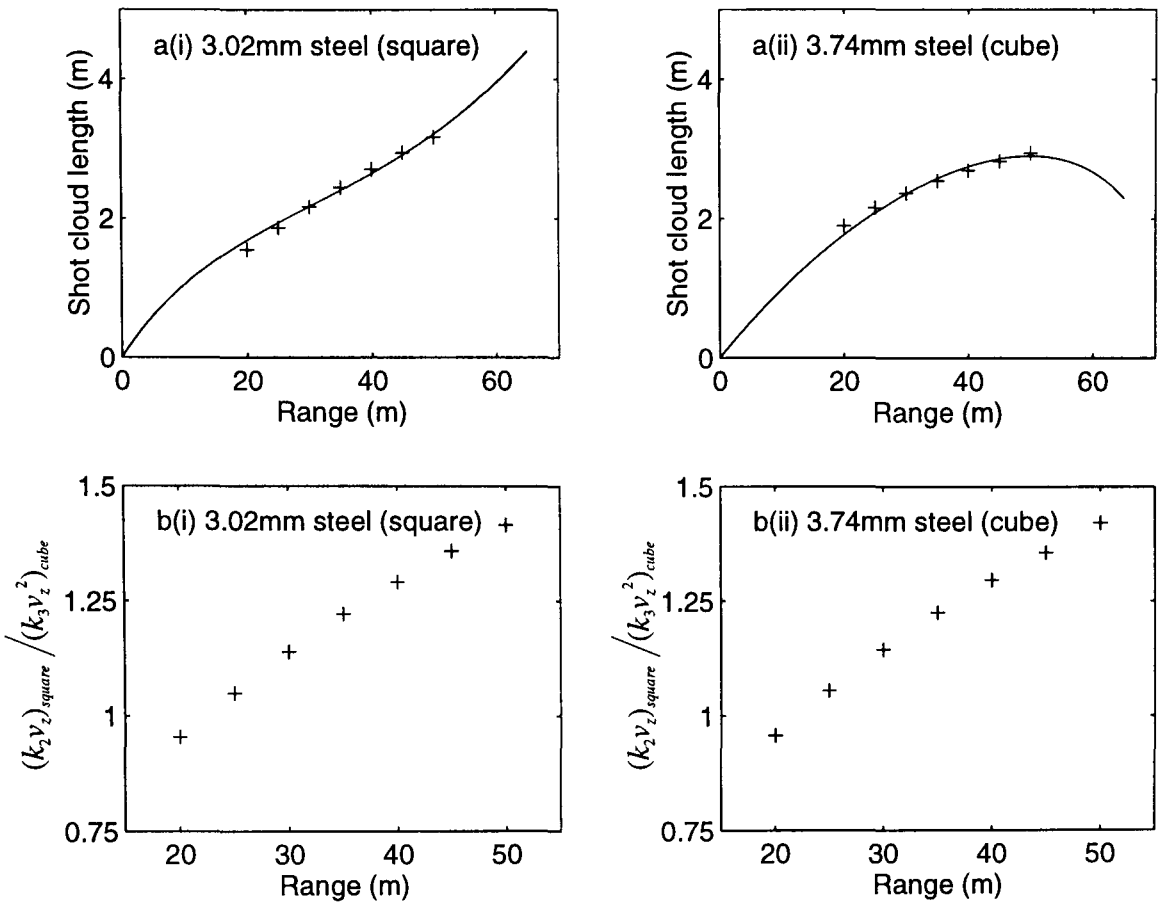

Figure 5.4 *(a) The shot cloud length as a function of range for steel pellets obeying (i) a square-law of air resistance (28g load of #4 steel shot using 0.030" choke) fitted to the cube law theory and (ii) a cube-law of air resistance (28g load of #1 steel shot using 0.020" choke) fitted to the square law theory. (b) The ratio of* $(k_2 v_z)_{square} / (k_3 v_z^2)_{cube}$ *from the width expression as a function of range.*

In the derivations of the (5.13) and (5.16) for the deviation of the z-component of velocity from the mean value $\langle v_z \rangle$, it was assumed that the magnitude of this deviation was much smaller than $\langle v_z \rangle$. This is verified by calculating $\sqrt{\langle U^2(t) \rangle}$ or $\sqrt{\langle u^2(t) \rangle}$ from (5.29) and (5.36), and dividing by the appropriate expression for v_z given by (5.4) or (5.7). From this the following ratios are obtained (5.41) for the square law and (5.42) for the cube law. The maximum values of these ratios (Figure 5.5) for the square law and cube law case are 5.1×10^{-3} and 55.5×10^{-3}, respectively, justifying the approximation.

$$\frac{\sqrt{\langle U^2(t) \rangle}}{v_z(t)} = \frac{1}{(1 + k_2 v_0 t)} \left\{ \alpha + 6 k_2^2 \beta \left[(1 + k_2 v_0 t)^5 - 1 \right] \right\}^{1/2} \qquad (5.41)$$

$$\frac{\sqrt{\langle u^2(t) \rangle}}{v_z(t)} = \frac{1}{(1 + 2 k_3 v_0^2 t)} \left\{ \alpha + 21 k_3^2 v_0^2 \gamma \left[(1 + 2 k_3 v_0^2 t)^4 - 1 \right] \right\}^{1/2} \qquad (5.42)$$

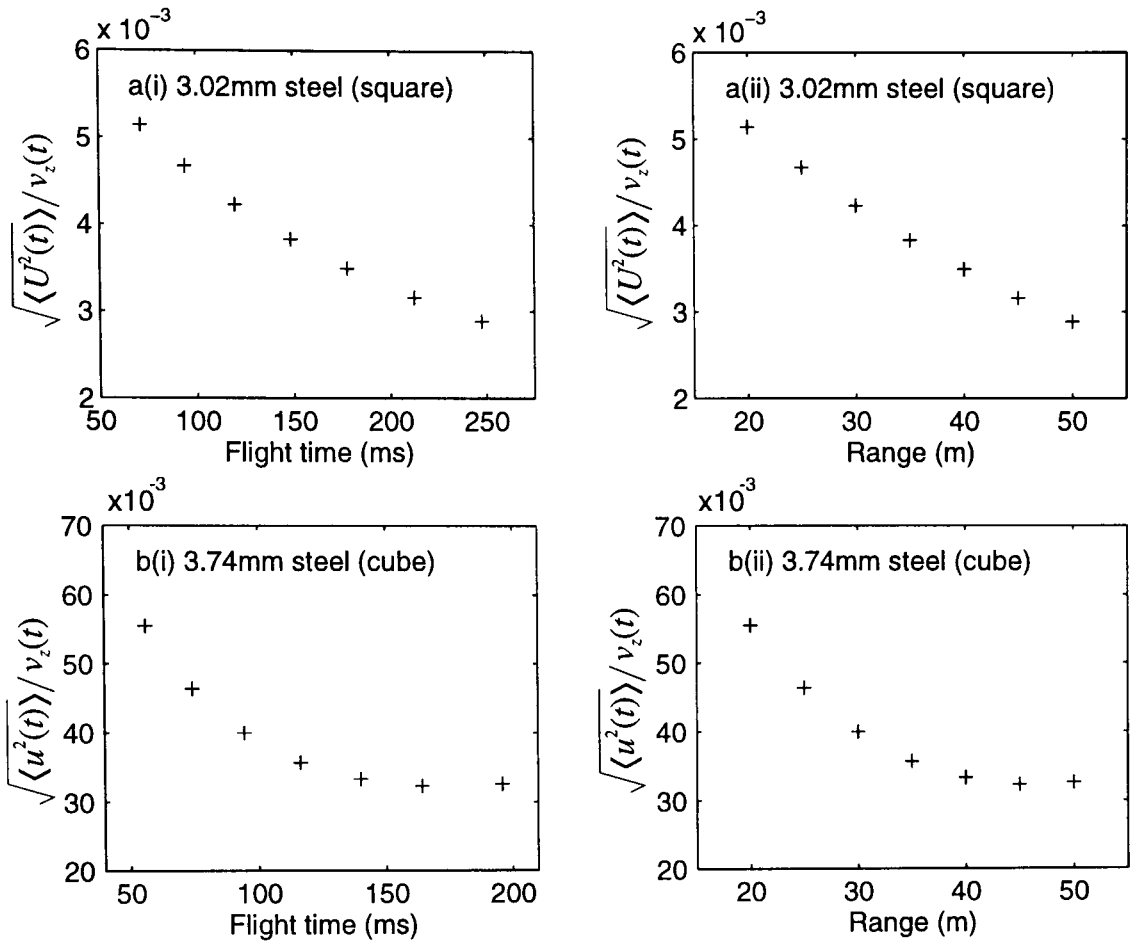

Figure 5.5 *The ratio of (a)* $\sqrt{\langle U^2(t)\rangle}$ *or (b)* $\sqrt{\langle u^2(t)\rangle}$ *to* v_z *as a function of (i) time and (ii) range for square law (28g load of #4 steel shot using 0.030" choke) and cube law (28g load of #1 steel shot using 0.020" choke) experimental data.*

The constants A and α in the theory are non-dimensional measures of the initial spread of the transverse velocity components. Reducing the bore diameter by tightening the choke should reduce this spread whilst increasing the spread of velocities in the z-direction. The types of pellets (28g load of #4 (3.02mm) steel shot) employed earlier for comparison with the square law theory were used to study the effect of choke (0.010" and 0.030" choke) on the fitted parameters. In fact, the choke was reduced in this test to 0.010" constriction. In Table 5.1, the values of the constants k_2, v_0, A, B, α, and β in the theory are given for two different chokes. The result of increasing the choke show that k_2 is, as expected, unaffected by choke since this constant is determined by the characteristics of a pellet (steel pellets, shape unaffected by choke) and the air density and is independent of the launch conditions. When the choke is tightened, the value v_0 increases while the transverse spread of velocities (determined by A) decreases. Tightening the choke also increases the spread of velocities in the z-direction (determined by α). This behaviour is confirmed by high speed photography of shot

clouds close to the muzzle [16]. The in-flight effects (determined by B and β) are also seen to increase as the choke is tightened. This may be due to the fact that the shot cloud is less diffuse for a greater fraction of the total measured flight-time, thereby increasing the interaction between pellets.

Constants	Choke constriction	
	0.010"	0.030"
k_2 (m^{-1})	0.0193	0.0193
v_0 (m/s)	330	339
A (dimensionless)	2.29×10^{-4}	0.87×10^{-4}
B (m^2)	0.045	0.054
α (dimensionless)	4.85×10^{-5}	5.69×10^{-5}
β (m^2)	3.44×10^{-6}	3.69×10^{-6}

Table 5.1 *Values of the constants in the square-law model, expressions (5.22) and (5.34), obtained by a least-squares fit to square law experimental data (28g load of #4 (3.02mm) steel shot) for two different chokes.*

The square and cube law expressions were also found to be appropriate for describing the shot cloud length and width for non-spherical pellets (e.g. lead) as long as the velocities lay within one or other of the velocity regimes. A larger deceleration constant, k_2 or k_3, was the result of an increase in pellet deformation caused by tightening the choke. In Figure 5.6 the averaged data points for the width and length of a shot cloud, generated from a 36g load of #BB lead shot (0.010" choke), with associated lead pellet velocities in the cube law regime are shown. Using the corresponding expression the theoretical curve again shows excellent qualitative agreement between experiment and theory.

The derived expressions for shot cloud length and width are comprised of two terms, the first term represents the launch effects and the second term describes the in-flight effects. By separating these two terms, their overall influence on a shot clouds development can be examined. From the curves it can be seen that the launch effects for

both the width and length have a dominating influence at the early stages of flight with the in-flight effect gradually increasing to become the major influence at large *t*. The point in time, or range, where the in-flight effects become greater than the launch effects has been observed to vary considerably between different loads of pellets obeying either a square or cube law of air resistance. However, in general the launch conditions have a greater prominence in the shot cloud width (Figure 5.6(a)) where they typically have the larger influence over the measurement range. This is confirmed in section 3.2.1 where the shot cloud width at 40 yards were seen to be influenced by the choke constriction. In the case of the shot cloud length (Figure 5.6(b)) the launch effects tend to level off over the measurement ranges, unlike the width where they increase with range, allowing the in-flight effects to have a more dominant role. This greater influence from the in-flight effects masks the launch effects thus explaining why in section 3.2.1 the choke seemed to have no consistent effect on the shot cloud length.

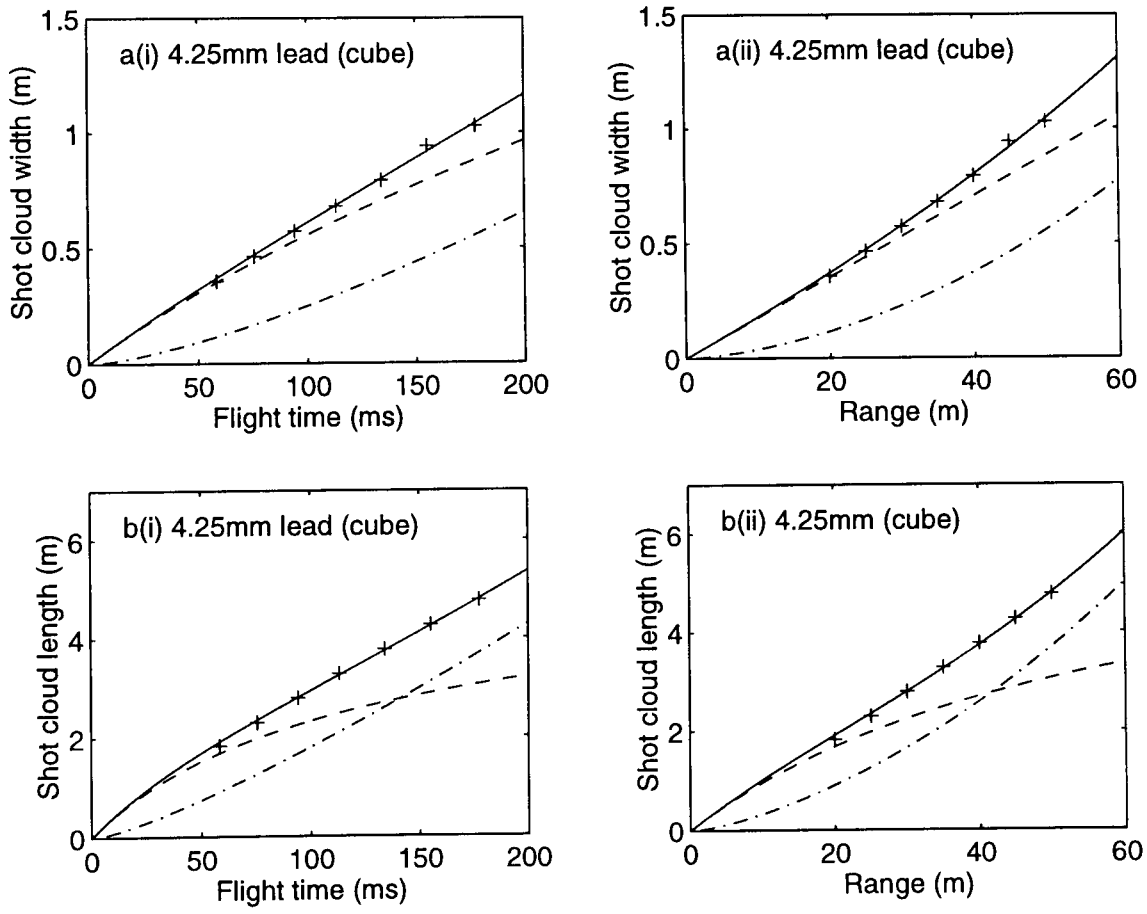

Figure 5.6 *The shot cloud (a) width and (b) length in metres for lead pellets obeying a cube-law of air resistance (36g load of #BB lead shot using 0.010" choke) as a function of (i) flight time and (ii) range. The crosses represent average data points and the theoretical curves (solid line) obtained by a least-squares fit of the corresponding random force model expressions are split into the launch (--) and in-flight (-.) effects.*

5.3 VELOCITY DEPENDENT RANDOM FORCE MODEL

5.3.1 Scaling to pellet velocity

In the previous section expressions were derived for the transverse and longitudinal spread of a shot cloud using a model based on a random force. The model was shown to give good qualitative agreement with the experimental data between 20-50m. However, from the initial assumption the random force term $F(t)$, which describe the irregularities affecting the motion of the pellets in flight, could have the same variance over the whole of the shot cloud flight time and would even have an influence on stationary pellets. It was therefore decided that this random nature was not the best assumption on physical grounds. Therefore to modify the model in section 5.2, the random force term $F(t)$ is scaled by the longitudinal velocity of the pellets, so that the equation of motion of a single sphere obeying a square-law of air resistance now becomes

$$\dot{\underline{v}} = k_2 v^2 \hat{\underline{v}} + \frac{\langle v_z \rangle}{v_0} \underline{F}(t) \quad . \tag{5.43}$$

Division by v_0 allows $\underline{F}(t)$, and hence D_x and D_z, to be dimensionally the same as it was in the velocity-independent model of the force. The scaling factor for the random force term has already been defined in (5.4), so taking the components of (5.43) and using the same arguments as in section 5.3 the x- and z-deceleration terms are found to be

$$\dot{v}_x = -k_2 v_x v_z + \frac{F_x(t)}{(1 + k_2 v_0 t)} \quad , \tag{5.44}$$

and

$$\dot{v}_z = -k_2 v_z^2 + \frac{F_z(t)}{(1 + k_2 v_0 t)} \quad . \tag{5.45}$$

Using the same procedure as in section 5.2.1, the first approximation, Equation (5.12) is substituted into (5.45) to give

$$\dot{U} = -\frac{2k_2 v_0}{(1+k_2 v_0 t)} U + \frac{F_z(t)}{(1+k_2 v_0 t)} \quad , \tag{5.46}$$

from which the deceleration of the transverse velocity components is obtained as

$$\dot{v}_z = -\frac{k_2 v_0}{(1+k_2 v_0 t)} v_x + \frac{F_x(t)}{(1+k_2 v_0 t)} \quad . \tag{5.47}$$

Similarly for pellets that are obeying a cube law of air resistance, the equations of motion are

$$\dot{u} = -\frac{3k_3 v_0^2}{(1+2k_3 v_0^2 t)} u + \frac{F_z(t)}{(1+2k_3 v_0^2 t)^{1/2}} \tag{5.48}$$

and

$$\dot{v}_x = -\frac{k_3 v_0^2}{(1+2k_3 v_0^2 t)} v_x + \frac{F_x(t)}{(1+2k_3 v_0^2 t)^{1/2}} \tag{5.49}$$

5.3.2 Lateral pellet distribution

An identical analytical process to that in section 5.2.2 is used to determine the width of a cloud of pellets, whereby the variance in the x-components of the pellets is calculated. For the square-law velocity dependence of the force due to air resistance, Equation (5.47) is integrated twice to obtain an expression for $x(t)$ in terms of $F_x(t)$. Using the integrating factor method, the first integral is

$$v_x(t) = \frac{v_{x0}}{(1+k_2 v_0 t)} + \frac{1}{(1+k_2 v_0 t)} \int_0^t F_x(t')dt' \quad . \tag{5.50}$$

The variation of the transverse displacements, given by (5.51), is obtained by taking the ensemble average over all the pellets after squaring (5.50). We find

$$\left\langle x^2(t)\right\rangle = \frac{\left\langle v_{x0}^2\right\rangle}{k_2^2 v_0^2}\left[\ln(1+k_2 v_0 t)\right]^2 + \int_0^t\int_0^t \frac{dt''d\tau''}{(1+k_2 v_0 t'')(1+k_2 v_0 \tau'')}\int_0^{t''}\int^{\tau''}\left\langle F_x(t')F_x(\tau')\right\rangle dt'd\tau' \ . \tag{5.51}$$

Using the same Markovian random process, Equation (5.21), to describe the random force it is shown in Appendix H.5 that the evaluation of (5.51) in closed form results in

$$W^2(t) = \frac{A}{k_2^2}\left[\ln(1+k_2 v_0 t)\right]^2 + \frac{27B}{2}\left[2k_2 v_0 t - 2\ln(1+k_2 v_0 t) - \left\{\ln(1+k_2 v_0 t)\right\}^2\right] \ , \tag{5.52}$$

where A and B are the same parameters as in (5.22). In the case of the cube-law velocity dependence of air resistance, integration of (5.49) gives

$$v_x(t) = \frac{v_{x0}}{(1+2k_3 v_0^2 t)^{1/2}} + \frac{1}{(1+2k_3 v_0^2 t)^{1/2}}\int_0^t F_x(t')dt' \tag{5.53}$$

and a further integration results in

$$x(t) = \frac{v_{x0}}{k_3 v_0^2}\left[(1+2k_3 v_0^2 t)^{1/2} - 1\right] + \int_0^t \frac{dt''}{(1+2k_3 v_0^2 t'')^{1/2}}\int_0^{t''} F_x(t')dt' \ . \tag{5.54}$$

The variance, by a similar argument to that used earlier, is given by

$$\left\langle x^2(t)\right\rangle = \frac{\left\langle v_{x0}^2\right\rangle}{k_3^2 v_0^4}\left[(1+2k_3 v_0^2 t)^{1/2} - 1\right]^2$$

$$+\int_0^t\int_0^t \frac{dt''d\tau''}{(1+2k_3 v_0^2 t'')^{1/2}(1+2k_3 v_0^2 \tau'')^{1/2}}\int_0^{t''}\int^{\tau''}\left\langle F_x(t')F_x(\tau')\right\rangle dt'd\tau' \ . \tag{5.55}$$

Again, a closed form expression is obtained when the correlation function (5.21) is inserted in to (5.55). In Appendix H.6 the evaluation of this equation is shown, which enables us to derive the shot cloud width with the same parameters A and C as (5.27):

$$W^2(t) = \frac{A}{k_3^2 v_0^2}\left[(1+2k_3 v_0^2 t)^{1/2} - 1\right]^2$$

$$+ 5C\left\{(1+2k_3 v_0^2 t)^2 - 6(1+2k_3 v_0^2 t) + 8(1+2k_3 v_0^2 t)^{1/2} - 3\right\} . \qquad (5.56)$$

5.3.3 Longitudinal pellet distribution

Using the equivalent method from section 5.2.3, the shot cloud length for the square-law velocity dependence of air resistance is found from the solution of (5.46) to be

$$U(t) = \frac{U_0}{(1+k_2 v_0 t)^2} + \frac{1}{(1+k_2 v_0 t)^2}\int_0^t (1+k_2 v_0 t')F_z(t')dt' \quad , \quad (5.57)$$

and hence from (5.12) the longitudinal velocity component is given by

$$v_z(t) = \frac{v_0}{(1+k_2 v_0 t)} + \frac{U_0}{(1+k_2 v_0 t)^2} + \frac{1}{(1+k_2 v_0 t)^2}\int_0^t (1+k_2 v_0 t')F_z(t')dt' . \quad (5.58)$$

The variance of the displacements, obtained as before by averaging over the pellets after integrating (5.58) and assuming $\langle U_0 \rangle$=0, gives

$$\left\langle z^2(t)\right\rangle = \frac{\left\langle U_0^2\right\rangle t^2}{(1+k_2 v_0 t)^2}$$

$$+\int_0^t\int_0^t \frac{dt''d\tau''}{(1+k_2 v_0 t'')^2(1+k_2 v_0 \tau'')^2}\int_0^{t''}\int_0^{\tau''}(1+k_2 v_0 t')(1+k_2 v_0 \tau')\left\langle F_z(t')F_z(\tau')\right\rangle dt'd\tau' .$$

(5.59)

Using the delta-function correlation, given by (5.33), it is possible once again to evaluate the variance in closed form and identify this with the square of the length of the shot cloud to obtain

$$L^2(t) = \frac{\alpha(k_2 v_0 t)^2}{k_2^2(1+k_2 v_0 t)^2} + 5\beta\left\{6(1+k_2 v_0 t)^{-1} - 2(1+k_2 v_0 t)^{-2} + 2(1+k_2 v_0 t) - 6\right\} \ , \tag{5.60}$$

where a and b are the same parameters as in (5.34). For the cube-law velocity dependence of air resistance, integration of (5.48) produces

$$u(t) = \frac{u_0}{(1+2k_3 v_0^2 t)^{3/2}} + \frac{1}{(1+2k_3 v_0^2 t)^{3/2}} \int_0^t (1+2k_3 v_0^2 t') F_z(t') dt' \ , \tag{5.61}$$

and using (5.15) an expression for the z-component of velocity is obtained:

$$v_z(t) = \frac{v_0}{(1+2k_3 v_0^2 t)^{1/2}} + \frac{u_0}{(1+2k_3 v_0^2 t)^{3/2}} + \frac{1}{(1+2k_3 v_0^2 t)^{3/2}} \int_0^t (1+2k_3 v_0^2 t') F_z(t') dt' \ . \tag{5.62}$$

The variance in the displacements in this case is found by the same procedure used previously where (5.62) is integrated twice and averaged over all the pellets to give

$$L^2(t) = \frac{\alpha}{k_3^2 v_0^2}\left[1 - \frac{1}{(1+2k_3 v_0^2 t)^{1/2}}\right]^2$$

$$+ \frac{14\gamma}{5}\left\{(1+2k_3 v_0^2 t)^2 + 24(1+2k_3 v_0^2 t)^{-1/2} - 10(1+2k_3 v_0^2 t)^{-1} - 15\right\} \ . \tag{5.63}$$

5.3.4 Appropriateness of model

In scaling the random force term $F(t)$ by the pellet longitudinal velocity v_z, alternative expressions were derived in section 5.3.2 and 5.3.3 for the shot cloud width and length appropriate to either a square or cube law of air resistance. When comparing these expressions to the same experimental data produced by the specially prepared loads of pellets described in section 5.2.4, there was no obvious visual difference between the fit obtained from the two types of random force models (section 5.2 and 5.3). The

assumption that the magnitudes of (5.46) and (5.48) are much smaller than $\langle v_z \rangle$ was also justified for the new model. When fitting the new model to the wrong experimental data the width was seen to be insensitive to the shot cloud width expression used and the lengths gave an unrealistic contraction in some cases once again. Therefore expressions (5.52), (5.60), (5.56) and (5.63) show the same excellent qualitative agreement between theory and the appropriate experimental data as the model described in section 5.2.4. However, statistically the new model with the scaled random force was found to give a slightly lower value of d_n, thus producing a better fit to the experimental data. This is shown in Table 5.2 where the normalized deviations d_n of the two models for the same experimental data are given.

Expression	Normalized deviation (d_n) to appropriate experimental data	
	Shot cloud width	Shot cloud length
Square law expressions (section 5.2)	0.0087 (5.22)	6.9×10^{-5} (5.34)
Square law expressions (section 5.3)	0.0060 (5.52)	1.63×10^{-5} (5.60)
Cube law expressions (section 5.2)	0.0037 (5.27)	1.34×10^{-4} (5.39)
Cube law expressions (section 5.3)	0.0020 (5.56)	1.02×10^{-4} (5.63)

Table 5.2 *The normalized deviations d_n associated for the two different models with the corresponding expression (given in brackets) to the appropriate experimental data.*

The nature of the shot cloud width and length generated by both the cube law and square law expressions derived in section 5.2 behaves as $t^{3/2}$ for large time t, where the in-flight effects are the dominant factor. This generates a point of inflection in the development of the shot cloud length when the in-flight effects become greater than the launch effects. In Figures 5.7 and 5.8, the predicted nature of the shot cloud widths and lengths from the two types of random force models are shown for large flight times (t) when fitted to the appropriate experimental data. The nature of the shot cloud width and

length predicted by the random force model described in section 5.2 may appear to be unrealistic. This may be due to modelling the random force as independent of the velocity. For this reason, the expressions in this section were derived from the alternative model with a random force being scaled by the longitudinal velocity. From these expressions (Figure 5.7 and 5.8) the square law and cube law expressions behave as $t^{1/2}$ and t, respectively, with large time t and do not cause a point of inflection. This seemed to show a more sensible development of the shot cloud and is proved to be a more appropriate model by the lower normalized deviation, d_n. However, over the measurement ranges (20-50m) there is negligible difference between the accuracy of the two models to the appropriate experimental data. The natures of these expressions for large t are not relevant to a shot cloud as it will either have reverted to square law behaviour or stationary. Therefore the expressions for a cube law or square law have a limited time period which means that both random force models are equally appropriate over the measurement range.

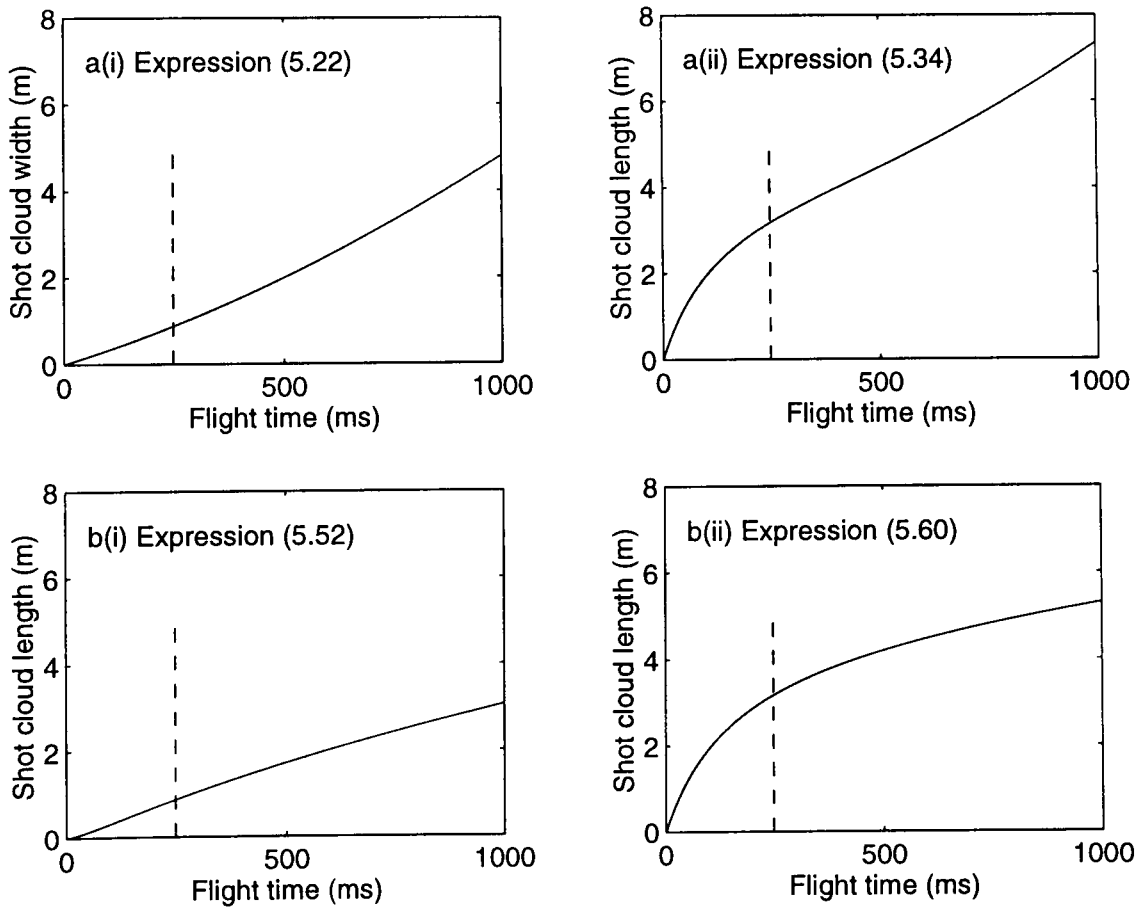

Figure 5.7 *The (a) random force model and (b) velocity dependent random force model corresponding square law prediction of the shot cloud (i) width and (ii) length for large time when using the appropriate experimental data (28g load of #4 (3.02mm) steel shot using 0.030" choke). The dotted line represents the flight time at 50m.*

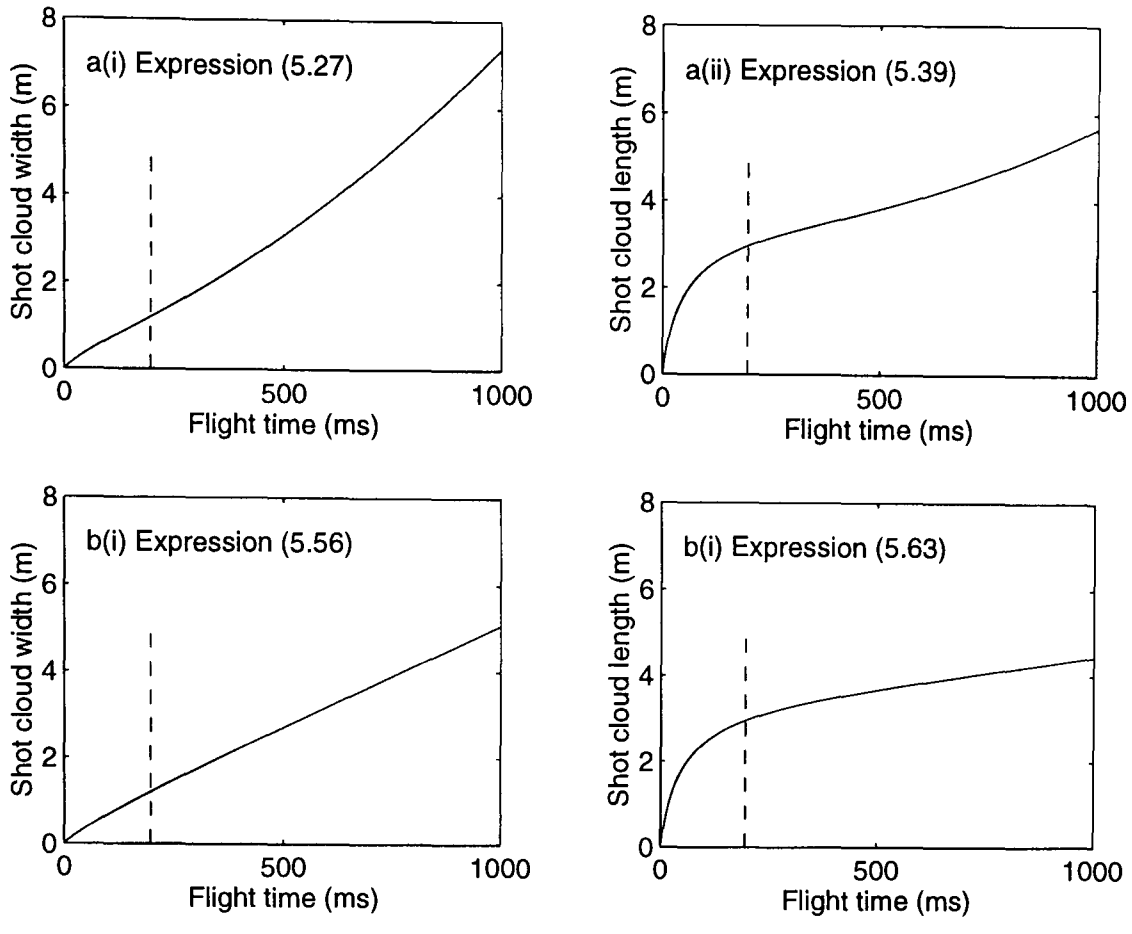

Figure 5.8 *The (a) random force model and (b) velocity dependent random force model corresponding cube law prediction of the shot cloud (i) width and (ii) length for large time when using the appropriate experimental data (28g load #1 (3.74mm) steel shot using 0.020" choke). The dotted line represents the flight time at 50m.*

5.4 SUMMARY

In this Chapter 2 methods are presented for modelling the dispersion of pellets within a shot cloud as it develops in flight. These models are based on the motion of a single sphere, and on the idea of a random force as used in diffusion theory. In the first model a random force was simply added to the equation of motion of a single sphere, whereas the second model weighted the random force by the average longitudinal velocity of the pellets. Statistical averages over all the pellets were then taken to obtain expressions for the width and length of the shot cloud. The theory has been applied to two specific velocity regimes of practical interest: the square-law and cube-law of air resistance. Analytical results were derived and a two parameter fit of the models was carried out using experimental data. The measurement system for the external ballistics of shotguns, as describe in Chapter 2, was used to measure their overall length and width as a function of flight time and range. Experiments were carried out using specially loaded ammunition operating in each of the two velocity regimes mentioned above.

From the expressions it was possible to separate the launch and in-flight effects. It was shown that the launchs effects were the major influence on the shot cloud width and the in-flight effects were more dominant in the shot cloud length masking the possible launch effects over the measurement ranges.

For both models excellent qualitative agreement between theory and experiment, over the measurement range, was obtained for both square-law and cube-law tests. However, the velocity dependent random force model produced a slightly improved fit with a more realistic development of the shot cloud for larger values of time *t*. This model also scaled the magnitude of the random force with velocity so that the pellets would not experience any random forces if they were stationary. This good agreement between theory and experimental data supports the appropriateness of the random force model approach to shot cloud ballistics. It must be noted that cube law pellets will have to pass through the square law regime before they terminate so the corresponding models has a limited time period.

Chapter 6

Conclusions and suggestion for further work

6.1 DISCUSSION OF RESULTS

The main objectives of this investigation were to establish a better understanding of the behaviour of shot clouds as they evolve in time and space, and to develop the limited work on ensembles of spheres travelling at velocities in the vicinity of Mach 1. It has emerged clearly from this work that no satisfactory theory exists at present which can predict the downrange behaviour of shot clouds in sufficient detail as to render measurements superfluous. In this investigation, a unique external shotgun ballistics measurement facility was designed and implemented to obtain experimental data on the distribution of pellets within a shot cloud. Theoretical models were also derived to describe the behaviour of shot clouds and then compared to experimental data to assess their validity. The principal achievements, limitations and results of this investigation will now be summarised and discussed.

Following a general introduction to shooting terms and sphere aerodynamics in Chapter 1, Chapter 2 describes the external shotgun ballistics measurement facility. A proof barrel with exchangeable choke and chamber tubes was used to launch the pellets as a shot cloud. The choke and chamber tube profiles were standardized to limit the number of variables in the launch conditions. With standardized launch conditions, any variations in the experimented data could be associated to the atmospheric condition or the ammunition. In adapting the barrel to take different cartridge lengths pressure readings were then not possible, thus preventing internal ballistic measurements. However, this was acceptable as the primary interest of the investigation was in the dynamics of shot clouds.

A muzzle probe was attached to the barrel. This probe registers the shot column exiting the muzzle, by breaking a wire, to within ±25μs. This uncertainty was determined to have negligible influence on the remaining timing measurements. The simplicity of the broken wire probe illustrated that high technology design is not always the best option for achieving reliable results. This concept was continued throughout the measurement facility wherever possible to avoid complex electronics experiencing the unstable ballistic environment.

The shot cloud was detected at ranges close to the muzzle by skyscreens. A string of screens out to 8m registered shot clouds as they travelled downrange. From the corresponding flight times-range data, near-muzzle velocity information was obtained on shot clouds. The near-muzzle performance of the shot cloud was not originally envisaged as part of the investigation, but the introduction of the skyscreens enhanced the measurement facility and produced additional information on the development of shot clouds. The skyscreens were designed for single rifle rounds (typically 5.56mm) travelling around Mach 2-3. Because of this they could not resolve the smaller, lower velocity pellets associated with shotgun ammunition. However, the leading edge of the shot column could be detected reliably out to 8m because of the compact mass of shot clouds. Results using this larger and slower projectile, compared to the 5.56mm bullet, meant that the RC circuits of the skyscreens produced a poor transient response. Therefore trailing edge flight time information could not be reliably extracted from the skyscreens.

The ballistics target was designed to meet contractual and research requirements. Its simplicity and robustness created a reliable measurement system which withstood the rigorous outdoor weather usage and the destructive nature of the shotgun. The 3.6m square target intercepted every pellet used over the measurement range for the ammunition and gun combination used during this investigation. The pellet impacts generated voltage impulses which when combined produced the shot cloud profile, a unique feature of this measurement facility. This simple display enabled the identification of stray pellets and gave much useful quality information on the consistency of the ammunition being tested. From the shot cloud profile, timing information was routinely obtained on the leading and trailing edges of the shot cloud. However, timing information for every pellet was not always possible due to the maximum rate of arrival of pellets being too high for the single-impulse response of the detector array, especially at close ranges. The leading edge data, dominated by the propagation delay through the polycarbonate, was the most accurate flight time measurement with a maximum uncertainty of $\pm 0.1\%$. A greater uncertainty of $\pm 0.75\%$ was observed in the trailing edge flight time data and was controlled by the ringing time of the detection panels. These uncertainties were satisfactory since the variation,

generated by the ammunition, in the corresponding flight times was several times larger at 1-3%. The only disadvantage of the ballistics target was that it intercepted the shot cloud and prevented continuous measurements on the same shot cloud downrange. With the variations in ballistic performance observed between shotgun ammunition from the same batch, an average was required to obtain representative results, thus reducing the significance of this limitation.

The ballistics target was unable to generate lateral position information to the desired accuracy requirements. Therefore an alternative system was established based on the traditional pattern testing method to obtain the lateral pellet distribution. By firing at a sheet of paper which was then back lit, the pattern images were scanned into a computer using a CCD camera. From the image, the co-ordinates of every pellet intercepted by the paper could be determined to within 2mm. This process increased the accuracy of the traditional measurement and also automated the once time consuming task.

In theory, the pattern paper, and therefore the light box, could be made to any size so as to encompass the whole lateral spread of the shot cloud. However, for the contract it was required to capture all the pellets from realistic choke, ammunition and range combinations. A 1.5m square pattern sheet was found, and used, to meet these contractual requirements whilst being a manageable size to handle. Unfortunately a consequence of this limited paper size was that when extreme choke and range combinations were used for research purposes, the lateral spread occasionally became larger than the pattern paper. In not retrieving all the pellets, errors in the calculated pattern centre and the radial standard deviation of the pellet co-ordinates occurred. Therefore the standard deviation was found by alternative methods, such as fitting the pellet distribution to a Gaussian, or taking the pellet count in a 30" circle, and the pellet centre was thought to be unaffected by the missing few percent of pellets.

The individual monitoring of small individual impact areas within the target array illustrated the capability of the ballistics measurement system to reproduce 3-dimensional outlines of shot clouds. From the outlines it was discovered that there was no constant shape to shot clouds produced by cartridges from the same batch. With the

inconsistency in the shape no additional information could be determined on the development of shot clouds. However, combining the information from the fired pellet shape and the general 3D shot cloud shapes, it is concluded that the most spherical pellets travel in the leading edge of the shot cloud and are found in the pattern centre, unlike the deformed outer region pellets in the pattern being associated with the trailing edge. The main achievements of the reconstruction of a shot cloud was the ability to design such a system and the general observed shapes of the shot cloud.

Chapter 3 addressed the issue of the shot cloud phenomena and showed that from a batch of cartridges a variation in the shot clouds ballistic performance is expected. The leading edge flight times of the shot cloud, ignoring stray pellets, were found to be the most consistent and easily identifiable measurement from the system, whereas the trailing edge had a greater variability and uncertainty in identification. The lateral distribution of pellets was determined to have the greatest variation in the shot cloud and the combination of these factors caused the inconsistency in the shot cloud shapes seen in the 3-dimensional reconstruction. With the variation in ballistics between cartridges from the same batches a sufficient number was necessary to be tested to obtain a reliable average result. A compromise of 10 cartridges per ranges was used as a practical optimum between a reliable average and an excessive acquisition time. Therefore the ballistics of one shot cloud cannot give a true reflection of the general characteristics of the load, especially lateral pellet distribution.

The effect of choke on the longitudinal and lateral distribution of pellets in a shot cloud was examined. It was found that the launch condition had no constant affect on the shot cloud lengths. This is thought, and shown in Chapter 5, to be caused by the in-flight effects having similar magnitude to the launch effects, thus masking the effects of choke at the measurement ranges. In the case of the lateral distribution the pellet dispersion decreased with an increase in choke constriction until 0.030" where the distribution was seen to level off irrespective of pellet material. With the limited choke profiles available to the investigation, this characteristic requires confirmation for other choke profiles. For the lateral distribution, the launch effects are shown in Chapter 5 to be

more dominant than the in-flight effects, and therefore still influence the dispersion over the measurement range.

Over this investigation an attempt was made to summarize the shot cloud phenomenon, such as effects of pellet diameter, loads, and internal gun ballistics on the downrange performance of shot clouds. This was not possible, as to produce reliable comparative ballistics for the contract, a standard proof barrel was used with certain choke constriction and profiles for particular pellet material and thus constrained the possible variation in launch condition. Further, variation in pellet diameters and load weights were reliant on the ammunition sent for testing and the limited supply of specially loaded cartridges for research. Therefore experiments were planned around the contract constraints and the limited supplies of ammunition. This made it difficult to do long runs of choke tests at different ranges. However, from the observed choke effects and ammunition variation on the distribution of pellets in a shot cloud it is concluded that it is not possible to summarize the shot cloud phenomena and make ballistics measurement redundant.

The intuitive conclusion from the observation of the shot cloud profiles, and confirmed by the calculation of the shot cloud length, is that the longitudinal spread of pellets is more compact for steel loads than for lead. This is thought to occur because the minor deformation seen in steel pellets after firing generates a smaller variation in drag on the pellets. The greater variation in deformation and therefore associated drag on the other pellet materials means that the pellets string out due to their different aerodynamic performances (in-flight effects). As steel pellets were found to be fairly spherical after firing, their experimental results were used to assess the validity of theoretical models based on the motion of a single sphere.

The conclusions drawn from the analysis of the pellet distribution within a shot cloud, irrespective of pellet material, choke and range, were that the lateral distribution of pellets in the x- and y-axis are symmetrical with a Gaussian nature. The combination of these two distributions was then proved to produce a Gaussian radial pellet density distribution which varies linearly with flight time over the measurement range. These

findings on the lateral distribution have been assumed in the shooting community from observation, but in this investigation they have been established statistically. Additionally, it was found that a Rayleigh distribution best described the longitudinal spread of pellets and that a Poisson process is appropriate in assessing the hit probability for all pattern data obtained during this investigation. The issue of pattern quality can be addressed by the variability in pellet distribution between alike cartridges and their hit probability distribution. All of the findings in this investigation have been produced by averaging over at least 10 cartridges, thus giving a large number of samples (1000-5000 pellets). However, the individual distribution from single cartridges may not resemble these due to the relatively lower number of samples (100-500 pellets).

In Chapter 4, the raw time-range data was condensed and summarised to obtain the ballistic characteristics of shot clouds. Two expressions were derived using the assumption that the pellets travel independently between 20-50m and at velocities below $0.5M$ (square law) or between $0.5M$ to $1.4M$ (cube law). From the nature of the shot cloud deceleration characteristics, determined from the experimental data, this suggested the pellets behave like individual spheres over the measurement ranges. A simplistic model for the drag coefficient was employed, where C_D was assumed to be proportional to velocity between Mach 0.5 and 1.4. However, to derive an accurate expression for the drag coefficient behaviour would involve a more complex function to describe the air resistance on a pellet, thus removing the simplicity of the assumed cube law model. For validating any theory, ammunition was selected so that the pellet velocities over the measurement range lay within either of the two velocity regimes.

From the experimental data generated by the ballistics target and the skyscreens it was shown not to be good practice to extrapolate from the muzzle to the measurement ranges or vice versa. This is because the strong interaction between pellets at the muzzle and the relative individuality of each pellet at ranges greater than 20m cannot be realistically represented by the same model. Therefore the expressions derived from the equation of motion of a single sphere are only appropriate for ranges where the pellets are independent.

The corresponding time-range expression for the square law and cube law of air resistance both produce their own deceleration constant. Using the wide range of experimental data on different pellet diameters and materials, a relationship between the deceleration constant and the combination of pellet properties and atmospheric conditions was obtained for both laws of air resistance. From these two relationships an approximation to the drag coefficient (C_D) was calculated for the leading edge pellets in a shot cloud, irrespective of size or material, thus updating the assumed drag coefficient model. With the different trailing edge pellet deformation associated with each material, it was not possible to obtain a general relationship for their deceleration characteristics. The trailing edge data was therefore separated into the different materials and a relationship between their pellet diameter and deceleration constant was obtained. This approach of calculating the deceleration constant of pellets in a shot cloud is valid only when associating the results with the square or cube law models. However, it does not give any additional information about the true shape of the drag coefficient other than an approximation within the velocity limits of each regime.

A synthesis model was derived from the equation of motion of a single sphere and, together with the updated drag coefficient, characteristics of the downrange ballistics of a shot cloud were predicted. The synthesis model was not limited to any velocity regimes due to a built-in model of the drag coefficient characteristics which adjusted the drag force acting on a pellet according to its velocity. Additionally, the model is not dependent on an assumed law of air resistance and can be adapted to any relationship between the drag coefficient and velocity. This model showed good qualitative agreement with experimental data when initiated after the equivalent time when the pellets became independent. The poor agreement found between the experimental data and theory when the model was started at t_0 reinforces the inappropriateness of extrapolating data from the muzzle to measurement ranges or vice-versa. A consequence of the large variation in trailing edge pellet performance meant that this model could not accurately predict the longitudinal distribution of pellets in the shot cloud for pellet materials other than steel. It was also difficult to input accurate leading and, especially, trailing edge flight times and velocities without making actual measurements.

Chapter 5 presented two stochastic models which were developed for describing the ballistic behaviour of a shot cloud as it develops over time. The equation of motion of a single sphere was perturbed by the addition of a random force term, and the width and length of the cloud were determined by performing ensemble averages. This theory was applied to both square-law and cube-laws of air resistance and both models were found to give excellent qualitative agreement to the appropriate experimental data taken over the measurement range. Statistically the model which scaled the random force by the average longitudinal velocity produced a slightly better fit and a more realistic shape to the shot cloud length and width for large t. However, extending both the cube law and square law too far beyond the experimental data becomes inappropriate as the shot cloud behaviour changes. For example, a cube law pellet becomes a square law pellet. Therefore, due to their small statistical difference in fits, both models are appropriate for describing the dispersion of pellets within a shot cloud for pellets remaining in one or other velocity regime.

The structure of the derived expressions was beneficial in observing the launch and in-flight effects on the shot cloud. From separating these two terms from the overall longitudinal and lateral spread it could be seen that the launch effects are initially greater in magnitude than those which develop in flight. The most dominant effect depended on the development of the in-flight effects. For example, the launch effects were seen to be generally larger in magnitude than the in-flight effects for the lateral spread over the measurement ranges, whereas the in-flight effects are predominate for the longitudinal dispersion. This was confirmed by experimental data where the choke (launch effects) was seen to effect the shot cloud width at 40 yards, but have no consistent effect on the length.

The good agreement between theory and experiment shown in Chapter 5 supports the appropriateness of a random force approach to shot cloud ballistics. However, the models are simple and do not include fundamental information on pellet deformation, the nature of the initial distributions (other than its σ), or the nature of the random forces and the pellet collisions on the dispersion of pellet without further assumptions or more data on these properties.

6.2 CONCLUSIONS

A fundamentally new external ballistics measurement facility for shotgun ammunition was designed and implemented to measure the downrange ballistic performance of shot clouds. From the experimental data it was determined statistically that the lateral distribution of pellet, effected by altering the internal ballistics of a gun, obeys a radial Gaussian density distribution and the longitudinal distribution, dominated by the in-flight effects of the pellets, is best described as a Rayleigh distribution. The combination of theory on a single sphere and experimental data has produced additional data on the deceleration characteristics of the pellets. This data was then used to predict the downrange ballistics of the shot cloud over ranges where the pellets are independent of one another. Finally, a stochastic model was developed for describing the behaviour of a shot cloud of spherical projectiles. Over this investigation good agreement has been achieved between experiment and theory to advance the science of shot cloud ballistics.

6.3 POSSIBLE FUTURE WORK

The measurement facility described in Chapter 2 is adequate for determining the average ballistic performance of shot clouds as they develop in space and time. To increase the understanding of the shot clouds development it is desired to track an individual shot cloud over the measurement range whilst generating data on the lateral and longitudinal pellet distribution. An alternative measurement system would be required which did not stop the pellets whilst producing timing and lateral positional information on all the pellets. Therefore the system would have to be able to resolve individual pellets travelling in the vicinity of the speed of sound. It is thought with the ever increasing refinements to radar a suitable system might be developed to meet these specifications. For example, the combination of longitudinal and transverse radars to get the distribution of pellets in each direction.

When this investigation started, the main requirement was to obtain ballistic data on shot clouds at realistic shooting ranges, say, 20-50m. The skyscreens were later added to the facility, but only gave limited data on the initial development of the shot clouds.

Since the initial spread of pellets has an effect on the downrange ballistics, it would be desirable to obtained greater information on this early stage of the development of the shot cloud. It has been shown in the past that high speed photography can achieve this information, but little research was carried out. Therefore it is suggested that high speed photography should be used to investigate the effects of choke on the initial spread of pellets. From these results it would possible to determine if the limiting factors on the pellet distributions over the measurement ranges are caused by the choke or the in-flight effects.

There are many variables which effect the ballistics of shot clouds, such as the launch condition (internal ballistics of the gun), cartridge and pellet properties and the interactive and individual performances of the pellets. During this investigation it has only been possible to examine the effects of a few of these properties due to the limited selection of pellet diameters, load weights, choke constriction and profiles. To fully understand the behaviour of shot clouds, all combinations of these effects need to be examined, especially detailed inspection near the muzzle.

The nature of the lateral and longitudinal distribution have been established from experimental data, but not from more basic theory. It would complete the analysis of the pellet distribution within a shot cloud if the lateral Gaussian distribution and the longitudinal Rayleigh distributions can be derived from first principles. Finally, the area of clumping, or holes in the lateral pellet distribution, needs to be investigated as there is no complete mathematical explanation for this phenomenon.

REFERENCES

1 Journeé Le Général, "Tir des Fusils de Chasse", (ed. Gauthier-Villars et Cie.) Paris, 3rd edition.

2 Lowry E.D., "Aerodynamic Performance of Lead and Iron Shotshell Loads", Olin Corporation, Winchester Division, Feb. 1970.

3 Burrard G., "The Modern Shotgun", Southampton Ashford Publishing 1985.

4 Charters A.C. and Thomas R.N., "The Aerodynamic Performance of Small Spheres from Subsonic to Supersonic Velocities", *Journal of Aeronautical Sciences*, pp. 469-476, Oct. 1945.

5 Bailey A.B. and Hiatt J., "Sphere Drag Coefficients for a Broad Range of Mach and Reynolds Numbers", *AIAA Journal*, Vol. 10, PP. 136-140, Nov. 1972.

6 Bailey A.B. and Starr R.F., "Sphere drag at Transonic Speeds and High Reynolds numbers", *AIAA Journal*, pp. 1631, Nov. 1976.

7 Lunnon R.G., "Fluid Resistance to Moving Spheres", *Proceedings of the Royal Society A*, No. 118, pp. 681-695, 1928.

8 Bacon D.L. and Reid E.L., "Experiments on Spheres in Wind Tunnels and in Air", *N.A.C.A Report*. No. 185.

9 Lam S.S.W. and Pollock N., "An Experimental Study of Transonic Flow Past a Sphere", *Tenth Australasian Fluid Mechanics Conference*, University of Melbourne, pp. 11.13-11.16, Dec. 1989.

10 Donovan W.F., "Retardation and Condition of Shot Pellets in Free Flight", *Ballistics Research Laboratories Technical Note* BRL TN 1653, Aberdeen Proving Ground, Maryland, USA. Apr. 1967.

11 Lee K.C., "Aerodynamic Interaction Between Two Spheres of Reynolds Numbers around 10^4", *Aeronautical Quarterly*, pp. 371-385. Nov. 1978.

12 "Lead Poisoning in Waterfowl: Internal Update Report", *JNCC* report, No. 252, 1995.

13 Giblin R.A. and Compton D.J., "A Ballistics Measurement System to Assist the Development and Evaluation of Non-Toxic Shot", *U.K. Department of the Environment Report*, March 1996.

14 Brindle J., "Shotgun Shooting: Techniques and Technology", Learnex (Publishers) Ltd, 1995.

15 "Oxford English Dictionary", Oxford University Press, 1980.

16 Lowry E.D., "A Waterfowl Lethality Model", Western Washington University, M.Sc Thesis, 1981.

17 "Eley Shooter's Diary ", Eley Hawk Ltd. 88th Edition.

18 Lowry E.D., "The Effect of a Shot String?", *American Rifleman*, pp. 36-39, Nov. 1979.

19 Goldstein S., "Modern Developments on Fluid Dynamics", Chapter 1, Oxford University Press, 1938.

20 Houghton E.L. and Carpenter P.W., "Aerodynamics for Engineering Students" Chapter 6 in *Viscous Flow and Boundary Layers*, Edward Arnold, 1993.

21 de Mestre N., "The Mathematics of Projectiles in Sport", Cambridge University Press, 1990.

22 Schlichting H., "Boundary-Layer Theory", Chapter 1, McGraw-Hill, 1960.

23 Rosenhead L., "Laminar Boundary Layers", Chapter 1, Oxford University Press, 1963.

24 Braun W.F., "Aerodynamics Data for Small Arms Projectiles", *Ballistics Research Laboratories Technical Note* No. 1630, Aberdeen Proving Ground, Maryland, USA. Apr. 1973.

25 Ross F.W. and Willmarth W.W., "Some Experimental Results on Sphere and Disk Drag", *AIAA Journal*, Vol. 9, pp. 285-291, Feb. 1971.

26 Fage A., "Experiments on a Sphere at Critical Reynolds Number", *A.R.C. Reports and Memoranda*, No. 1766, Sept. 1936.

27 Achenbach E., "The Effect of Surface Roughness and Tunnel Blockage on the Flow Past Spheres", *Journal of Fluid Mechanics*, Vol. 65, pp. 113-125, 1974.

28 Achenbach E., "Experiments on the Flow Past Spheres at Very High Reynolds Numbers", *Journal of Fluid Mechanics*, Vol. 54, pp. 565-575, 1972.

29 Sherman F.S., "A Survey of Experimental Results and Methods for the Transition Regime of Rarefied Gas Dynamics", *Proceedings of the Third International Symposium on Rarefied gas Dynamics*, Vol. II, Academic Press, New York, pp. 228, 1963.

30 Jaikrishnan K.R., Szeri A.Z. and Rohrer W.M., "A Study of transonic Flow around Spheres", *Journal of Fluid Mechanics*, Vol. 80, pp. 17-31, 1977.

31 Suryanarayana G.K., Pauer H. and Meier G.E.A., "Bluff-Body Drag Reduction by Passive Ventilation", *Experiments in Fluids*, pp. 73-81, 1993.

32 Jayaweera K.O.L.F. and Mason B.J., "The Behaviour of Clusters of Spheres Falling in a Viscous Fluid: Part I Experiments", *Journal of Fluid Mechanics*, Vol. 20, pp. 121-128, 1964.

33 Hocking L.M., "The Behaviour of Clusters of Spheres Falling in a Viscous Fluid: Part II Slow Motion Theory", *Journal of Fluid Mechanics*, Vol. 20, pp. 129-139, 1964.

34 Bretherton F.P., "Inertial Effects on Clusters of Spheres Falling in a Viscous Fluid", *Fluid Journal of Fluid Mechanics*, Vol. 20, pp. 401-410, 1964.

35 Hamielec A.E., Hoffman T.W. and Ross L.L, "Numerical Solution of the Navier-Stokes Equation for Flow Past Spheres: Part I Viscous flow around Spheres with and without Radial Mass Efflux", *A.I.Ch.E. Journal*, pp. 212-219, Mar. 1967.

36 Lowry E.D., Presentation at the *sport writers conference*, East Alton, Illinois, USA, 1962.

37 Thomas G., "Shotguns and Cartridges for Game and Clays", A&C Black London, 1987.

38 Oberfell G. and Thompson C., "The Mysteries of Shotgun Patterns", Oklahoma State University Press, Stillwater, 1960.

39 Roach S.A., "The Theory of Random Clumping", Mathuen and Co. Ltd., 1968.

40 Compton D.J. and Giblin R.A., "A Measurement System for the External Ballistics and Pattern Analysis of Shot clouds", *Proceedings of the 1st Conference on Non-Toxic Shot*, Royal Military College of Science, ISBN: 0 86038 022 X, pp. 33-55, May 1996.

41 Qualye P.P., "The truth about shot string", *American Rifleman*, Oct. 1925.

42 Lu S.-T., Chou C. and Lee M.-T., "Electro-Optical Target System for Position and Speed Measurement", *IEE Proceedings-A*, Vol. 140, pp. 252-256, Jul., 1993.

43 Terma Electronik AS (Denmark), Report on tests carried out in collaboration with University College London at the Royal Military College of Science (Shrivenham), Sept. 1992.

44 Fuller P., Formerly of DRA Fort Halstead, Private Communication.

45 Barlow R.J., "Statistics", John Wiley & Sons, 1989.

46 Bevington P.R., "Data Reduction and Error Analysis for the Physical Sciences", McGraw-Hill, 1992.

47 Farrar C.L. and Leeming D.W., "Military Ballistics-A Basic Manual", Chapter 3 in *Intermediate ballistics*, Brassey's Publishers Ltd., 1982.

48 Lowry, E.D., Private Communication.

49 Bearman P., Head of the Department of Aeronautics at Imperial College London, Private Communication.

50 "CRC Handbook of Chemistry and Physics", CRC Press, Inc. Boca Raton, pp. 55-20.

51 Haken H., "Synergetics", Chapter 6, Berlin: Springer-Verlag, 1983.

52 MacDonald D.K.C., "Noise and Fluctuations: an Introduction", New York and London: John Wiley and Sons. pp. 31-32, 1962.

Appendices

A. SHOT SIZE EQUIVALENTS

The pellets in a cartridge are conventionally given a nominal shot size to indicate their diameter. However, the metric pellet diameter equivalence of these nominal shot sizes vary for different countries. In Table A.1 the shot size equivalents are given between metric and the normal sizes for a selection of countries.

Metric (mm)	Shot size Equivalents (nominal)		
	English	American	Italian
4.1	BB	Air rifle	00
3.6	1	2	1 or 2
3.3	3	4	3
3.1	4	5	4
2.8	5	6	5
2.6	6	-	6
2.4	7	$7^1/_2$	$7^1/_2$
2.3	$7^1/_2$	8	8
2.2	8	-	-
2.0	9	9	$9^1/_2$

Table A.1 *The metric equivalents for the nominal shots sizes from a selection of countries.*

Note the average measure metric pellet diameter is used for any calculation used during this investigation.

B. LATERAL DISTRIBUTION : *X*- AND *Y*- AXIS

To examine the nature of the lateral pellet density distribution on the horizontal (x-axis) and vertical (y-axis) direction, consecutive horizontal and vertical 75mm strips about the centre of 10 patterns were taken. In Figure 3.2.3 it was seen that the distribution had the characteristics of Gaussian and described by (3.6). This same relationship is seen in Figure B.1-B.10 for a range of pellet diameters, materials, chokes and ranges. A least squares fit of (3.6) was also performed and overlaid on the plots.

$$\rho(r) = \frac{1}{\sigma\sqrt{2\pi}} \exp^{-r^2/2\sigma^2} \tag{3.6}$$

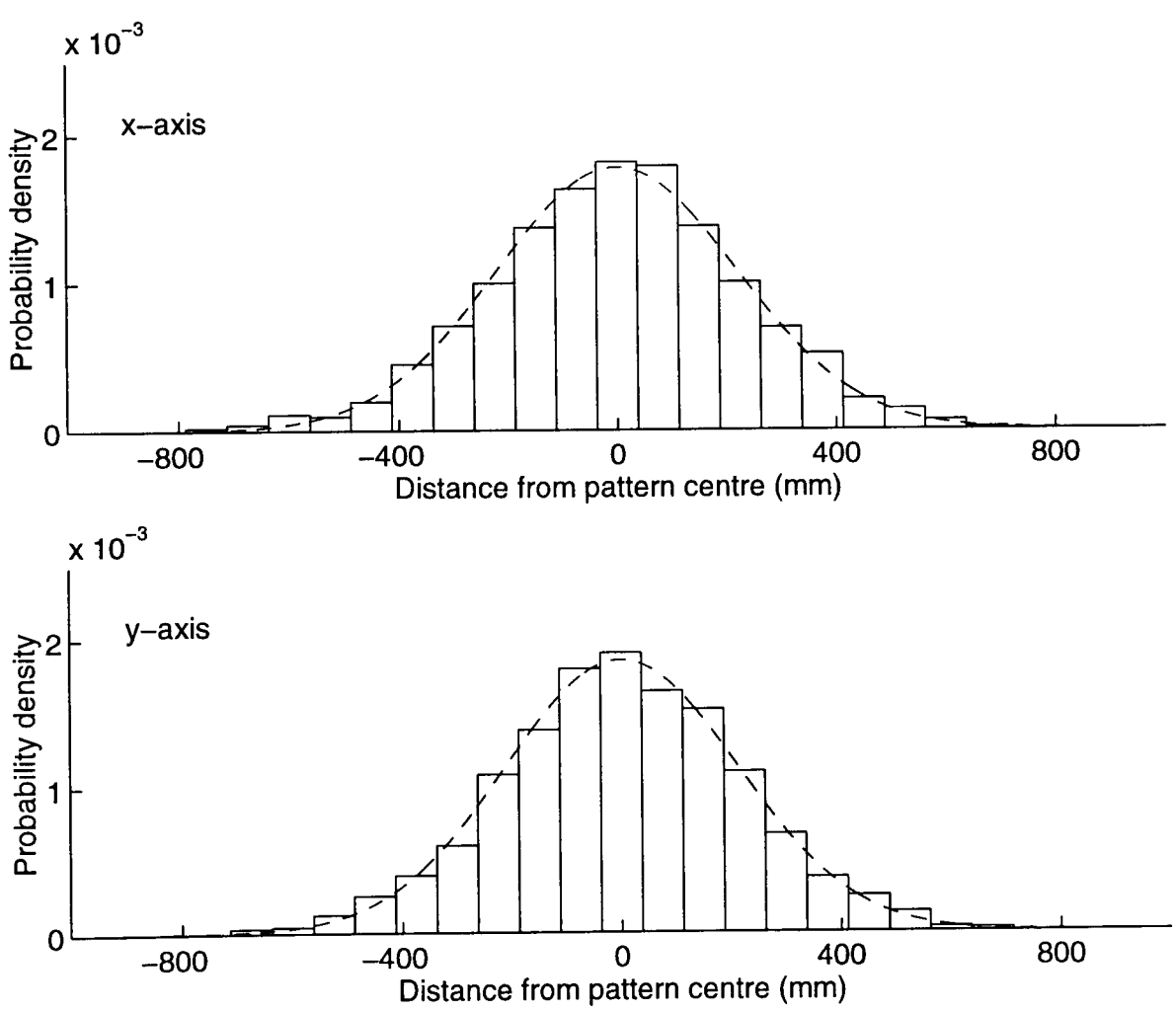

Figure 3.23 *The average probability densities for consecutive horizontal (x) and vertical (y) 75mm strips averaged about the centre of 10 patterns are given for a 36g load of #4 lead shot (0.030" choke) at 40 yards.*

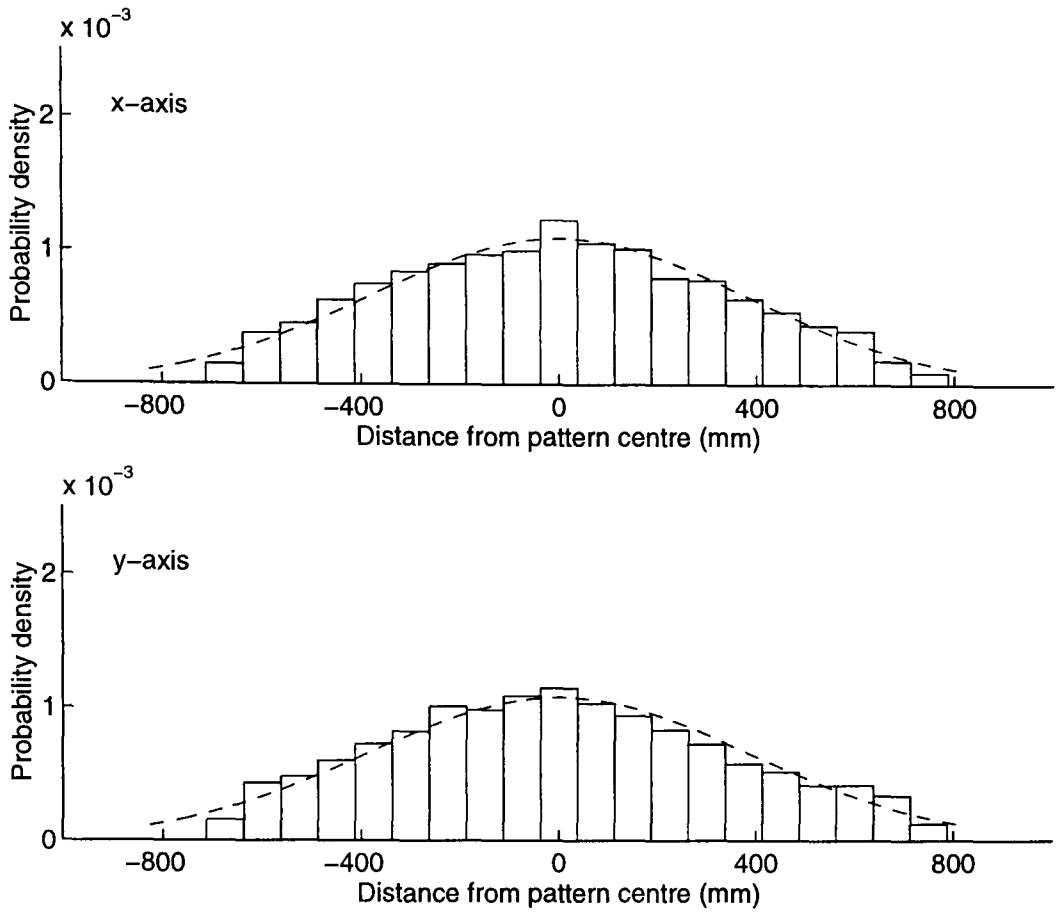

Figure B.1 *The probability densities for consecutive horizontal (x) and vertical (y) 75mm strips averaged about the centre of 10 patterns are given for a 28g load of #7$^1/_2$ lead shot (0.000" choke) at 40 yards.*

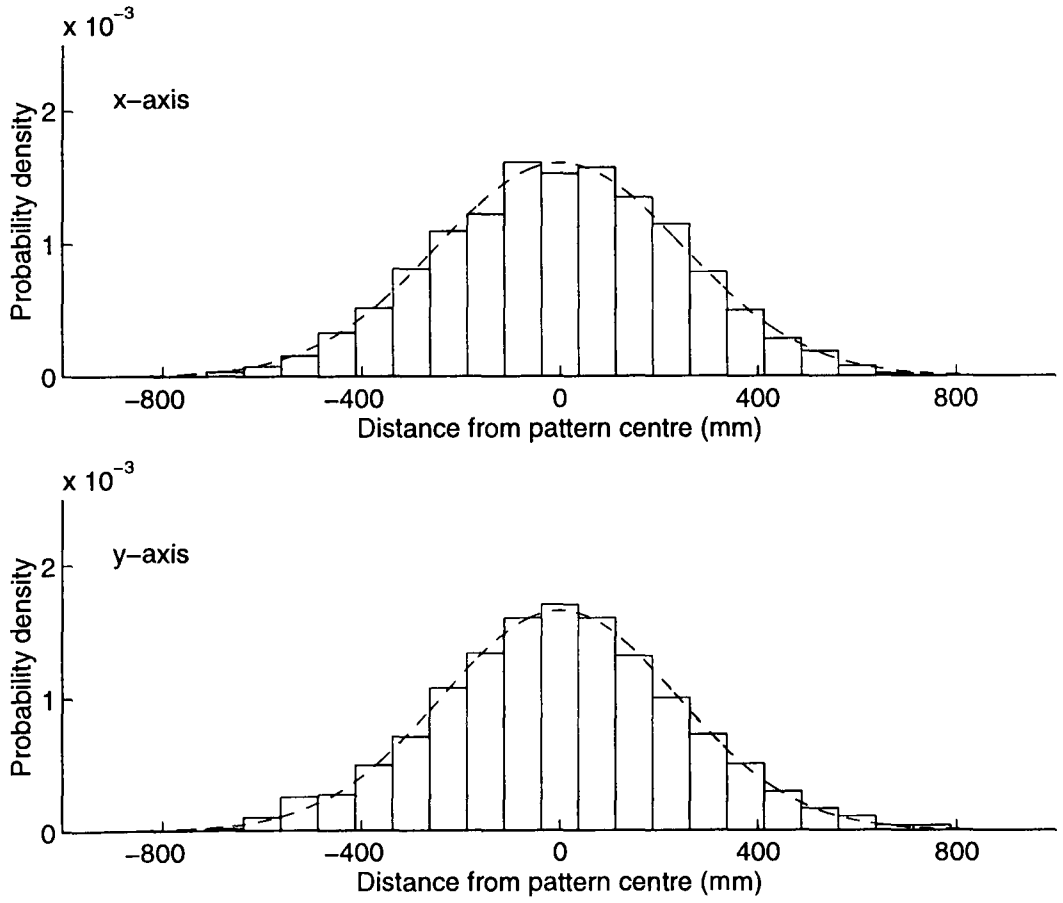

Figure B.2 *The probability densities for consecutive horizontal (x) and vertical (y) 75mm strips averaged about the centre of 10 patterns are given for a 28g load of #7$^1/_2$ lead shot (0.040" choke) at 40 yards.*

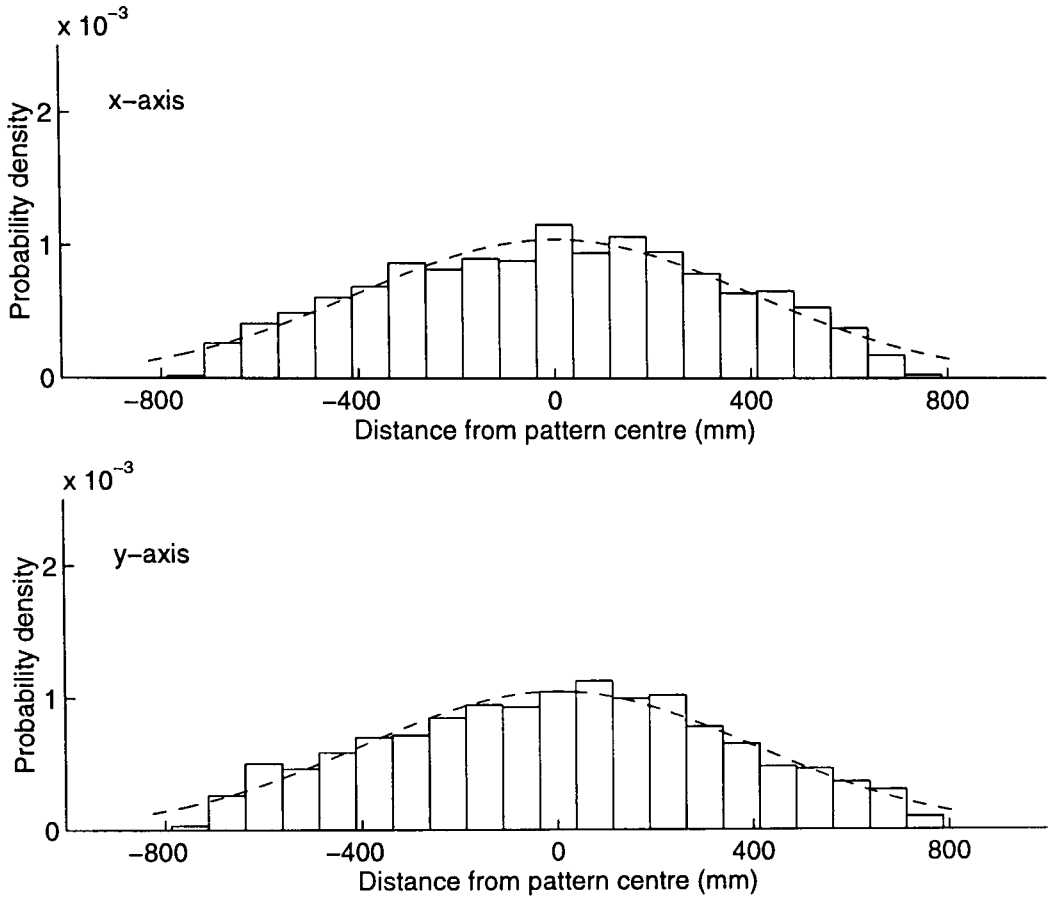

Figure B.3 *The probability densities for consecutive horizontal (x) and vertical (y) 75mm strips averaged about the centre of 10 patterns are given for a 32g load of #3 steel shot (0.000" choke) at 40 yards.*

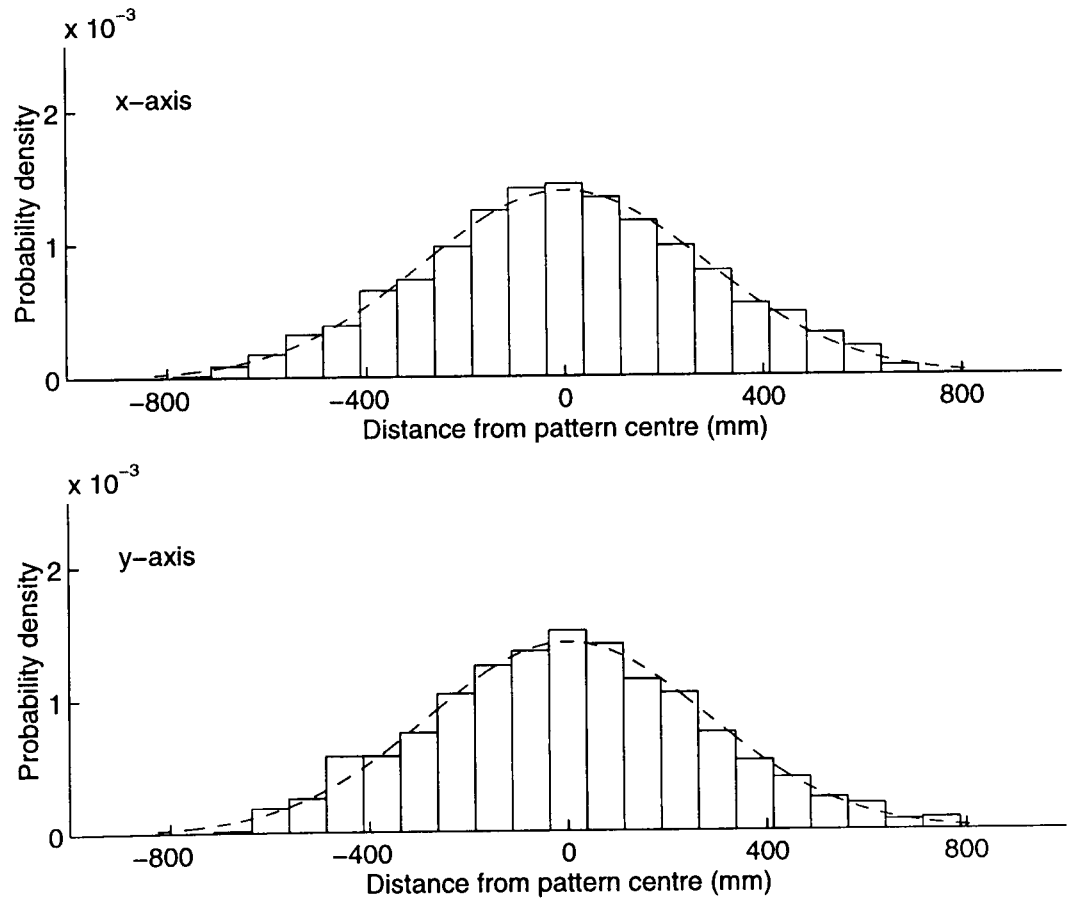

Figure B.4 *The probability densities for consecutive horizontal (x) and vertical (y) 75mm strips averaged about the centre of 10 patterns are given for a 32g load of #3 steel shot (0.040" choke) at 40 yards.*

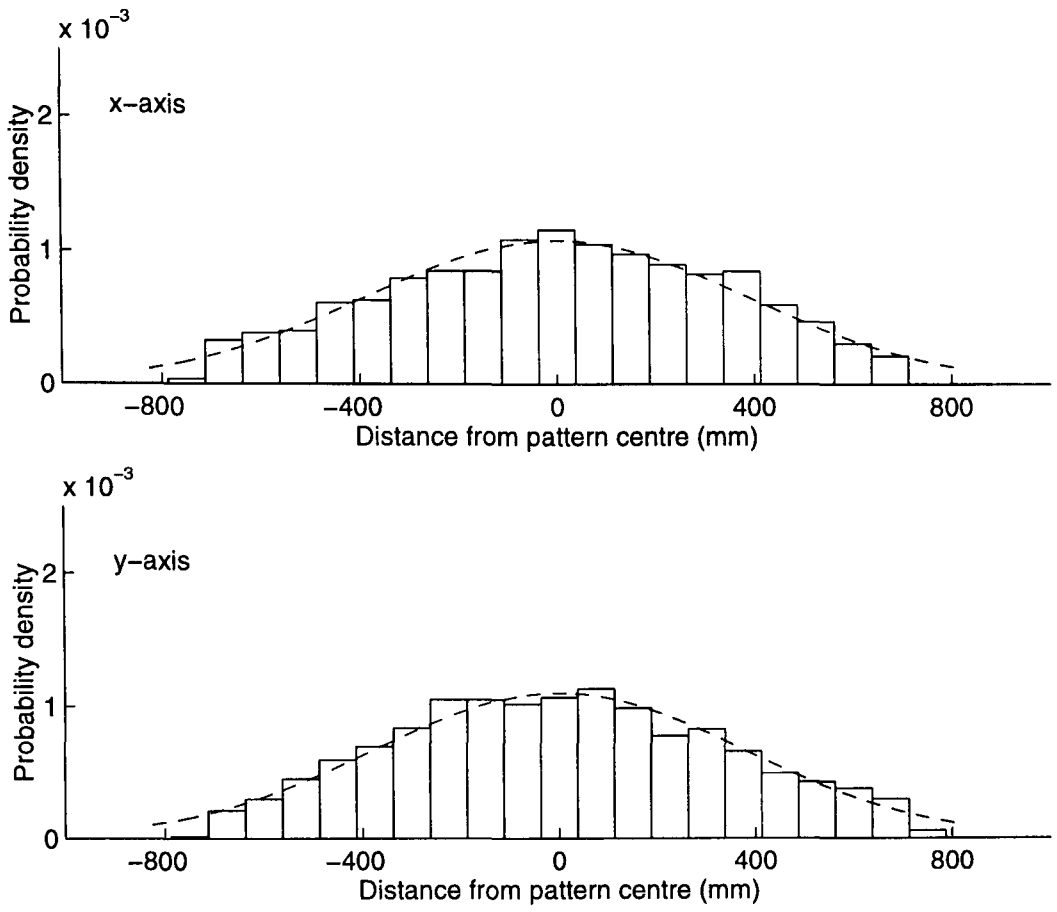

Figure B.5 *The probability densities for consecutive horizontal (x) and vertical (y) 75mm strips averaged about the centre of 10 patterns are given for a 36g load of #3 bismuth shot (0.000" choke) at 40 yards.*

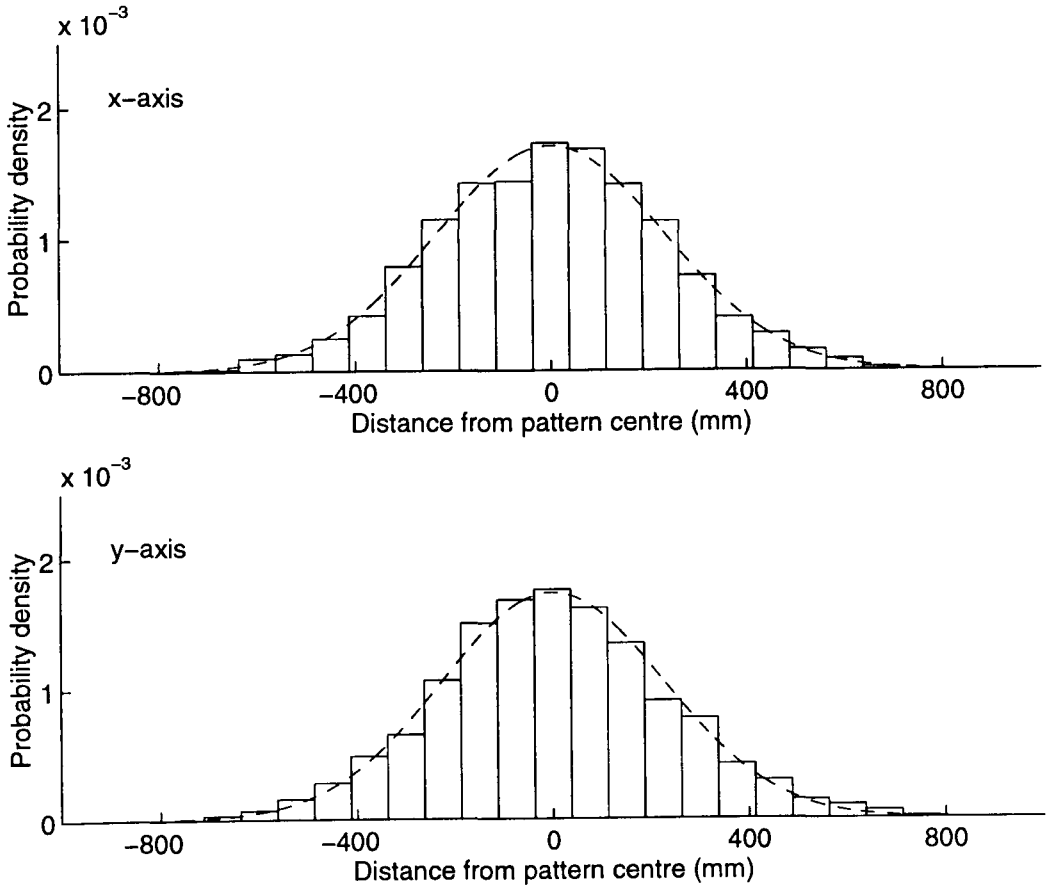

Figure B.6 *The probability densities for consecutive horizontal (x) and vertical (y) 75mm strips averaged about the centre of 10 patterns are given for a 36g load of #3 bismuth shot (0.040" choke) at 40 yards.*

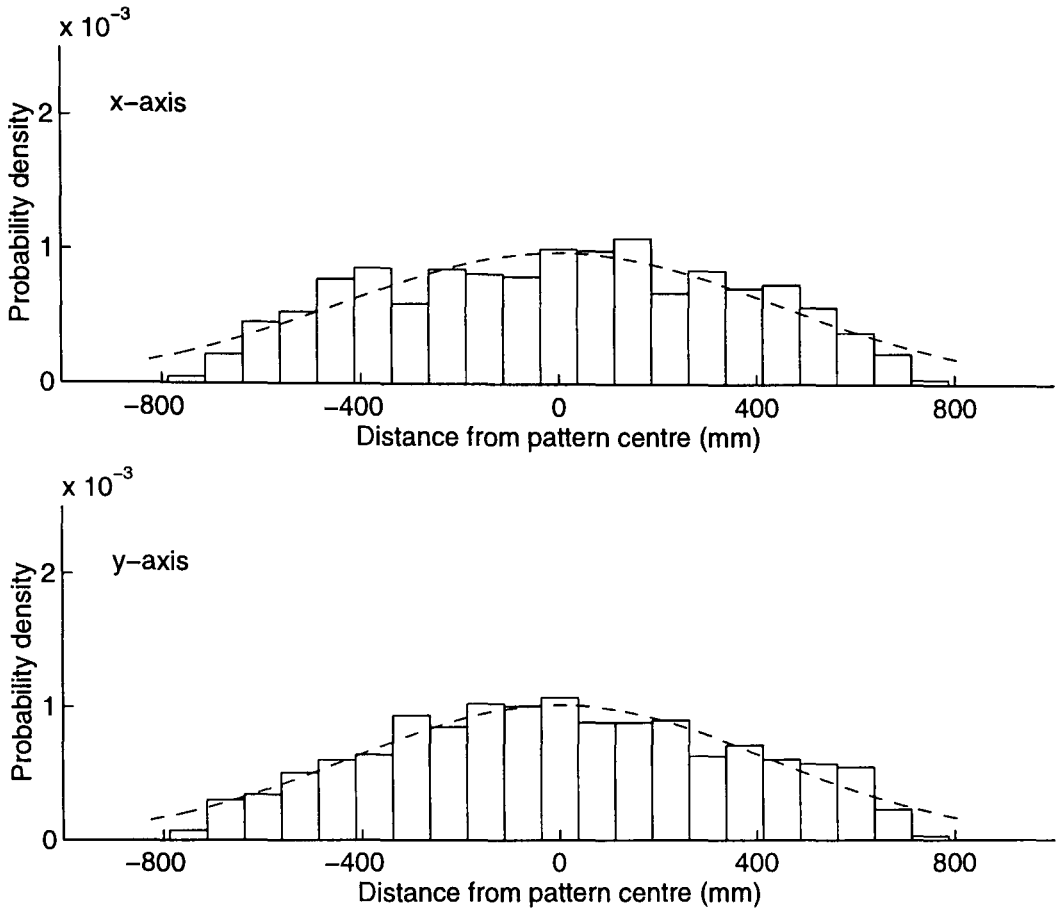

Figure B.7 *The average probability densities for consecutive horizontal (x) and vertical (y) 75mm strips averaged about the centre of 10 patterns are given for a 30g load of #4 zinc shot (0.000" choke) at 40 yards.*

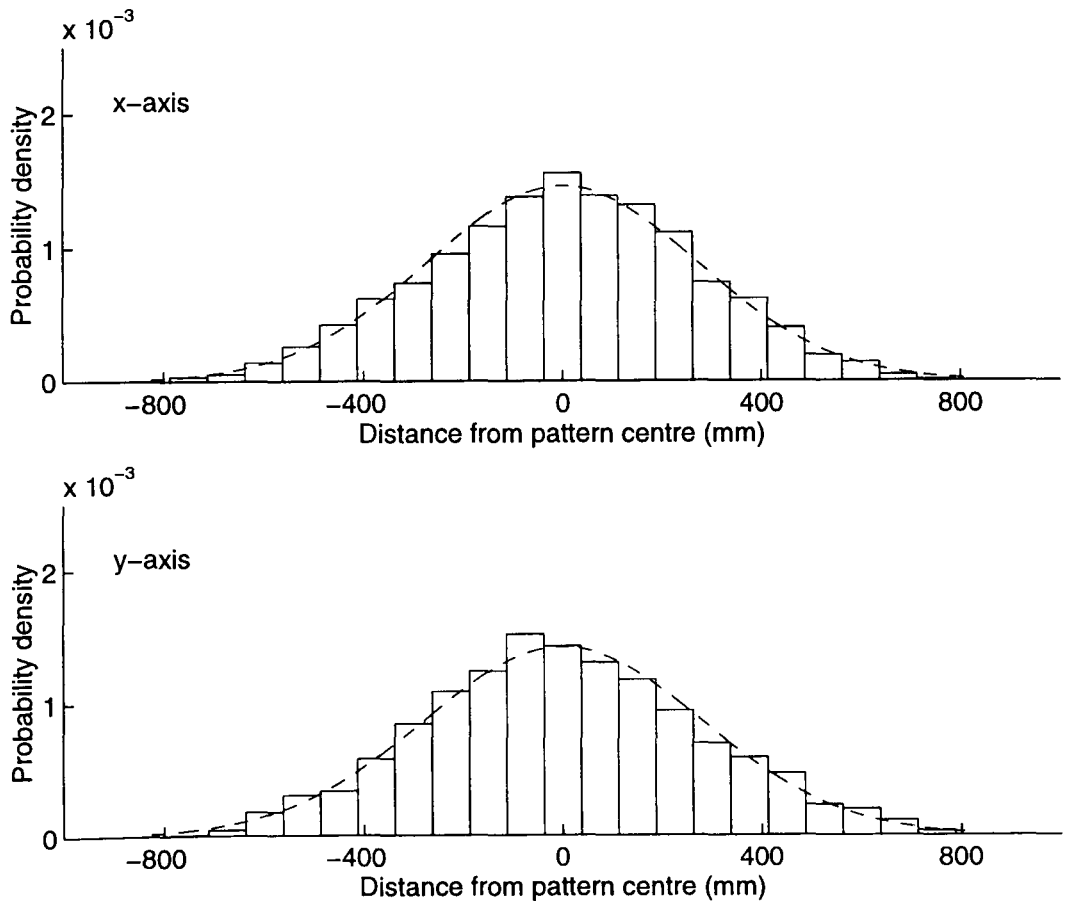

Figure B.8 *The probability densities for consecutive horizontal (x) and vertical (y) 75mm strips averaged about the centre of 10 patterns are given for a 30g load of #4 zinc (0.040" choke) at 40 yards.*

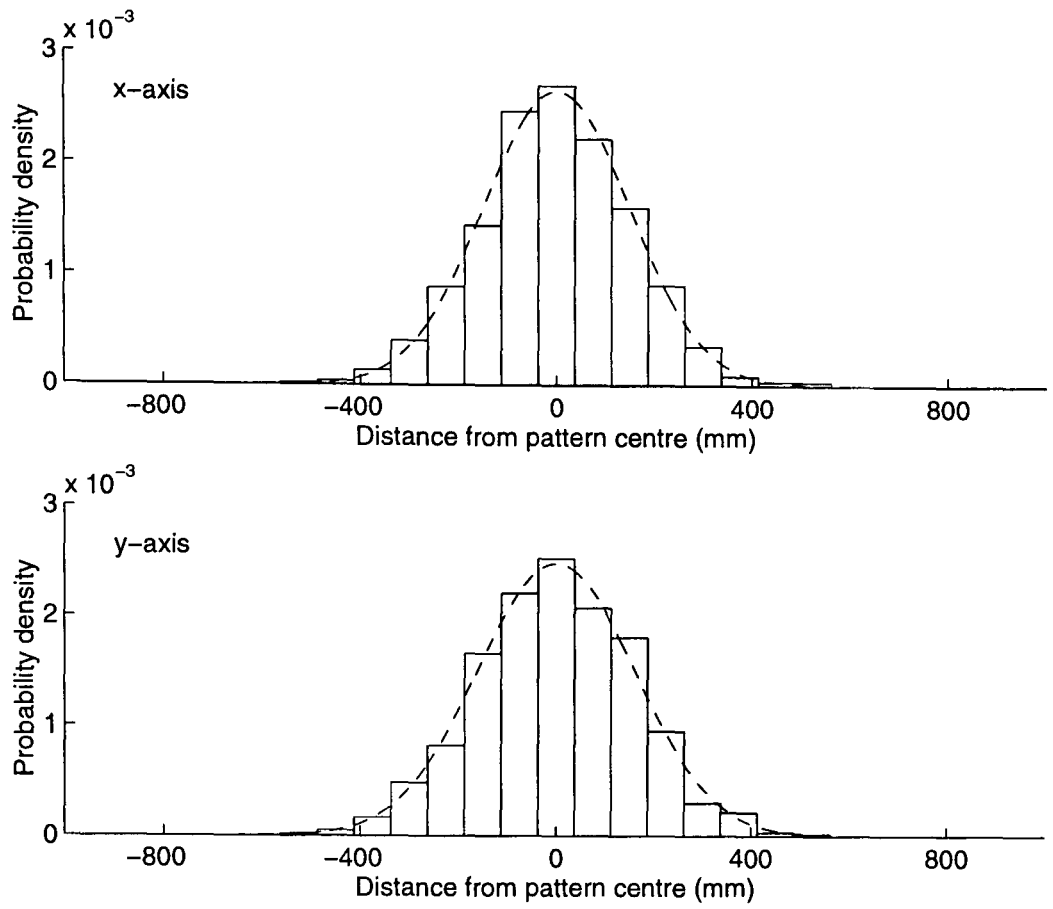

Figure B.9 *The probability densities for consecutive horizontal (x) and vertical (y) 75mm strips averaged about the centre of 10 patterns are given for a 36g load of #BB lead shot (0.010" choke) at 20m.*

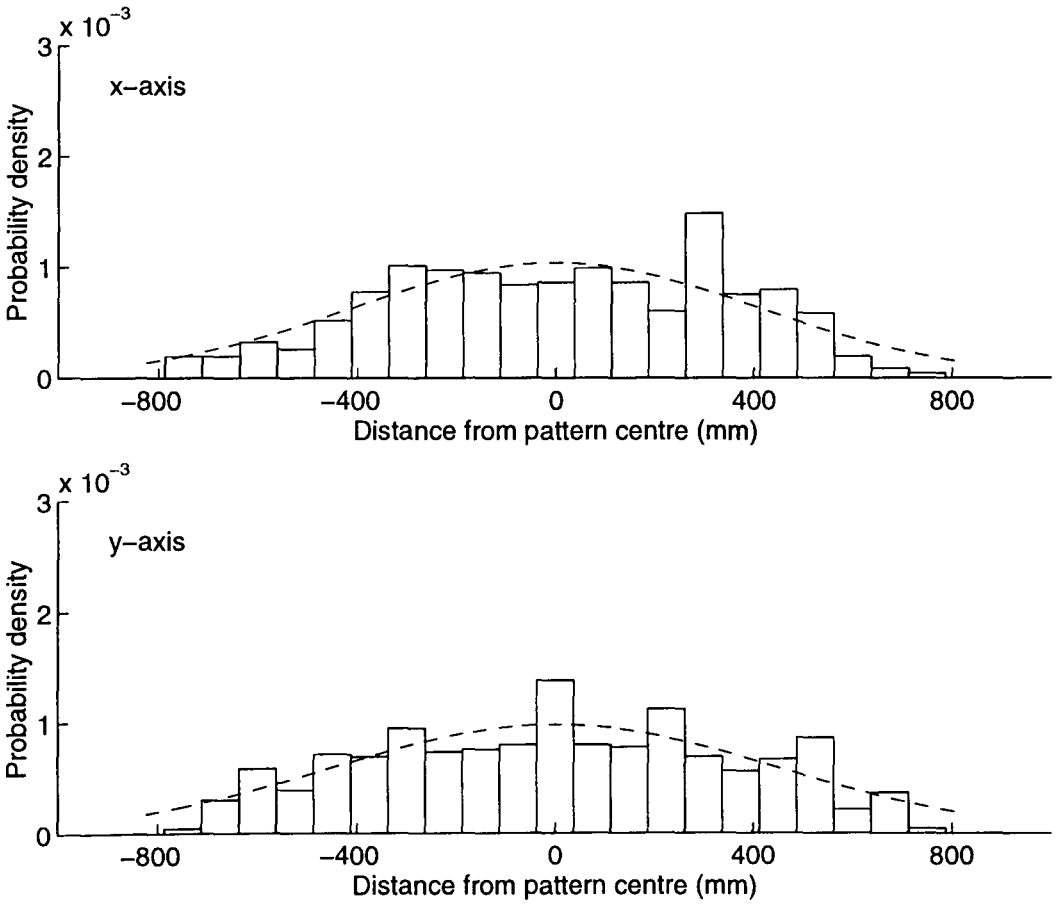

Figure B.10 *The probability densities for consecutive horizontal (x) and vertical (y) 75mm strips averaged about the centre of 10 patterns are given for a 36g load of #BB lead shot (0.010" choke) at 50m.*

C. χ^2 DISTRIBUTION

To make judgements and decisions about the goodness-of-fit, the relevant quantity is called the χ^2 probability, as given in (3.10). In Table C.1 the probabilities of χ^2 are taken from Barlow [45] for a range of χ^2 and degrees of freedom (n).

$$P(\chi^2;n)=\int_{\chi^2}^{\infty} P(\chi'^2;n)d\chi'^2 \qquad (3.10)$$

Degrees of freedom	χ^2 Distribution							
(n)	P=0.99	0.98	0.95	0.90	0.80	0.70	0.50	0.30
1	0.000157	0.000628	0.00393	0.0158	0.0642	0.148	0.455	1.074
2	0.0201	0.0404	0.103	0.211	0.446	0.713	1.386	2.408
3	0.115	0.185	0.352	0.584	1.005	1.424	2.366	3.665
4	0.297	0.429	0.711	1.064	1.649	2.195	3.357	4.878
5	0.554	0.752	1.145	1.610	2.343	3.000	4.351	6.064
6	0.872	1.134	1.635	2.204	3.070	3.828	5.348	7.231
7	1.239	1.564	2.167	2.833	3.822	4.671	6.346	8.383
8	1.646	2.032	2.733	3.490	4.594	5.527	7.344	9.524
9	2.088	2.532	3.325	4.168	5.380	6.393	8.343	10.656
10	2.558	3.059	3.940	4.865	6.179	7.267	9.432	11.781
11	3.053	3.609	4.575	5.578	6.989	8.148	10.341	12.899
12	3.571	4.178	5.226	6.304	7.807	9.034	11.340	14.011
13	4.107	4.765	5.892	7.042	8.634	9.926	12.340	15.119
14	4.660	5.368	6.571	7.790	9.467	10.821	13.339	16.222
15	5.229	5.985	7.261	8.547	10.307	11.721	14.339	17.322
16	5.812	6.614	7.962	9.312	11.152	12.624	15.338	18.418
17	6.408	7.255	8.672	10.085	12.002	13.531	16.338	19.511
18	7.015	7.906	9.390	10.865	12.857	14.440	17.338	20.601
19	7.633	8.567	10.117	11.651	13.716	15.325	18.338	21.689
20	8.260	9.237	10.851	12.443	14.578	16.266	19.337	22.775

Table C.1 *The χ^2 distribution.*

D. LATERAL DISTRIBUTION : RADIAL

To determine the nature of lateral radial pellet density distribution, the average pellet density within annulii have equal area, so the radii increments of the circles decreases from the pattern centre, were taken over 10 patterns. In Figure 3.27 the Gaussian characteristics, Equation (3.17), are seen in the radial distribution. This relationship is also seen in Figure D.1-D.10 for the same range of pellet diameters, materials, chokes and ranges shown in Appendix B. A least squares fit of (3.17) was also performed and overlaid on the plots.

$$\rho = \rho_0 e^{-r^2/2\sigma^2} \tag{3.17}$$

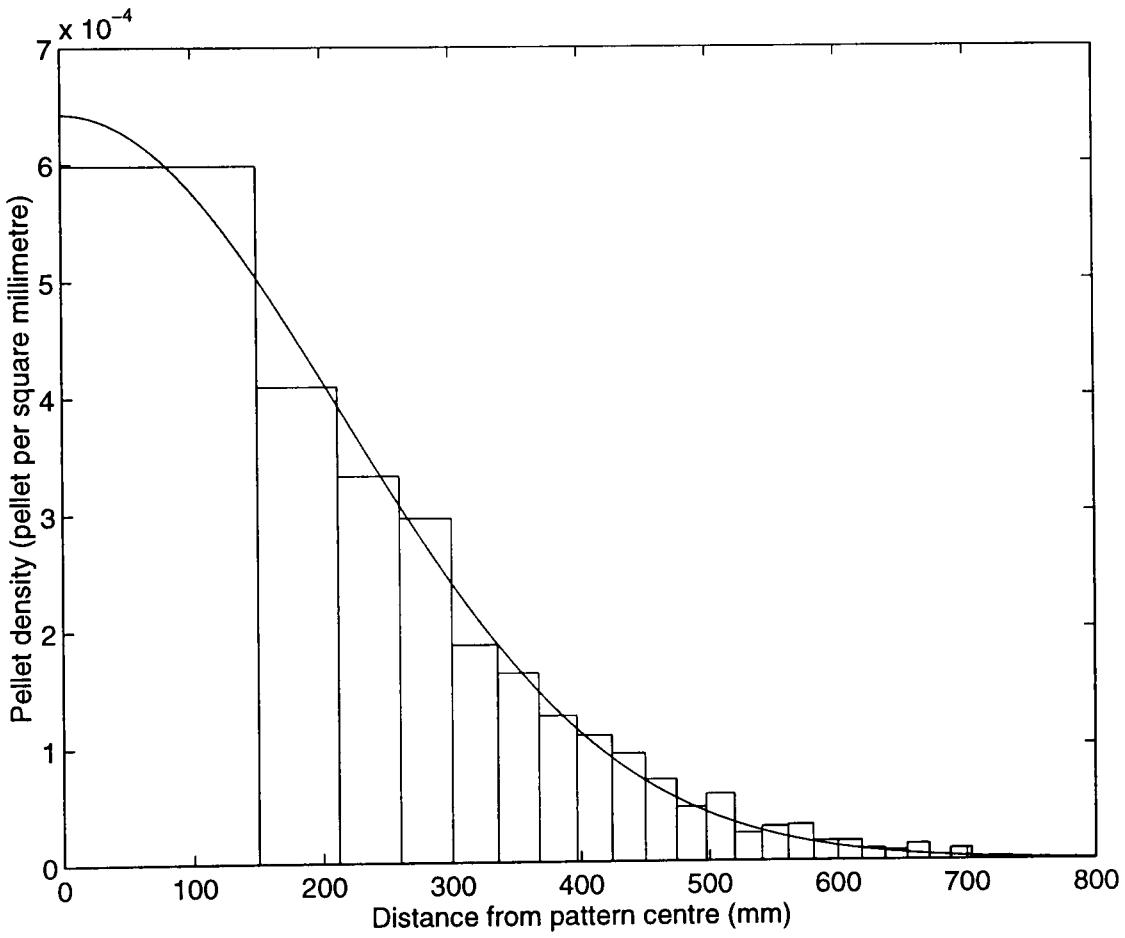

Figure 3.27 *The average radial distribution of pellet density averaged over 10 patterns for a 36g load of #4 lead shot (0.030" choke) at 40 yards. The histogram shows the calculated pellet densities in zones, or annuli, of equal area, and the curve is a fitted Gaussian.*

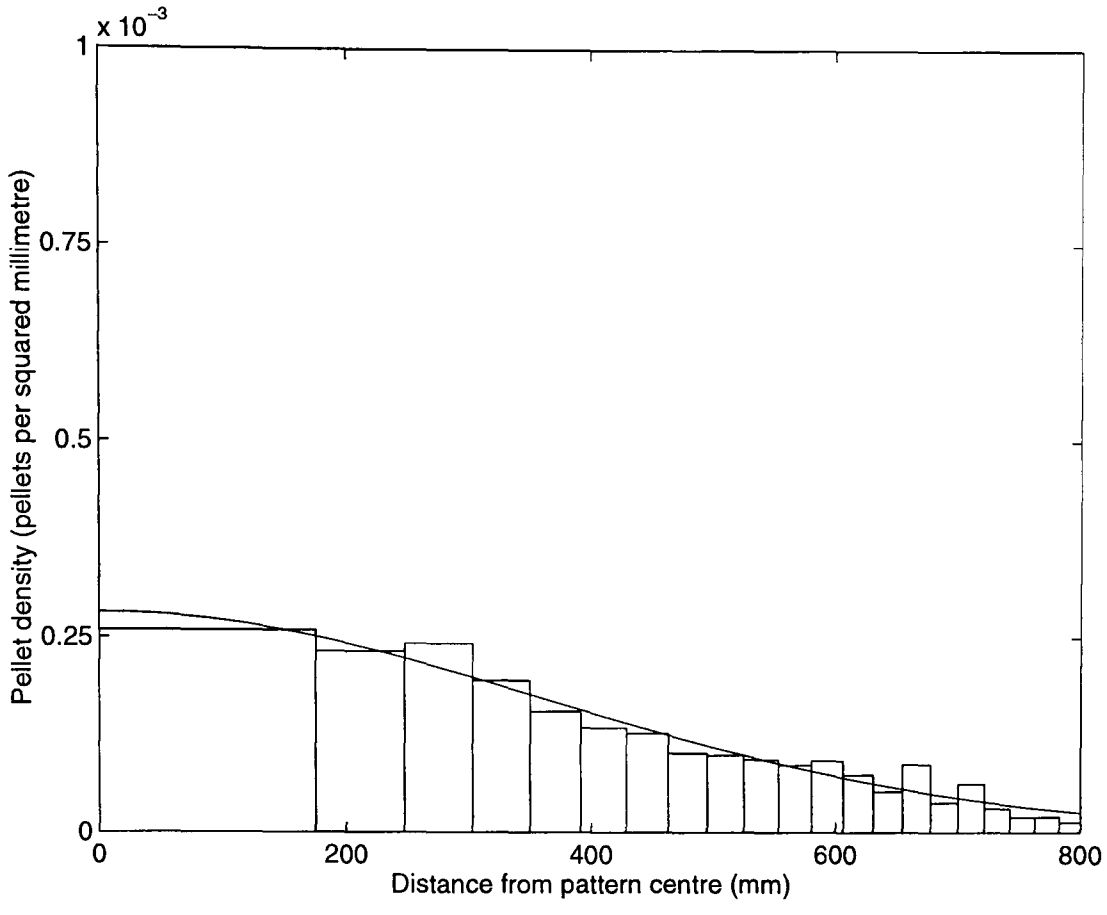

Figure D.1 *The average radial distribution of pellet density averaged over 10 patterns for a 28g load of #7$^1/_2$ lead shot (0.000" choke) at 40 yards. The histogram shows the calculated pellet densities in zones, or annuli, of equal area, and the curve is a fitted Gaussian.*

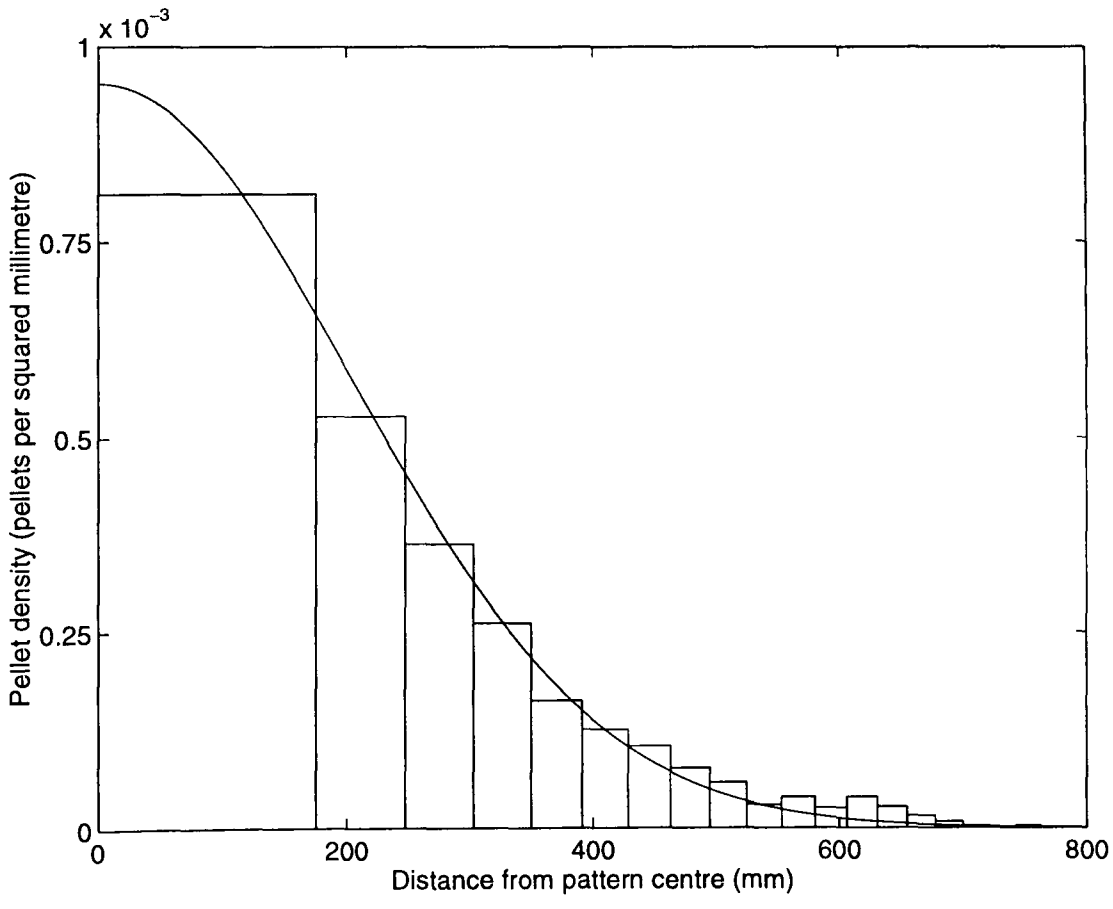

Figure D.2 *The average radial distribution of pellet density averaged over 10 patterns for a 28g load of #7$^1/_2$ lead shot (0.040" choke) at 40 yards. The histogram shows the calculated pellet densities in zones, or annuli, of equal area, and the curve is a fitted Gaussian.*

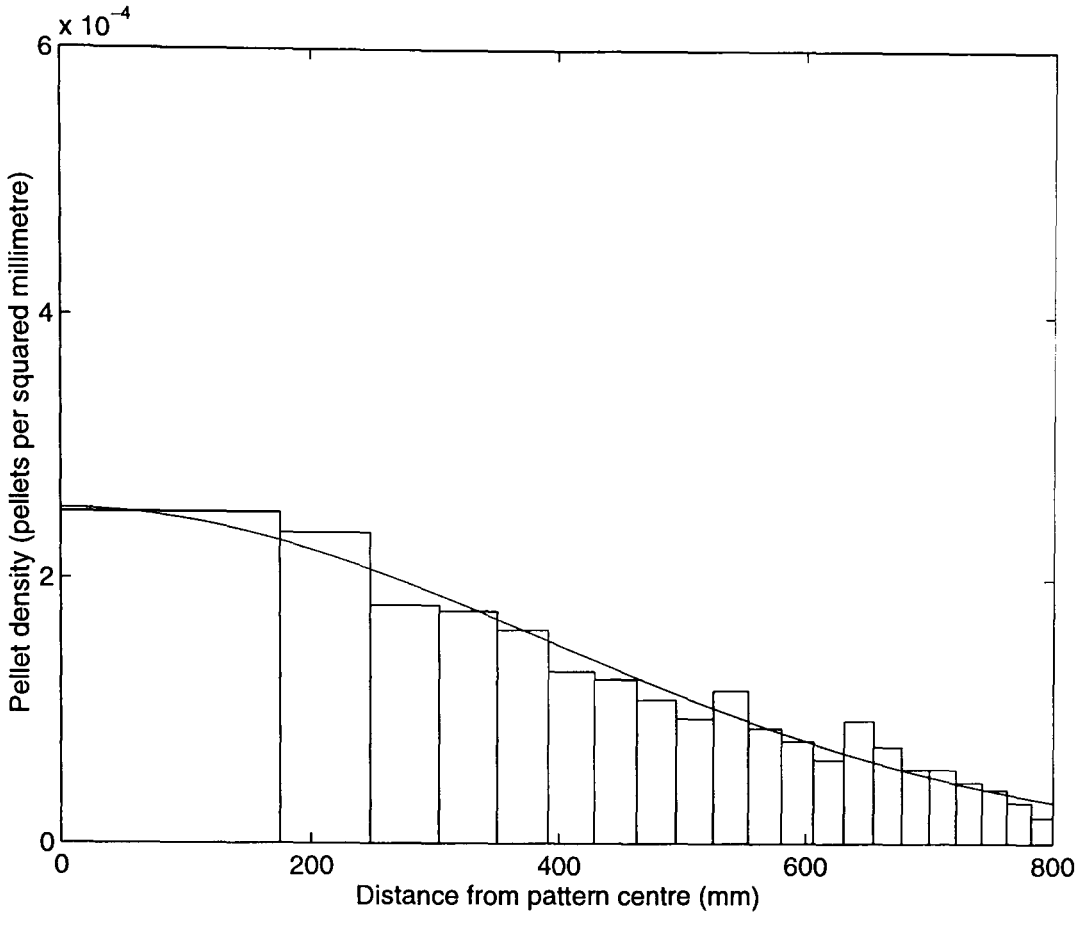

Figure D.3 *The average radial distribution of pellet density averaged over 10 patterns for a 32g load of #3 steel shot (0.000" choke) at 40 yards. The histogram shows the calculated pellet densities in zones, or annuli, of equal area, and the curve is a fitted Gaussian.*

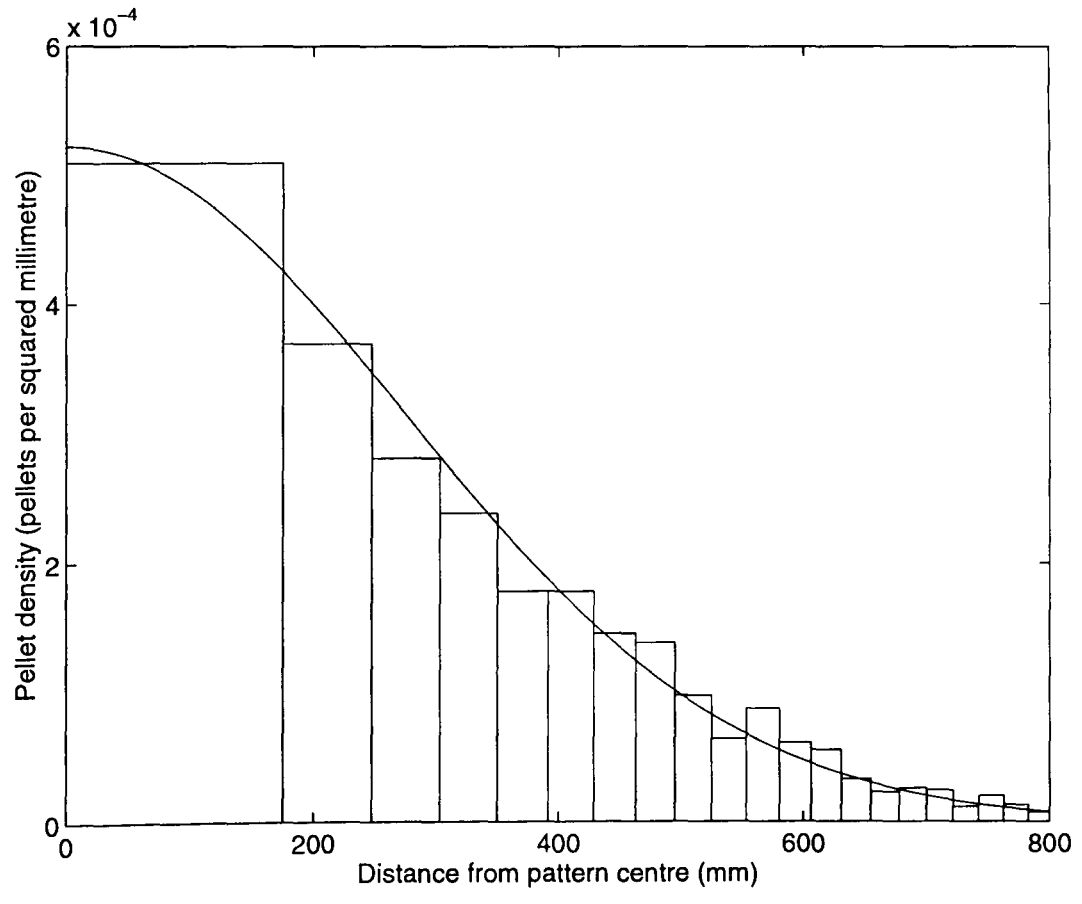

Figure D.4 *The average radial distribution of pellet density averaged over 10 patterns for a 32g load of #3 steel shot (0.040" choke) at 40 yards. The histogram shows the calculated pellet densities in zones, or annuli, of equal area, and the curve is a fitted Gaussian.*

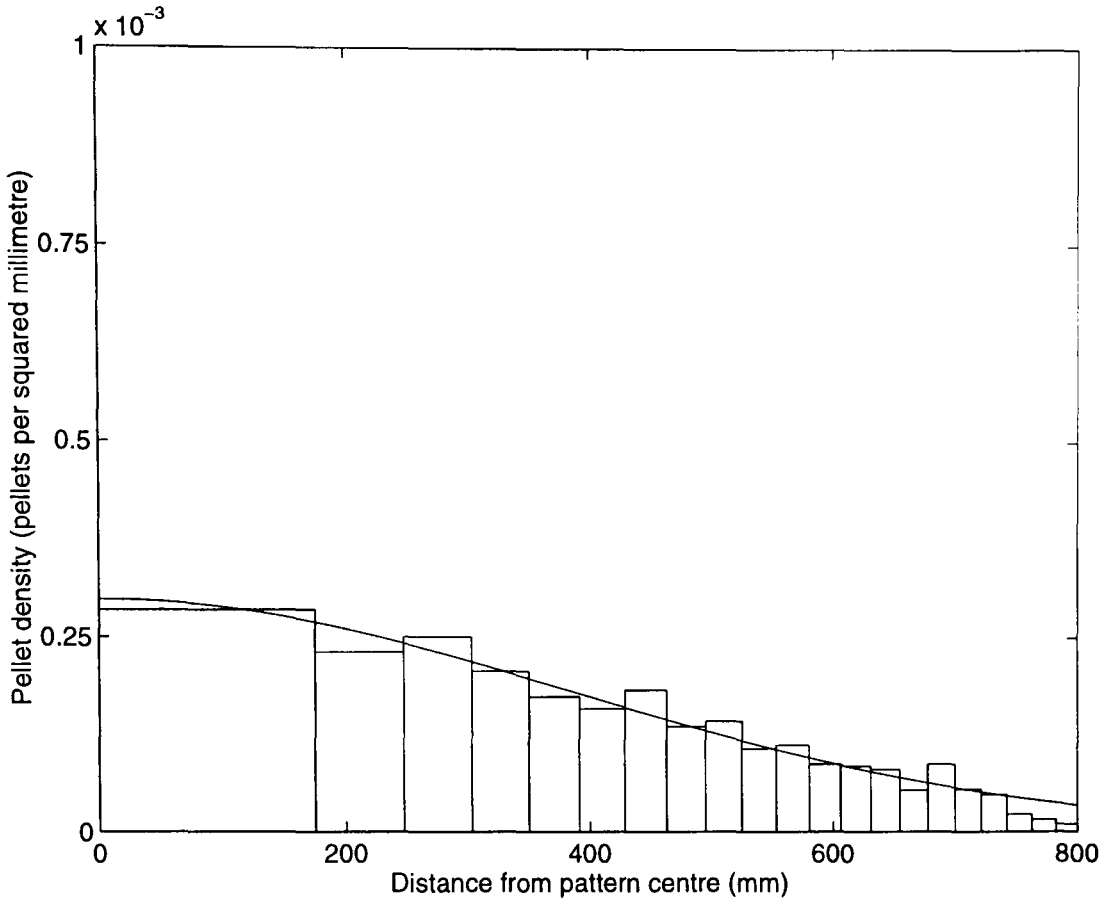

Figure D.5 *The average radial distribution of pellet density averaged over 10 patterns for a 36g load of #3 bismuth shot (0.000" choke) at 40 yards. The histogram shows the calculated pellet densities in zones, or annuli, of equal area, and the curve is a fitted Gaussian.*

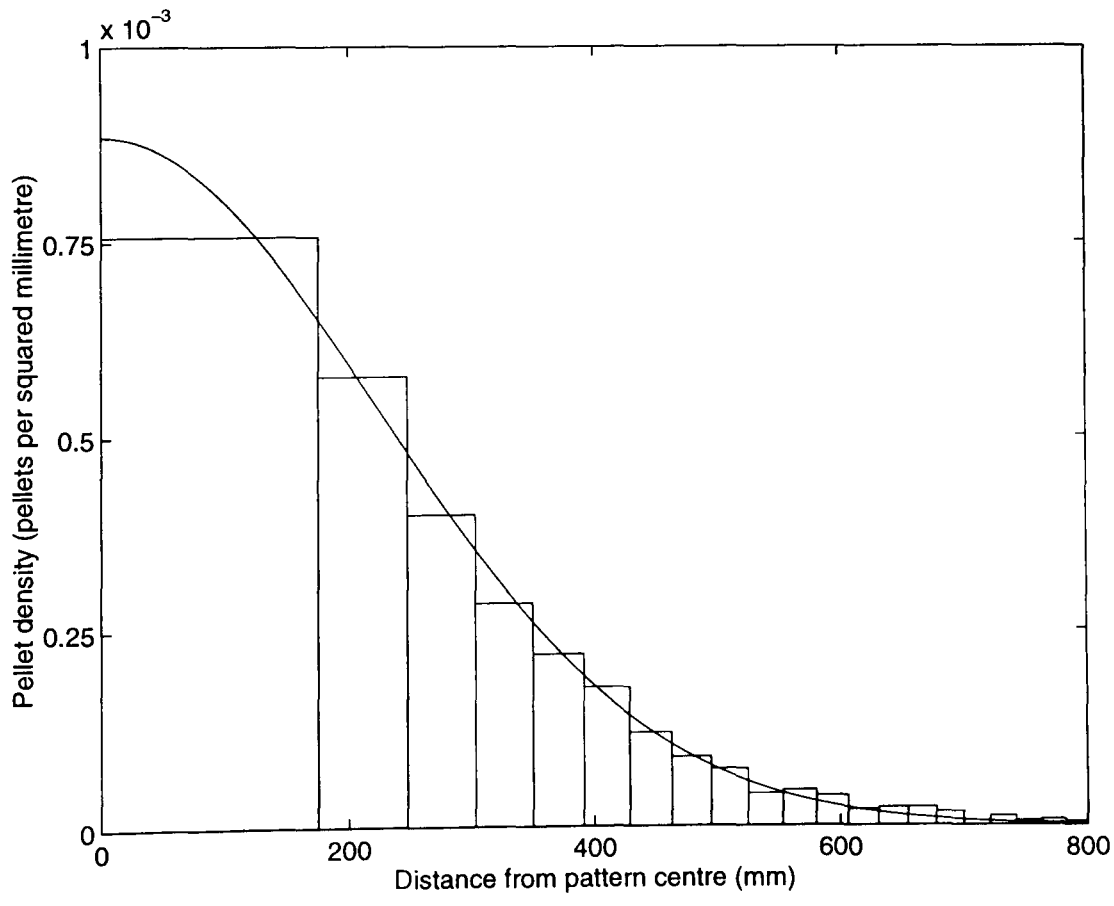

Figure D.6 *The average radial distribution of pellet density averaged over 10 patterns for a 36g load of #3 bismuth shot (0.040" choke) at 40 yards. The histogram shows the calculated pellet densities in zones, or annuli, of equal area, and the curve is a fitted Gaussian.*

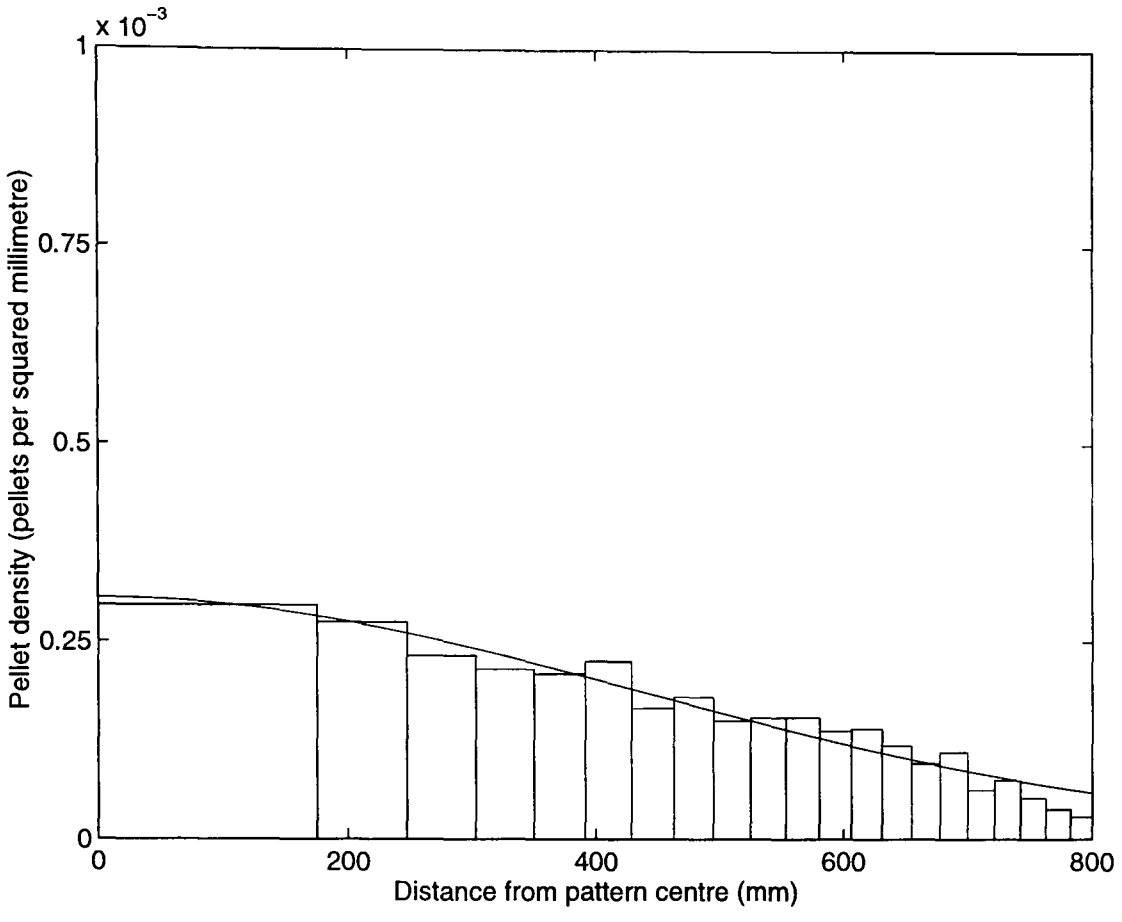

Figure D.7 *The average radial distribution of pellet density averaged over 10 patterns for a 30g load of #4 zinc shot (0.000" choke) at 40 yards. The histogram shows the calculated pellet densities in zones, or annuli, of equal area, and the curve is a fitted Gaussian.*

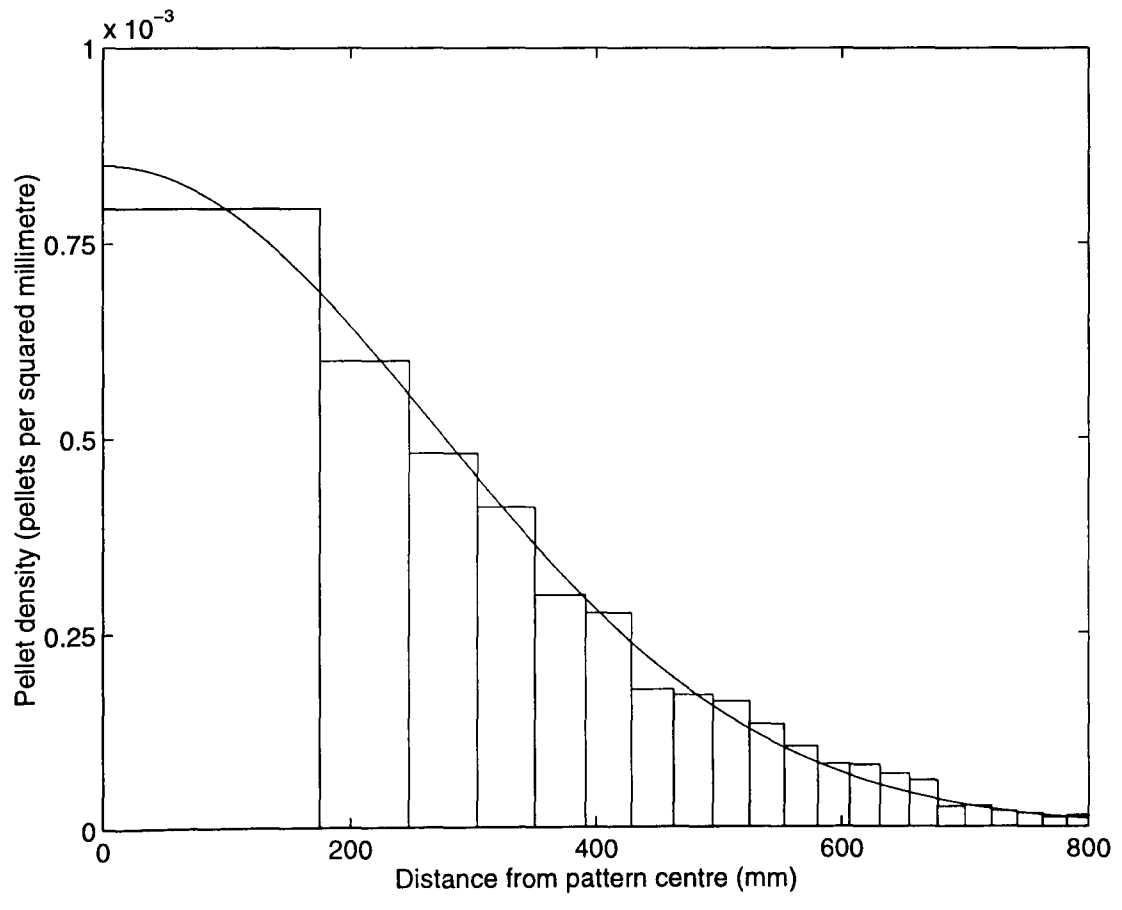

Figure D.8 *The average radial distribution of pellet density averaged over 10 patterns for a 30g load of #4 zinc shot (0.040" choke) at 40 yards. The histogram shows the calculated pellet densities in zones, or annuli, of equal area, and the curve is a fitted Gaussian.*

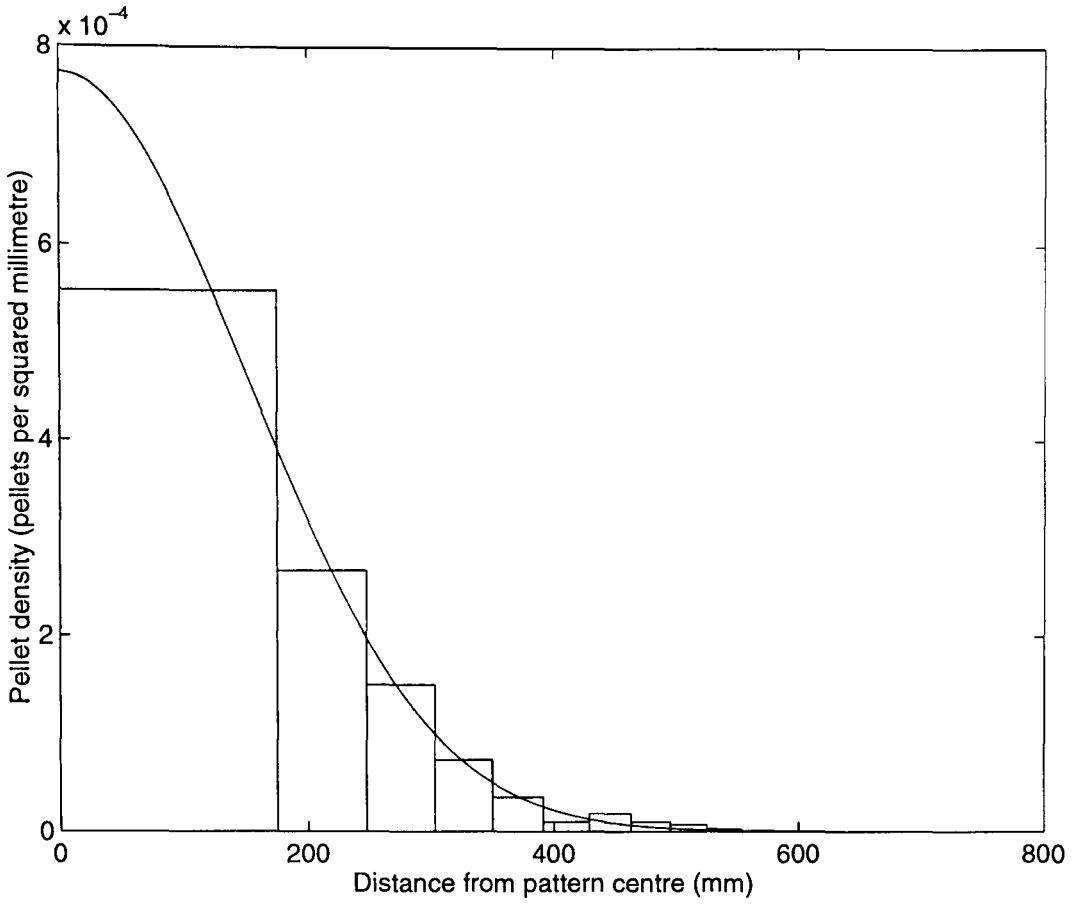

Figure D.9 *The average radial distribution of pellet density averaged over 10 patterns for a 36g load of #BB lead shot (0.010" choke) at 20m. The histogram shows the calculated pellet densities in zones, or annuli, of equal area, and the curve is a fitted Gaussian.*

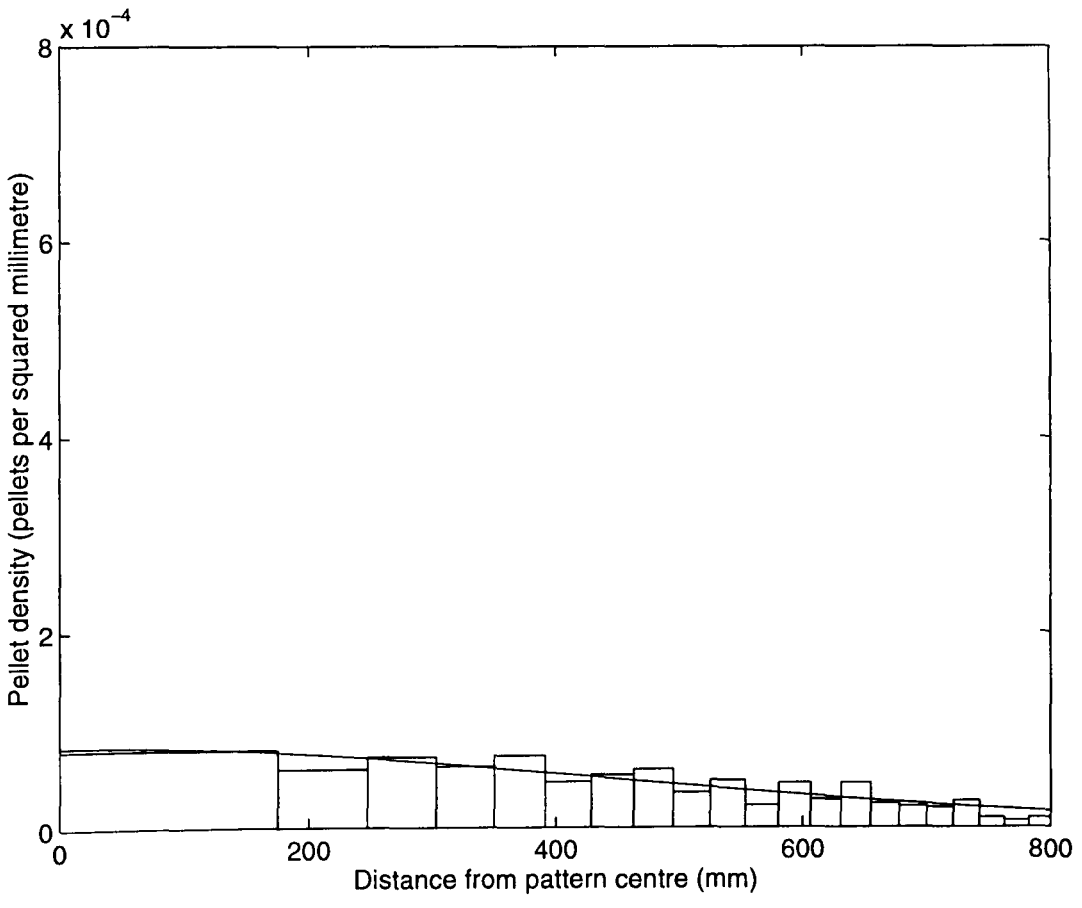

Figure D.10 *The average radial distribution of pellet density averaged over 10 patterns for a 36g load of #BB lead shot (0.010" choke) at 50m. The histogram shows the calculated pellet densities in zones, or annuli, of equal area, and the curve is a fitted Gaussian.*

E. HIT PROBABILITY DISTRIBUTION

To illustrate the appropriateness of the Poisson distribution on the lateral dispersion of pellets in a shot cloud, a linear relationship should result from (3.34). This linear relationship was shown in Figure 3.33 where the average number of pellets and the probability of find 0, 1, 2 and 3 pellets, in areas equivalent to a 100mm diameter circle, were found. In Figure E.1-E.4 the Poisson distribution for the same range of pellet diameters and materials as that in Appendix B and D are shown.

$$\overline{H} = \ln\left[\frac{\overline{H}^{H}}{H!\,p(H)}\right] \tag{3.34}$$

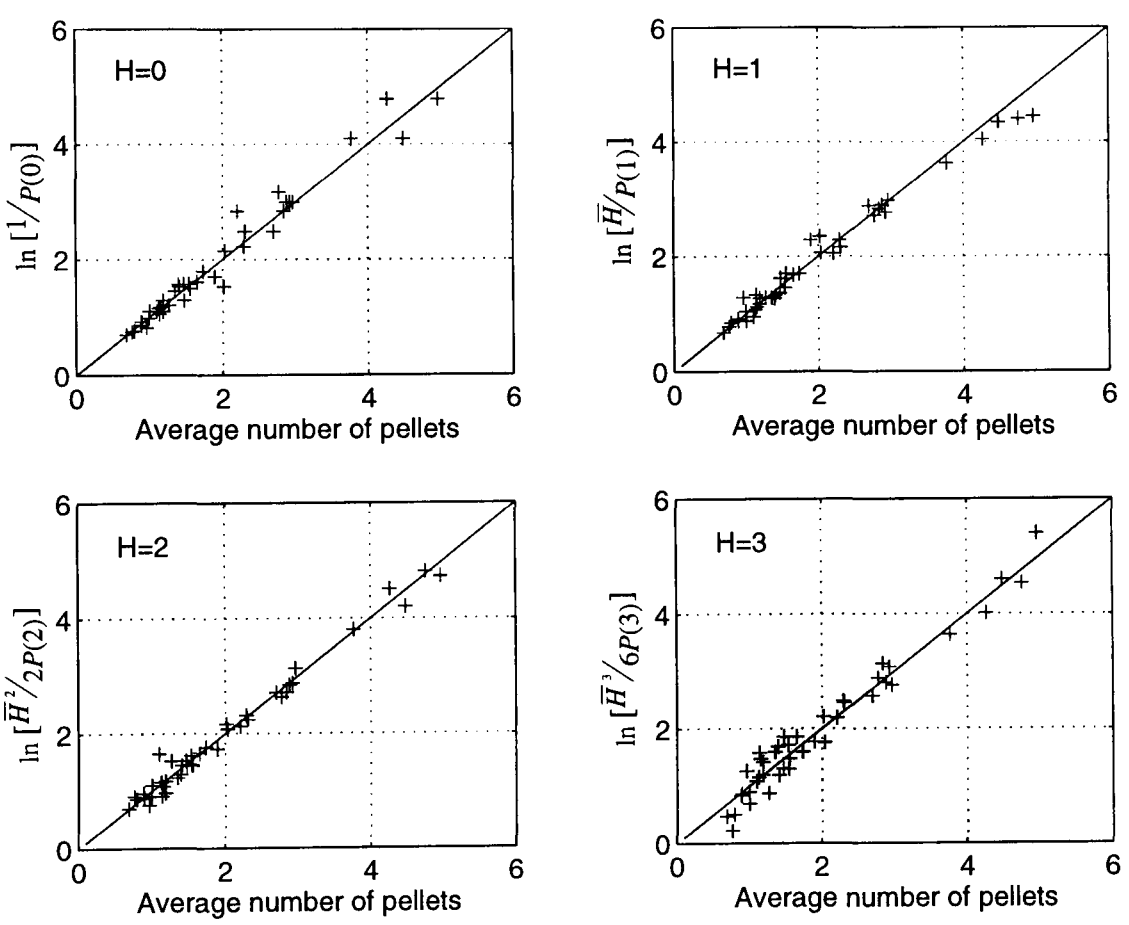

Figure 3.33 *The relationship between the measure average pellet counts ($\overline{H}$) in areas, A, of similar pellet densities and their corresponding probabilities of finding 0, 1, 2 and 3 pellet for a 36g load of #4 lead shot (0.000" - 0.050" choke) at 40 yards. The area A chosen in that of a 100mm diameter circle and the solid line represents the theoretical Poisson distribution.*

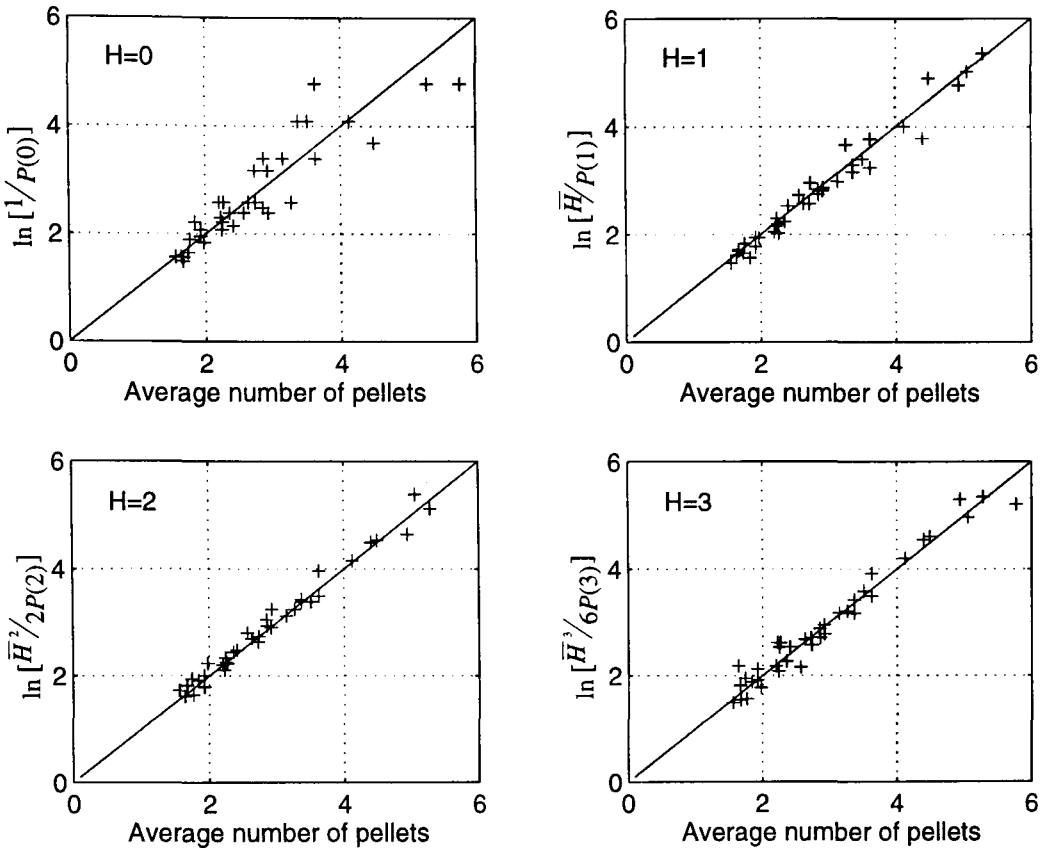

Figure E.1 *The relationship between the measure average pellet counts ($\overline{H}$) in areas, A, of similar pellet densities and their corresponding probabilities of finding 0, 1, 2 and 3 pellet for a 28g load of #7½ lead shot (0.000" - 0.050" choke) at 40 yards. The area A chosen in that of a 100mm diameter circle and the solid line represents the theoretical Poisson distribution.*

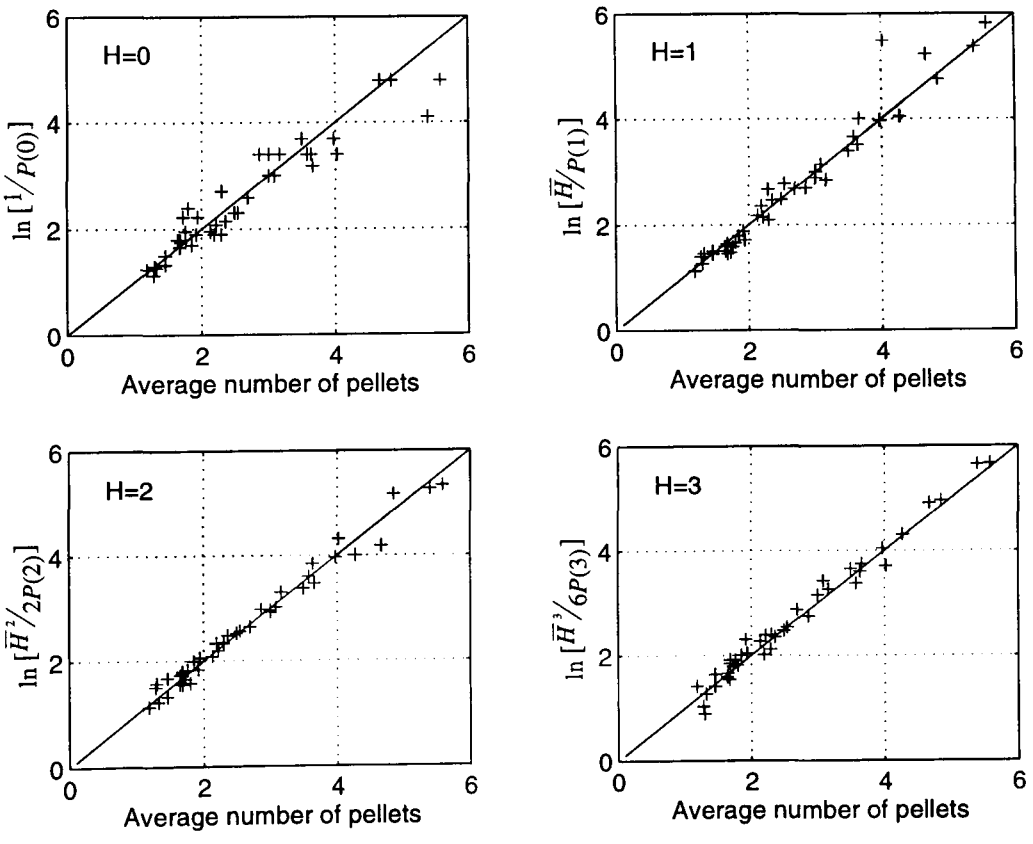

Figure E.2 *The relationship between the measure average pellet counts ($\overline{H}$) in areas, A, of similar pellet densities and their corresponding probabilities of finding 0, 1, 2 and 3 pellet for a 32g load of #3 steel shot (0.000" - 0.050" choke) at 40 yards. The area A chosen in that of a 100mm diameter circle and the solid line represents the theoretical Poisson distribution.*

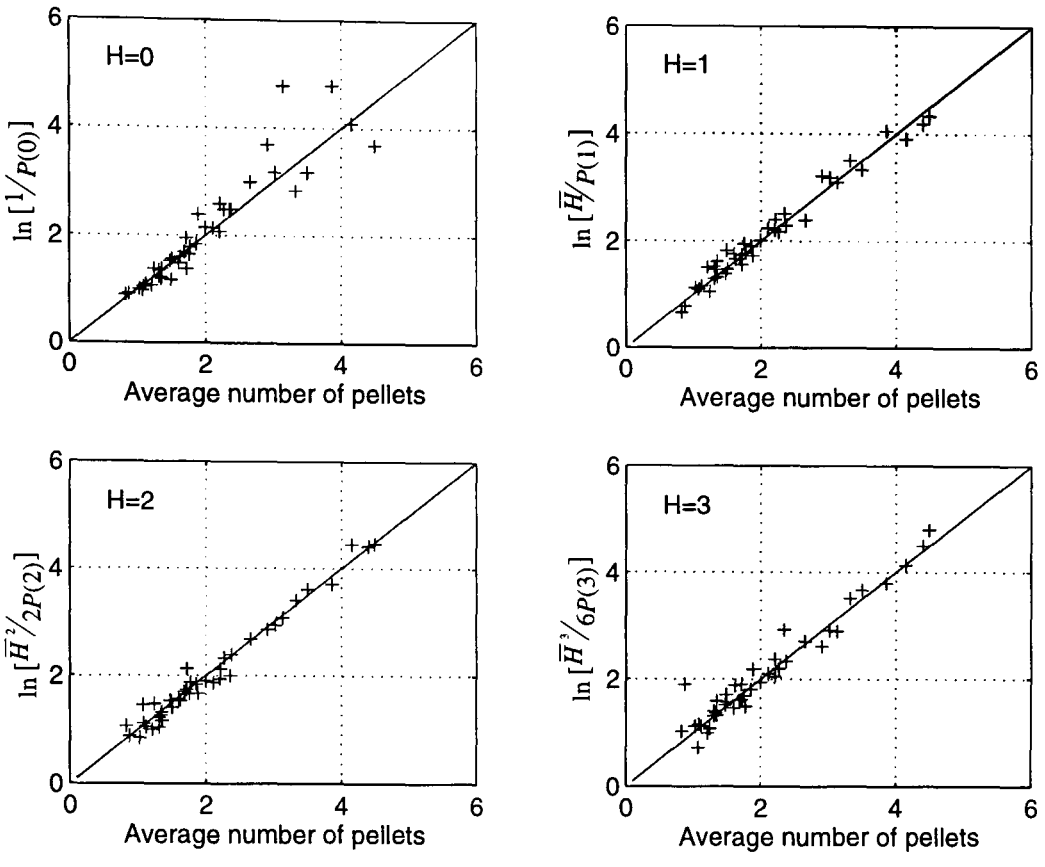

Figure E.3 *The relationship between the measure average pellet counts ($\overline{H}$) in areas, A, of similar pellet densities and their corresponding probabilities of finding 0, 1, 2 and 3 pellet for a 36g load of #3 bismuth shot (0.000" - 0.050" choke) at 40 yards. The area A chosen in that of a 100mm diameter circle and the solid line represents the theoretical Poisson distribution.*

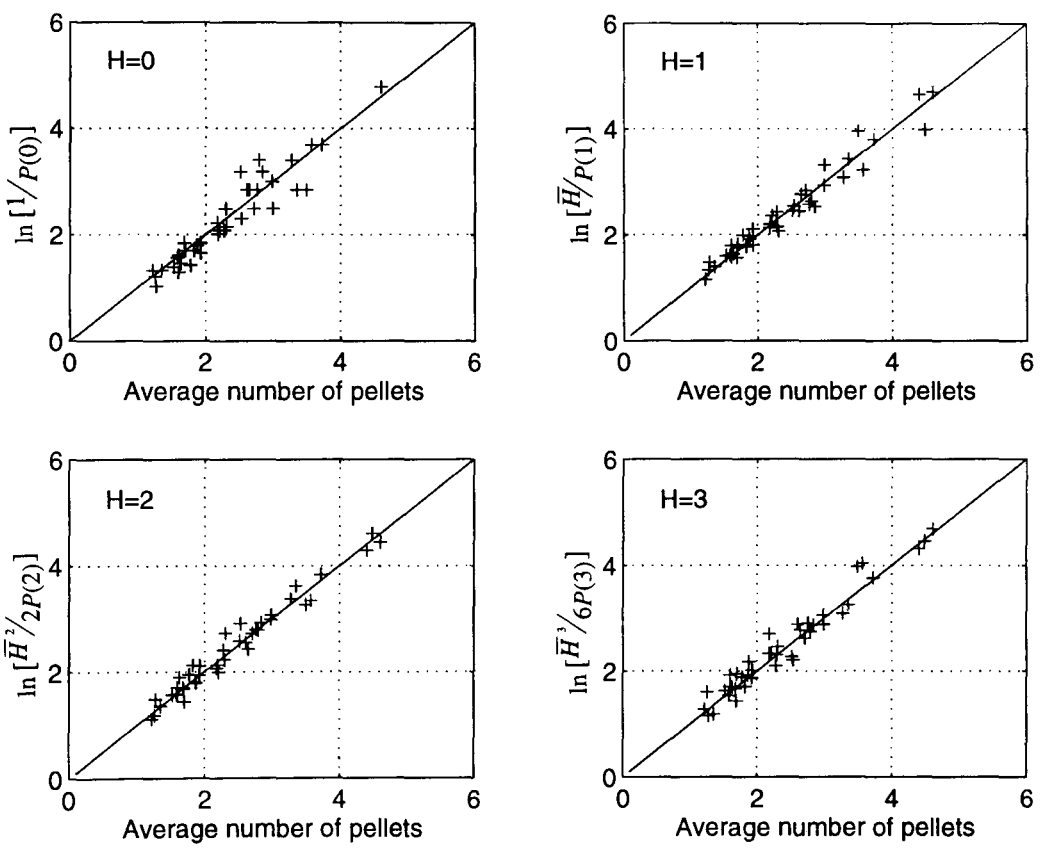

Figure E.4 *The relationship between the measure average pellet counts ($\overline{H}$) in areas, A, of similar pellet densities and their corresponding probabilities of finding 0, 1, 2 and 3 pellet for a 30g load of #4 zinc shot (0.000" - 0.050" choke) at 40 yards. The area A chosen in that of a 100mm diameter circle and the solid line represents the theoretical Poisson distribution.*

F. SAMPLE BALLISTICS REPORT

This is the ballistics report for the 36g load of #3 lead shot using 0.030" choke described in Chapter 2.

Pattern information is given at 40 yds (36.6m) because this is the standard UK test range.

The reference to a "5ft square" means that the total number of impacts on the 1.5m (approx. 5ft) square pattern paper is noted.

On the last page of the report, the "ref." numbers 1-10 refer to individual patterns.

"Std. Dev." refers to the sample standard deviation of the batch tested.

"*pv*" is the ratio of the sample standard deviation to the average, expressed as a percentage. It is a convenient measure of consistency within the batch tested.

G. EFFECTS OF AIR DENSITY ON FLIGHT TIME

G.1 The effect of air density on cube law pellets

For identical pellets travelling in different atmospheres, their deceleration constants (k_3) are controlled by the air density (ρ_a). Therefore a small change in the deceleration constant

$$k_3 \rightarrow k_3 + \delta k_3 \tag{G.1}$$

effects the flight time, expression (4.7), of a pellet at range R by

$$t \rightarrow t + \delta t = \frac{R}{v_0} + \frac{(k_3 + \delta k_3)R^2}{2} \tag{G.2}$$

and as R/v_0 is a constant at a given range

$$\delta t = \frac{\delta k_3 R^2}{2} \tag{G.3}$$

Converting the small change in flight time (δt) into a ratio of total flight time t, we have

$$\frac{\delta t}{t} = \frac{\delta k_3 \, R^2/2}{R/v_0 + 2/k_3 v_0 R} = \frac{\delta k_3/k}{1 + 2/k_3 v_0 R} \tag{G.4}$$

From (4.14) it can be seen that for identical pellets

$$\frac{\delta k_3}{k_3} = \frac{\delta \rho_a}{\rho_a} \quad . \tag{G.5}$$

Therefore the percentage increase in flight time generated by a percentage increase in air density is shown in Figure G.1 and given by

$$\frac{\delta t}{t} = \frac{\delta \rho_a / \rho_a}{1 + 2/k_3 v_0 R} \tag{G.6}$$

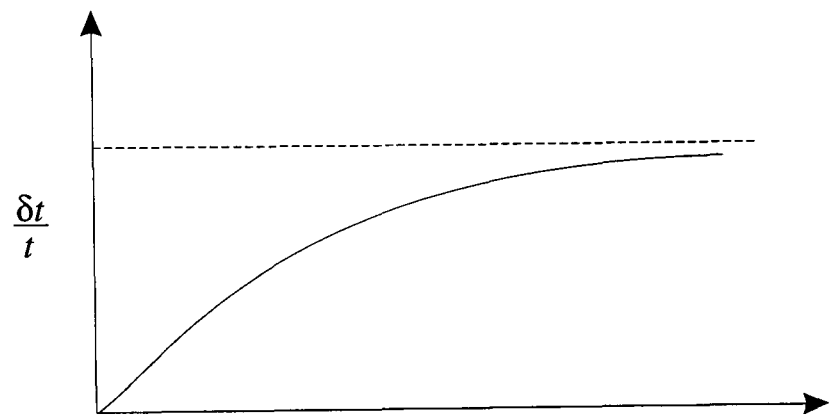

Figure G.1 *The nature of the percentage increase in flight time ($\delta t/t$), on a pellet obeying a cube law, with range for a small increase in air density ($\delta\rho_d/\rho_a$).*

G.2 The effect of air density on square law pellets

A small change in the deceleration constant of a pellet in the square law

$$k_2 \rightarrow k_2 + \delta k_2 \tag{G.7}$$

effects the flight time (4.8) of a pellet at range R by (G.8).

$$t \rightarrow t + \delta t = \frac{1}{(k_2 + \delta k_2)v_0}\left(e^{(k_2+\delta k_2)R} - 1\right) \tag{G.8}$$

Therefore,

$$\delta t = \frac{1}{(k_2 + \delta k_2)v_0}\left(e^{(k_2+\delta k_2)R} - 1\right) - \frac{1}{k_2 v_0}\left(e^{k_2 R} - 1\right) \tag{G.9}$$

$$\delta t = \frac{1}{k_2 v_0}\left[e^{k_2 R} R\delta k_2 - \frac{\delta k_2}{k_2}\left(e^{k_2 R} - 1\right)\right] \tag{G.10}$$

and converting the small change in flight time (δt) into a ratio as before we obtain

$$\frac{\delta t}{t} = \left[\frac{e^{k_2 R} R\delta k_2}{e^{k_2 R} - 1} - \frac{\delta k_2}{k_2}\right] \tag{G.11}$$

$$= \frac{\delta k_2}{k_2}\left[\frac{k_2 R}{1 - e^{-k_2 R}} - 1\right]$$

From (4.14) it can be seen that for identical pellets

$$\frac{\delta k_2}{k_2} = \frac{\delta \rho_a}{\rho_a} \quad . \tag{G.12}$$

Therefore the percentage increase in flight time generated by a percentage increase in air density is shown in Figure G.2 and given by

$$\frac{\delta t}{t} = \frac{\delta \rho_a}{\rho_a}\left[\frac{k_2 R}{1 - e^{-k_2 R}} - 1\right] \quad . \tag{G.13}$$

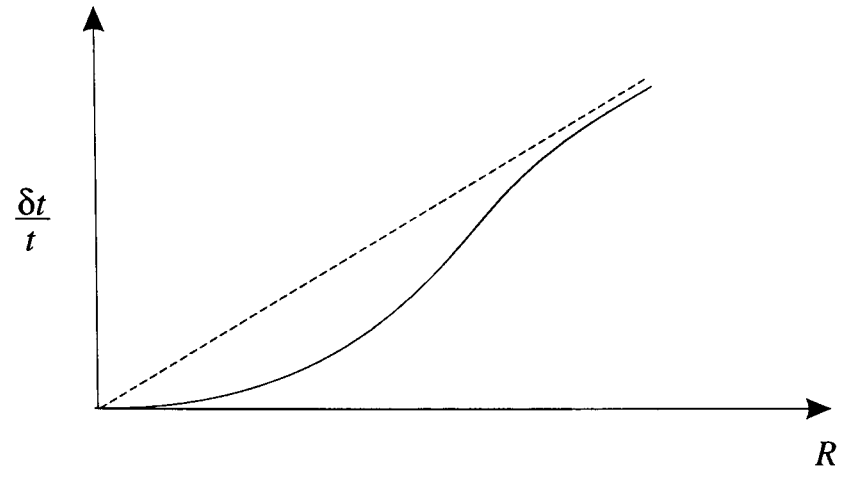

Figure G.2 *The nature of the percentage increase in flight time (dt/t), on a pellet obeying a square law, with range for a small increase in air density ($\delta\rho_a/\rho_a$).*

H. IN-FLIGHT TERMS FOR STOCHASTIC MODELS

H.1 In-flight width term (square law random force model)

The in-flight terms in (5.20) are evaluated in this section using the correlation function (5.21). The required integral is

$$I = D_x \int_0^t \int_0^t \frac{dt''d\tau''}{(1+k_2 v_0 t'')(1+k_2 v_0 \tau'')} \int_0^{t''} \int_0^{\tau''} (1+k_2 v_0 t')(1+k_2 v_0 \tau')\delta(t'-\tau')dt'd\tau' \quad . \tag{H.1}$$

Considering the inner double integral in this expression. The delta-function sets t' equal to τ'. In the t', τ'-plane, integration is therefore performed along the line $t'=\tau'$, the upper limit being determined by the relative sizes of t'' and τ''. Integration ceases at t'' if $t''<\tau''$ and at τ'' if $t''>\tau''$, as shown in Figure H.1.

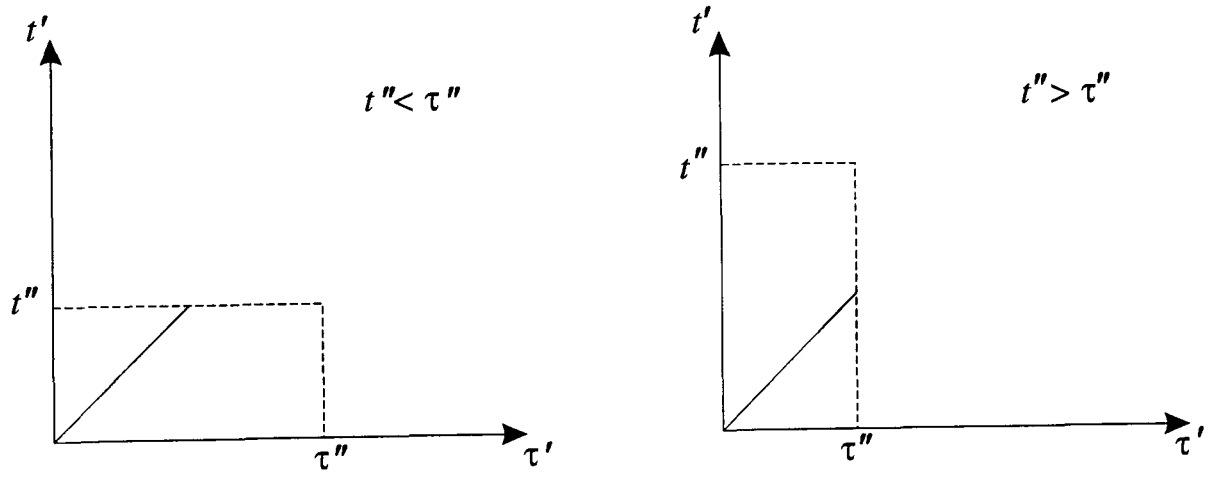

Figure H.1 *The integration in the t', τ'-plane showing the upper limit of integration as the minimum of t' and τ'.*

Hence the required limit is the minimum of t'' and τ'', which is written as $t_o=\min(t'',\tau'')$. Substituting this into (H.1)

$$I = D_x \int_0^t \int_0^t \frac{dt''d\tau''}{(1+k_2 v_0 t'')(1+k_2 v_0 \tau'')} \int_0^{t_0} (1+k_2 v_0 t')^2 dt'$$

$$I = D_x \int_0^t \int_0^t \frac{dt''d\tau''}{(1+k_2 v_0 t'')(1+k_2 v_0 \tau'')} \frac{1}{3k_2 v_0}\left[(1+k_2 v_0 t_0)^3 - 1\right] \quad . \quad \text{(H.2)}$$

The integration over the square of side equal to t in the t'', τ''-plane must be done in two parts since above the line $t''=\tau''$, t_0 is equal to τ'', while below this line t_0 equals t''. Hence performing the integration over τ'' first gives

$$I = \frac{D_x}{k_2 v_0} \int_0^t \frac{dt''}{(1+k_2 v_0 t'')} \left[\int_0^{t''} \frac{(1+k_2 v_0 \tau'')^3 - 1}{(1+k_2 v_0 \tau'')} d\tau'' + \int_{t''}^t \frac{(1+k_2 v_0 t'')^3 - 1}{(1+k_2 v_0 \tau'')} d\tau'' \right]$$

$$= \frac{D_x}{k_2 v_0} \int_0^t \frac{dt''}{(1+k_2 v_0 t'')} \left\{ \frac{1}{3k_2 v_0}\left[(1+k_2 v_0 t'')^3 - 1\right] - \frac{1}{k_2} \ln(1+k_2 v_0 t'') \right.$$

$$\left. + \left[(1+k_2 v_0 t'')^3 - 1\right] \frac{1}{k_2 v_0} \ln\left(\frac{1+k_2 v_0 t}{1+k_2 v_0 t''}\right) \right\}$$

$$= \frac{D_x}{3k_2^2 v_0^2} \int_0^t \frac{dt''}{(1+k_2 v_0 t'')} \left\{ \frac{1}{3}(1+k_2 v_0 t'')^3 - \frac{1}{3} + \left[(1+k_2 v_0 t'')^3 - 1\right] \ln(1+k_2 v_0 t) \right.$$

$$\left. - (1+k_2 v_0 t'')^3 \ln(1+k_2 v_0 t'') \right\} \quad .$$

(H.3)

This integral is now straightforward, if tedious, to evaluate and the in-flight terms are found to be

$$I = \frac{2D_x}{27k_2^3 v_0^3} \left\{ (1+k_2 v_0 t)^3 - 1 - 3\ln(1+k_2 v_0 t) - \frac{9}{2}\left[\ln(1+k_2 v_0 t)\right]^2 \right\} \quad .$$

(H.4)

H.2 In-flight width term (cube law random force model)

The in-flight terms in (5.26) are evaluated in this section using the correlation function (5.21). The required integral is

$$I = D_x \int_0^t \int_0^t \frac{dt''d\tau''}{\left(1+2k_3v_0^2t''\right)\left(1+2k_3v_0^2\tau''\right)} \int_0^{t''} \int_0^{\tau''} \left(1+2k_3v_0^2t'\right)^{1/2} \left(1+2k_3v_0^2\tau'\right)^{1/2} \delta(t'-\tau')dt'd\tau' \,. \tag{H.5}$$

Using the same upper limits as shown in Figure H.1 and used in Appendix H.1

$$I = D_x \int_0^t \int_0^t \frac{dt''d\tau''}{\left(1+2k_3v_0^2t''\right)^{1/2}\left(1+2k_3v_0^2\tau''\right)^{1/2}} \frac{1}{4k_3v_0^2} \left[\left(1+2k_3v_0^2t_0\right)^2 - 1\right] \,. \tag{H.6}$$

Here again the integration over the square of side equal to t in the t'', τ''-plane must be done in two parts. Hence performing the integration over τ'' first gives

$$I = \frac{D_x}{4k_3^2v_0^4} \int_0^t \frac{dt''}{\left(1+2k_3v_0^2t''\right)^{1/2}} \left[\left(1+2k_3v_0^2t''\right)^2 \left(1+2k_3v_0^2t\right)^{1/2} - \frac{4}{5}\left(1+2k_3v_0^2t''\right)^{5/2} - \left(1+2k_3v_0^2t''\right)^{1/2} + \frac{4}{5}\right] \,. \tag{H.7}$$

Then from the integrating (H.7) the in-flight effects are found to be

$$I = \frac{D_x}{60k_3^3v_0^6} \left\{24\left(1+2k_3v_0^2t\right)^{1/2} + \left(1+2k_3v_0^2t\right)^3 - 15\left(1+2k_3v_0^2t\right) - 10\right\} \,. \tag{H.8}$$

H.3 In-flight length terms (square law random force model)

The in-flight terms in (5.32) are evaluated in this section using the correlation function (5.33). The required integral is

$$I = D_z \int_0^t \int_0^t \frac{dt''d\tau''}{\left(1+k_2 v_0 t''\right)^2 \left(1+k_2 v_0 \tau''\right)^2} \int_0^{t''} \int_0^{\tau''} \left(1+k_2 v_0 t'\right)^2 \left(1+k_2 v_0 \tau'\right)^2 \delta(t'-\tau')dt'd\tau' \quad . \tag{H.9}$$

Using the same upper limits as shown in Figure H.1 and used in Appendix H.1

$$I = D_z \int_0^t \int_0^t \frac{dt''d\tau''}{\left(1+k_2 v_0 t''\right)^2 \left(1+k_2 v_0 \tau''\right)^2} \frac{1}{5k_2 v_0}\left[\left(1+k_2 v_0 t_0\right)^5 - 1\right] \quad . \tag{H.10}$$

Here again the integration over the square of side equal to t in the t'', τ''-plane must be done in two parts. Hence performing the integration over τ'' first gives

$$I = \frac{D_z}{5k_2^2 v_0^2} \int_0^t \frac{dt''}{\left(1+k_2 v_0 t''\right)^2}\left[\frac{5}{4}\left(1+k_2 v_0 t''\right)^4 + \frac{1}{\left(1+k_2 v_0 t\right)}\left[1-\left(1+k_2 v_0 t''\right)^5\right] - \frac{5}{4}\right] \quad . \tag{H.11}$$

Then from the integrating (H.11) the in-flight effects are found to be

$$I = \frac{D_z}{60k_2^3 v_0^3}\left\{\left(1+k_2 v_0 t\right)^3 - 6\left(1+k_2 v_0 t\right)^{-2} + 15\left(1+k_2 v_0 t\right)^{-1} - 10\right\} \tag{H.12}$$

and rearranging gives

$$I = \frac{D_z \left(k_2 v_0 t\right)^2}{60k_2^3 v_0^2 \left(1+k_2 v_0 t\right)^2}\left\{10 + 5k_2 v_0 t + \left(k_2 v_0 t\right)^2\right\} \tag{H.13}$$

H.4 In-flight length terms (cube law random force model)

The in-flight terms for the cube law random force model are evaluated in this section using the correlation function (5.33). The required integral is

$$I = D_z \int_0^t \int_0^t \frac{dt''d\tau''}{\left(1+2k_3v_0^2t''\right)^{3/2}\left(1+2k_3v_0^2\tau''\right)^{3/2}} \int_0^{t''}\int_0^{\tau''}\left(1+2k_3v_0^2t'\right)^{3/2}\left(1+2k_3v_0^2\tau'\right)^{3/2}\delta(t'-\tau')dt'd\tau' \ . \tag{H.14}$$

Using the same upper limits as shown in Figure H.1 and used in Appendix H.1

$$I = D_z \int_0^t \int_0^t \frac{dt''d\tau''}{\left(1+2k_3v_0^2t''\right)^{3/2}\left(1+2k3v_0^2\tau''\right)^{3/2}} \frac{1}{8k_3v_0^2}\left[\left(1+2k_3v_0^2t_0\right)^4 - 1\right] \ . \tag{H.15}$$

Here again the integration over the square of side equal to t in the t'', τ''-plane must be done in two parts. Hence performing the integration over τ'' first gives

$$I = \frac{D_z}{8k_3^2v_0^4}\int_0^t \frac{dt''}{\left(1+2k_3v_0^2t''\right)^{3/2}}\left[\frac{8}{7}\left(1+2k_3v_0^2t''\right)^{7/2} + \left(1+2k_3v_0^2t''\right)^4\left(1+2k_3v_0^2t''\right)^{1/2} + \left(1+2k_3v_0^2t''\right)^{1/2} - \frac{8}{9}\right] \ . \tag{H.16}$$

Then from the integrating (H.7) the in-flight effects are found to be

$$I = \frac{D_z}{168k_3^3v_0^6}\left\{\left(1+2k_3v_0^2t\right)^3 - 28 - 48\left(1+2k_3v_0^2t\right)^{-1/2} - 21\left(1+2k_3v_0^2t\right)^{1/2}\right\} \ . \tag{H.17}$$

H.5 In-flight width term (square law velocity dependent random force model)

The in-flight terms in (5.51) are evaluated in this section using the correlation function (5.21). The required integral is

$$I = D_x \int_0^t \int_0^t \frac{dt''d\tau''}{(1+k_2 v_0 t'')(1+k_2 v_0 \tau'')} \int_0^{t''} \int_0^{\tau''} \delta(t'-\tau')dt'd\tau' \,. \qquad \text{(H.18)}$$

Using the same upper limits as shown in Figure H.1 and used in Appendix H.1

$$I = D_x \int_0^t \int_0^t \frac{dt''d\tau''}{(1+k_2 v_0 t'')(1+k_2 v_0 \tau'')}\, t_0 \,. \qquad \text{(H.19)}$$

Here again the integration over the square of side equal to t in the t'', τ''-plane must be done in two parts. Hence performing the integration over τ'' first gives

$$I = \frac{D_x}{k_2^2 v_0^2} \int_0^t \frac{dt''}{(1+k_2 v_0 t'')} \Big\{ k_2 v_0 t'' - \ln(1+k_2 v_0 t'')^2 + k_2 v_0 t'' \big[\ln(1+k_2 v_0 t) - \ln(1+k_2 v_0 t'') \big] \Big\} \,. \qquad \text{(H.20)}$$

Then from the integrating (H.20) the in-flight effects are found to be

$$I = \frac{D_x}{(k v_0)^3} \Big\{ 2k_2 v_0 t - 2\ln(1+k_2 v_0 t) - \big[\ln(1+2k_2 v_0 t) \big]^2 \Big\} \,. \qquad \text{(H.21)}$$

H.6 In-flight width term (cube law velocity dependent random force model)

The in-flight terms in (5.55) are evaluated in this section using the correlation function (5.21). The required integral is

$$I = D_x \int_0^t \int_0^t \frac{dt''d\tau''}{\left(1+2k_3v_0^2t''\right)^{1/2}\left(1+2k_3v_0^2\tau''\right)^{1/2}} \int_0^{t''}\int_0^{\tau''} \delta(t'-\tau')dt'd\tau' \,. \qquad \text{(H.22)}$$

Using the same upper limits as shown in Figure H.1 and used in Appendix H.1

$$I = D_x \int_0^t \int_0^t \frac{dt''d\tau''}{\left(1+2k_3v_0^2t''\right)^{1/2}\left(1+2k_3v_0^2\tau''\right)^{1/2}} \; t_0 \;\; . \qquad \text{(H.23)}$$

Here again the integration over the square of side equal to t in the t'', τ''-plane must be done in two parts. Hence performing the integration over τ'' first gives

$$I = \frac{D_x}{2k_3^2v_0^4} \int_0^t \frac{dt''}{\left(1+2k_3v_0^2t''\right)^{1/2}} \left\{ \frac{1}{2}\left(1+2k_3v_0^2t''\right)^{3/2} + \frac{2}{3} - +\left(1+2k_3v_0^2t''\right)^{1/2} \right.$$
$$\left. 2k_3v_0^2t''\left[\left(1+2k_3v_0^2t\right)^{1/2} - \left(1+2k_3v_0^2t''\right)^{1/2}\right]\right\} \,. \qquad \text{(H.24)}$$

Then from the integrating (H.24) the in-flight effects are found to be

$$I = \frac{D_x}{12k_3v_0^2} \left\{ \left(1+2k_3v_0^2t''\right)^2 - 6\left(1+2k_3v_0^2t''\right) + 8\left(1+2k_3v_0^2t''\right)^{1/2} - 3 \right\} \,. \qquad \text{(H.25)}$$

H.7 In-flight length terms (square law velocity dependent random force model)

The in-flight terms in (5.59) are evaluated in this section using the correlation function (5.33). The required integral is

$$I = D_z \int_0^t \int_0^t \frac{dt''d\tau''}{\left(1+k_2 v_0 t''\right)^2 \left(1+k_2 v_0 \tau''\right)^2} \int_0^{t''} \int_0^{\tau''} \left(1+k_2 v_0 t'\right)\left(1+k_2 v_0 \tau'\right)\delta(t'-\tau')dt'd\tau' \quad . \tag{H.26}$$

Using the same upper limits as shown in Figure H.1 and used in Appendix H.1

$$I = D_z \int_0^t \int_0^t \frac{dt''d\tau''}{\left(1+k_2 v_0 t''\right)^2 \left(1+k_2 v_0 \tau''\right)^2} \frac{1}{3k_2 v_0}\left[\left(1+k_2 v_0 t_0\right)^3 - 1\right] \quad . \tag{H.27}$$

Here again the integration over the square of side equal to t in the t'', τ''-plane must be done in two parts. Hence performing the integration over τ'' first gives

$$I = \frac{D_z}{3k_2^2 v_0^2} \int_0^t \frac{dt''}{\left(1+k_2 v_0 t''\right)^2}\left[\frac{3}{2}\left(1+k_2 v_0 t''\right)^2 + \frac{\left(1+k_2 v_0 t''\right)^3}{\left(1+k_2 v_0 t\right)} + \frac{1}{\left(1+k_2 v_0 t''\right)} - \frac{3}{2}\right] \quad . \tag{H.28}$$

Then from the integrating (H.28) the in-flight effects are found to be

$$I = \frac{D_z}{6k_2^3 v_0^3}\left\{6\left(1+k_2 v_0 t\right)^{-1} - 2\left(1+k_2 v_0 t\right)^{-2} + 2\left(1+k_2 v_0 t\right) - 6\right\} \tag{H.29}$$

H.8 In-flight length terms (cube law velocity dependent random force model)

The in-flight terms for the cube law velocity dependent random force model are evaluated in this section using the correlation function (5.33). The required integral is

$$I = D_z \int_0^t \int_0^t \frac{dt''d\tau''}{\left(1+2k_3v_0^2t''\right)^{3/2}\left(1+2k_3v_0^2\tau''\right)^{3/2}} \int_0^{t''}\int_0^{\tau''}\left(1+2k_3v_0^2t'\right)\left(1+2k_3v_0^2\tau'\right)\delta(t'-\tau')dt'd\tau' \ . \tag{H.30}$$

Using the same upper limits as shown in Figure H.1 and used in Appendix H.1

$$I = D_z \int_0^t \int_0^t \frac{dt''d\tau''}{\left(1+2k_3v_0^2t''\right)^{3/2}\left(1+2k3v_0^2\tau''\right)^{3/2}} \frac{1}{6k_3v_0^2}\left[\left(1+2k_3v_0^2t_0\right)^3-1\right] \ . \tag{H.31}$$

Here again the integration over the square of side equal to t in the t'', τ''-plane must be done in two parts. Hence performing the integration over τ'' first gives

$$I = \frac{D_z}{6k_3^2v_0^4}\int_0^t \frac{dt''}{\left(1+2k_3v_0^2t''\right)^{3/2}}\left[\frac{6}{5}\left(1+2k_3v_0^2t''\right)^{5/2} + \frac{\left(1+2k_3v_0^2t''\right)^3}{\left(1+2k_3v_0^2t\right)^{1/2}} + \left(1+2k_3v_0^2t''\right)^{-1/2} - \frac{6}{5}\right] \ . \tag{H.32}$$

Then from the integrating (H.32) the in-flight effects are found to be

$$I = \frac{D_z}{60k_3^3v_0^6}\left\{\left(1+2k_3v_0^2t\right)^2 + 24\left(1+2k_3v_0^2t\right)^{-1/2} - 10\left(1+2k_3v_0^2t\right)^{-1} - 15\right\}. \tag{H.33}$$